



# **Hydrodynamic and mass transfer study of micro-packed beds in single- and two-phase flow**

**Thèse**

**Ali Faridkhou**

**Doctorat en génie chimique**  
Philosophiae Doctor (Ph.D.)

Québec, Canada

© Ali Faridkhou, 2015



## Résumé

Les micros-lit fixes sont des milieux poreux miniaturisés ralliant les avantages à la fois des microréacteurs et des lits fixes, comme par exemple en terme de rapport surface/volume très élevé conduisant à des taux de transfert de chaleur et de matière intensifiés. Par conséquent, la caractérisation hydrodynamique des micros-lits fixes est nécessaire afin d'appréhender de manière objective les phénomènes de transfert et les modes de contact entre phases. Ensuite l'importance des micros-lits fixes est mise en évidence tandis que les approches pour construire des bases de recherche sur les micros-lits fixes y sont explicitées.

Notre recherche commence par l'étude des régimes d'écoulement, des transitions de régime d'écoulement de la multiplicité de l'hydrodynamique et du transfert de matière liquide-solide dans les micros-lits fixes. Cette étude est réalisée au moyen d'une méthode de visualisation par microscopie optique à la paroi et le traitement d'image qui s'en suit pour la partie hydrodynamique et d'une méthode électrochimique basée sur l'oxydoréduction du couple complexes ferri/ferreux hexacyanure pour la partir sur le transfert de matière.

Les résultats de perte de charge et de rétention de liquide ont été discutés par rapport aux régimes d'écoulement mis en place et des observations pariétales rendues possibles par microscopie optique. L'effet de la taille des particules et de la géométrie du canal sur les transitions de régimes d'écoulement, le comportement transitoire et le phénomène d'hystérèse ont également été abordés. Finalement, les résultats des expériences hydrodynamiques ont été obtenus en faisant face à de nombreux défis pour lesquels nous avons formulé de nombreuses recommandations en vue d'investigations futures.

La détermination expérimentale du coefficient de transfert de masse liquide-solide ( $k_{LS}$ ) par la technique électrochimique a été effectuée dans un micro-lit fixe rempli de couches de particules de graphite non-sphériques servant de cathode et d'anode. Les expériences ont été réalisées pour un écoulement monophasique en régime de diffusion limitée. Finalement, la correspondance de valeurs de  $k_{LS}$  avec les corrélations construites sur la base d'études sur les lits fixes à l'échelle macroscopique a été discutée.





## Abstract

Micro-packed beds are miniaturized packed beds having the advantages of both microreactors (high surface-to-volume ratios leading to intensified heat and mass transfer rates, increased safety, etc.) and packed beds (effective contact between the phases) that have the potential to be successfully employed for purposes such as catalyst screening and production of hazardous materials. To assess this potential, hydrodynamic characterization of micro-packed beds is necessary as they address the actual flow phenomena and provide suggestions to improve the contacting patterns between phases for enhanced performances. This work starts with a brief review on process intensification via microreactors. Then the importance of micro-packed beds is highlighted while the approaches to build research foundations on micro-packed beds are discussed.

Our research begins by studying the flow regimes, transitions in flow regime and hydrodynamic multiplicity in micro-packed beds mostly by means of microscopic wall visualization and image processing. Results on pressure drop and liquid holdup have been obtained and discussed in terms of flow regimes and wall-flow image analyses. In addition, residence time distributions of the liquid in micro-packed beds have been obtained according to two techniques, by an impulse tracing method (electrolyte tracer injection) and wall visualization with optical microscopy. The effect of particle size and channel geometry (circular vs. square) has also been investigated in terms of flow regime transitions, transient behavior and hysteresis. Finally, challenges and recommendations thereof to surpass the many difficulties encountered are methodically explained to facilitate future investigations.

Experimental determination of liquid-solid mass transfer coefficient ( $k_{LS}$ ) via a linear polarization method was also carried out in a micro-packed bed filled with layers of non-spherical graphite particles serving as cathode and anode for the Redox ferri/ferrocyanide electrochemical reaction. Experiments concerned single-phase liquid flow within the diffusion-limited regime. Particle size analysis and image processing were used to evaluate deviations from spherical geometry of the graphite particles to determine liquid-solid mass transfer coefficient. Finally, the correspondence of  $k_{LS}$  values with macro-scale packed bed correlations was discussed.



## Table of Contents

Résumé.....	iii
Abstract.....	v
List of tables.....	xi
List of figures.....	xiii
Acknowledgment.....	xxiii
Foreword.....	xxv
Introduction.....	1
1.1 Process intensification.....	1
1.2 Microreactors and their advantages.....	2
1.3 Microreactors and industrial producers.....	5
1.4 Microreactors designs and applications.....	7
1.5 Micro-packed beds (packed microreactors).....	10
1.6 Hydrodynamic study of micro-packed beds.....	17
1.6.1 Micro- vs. macro-scale hydrodynamics.....	17
1.6.2 Research methodologies for hydrodynamic studies.....	20
1.6.3 Literature on the hydrodynamic study of micro-packed beds.....	27
1.6.4 Visualizations in micro-packed beds.....	33
1.7 Mass transfer study of micro-packed beds.....	35
1.8 Scope of thesis.....	37
1.9 Nomenclature.....	39
1.10 References.....	41
2 Hydrodynamics of gas-liquid cocurrent flows in micro-packed beds - Wall visualization study.....	51
2.1 Introduction.....	53

2.2	Experimental.....	55
2.2.1	Setup .....	55
2.2.2	Methodology.....	56
2.2.3	Image Processing.....	57
2.3	Results and discussion.....	59
2.3.1	Flow Regimes .....	59
2.3.2	Onset of Flow Regime Transitions.....	62
2.3.3	Hysteresis.....	65
2.4	Conclusions.....	71
2.5	Nomenclature.....	73
2.6	References.....	74
3	Hydrodynamics of gas-liquid micro-fixed beds – Measurement approaches and technical challenges.....	79
3.1	Introduction.....	81
3.2	Experimental section .....	82
3.2.1	Microreactor packing procedure.....	82
3.2.2	RTD setup fabrication and methodology.....	83
3.2.3	Visualization setup and methodology.....	87
3.3	Results and discussion.....	92
3.3.1	Effect of tracer input location.....	92
3.3.2	Misconstrue in flow regime designation.....	95
3.3.3	Pressure drop, bed porosity and liquid holdup .....	98
3.3.4	Near wall RTD determination .....	101
3.4	Conclusion.....	104
3.5	Nomenclature.....	105

3.6	References .....	106
4	Two-phase flow hydrodynamic study in micro-packed beds – The effect of bed geometry and particle size.....	109
4.1	Introduction .....	111
4.2	Experimental .....	112
4.2.1	Setup.....	112
4.2.2	Methodology .....	114
4.3	Results and discussion.....	118
4.3.1	Flow regime transition within the bed.....	118
4.3.2	Hysteresis and the effect of particle size .....	124
4.3.3	Transient behavior.....	128
4.4	Conclusion.....	131
4.5	Nomenclature .....	132
4.6	References .....	133
5	Determination of liquid-solid mass transfer coefficient in micro-packed beds using the limiting current technique.....	137
5.1	Introduction .....	139
5.2	Experimental .....	141
5.2.1	Setup.....	141
5.2.2	Methodology .....	143
5.3	Results and discussions .....	148
5.3.1	Single-phase liquid flow.....	148
5.3.2	Gas-liquid flow.....	156
5.4	Conclusions .....	158
5.5	Nomenclatures.....	159

5.6	References.....	160
6	Thesis conclusion.....	163
6.1	Key contributions.....	163
6.2	Suggested future work.....	165
6.3	References.....	167

## List of tables

<b>Table 1-1:</b> Surface to volume ratio for some conventional and micro-scale process units <sup>4-6</sup> .....	3
<b>Table 1-2.</b> Summary of the most common designs of microreactors along with their applications mentioned in the open literature .....	8
<b>Table 1-3.</b> Physical properties of air and water at 20°C and 1 atm. ....	18
<b>Table 1-4.</b> Comparison of dimensionless numbers appearing in hydrodynamic studies in both macro- and micro-scale.....	19
<b>Table 1-5.</b> Path 1, how to build research foundations on micro-packed beds by their comparison with microchannels (similarity of scale) .....	23
<b>Table 1-6.</b> Path 2, how to build research foundations on micro-packed beds by their comparison with macro-packed beds (similarity of operation) .....	25
<b>Table 2-1.</b> Properties of Working Fluids.....	57
<b>Table 4-1.</b> Operating conditions for studying the effect of capillary shape and particle size on pressure drop, flow regimes and micro-packed bed transient behavior ( $U_{GS} = 21.3$ cm/s).....	116
<b>Table 5-1.</b> Selected macro-scale correlations (in terms of Sherwood number) proposed for determination of liquid-solid mass transfer coefficient .....	151





## List of figures

- Figure 1-1.** Photomicrograph of the micro-packed bed loaded with catalyst (Top). Schematic of the multichannel reactor design illustrating fluid manifold to 10 parallel fixed-bed reaction channels (A). Photomicrograph of multichannel reactor chip (B). Adapted from Losey et al (2001)<sup>28</sup> ..... 11
- Figure 1-2.** Comparison of cross flow against typical axial (tube) flow (a). A section of the cross flow reactor packed with 60 micron glass beads (b) and the overall picture of cross-flow microreactor (c). Adapted from Ajmera et al. (2002)<sup>43</sup> ..... 12
- Figure 1-3.** Radial flow micro-packed bed. Schematic (a), fabricated device (b), vaporization region (c) and catalyst particle filter (d). Adapted from Pattekar and Kothare (2005)<sup>27</sup> ..... 13
- Figure 1-4.** Transparent micro-packed bed strengthened with metal deposition used for high pressure hydrogenation. Overall view of micro-packed bed (a), schematic of gas-liquid-solid contact (b). Adapted from Trachsel et al. (2008)<sup>47</sup> ..... 15
- Figure 1-5.** Micro-packed bed arrangement (a) combination with Raman spectroscopy (b). Adapted from Cao et al. (2011)<sup>51</sup> ..... 16
- Figure 1-6.** Schematic representation of macro- and micro-scale. A stirred tank (left) and a microreactor (right) both used for gas-liquid contact. Length scales are indications of the characteristic lengths. .... 18
- Figure 1-7.** Experimental setup for contribution b) by Márquez et al.<sup>103</sup> ..... 30
- Figure 1-8.** Typical images encountered during CO<sub>2</sub>-water flow in the micro-channel with  $d_h = 400 \mu\text{m}$  (flow from left to right with observation point at a distance of 3 cm from entrance): (a) bubbly flow ( $j_G = 0.16 \text{ m/s}$ ,  $j_L = 1.0 \text{ m/s}$ ); (b) bubbly flow ( $j_G = 0.29 \text{ m/s}$ ,  $j_L = 1.0 \text{ m/s}$ ); (c) Taylor flow ( $j_G = 0.16 \text{ m/s}$ ,  $j_L = 0.04 \text{ m/s}$ ,  $Ca = 0.0028$ ,  $Re_L = 80$ ); (d) Taylor flow ( $j_G = 1.28 \text{ m/s}$ ,  $j_L = 1.0 \text{ m/s}$ ,  $Ca = 0.031$ ,  $Re_L = 913$ ); (e) unstable slug flow ( $j_G = 1.74 \text{ m/s}$ ,  $j_L = 0.51 \text{ m/s}$ ); (f) unstable slug flow ( $j_G = 2.14 \text{ m/s}$ ,  $j_L = 0.51 \text{ m/s}$ ); (g) bubble-train slug flow ( $j_G = 2.07 \text{ m/s}$ ,  $j_L = 1.0 \text{ m/s}$ ); (h) slug-annular flow ( $j_G = 7.51 \text{ m/s}$ ,  $j_L = 0.20 \text{ m/s}$ ); (i) churn flow ( $j_G = 12.7$

m/s,  $j_L = 1.0$  m/s); (j) churn flow ( $j_G = 31$  m/s,  $j_L = 0.51$  m/s); (k) annular flow ( $j_G = 21.5$  m/s,  $j_L = 0.02$  m/s), Adapted from Yue et al. (2008)<sup>53</sup> ..... 34

**Figure 1-9.** Experimental setup for the meandering microchannel (top-left), Schematic of the microchannel; network and the field of view (top-right) and RTD curves for segmented gas–liquid flow ( $j_L = 3.1$  mm/s,  $j_G = 21.7$  mm/s) at different lengths along device (bottom). Adapted from Trachsel et al. (2005)<sup>71</sup> and Günther et al. (2004)<sup>74</sup> ..... 35

**Figure 1-10.** Top view of the micro-packed bed outlet filter for solids immobilization (a) and 320 $\mu$ m fused-silica square microchannel packed with 80 $\mu$ m copper particles (b). Adapted from Tidona et al. (2012)<sup>29</sup> ..... 37

**Figure 2-1.** Experimental Setup: 1) Gas cylinder; 2) Syringe pump; 3) Gas mass flow controller; 4) Microreactor; 5) Inverted microscope and objective lens; 6) Camera with frame grabber port; 7) Computer for image acquisition; 8) Drain ..... 56

**Figure 2-2.** Image processing procedure starting from raw image (top-left): a) image binarization without preprocessing b) image pre-processing c) binarization of pre-processed image and obtaining liquid and gas occupied mean areas..... 58

**Figure 2-3.** Dynamic variations of characteristic lengths for liquid (right) and gas (left) at four liquid superficial velocities. .... 60

**Figure 2-4.** Sequence of images taken for air and water system in the high interaction regime at  $U_{GS} = 25.5$  cm/s and  $U_{GL} = 19$  mm/s..... 61

**Figure 2-5.** Coefficient of variation of liquid as a function of liquid superficial velocity and constant gas superficial velocity: Maxima on curves correspond to transitions from low to high interaction flow regime. .... 62

**Figure 2-6.** Comparative flow regime map based on Charpentier and Favier coordinates. Regions to the left of each group represent low interaction flow regime while regions to the right indicate high interaction flow regime. Results for macro-scale groups I and II are extracted from Charpentier and Favier (1975).<sup>39</sup> ..... 64

**Figure 2-7.** Two-phase flow pressure drop versus liquid superficial velocity at constant gas superficial velocity ( $U_{GS} = 25.5$  cm/s). Lower curve: ascending liquid velocity

(imbibition or forward mode), upper curve: descending liquid velocity (drainage or backward mode). .....66

**Figure 2-8.** Fraction of liquid occupying bed texture nearby wall, as inferred from image analysis and processing, both in forward and backward conditions within zone (I) of pressure drop hysteresis curve. ....68

**Figure 2-9.** Comparison of the wetting patterns at the same gas and liquid superficial inlet velocities ( $U_{Gs}= 25.5$  cm/s,  $U_{Ls}= 1.1$  mm/s). a) original imbibition image, b) original drainage image, c) binarized imbibition image, d) binarized drainage image and e) comparative difference image of c) and d). .....69

**Figure 2-10.** Fraction of liquid occupying bed texture in both forward and backward conditions within zone (I) of the pressure drop hysteresis curve..... 70

**Figure 2-11.** Comparative percentage of the indifferent regions (green parts of Figure 9) within zone (I) of the pressure drop hysteresis curve. ....71

**Figure 3-1.** Two types of electrode configuration proposed for for RTD measurements. Old design of ring electrodes (left) and new design of point electrodes (right) installed on microreactor.....84

**Figure 3-2.** Experimental setup of the micro-fixed bed reactor for RTD and holdup determination .....85

**Figure 3-3.** Conductivity signals for the inlet (a) and outlet (b) upon using pure water as the liquid phase  $U_{Gs}=21.3$  cm/s,  $U_{Ls}= 1$  mm/s.....86

**Figure 3-4.** Experimental Setup for visualization experiments: 1) Gas cylinder 2) Syringe pump 3) Gas mass flow controller 4) Micro-reactor 5) Inverted Microscope and Objective lens 6) Camera with frame grabber port 7) Computer for image acquisition 8) Drainage.....88

**Figure 3-5.** Schematics of method 1 for RTD determination by microscopic imaging and dye injection (assuming ideal pulse injection) and monitoring the overall-averaged pixel values within the image ( $U_{Gs}= 10.6$  cm/s and  $U_{Ls}= 1.6$  mm/s).....90

**Figure 3-6.** Schematics of method 2 for RTD determination by microscopic imaging and dye injection by double detection and monitoring of the laterally averaged pixel values at the two left and right extremes of the image ( $U_{GS}= 10.6$  cm/s and  $U_{LS}= 1.6$  mm/s) ..... 91

**Figure 3-7.** Illustrative example of inverting the initially obtained RTD curves from microscopic imaging and dye injection into those commonly used. a) Initially obtained curves showing minima b) Inverted curves showing maxima..... 92

**Figure 3-8.** Two alternatives for tracer injection during hydrodynamic test on micro-fixed bed reactors. a) in liquid phase before gas-liquid contact b) in packed bed after gas-liquid contact ..... 93

**Figure 3-9.** Experimental inlet and outlet electrical conductance response curves with the fit of outlet response using a two-parameter PD RTD model for two cases: a) tracer injection in the liquid feeding line b) tracer injection in the packed bed downstream of the gas-liquid merging point. ( $U_{GS}= 21.3$  cm/s and  $U_{LS}= 1$  mm/s for both cases)..... 94

**Figure 3-10.** Sequence of four images taken for air and water system in during flow instability at  $U_{GS}= 21.3$  cm/s and  $U_{LS}= 1.6$  mm/s (left) and the binarized images (right)... 96

**Figure 3-11.** Variations in dimensionless liquid phase characteristic length (a,b) and electric conductivity (c,d) at  $U_{GS}= 21.3$  cm/s and  $U_{LS}= 1.6$  mm/s. a) dimensionless liquid phase characteristic length during flow instabilities due to loose packing b) dimensionless liquid phase characteristic length in dense-packing c) electric conductivity signals during flow instabilities due to loose packing d) electric conductivity signals in dense-packing..... 97

**Figure 3-12.** Pressure drop data for air-water, argon-water and hydrogen-water systems at (a)  $U_{LS}=1$  mm/s and (b)  $U_{LS}=1.6$  mm/s ..... 99

**Figure 3-13.** Liquid holdup data for air-water, argon-water and hydrogen-water systems at (a)  $U_{LS}=1$  mm/s and (b)  $U_{LS}=1.6$  mm/s ..... 100

**Figure 3-14.** Actual RTD data obtained by monitoring the changes in the overall averaged pixel values and fitted against the curves representing a) small deviations from plug flow and b) large deviations from plug flow ..... 102

**Figure 3-15.** Experimental inlet and outlet gray level variation response curves (obtained by image acquisition from wall visualization) with the fit of outlet response using a two-parameter PD RTD model. ( $U_{GS}= 10.6$  cm/s and  $U_{LS}= 1.6$  mm/s)..... 103

**Figure 4-1.** Experimental Setup: 1) Gas cylinder; 2) Syringe pump; 3) Gas mass flow controller; 4) Differential pressure transducer; 5) Micro-reactor made with round/square capillary tube; 6) Inverted microscope and objective lens; 7) Camera with frame grabber port; 8) Computer for image acquisition; 9) Drain..... 114

**Figure 4-2.** Regions within the square micro-fixed bed axial length used for visualization on flow regime transition..... 115

**Figure 4-3.** Definition of transient time taken as the time span between two steady states (top) and the method for its determination (bottom)..... 117

**Figure 4-4.** Dynamic variations in dimensionless liquid-phase characteristic length at  $U_{GS} = 21.3$  cm/s and for four regions within the axial length of the square micro-fixed bed with particles of 106-125  $\mu\text{m}$  (columns (a) and (b) represent first and second half of micro-fixed bed, respectively, according to Figure 2).  $U_{LS} = 12.8$  mm/s (4-4-1-a and 4-4-1-b),  $U_{LS} = 14.9$  mm/s (4-4-2-a and 4-4-2-b),  $U_{LS} = 17.0$  mm/s (4-4-3-a and 4-4-3-b) and  $U_{LS} = 19.2$  mm/s (4-4-4-a and 4-4-4-b)..... 119

**Figure 4-5.** Pressure drop variations against liquid superficial velocity (at iso-G conditions) for a) circular geometry and b) square geometry..... 121

**Figure 4-6.** Pressure drop variations against liquid superficial velocity (at iso-G conditions) at two different range of particle sizes: a)  $D/d_p \approx 20$  and b)  $D/d_p \approx 10$ ..... 123

**Figure 4-7.** Effect of decreasing particle size (increasing  $D/d_p$  ratio) on wetting pattern hysteresis at the same gas and liquid superficial velocities ( $U_{GS} = 25.5$  cm/s,  $U_{LS} = 1.1$  mm/s) for a)  $D/d_p \approx 10$  (adapted from Faridkhou and Larachi [7]) and b)  $D/d_p \approx 20$  (current work)..... 125

**Figure 4-8.** (a, c): Fraction of liquid occupying bed texture in both imbibition and drainage, and comparative percentage of indifferent regions (green parts of Figure 8a) adapted from Faridkhou and Larachi [7], for  $D/d_p \approx 10$ . (b, d): Fraction of liquid-occupying

bed texture in both imbibition and drainage, and the comparative percentage of the indifferent regions (green parts of Figure 8b) as current work for  $D/d_p \approx 20$ . ..... 127

**Figure 4-9.** Effect of geometry on the dimensionless transient time of micro-fixed beds at a)  $D/d_p \approx 20$  and b)  $D/d_p \approx 10$ . ..... 129

**Figure 4-10.** Effect of particle size (column-to-particle diameter ratio) on the dimensionless transient time in micro-fixed bed of a) circular geometry and b) square geometry. .... 130

**Figure 5-1.** Schematic of the I-V curve obtained from limiting-current technique 141

**Figure 5-2.** Experimental setup of the micro-fixed bed reactor for liquid-solid mass transfer studies. .... 142

**Figure 5-3.** Images of graphite particles of two different sizes: Group A (top) Group B (bottom) ..... 146

**Figure 5-4.** Size distribution based on equivalent diameter for graphite particles of a) Group A and b) Group B. .... 147

**Figure 5-5.** I-V curve in single-phase liquid flow experiments for graphite particles of a) Group A and b) Group B ..... 149

**Figure 5-6.** Liquid-solid mass transfer coefficients for group B graphite particles in both a) direct and b) dimensionless form comparing the logarithmic and arithmetic averaging approach for evaluating ferricyanide concentration ..... 150

**Figure 5-7.** Experimental liquid-solid mass transfer coefficients for group B graphite particles versus predicted results with macro-scale correlations. .... 152

**Figure 5-8.** Volumetric liquid-solid mass transfer coefficients for group B graphite particles (♦) compared with those determined by Tidona et al. (2013) with 80µm particles and different D/d ratios. All data are for single-phase liquid flow experiments. .... 153

**Figure 5-9.** Comparison of volumetric liquid-solid mass transfer coefficients for single-phase liquid flow experiments at micro- and macro-scale. .... 154

**Figure 5-10.** Comparison of experimental liquid-solid mass transfer coefficients with predictions of Larachi et al. (2003) correlation a)  $k_{LS}$  vs  $U_{LS}$  , b) Sherwood number vs. Reynolds number ..... 155

**Figure 5-11.** Examples of peculiar results obtained for two-phase flow experiments presumably due to the high flow rate of the gas phase compared to the liquid phase. .... 157





”We live on an island surrounded by a sea of ignorance. As our island of knowledge grows, so does the shore of our ignorance.”

John Archibald Wheeler

”It is better to deserve honors and not have them than to have them and not to deserve them.”

Mark Twain



# Acknowledgment

This thesis would not have been possible without the love, support and patience of my family, friends and especially my advisor.

Before I acknowledge all the people at Laval University, I would like to begin by acknowledging the support of my parents and parents-in-law for their continued long distance encouragements and supports which gave me great comfort in both brightest and darkest days of my work.

Every good thesis starts and goes on with a good advisor. I could not have asked for a better advisor than Professor Faiçal Larachi. I really enjoyed working with him despite the tough times that I always had to meet his extremely high expectations. It's a shame that there is no chance to go back in time and try out more ideas that came up during our discussions. I am deeply indebted for his advisement and mentorship and I am quite positive that I will be more thankful to him for what he taught me when I start a new career in the future.

My genuine appreciations to Dr. Mohsen Hamidipour for showing me the initial set up and the subsequent trainings required to start my project. I would also like to thank Dr. Jean-Nöel Tourvieille for all his helps and feedbacks on the limiting current technique used for mass transfer study in chapter 5. My sincere gratefulness to all my friends especially Pouya Hajiani, Amin Sarvaramini, Ali Entezari, Shahab Boroun and Amir Monfared for creating a pleasant working atmosphere. Special thanks to Dr. Gnouyaro Palla Assima for being a great confidant and also for his efforts to translate parts of this thesis into French.

I would like to thank the chemical engineering department technicians: Marc Lavoie, Jean-Nicholas Ouellet and especially Jerome Noël for his outstanding helps in the fabrication phase of micro-packed beds.

Last but not least, my great gratitude to my amazing wife, Afrooz, who was always there for me in joy and sorrow. Thanks to her perpetual love and heart-warming words, I managed to hold on during some hard and stressful days I had. After these four years of graduate study, I can't wait for the next forty years, or however long God blesses me to be with her.



## Foreword

This PhD thesis comprises six chapters starting with the introduction, chapter 1, and ending with a conclusion, chapter 6. Chapters 2-4 represent articles published in the scientific journals while chapter 5 will be submitted for publication shortly. The articles representing chapters 2-4 are listed below:

**A. Faridkhou**, F. Larachi, Hydrodynamics of gas-liquid concurrent flows in micropacked beds-wall visualization study , *Industrial Engineering Chemistry Research*, 2012, 51 (50) 16495-16504.

**A. Faridkhou**, M. Hamidipour, F. Larachi, Hydrodynamics of gas-liquid micro-fixed beds – Measurement approaches and technical challenges, *Chemical Engineering Journal*, 223 (2013) 425-435.

**A. Faridkhou**, F. Larachi, Two-phase flow hydrodynamic study in micro-packed beds – Effect of bed geometry and particle size, *Chemical Engineering and Processing*, 78 (2014) 27-36.

Some results of these studies were presented in the following conferences:

M. Hamidipour, **A. Faridkhou**, I. Iliuta, D. Schweich and F. Larachi, Hydrodynamics of gas-liquid micro-packed beds- experiment and modeling, CAMURE Conference, 2011, Naantali, Finland

**A. Faridkhou**, M. Hamidipour, F. Larachi, Visualization of flow patterns in micro-packed bed reactors- 61st Canadian Chemical Engineering Conference, 2011, London, ON, Canada

**A. Faridkhou**, F. Larachi, Hydrodynamic studies of micro-packed beds– CGCC Conference, 2012, Québec, QC, Canada

**A. Faridkhou**, I. Iliuta, M. Hamidipour, D. Schweich, F. Larachi, Two-phase flow in micro-packed beds –GLS Conference, 2012, Marrakech, Morocco

**A. Faridkhou**, F. Larachi, Hydrodynamics of two-phase flow in catalytic micro-packed beds –CGCC Conference, 2013, Montréal, QC, Canada

**A. Faridkhou**, J. N. Tourvieille, R. Philippe, C. de Bellefon., F. Larachi, Hydrodynamics in structured and randomly packed microreactors: a comparative perspective- CAMURE Conference, 2014, Lyon, France

# Introduction

## 1.1 Process intensification

The term process intensification (PI) without any doubt has opened up a new horizon through which various processes can be modified in order to improve their performance. During the last two decades, a number of definitions have been proposed for the term each trying to address the key features as well as the benefits that can be achieved via this approach. A rather comprehensive definition for process intensification is the one by Stankiewicz and Moulijn as: “Any chemical engineering development that leads to a substantially *smaller, cleaner and more energy efficient* technology is process intensification”.<sup>1</sup>

Considering the definition above, process intensification can be achieved by two different means: 1) equipment (hardware) and 2) methods (software).<sup>2</sup> PI through hardware approach means that there are certain types of process equipment having inherently higher performance compared to other ones designed for the same purpose. Leaning toward using these more efficient units, fulfills the aim of process intensification. For instance, using compact plate and frame heat exchangers greatly improves heat transfer in comparison with an ordinary shell and tube design. Therefore, they serve to intensify the heat transfer process. Software approach, on the other hand, relies on innovative ideas suggesting that either certain methods can be combined or totally new alternatives shall be utilized instead of conventional methods to achieve PI. These include using cyclic operations rather than steady state ones to intensify the rate of heat and mass transfer in a process unit, for example, or perform reactive separations to increase the component splitting efficiency.

In the realm of chemical engineering, one of the main objectives in many macro-scale process units is promoting mass transfer. This can be reached at the expense of higher energy dissipations (unfavourable) to cause more vigorous contacting of the fluids in terms of turbulence (favourable) and thus creating more interfacial area (e.g. higher power inputs to gas-liquid stirred tank reactors).<sup>2</sup> This coupling of mass transfer and hydrodynamics might not be completely within the goal of process intensification in this case. The question arising

here is: how can we enhance heat and mass transfer in a process without hindering the achievements of process intensification? One answer to this question might be: “those equipment possessing high surface to volume ratios which are potentially creating large interfacial area can be thought as major candidates for process intensification”. This is the case for miniaturized equipment operating at small scales called microreactors which can be categorized in the hardware approach for process intensification. The remainder of this section deals with microreactors in particular.

## 1.2 Microreactors and their advantages

Miniaturization, as mentioned previously, serves as one of the main approaches for process intensification which has got numerous applications in many sectors of chemical industry. The common term in chemical engineering referring to miniaturized process units is “*microreactor*”. By definition, microreactors are “miniaturized chemical process units with characteristic dimensions of the internal fluid handling parts in the sub-millimetre range”.<sup>3</sup> Working at such dimensions imposes limitations in terms of cost and complicity and thus, there must exist remarkable advantages that make accepting these limitations worthwhile. This part outlines the main advantages offered by microreactors as wells as their applications in different research domains.

***High surface to volume ratio:*** Operation at reduced scales can have remarkable advantages especially when the system is downsized up to microscopic length scales. Upon reduction in the size of a system, its surface area to volume ratio increases (in the order of 1500-27000 m<sup>2</sup>/m<sup>3</sup>). Table 1-1 outlines the surface to volume ratios for some of the conventional process equipment along with those of some micro-process equipment.



**Table 0-1:** Surface to volume ratio for some conventional and micro-scale process units<sup>4,6</sup>

<b>Equipment</b>	<b>Surface to volume ratio (m<sup>2</sup>/m<sup>3</sup>)</b>
Spray column	10-100
Shell and tube heat exchanger	50-100
Bubble column	50-600
Packed column (counter-current)	10-350
Packed column (co-current)	10-1700
Mechanically stirred bubble column	100-2000
Venturi injector	160-2500
Compact heat exchanger	850-1500
Micro-channel heat exchanger	>1500
Micro-bubble column	5100-14800
Falling film microreactor (300µm x 100 µm)	Up to 27000

Owing to the confined space and high surface to volume ratios, the existing phases will be interacting in a much more aggressive environment which drastically enhances heat and mass transfer.<sup>7</sup> This advantage comes into play especially in catalytic gas-phase reactors coated with active material on the inner walls.<sup>3, 8, 9</sup> In this case, it is the high interfacial area that results in highly enhanced mass transfer rates in microreactors as the phases are forced to mix over the catalyst in a constrained volume. Generally, for reactions occurring in mass transfer-limited regime, microreactors could be quite small while maintaining high productivity.<sup>10</sup> Moreover, for kinetic studies of catalytic reactions, where competition exists between the rate of diffusion to the catalyst sites and the rate of reaction, microreactors are

able to virtually eliminate mass transport resistance, making them an extremely useful tool for isolating reaction kinetics.<sup>11</sup>

High surface to volume ratios for microreactors also result in the dominance of surface effects over volumetric effects. Thus, over microscopic length scales, inertia forces may often turn out to be negligible in comparison with viscous or surface tension forces. In fact, surface forces in micro-scale play decisive roles in the system functionality.

***Excellent temperature control:*** For a given difference in physical properties (e.g. temperature, concentration, density and pressure), decreasing the linear dimensions increases the gradients and as a result, the driving forces for heat or mass transfer per unit volume or per unit area will also increase.<sup>8, 12</sup> Efficient heat transfer in microreactors eases temperature control and eliminates the formation of hot-spots due to localized reaction zones. Consequently, chemical reactions that are highly exothermic or containing explosive materials can be carried out in these units.<sup>9</sup>

***Small volume and short residence time:*** Small dimensions of microreactors are equivalent to lower material inventory and thus increased safety. From this perspective, microreactors have the potential to be used for the production of toxic materials<sup>13</sup> since the amount of released hazardous material would not pose any major risk in case of incidents.<sup>8, 9</sup> Another application stemming from small material inventory is the realm of catalyst testing (screening) in R&D divisions. Large amount of catalysts used for testing each type of catalyst in a batch reactor can be replaced by a few milligrams of catalysts tested in a continuous flow microreactors (fast transfer of research results into production.<sup>8</sup> Owing to a small hold-up in microreactors, the residence times will also be shorter which is in favour of product selectivity.<sup>3, 8</sup>

***Numbering-up:*** Another characteristic feature of microreactors is that the common scale-up approach used in macro-scale units can be successfully replaced by a so-called *numbering-up* (or scaling-out) approach which means that any change in capacity can be achieved by multiple repetition of basic units while, on the other hand, it guarantees that the basic feature of individual units will not be altered.<sup>3, 8</sup> This concept, however, has its own challenges as the microreactors must achieve uniform flow distribution to maintain same flow rate and residence time in each individual unit and there should exist an elaborate

reaction monitoring method.<sup>14</sup> Inlet regions in the reactor can be designed such that flow equipartition between the channels is ensured.<sup>9, 15</sup>

***Safety and waste minimization:*** Generally, production costs increase with a decrease in reactor volume. Therefore, it might seem that using microreactors for production purposes, considering the small reaction volume, may be unprofitable. However, one must note that microreactors still bring major cost savings due to other factors that normally counterbalance or at least justify high production costs. For instance, waste production will be minimized in microreactors since small amounts of material are tested. This enables the setup to test as many chemicals as possible during a certain period of time and transfer the research results into production. Smaller sizes also bring more safety to chemical processes which is also a key factor in producing hazardous materials, for instance.<sup>8, 9</sup>

### **1.3 Microreactors and industrial producers**

Despite their size, microreactors can outperform conventional reactors that are hundreds or thousands of times larger. Pressed by safety and environmental considerations, a large number of companies in fine chemicals, specialty chemicals, pharmaceuticals and consumer products are developing applications for microreactors.<sup>16</sup>

Chemical manufacturers are increasingly trying to exploit the advantages resulting from using microreactors. The companies include (but are not limited to): Switzerland-based Clariant, Sigma Aldrich subsidiary SAFC, Germany's BASF and Evonik Industries, Netherlands-based DSM, US-based DuPont, and pharmaceutical companies Schering-Plough, Sanofi Aventis, Roche, GlaxoSmithKline, Novartis and Astra Zeneca. Even consumer products giant Procter & Gamble has worked with them.<sup>17</sup>

Many of Sigma-Aldrich's products are produced under laboratory conditions in batches of 20 L. However, it has been stated that nearly 40 percent of these products can be produced in microreactors with little or no process modification according to the R&D management. For such cases, microreactors would reduce reaction time and cost. For example, the condensation of 2-trimethyl-silylethanol and p-nitrophenyl- chloroformate to produce 2-(trimethyl-silyl)ethyl 4-nitrophenyl carbonate requires 14 hours to complete in a conventional setup but only 18.4 minutes in a microreactor. Because contact between

reagents and products is so brief, the possibility that the desired product will degrade or that by-products will be formed is vastly reduced.<sup>18</sup>

Although most applications being developed for microreactors involve specialty chemicals, fine chemicals and pharmaceuticals, Velocys (a US-based company acquired by UK-based Oxford Catalysts) is focused on bulk chemicals. In contrast to most microreactor companies who offer small-scale microreactors without catalysts processing a liquid phase flow, Velocys microchannel reactors can incorporate heterogeneous catalysts and are able to process large amounts of reagents at a wide range of temperatures and pressures. Their technology encompasses ethylene production via the oxidative dehydrogenation of ethane, direct dimethylether (DME) production from syngas; the *Fischer-Tropsch* process; steam methane reforming; hydrocracking; and the production of methanol, styrene, vinyl acetate monomer, formaldehyde and ethylene oxide.<sup>17</sup>

Although microreactors will not replace the large petrochemical complexes that are the chemical industry's most intensive users of flow chemistry, there are circumstances where the size and portability of microreactors are more beneficial than economies of scale. For example, it is not cost-effective to transport biomass long distances for conversion to fuel as is the case in Velocys' biomass-to-liquids (BTL) project. In this case, Velocys has demonstrated a two-gallon-per-day BTL microreactor using a new, highly active *FT* catalyst developed by Oxford Catalysts. The device operated for more than 3,000 hours and achieved productivities of over 1,500 kg/m<sup>3</sup>/h. Standard fixed bed *FT* reactors typically operate at productivities of around 100 kg/m<sup>3</sup>/h and slurry bed *FT* reactors at around 200 kg/m<sup>3</sup>/h.<sup>17</sup>

In conclusion, it should be noted that using a continuous system of microreactors for commercial production entails investment costs which are probably higher than that of a batch plant. A number of items that might justify this replacement (due to costs saving) could be: 1) major yield improvement 2) reduced labor costs due to automation and 3) ability to develop versatile microreactors which are able to handle solid phase (in case of heterogeneous catalytic reaction) and 4) increased safety<sup>16</sup>

## 1.4 Microreactors designs and applications

The selection among various types of microreactors depends on a number of factors to be specified. These factors are (but not limited to):

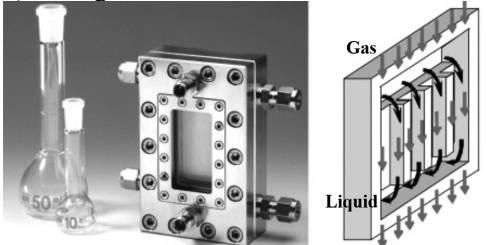
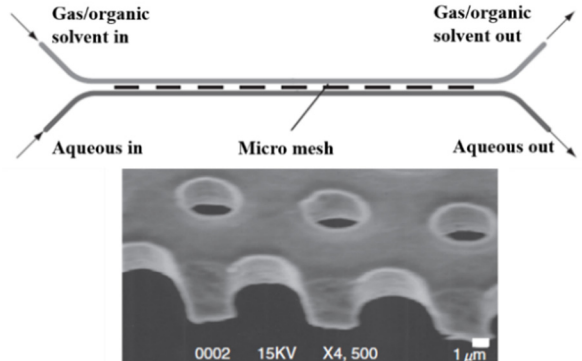
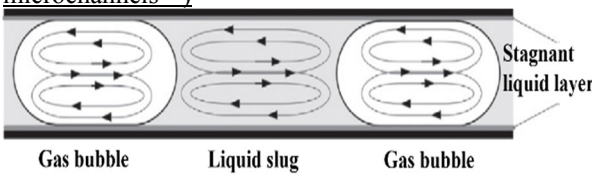
- Phases involved
- Residence time
- Catalytic or non-catalytic process
- Homogenous or heterogeneous catalyst
- Solid incorporation (in case a solid phase is involved)
- Desired contacting scheme between the phases
- Manufacturing costs , etc

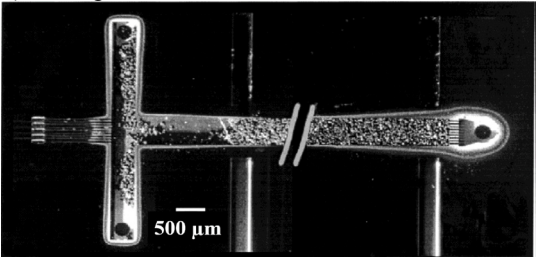
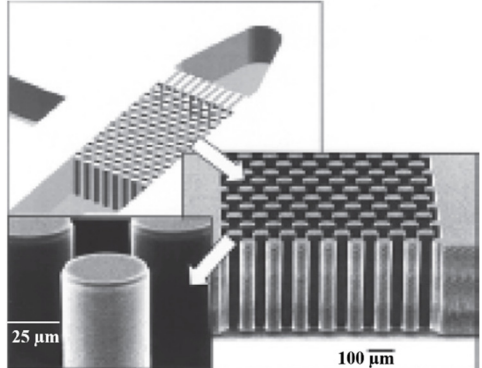
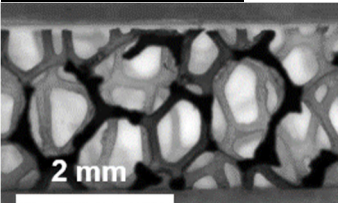
Different configurations have been reported in the literature each designed for a specific application. Table 1-2 summarizes some of the most common designs of microreactors along with their applications mentioned in the open literature. They can be generally categorized into the following three groups:

- Continuous phase microreactors (falling-film and mesh microreactors)
- Dispersed phase microreactors (segmented flow microreactors and micro-packed beds)
- Internally structured microreactors (pre-structured microreactors and foam microreactors)

Most of the microreactors reported in the literature are used for reactions involving multiple phases (i.e., liquid and gaseous reactants and products). Of the most common applications are catalytic hydrogenations. Hydrogenation reactions are ubiquitous throughout fine chemicals and pharmaceutical processing and account for about 20% of all the reactions in these fields. Catalytic hydrogenations are fast and highly exothermic and since hydrogen is only slightly soluble in most organic solvents, mass transfer of the hydrogen to the liquid phase can often be the rate-limiting step. Consequently, reactor performance and product selectivity are often strongly influenced by mass transfer while heat removal is also an important aspect. Both issues may be addressed by using microstructured devices.<sup>11, 19</sup>

**Table 0-2.** Summary of the most common designs of microreactors along with their applications mentioned in the open literature

Category	Basis of operation	Highlights	Applications
<b>Continuous phase microreactors</b>			
<p>1) <u>Falling-film microreactor</u></p> 	<p>1) Gravity flow of liquid film over a solid plate with a side-by-side flow of gas phase</p> <p>2) Heat removal from the reactor by placing a microstructured heat exchanger beneath the setup</p>	<p>1) Excellent temperature control (prevents hotspots)</p> <p>2) Small holdup and short contact time</p> <p>3) Small thickness of liquid film prevents large mass transfer resistance as in similar macro-scale units</p>	<p>1) Hydrogenation of nitrobenzene<sup>20</sup></p> <p>2) Evaporation of hydrogen peroxide for partial oxidation of propene to methyloxirane<sup>21</sup></p>
<p>2) <u>Mesh microreactor</u></p> 	<p>1) Separate gas and liquid flows through separate compartments separated by a porous wall (mesh) for contact between the phases.</p> <p>2) Are more suited for immiscible fluids at low to moderate flow rates.</p>	<p>1) The combination of a high gas–liquid interfacial area with a thin fluid layer results in high volumetric mass transfer coefficients.</p> <p>2) Phase separation is not required.</p> <p>3) Low pressure drop</p> <p>4) Could be used in the batch mode as well</p> <p>5) No risk of flooding</p>	<p>1) Hydrogenation of <math>\alpha</math>-methylstyrene<sup>22</sup></p> <p>2) Absorption of oxygen into aqueous alkaline pyrogallol<sup>23</sup></p>
<b>Dispersed phase microreactors</b>			
<p>1) <u>Segmented flow microreactors (also known as microchannels<sup>24</sup>)</u></p> 	<p>Simultaneous gas and liquid feeding into a channel in the millimeter or submillimeter range which can be straight or meandering. The walls may also be coated with active catalyst.</p>	<p>1) Mostly operated at Taylor flow (or slug flow) regime</p> <p>2) Phase coalescence is prevented and a recirculating flow pattern forms inside the liquid slug</p> <p>3) Liquid film thickness is a function of the capillary number (Ca)</p>	<p>1) hydrogenation of 4-nitrobenzoic acid to 4-aminobenzoic acid<sup>25</sup></p> <p>2) hydrogenation of 2-butyne-1,4-diol to <i>cis</i>-2-butene-1,4-diol and butane-1,4-diol<sup>26</sup></p>

Category	Basis of operation	Highlights	Applications
<p>2) Micropacked beds</p> 	<p>1) Catalyst particles, in the form of powder, are loaded into a micro-tube in the millimeter or submillimeter range while gas and liquid phases are fed into the tube. 2) Solid phase should be immobilized inside the micro-tube either by using a mesh grid at the outlet or by constricting the outlet.</p>	<p>1) Largest possible solid-catalyst surface for reaction and high mass transfer coefficients 2) Easy and less costly in terms of fabrication 3) High pressure drop 4) Available radial configurations for decreasing the pressure drop (up to one order of magnitude)<sup>27</sup></p>	<p>1) Cyclohexene hydrogenation<sup>28, 29</sup> 2) Hydrogen production for PEM fuel cells<sup>30</sup> 3) Fischer-Tropsch synthesis<sup>31, 32</sup></p>
<b>Internally-structured microreactors</b>			
<p>1) Pre-structured microreactors<sup>10</sup></p> 	<p>1) Direct integration of the catalyst support structures into the channels of the microreactor in the form of posts 2) Allows the precise definition of the bed properties such as the supports size, shape, arrangement and the void fraction<sup>19</sup></p>	<p>1) Lower pressure drop compared to micro-packed beds 2) Allows the precise definition of the bed properties, including the support's size, shape and arrangement, and the void fraction. 3) Broad applicability in enhancing the transport and active surface area for sensing, chemical, and biochemical conversion devices 4) High cost of manufacturing</p>	<p>1) Singlet oxygen production<sup>33</sup> 2) Cyclohexene hydrogenation<sup>19</sup> 3) hydrogenation of o-nitroanisole to o-anisidine<sup>11</sup> 4) Ozonolysis of organic reagents<sup>34</sup></p>
<p>2) Foam microreactors</p> 	<p>Simultaneous gas and liquid feeding into a channel in the millimeter or submillimeter packed with solid foams of high voidage.</p>	<p>1) High specific surface area and catalyst immobility 2) Low pressure drop 3) Difficulties in case of catalyst deactivation (foam replacement required)</p>	<p><math>\alpha</math>-methylstyrene catalytic hydrogenation over a layer of wash-coated Pd/Al<sub>2</sub>O<sub>3</sub><sup>35</sup></p>

## 1.5 Micro-packed beds (packed microreactors)

Currently, a large number of chemical industries rely on large scale multiphase catalytic packed bed reactors with co-current gas-liquid flow through solid packings<sup>36, 37</sup>. Merging the advantages of micro-scale operation and that of packed beds, micro-packed beds, also known as micro-fixed beds<sup>38</sup> (refer to Table 1-2), are promising tools with the potential to push the industry envelope even further. Today, a number of industrially well-known processes such as hydrogenation<sup>39</sup>, hydrodesulphurization<sup>40</sup> and Fischer-Tropsch synthesis<sup>31, 32, 41</sup> are being carried out in multiphase micro-packed beds. The synthesis of dangerous materials such as phosgene<sup>13</sup>, synthesis of products at explosive regimes<sup>42</sup>, production of compounds under highly exothermic reactions<sup>33</sup> are other possibilities that could be accomplished in micro-packed beds.

Different designs and applications of micro-packed beds have been presented in the literature each pointing out new applications. Meanwhile, some of the published research papers aim at partially circumventing the problems attributed to micro-packed beds such as high pressure drop.<sup>27, 43</sup> Probably one of the pioneering works on micro-packed beds was presented by Losey et al.<sup>28</sup> who successfully performed cyclohexene hydrogenation in a parallel configuration of micro-packed beds of 625  $\mu\text{m}$  x 300  $\mu\text{m}$  filled with 50  $\mu\text{m}$  catalyst particles of Pd/alumina (Figure 1-1). Their analysis of energy dissipation in micro-packed bed revealed that the energy required for the two phase flow in this miniaturized system scales appropriately with those of laboratory scale multiphase reactors. In addition, the multiphase flow behaviour (represented by the flow regime transition) in micro-packed bed is quite comparable with standard laboratory scale systems.



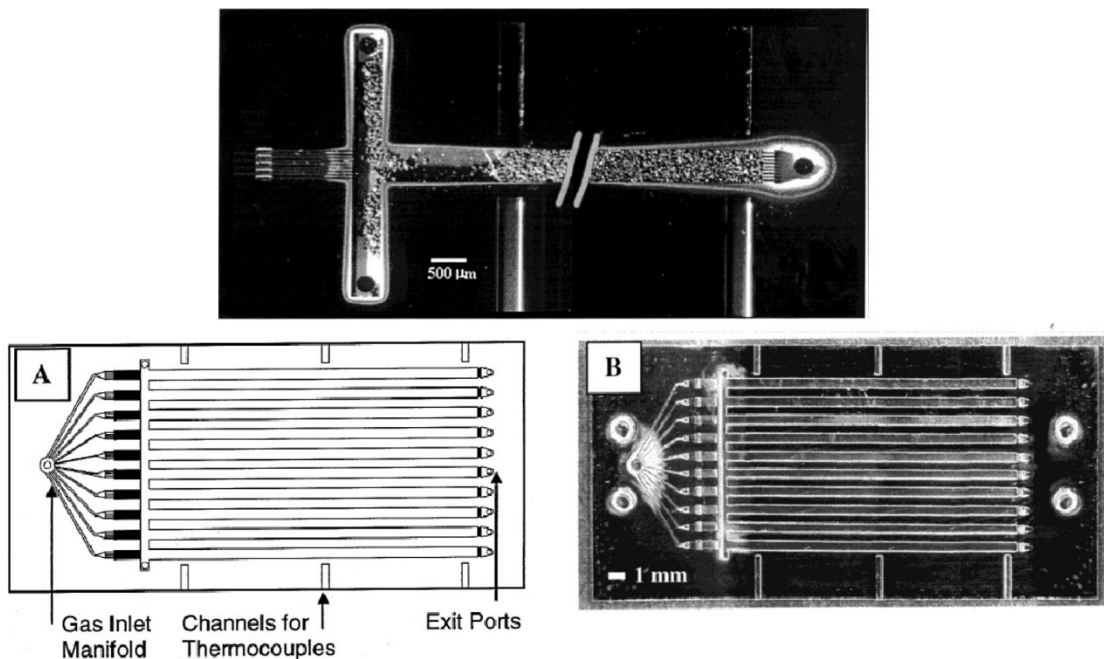


**Figure 0-1.** Photomicrograph of the micro-packed bed loaded with catalyst (Top). Schematic of the multichannel reactor design illustrating fluid manifold to 10 parallel fixed-bed reaction channels (A). Photomicrograph of multichannel reactor chip (B). Adapted from Losey et al (2001) <sup>28</sup>

Alternative configurations have been proposed to improve the performance of micro-packed bed reactors in terms of pressure drop, for instance. In a research contribution by Ajmera et al., a cross-flow microreactor was developed for catalyst testing purposes (Figure 1-2). The cross-flow configuration comprised of 256 shallow channels distributed over the width of the microreactor and filled with solid packing. The results obtained from both experiment and modeling confirm the even flow distribution across the microreactor with a pressure drop of nearly 1600 times less than axial flow micro-packed beds. The carbon monoxide oxidation was also chosen as a model reaction used for catalyst testing and it was concluded that the setup can be used for high throughput heterogeneous catalyst testing if coupled with appropriate sensors.

Miniaturized packed beds have been extensively applied within the past two decades with the purpose of providing on demand hydrogen for small fuel cells. Hydrogen production, in this case, is often achieved by conversion of hydrocarbon fuels to hydrogen-rich gas streams by a catalytic microreactor.<sup>44</sup> Among reactions that are typically investigated, methanol steam reforming is often preferred for two main reasons: 1) high hydrogen-to-

carbon ratio in methanol as compared to other fuels and 2) lower inter-carbon bonds enabling the reforming process at moderate temperatures in the range of 200-300°C.<sup>45</sup>

In another innovative design to reduce the pressure drop in packed bed microreactors, Pattekar and Kothare<sup>27</sup> introduced a novel micro-packed bed for fuel processing via methanol reforming to enable hydrogen delivery in miniaturized fuel cells for portable power generation (Figure 1-3).

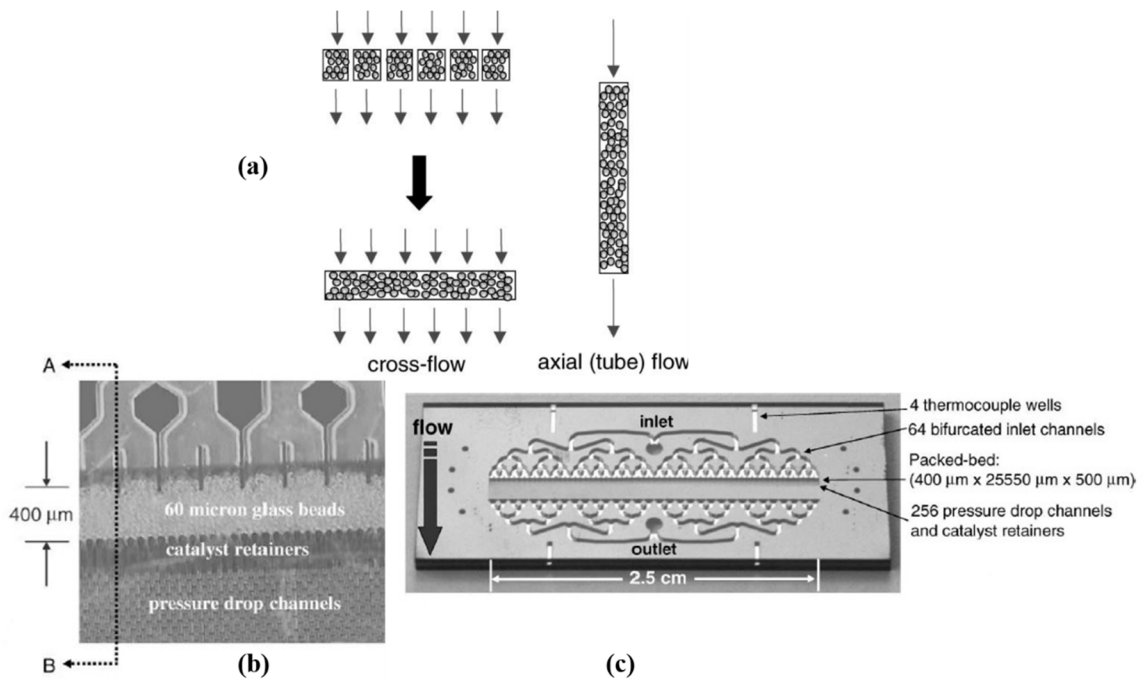


**Figure 0-2.** Comparison of cross flow against typical axial (tube) flow (a). A section of the cross flow reactor packed with 60 micron glass beads (b) and the overall picture of cross-flow microreactor (c). Adapted from Ajmera et al. (2002)<sup>43</sup>

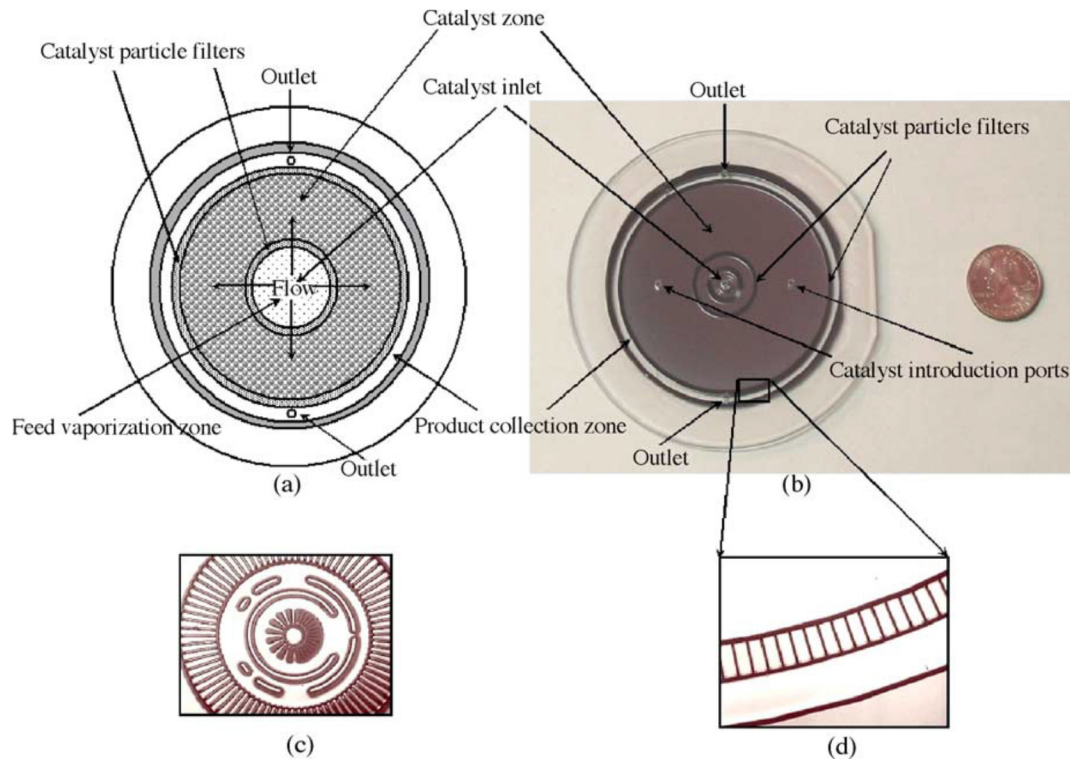


**Figure 0-3.** Radial flow micro-packed bed. Schematic (a), fabricated device (b), vaporization region (c) and catalyst particle filter (d). Adapted from Pattekar and Kothare (2005)<sup>27</sup>

Their setup included a radial flow micro-packed bed which was integrated with a micro-vaporizer used for hydrogen delivery using methanol reforming:



The idea of fabricating a radial micro-packed bed was implanted after Pattekar and Kothare demonstrated that performing the reforming process in a packed rectangular microchannel ( $400 \mu\text{m} \times 1000 \mu\text{m}$  packed with particles of  $50\text{--}70 \mu\text{m}$  in diameter) requires high energy inputs to overcome the high pressure drop ( $70\text{--}100 \text{ psig}$ ) although high conversions were achieved at low temperatures.<sup>30</sup> Utilizing the radial micro-packed bed, the conversion of methanol to hydrogen was greater than 98% and the flowrates were sufficient to supply hydrogen to a 20W fuel cell.

Hydrogenation of CO for methanol synthesis is a major application that can be achieved in micro-scale at high pressures (as methanol formation results in decrease in the number of moles). Bakhtiary-Davijany et al. proposed an integrated micro-packed bed reactor-heat exchanger for methanol synthesis from syngas using Cu/ZnO/Al<sub>2</sub>O<sub>3</sub> particles as catalyst.<sup>46</sup> The arrangement showed an isothermal operation at different operating conditions (due to outstanding heat removal capability) and maintained a promising productivity.

One of the great advantages of microreactors is in catalytic reactions where the reagents or products are toxic or explosive and cause problems in terms of handling. As an example, Inoue et al.<sup>42</sup> performed direct synthesis of hydrogen peroxide by passing the explosive gas mixture of hydrogen and oxygen over a micro-packed bed of palladium catalyst. The experimental setup is identical to one used by Losey et al.<sup>28</sup> for cyclohexene hydrogenation and in this case it promotes the free radical branching reactions at pressure range of 2-3 MPa that would give rise to explosion in a laboratory scale reactor. The key to safe operation of the micro-packed bed is to minimize the existence of voids especially at the inlet by filling the inlet zone of the bed with silica particles.

As for the safe on-site/ on-demand production of hazardous materials, Ajmera et al.<sup>13</sup> carried out phosgene synthesis ( $\text{Cl}_2 + \text{CO} \rightarrow \text{COCl}_2$ ) in a micro-packed bed identical to that used by Losey et al. and Inoue et al. The only extra feature was the protective coating to avoid corrosion due to the existence of chlorine in the system.

Operation at high pressures is much safer in micro-scale by cutting-edge microfabrication methods. If visualizations of the reaction section of micro-packed beds are desired as well, glass capillaries can be treated by thin film metallization for enhanced mechanical strength while maintaining the optical transparency. The micro-packed bed presented by Trachsel et al. with specifications as above was able to perform cyclohexene hydrogenation at high pressures (140 bar) and high temperatures (80°C) over the Pd catalyst particles within the bed.<sup>47</sup> The reaction experiment was performed in a micro-packed bed 36mm in length (340 μm in depth and 400 μm in width) where the catalyst particles were loaded. The gas and liquid streams were fed through a T-section at the start of the bed brought into contact in a static mixer comprised of some etched columns (diameter: 100 μm and spacing: 100 μm) according to Figure 1-4. A significant increase in the rate of reaction (by

one order of magnitude) was observed when hydrogenation takes place in the micro-packed bed at 51 Bar and 71°C instead of ambient conditions.

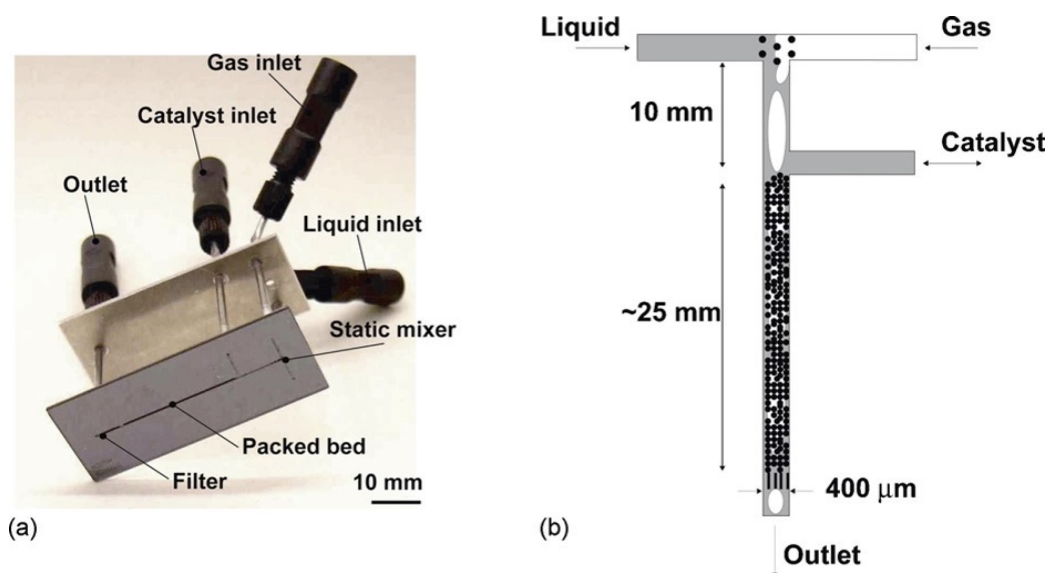


**Figure 0-4.** Transparent micro-packed bed strengthened with metal deposition used for high pressure hydrogenation. Overall view of micro-packed bed (a), schematic of gas-liquid-solid contact (b). Adapted from Trachsel et al. (2008)<sup>47</sup>

Recently, Tidona et al. extended the operating pressure envelope by doing CO<sub>2</sub> hydrogenation (reverse water-gas shift (RWGS) reaction) in a stainless steel capillary tube of 1000 μm in diameter with 1 wt% Pt/CeO<sub>2</sub> catalyst at 450°C and at a pressure range of 200-950 bar<sup>48</sup>. Although the CO conversion achieved in the microreactor was lower than the equilibrium of the reactions, the setup functionality at quite high pressures was confirmed.

Catalytic oxidation of alcohols is a quite well-known process with products typically utilized in pharmaceuticals, fragrances and polymers. Although it was initially found out that gold is the catalyst of interest for this type of reaction<sup>49</sup>, it was later discovered that the Au/Pd catalyst could tremendously enhance catalyst activity and increase selectivity<sup>50</sup>. Instead of performing the reaction in catalytic macro-scale packed beds which suffers from several drawbacks (e.g. flow maldistribution, incomplete wetting in packed-bed and associated external mass transfer limitations and temperature gradients), Cao et al. used the miniaturized packed bed reactor for oxidation of benzyl alcohol as demonstrated in Figure 1-5.<sup>51</sup> An *In situ* Raman spectroscopic study was coupled to the experiments so that the spectra indicated

the product (benzaldehyde) concentration profile along the bed length. It was also shown that the external mass transfer resistance could be ignored at certain gas-to-liquid flow ratios. However, internal mass transfer was present as reflected by the effect of changes in particle size on conversion.

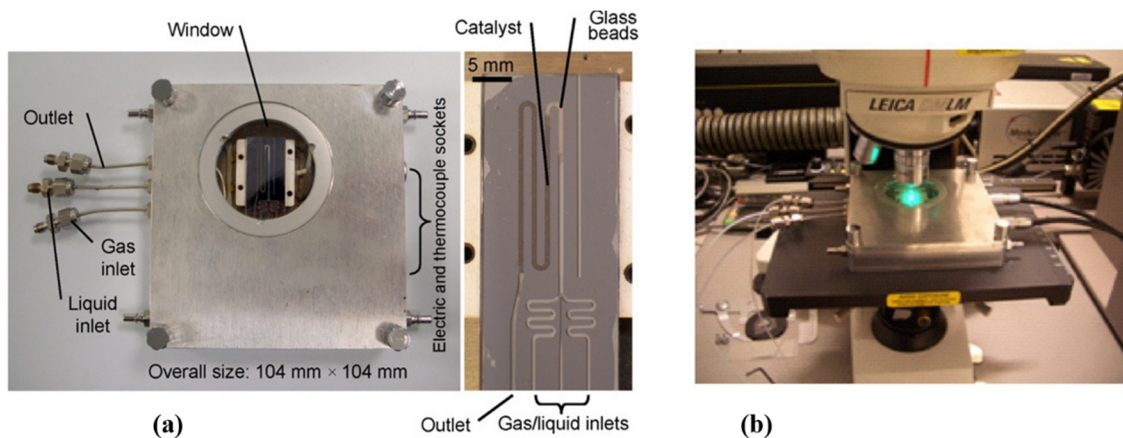


**Figure 0-5.** Micro-packed bed arrangement (a) combination with Raman spectroscopy (b). Adapted from Cao et al. (2011)<sup>51</sup>

The examples mentioned in this section demonstrate the wide application of micro-packed beds in chemical processing and how they can be successfully employed due to their satisfactory performance. However, it can be argued that in most of the research contributions on micro-packed beds, the nature of the contacting patterns between the phases has not been thoroughly investigated. This lies within the realm of hydrodynamic studies which enables researchers to identify certain contacting patterns between the phases that boost the micro-packed bed performance in terms of conversion and selectivity, for example. However, it is astonishing that hydrodynamic study of micro-packed beds has received quite a poor coverage in the open literature. Therefore, in the remainder of this chapter, the primary focus will be on hydrodynamics of micro-packed beds where differences between micro- and macro-scale hydrodynamics and methodologies that could be (or has been) adopted in studies of such kind of microreactors are highlighted. Some key contributions in the hydrodynamic study of micro-packed beds will be discussed in detail and the importance of visualization in

the hydrodynamic study of micro-packed beds will be pointed out. Mass transfer study of micro-packed beds is another subject that will be mentioned.

## **1.6 Hydrodynamic study of micro-packed beds**

Hydrodynamic studies if coupled with reaction engineering or mass transfer studies will culminate in positive outcomes. They can determine which type(s) of phase contacting patterns are more in favour of certain reactions in terms of performance or enhance inter-phase mass transfer. Therefore, one can say that results from hydrodynamic investigations in microreactors could be used as the feed to other fields of investigation thus enabling researches to narrow down their options for designing reaction or mass transfer experiments.

### **1.6.1 Micro- vs. macro-scale hydrodynamics**

Changing the scale of operation from macro to micro will greatly affect hydrodynamics as many forces that have crucial roles in macro-scale units lose their dominance upon downsizing the equipment. One of the most efficient ways to demonstrate this difference between the scales is by comparing the ratio of different forces in the form of dimensionless numbers.<sup>9</sup> Imagine two types of equipment for gas-liquid contact as shown in Figure 1-6. One is a macro-scale stirred tank with its blades sparging the gas bubbles in the liquid phase (tank diameter: 1 m, bubble diameters: 500  $\mu\text{m}$ ) and the other one is a microreactor commonly used for bringing gas and liquid phases into contact (microreactor diameter: 100  $\mu\text{m}$ ). By just focusing on flow phenomena in the two units, one can assume water and air as being the working fluids with their properties mentioned in Table 1-3. The velocity scale is also considered to be 1 m/s for the stirred vessel and 0.01 m/s for microreactor. For the macro-scale stirred vessel, a diameter of 1 m is assumed as characteristic length while in the case of microreactor the channel diameter (100  $\mu\text{m}$ ) represents the characteristic length. When gas/liquid flows are considered, bubble diameter is also regarded as a second length scale. Characteristic bubble diameters in heavily agitated tanks are about 500  $\mu\text{m}$ <sup>9</sup> whereas in a micro reactor the dimension of the bubbles is the same as the channel diameter.

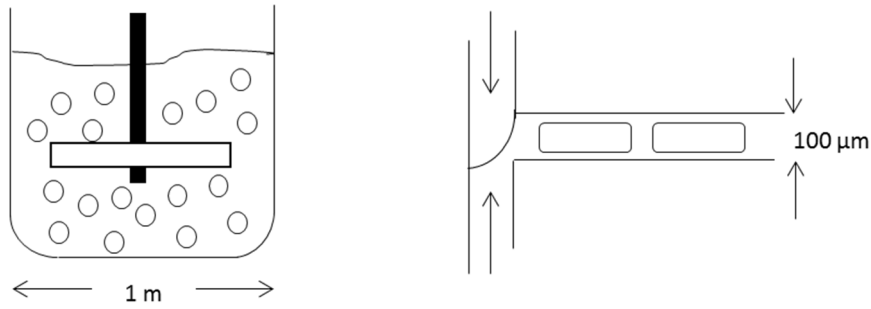


**Figure 0-6.** Schematic representation of macro- and micro-scale. A stirred tank (left) and a microreactor (right) both used for gas-liquid contact. Length scales are indications of the characteristic lengths.

**Table 0-3.** Physical properties of air and water at 20°C and 1 atm.

Properties	Gas (air)	Liquid (water)
$\rho$ (kg/m <sup>3</sup> )	1.188	998.21
$\mu$ (Pa.s)	$18.24 \times 10^{-6}$	$1 \times 10^{-3}$
$\sigma$ (N/m)	-	$72.7 \times 10^{-3}$

Based on assumptions and data mentioned above, it is possible to compare the relative importance of the different forces influencing flow phenomena in terms of dimensionless numbers as shown in Table 1-4. Characteristic lengths used in evaluating the dimensionless numbers are the diameters of the units unless stated otherwise. As can be observed from the Table 1-4 one might expect some variations with respect to hydrodynamic behaviours in macro and micro scale flow units due to differences observed in the magnitude of different forces. Moreover, it should be noted that the micro-scale representative in the above comparative example was a micro-channel in which a bubble occupies almost the entire cross section of the channel. However, in case of a packed microreactor, which is the main focus of our work, the characteristic length could be evaluated based on the packing diameter which is even less than the micro-channel diameter. Therefore, it can be concluded that for a packed microreactor, the significance of inertial and gravitational forces will be much more reduced



whereas the surface tension forces are more strengthened due to very small pore sizes within the packed microreactor. This will also lead to changes in terminologies when comparing macro-scale packed beds with their micro-scale counterparts. For example, in the case of two-phase flow in macro-scale packed beds, the term *trickle bed* can also be used in the same context due to the trickling of the liquid phase within the bed. However, applying the term in case of a micro-packed bed does not seem logical as the liquid flow within the micro-packed bed is not driven by gravitation.

**Table 0-4.** Comparison of dimensionless numbers appearing in hydrodynamic studies in both macro- and micro-scale.

Name	Formula	Physical interpretation	Typical macro value	Typical micro value	Comments
<b>Bond number</b>	$Bo = \frac{(\rho_l - \rho_g)L^2g}{\sigma}$	$\frac{\text{Gravitational force}}{\text{Surface tension force}}$	$3 \times 10^{-2}$	$1 \times 10^{-3}$	Relevant for bubble (droplet) flows. Length scale: bubble diameter
<b>Capillary number</b>	$Ca = \frac{\mu u}{\sigma}$	$\frac{\text{Viscous force}}{\text{Surface tension force}}$	$1 \times 10^{-2}$	$1 \times 10^{-4}$	Relevant for bubble (droplet) flows.
<b>Froude number</b>	$Fr = \frac{\rho_g u^2}{(\rho_l - \rho_g)gL}$	$\frac{\text{Inertial force}}{\text{Gravitational force}}$	$2 \times 10^{-1}$	$1 \times 10^{-4}$	Relevant for bubble (droplet) flows. Length scale: bubble diameter
<b>Reynolds number</b>	$Re = \frac{\rho L u}{\mu}$	$\frac{\text{Inertial force}}{\text{Viscous force}}$	$1 \times 10^6$	1	-
<b>Weber number</b>	$We = \frac{\rho_g L u^2}{\sigma}$	$\frac{\text{Inertial force}}{\text{Surface tension force}}$	$8 \times 10^{-3}$	$2 \times 10^{-7}$	Relevant for bubble (droplet) flows. Length scale: bubble diameter

The above comparison between the macro- and micro-scale suggests that the relative impact of different forces (e.g. gravitational, capillary) are different in the two scales and therefore, caution must be exercised in extending the macro-scale results and trends to micro-scale. Macro-scale studies can be inspiring in illuminating the experimental procedures required for studying the same units in micro-scale (although the experiments might need

some customization due to the drastic change in scale), however, the comparison above clearly demonstrates that the conclusions drawn from a macro-scale units might not be necessarily valid for the miniaturized unit (micro-scale). In section 1.6.3, some of the micro-scale studies inspired from similar research contributions in macro-scale are presented and the difference between the two scales are highlighted.

## 1.6.2 Research methodologies for hydrodynamic studies

Hydrodynamic studies generally revolve around subjects such as flow regimes, pressure drop, phase holdup, residence time distribution (RTD) and so forth. Therefore, in order to be able to put the pieces of hydrodynamic puzzle together, it is necessary to have preliminary and general definitions of the most common terms encountered in hydrodynamic studies. The terms including the following:

***Flow regimes:*** In multiphase flow reactors, regardless of the scale, the contacting pattern between the different phases flowing through the reactor is termed as flow regime which is primarily a function of the ratio of the flowing phases. This dependency, is often depicted as flow regime maps with each envelope (region) representing the loci of phase flow rates giving rise to a specific flow regime.

***Pressure drop:*** Pressure drop is a measure of the energy required to move the fluids through the reactor. Based on the type of fluid phases in contact with each other as well as the medium through which the fluids flow, several correlations and models have been proposed. The two cases of wider applications are gas-liquid flow in channels (or micro-channels) and gas-liquid flow in porous media (or micro-porous media). Correlations for these two categories can be classified as either homogeneous flow models (HFMs) or separated flow models (SFMs). HFMs treat a two-phase flow as a single-phase flow with properties evaluated from mixing rules (e.g. two-phase density and viscosity). When the velocities of both phases are similar (i.e., in the absence of any slip between the phases), the homogeneous flow model is found to be quite accurate. SFMs, on the other hand, are based on a two-phase frictional multiplier which is defined as the ratio of the pressure gradient of the liquid phase to that of the gas phase.

**Phase Holdup:** Phase Holdup is defined over a volume and can be regarded as the fraction of a volume occupied by a certain phase. For example, liquid holdup in a packed bed reactor is the ratio of the volume of liquid in the bed at any time to the volume of the empty reactor. As well as pressure drop, numerous correlations exist for phase holdup prediction in different multiphase flow reactors. The primary interest of this report, though, is on the liquid holdup in packed reactors.

**Residence time distribution (RTD) and axial dispersion:** It is obvious that in the case of ideal plug flow within a reactor, whether macro-scale or micro-scale, all the fluid elements reside in the reactor for the same period of time. Thus, there will only be one residence time for the ideal situation. However, in a non-ideal reactor, fluid elements have different residence times upon entering and exiting the reactor which changes the term into “residence time distribution (RTD)”. It is possible to calculate one “mean residence time” based on the RTD. In order to perform chemical reactions in microreactors with high selectivity, it is required to have a narrow residence time distribution. Generally, RTDs are experimentally determined using tracer injection methods and RTD plots are normally drawn in different units, but E-curves (exit age distribution versus time) are the most common format. When an ideal pulse of tracer is injected to a fluid entering a tubular reactor, the pulse spreads as it flows along the length. The spread of the signal can be assumed to be due to a diffusion process superimposed on the plug flow called dispersion. This can be regarded as a deviation from ideal plug flow reactor. In order to evaluate the dispersion occurring in the axial direction (termed axial dispersion coefficient:  $D$ ), it is required to calculate mean residence time and variance (spread) from the RTD curve.

**Flow field velocity:** One of the options for flow field velocity determination is to infer the motion of the bulk from the observed velocity of fluorescent particles that are injected into the fluid. Particle distributions in the flow of interest are recorded at two instants of time ( $t$  and  $t+\Delta t$  where  $\Delta t$  is in the order of nanoseconds) and from the change of the particle distribution over time, the flow field velocity is determined.<sup>52</sup> This method is called particle image velocimetry (PIV) and the similar process employed for microfluidic devices is called micro-particle image velocimetry ( $\mu$ -PIV). Regardless of the scale (whether Macro or

Micro), PIV can be used to obtain a two component velocity field over a two-dimensional plane.

To define research methodologies for micro-packed beds, it should be once more noted that micro-packed beds can be thought as a scaled-down packed bed reactor. In another word, they have similarities with both macro-scale packed beds (due to the operation and structure point of view) and microchannels (from the scale point of view). Therefore, in order to define methodologies for studying the micro-packed beds, one can benefit from both types of similarities and design two separate research paths. In one path, the literature on hydrodynamic study of microchannels are reviewed and the possibilities to adapt them with micro-packed beds are investigated. In the second path, the research contributions on the hydrodynamics of macro-scale packed beds are highlighted and the potential to carry out the same studies (with major or minor modification due the scale difference) for micro-packed beds is assessed. These two separate paths inspired from microchannels and macro-scale packed beds are summarized in Tables 1-5 and 1-6.

**Table 0-5.** Path 1, how to build research foundations on micro-packed beds by their comparison with microchannels (similarity of scale)

<b>Path 1: Microchannels vs Micro-packed beds</b>			
<b>Subjects of study on microchannels</b>	<b>Key point(s)</b>	<b>Selected references</b>	<b>Similar study on micro-packed beds?</b>
<b><i>Flow regimes and transitions</i></b>			
Effect of channel size	Decreasing channel diameter: <ul style="list-style-type: none"> <li>▪ Suppressing some flow regimes</li> <li>▪ Changing in boundaries of flow regime envelopes</li> </ul>	Yue et al. <sup>53</sup> Coleman and Garimella <sup>54</sup> Zhao and Bi <sup>55</sup>	No
Role of liquid phase surface tension	Decreasing the liquid surface tension: <ul style="list-style-type: none"> <li>▪ Shrinkage in the surface tension dominated regime envelope</li> </ul>	Waelchli and von-Rohr <sup>56</sup> Zhang et al. <sup>57</sup>	No
Effect of microchannel wall wettability or its roughness	Increasing the contact angle: <ul style="list-style-type: none"> <li>▪ Prevents liquid from spreading on the tube wall</li> <li>▪ Marked deviations in flow regime transition lines are observed</li> </ul> Changing wall roughness by treating the inner surface: <ul style="list-style-type: none"> <li>▪ Alters wettability by hindering spreading and stabilization of the liquid films attached to the wall</li> </ul>	Barajas and Panton <sup>58</sup> Cubaud et al. <sup>59</sup> Serizawa et al. <sup>60</sup>	No
Role of microchannel cross-sectional geometry	Changing the cross-sectional geometry from circular to square: <ul style="list-style-type: none"> <li>▪ Leads to changes in flow regime transition line due to the impact of liquid phase pulled to the corners of a square channel</li> </ul>	Coleman and Garimella <sup>54</sup> Triplett et al. <sup>61</sup>	No
Effect of microchannel inlet conditions	Modifying the inlet conditions from T-type to Smooth-type: <ul style="list-style-type: none"> <li>▪ Shifting from surface tension-dominated to inertia-dominated flow regime occurs at higher gas flow rates</li> </ul>	Qian and Lawal <sup>62</sup> Haverkamp et al. <sup>63</sup>	No
<b><i>Pressure drop</i></b>			
$\Delta P$ Prediction based on correlations for different flow regimes	<ul style="list-style-type: none"> <li>▪ For flow patterns such as slug-annular flow, annular flow and churn flow, frictional pressure drop can be predicted by the separated flow model</li> <li>▪ Homogenous flow model can only be applied to bubbly flow regime in which the liquid phase is less disturbed by the presence of small bubbles</li> <li>▪ None of the above models provide predictions for Taylor flow regime</li> </ul>	Yue et al. <sup>53, 64</sup>	No
$\Delta P$ Prediction based on correlation for Taylor flow regime	A model proposed for pressure drop prediction including the term (Re/Ca) meaning that friction factor in Taylor flow regime is independent of velocity but varies with liquid physical properties.	Kreutzer et al. <sup>65</sup>	No

<b>Path 1: Microchannels vs Micro-packed beds</b>			
<b>Subjects of study on microchannels</b>	<b>Key point(s)</b>	<b>Selected references</b>	<b>Similar study on micro-packed beds?</b>
Homogenous flow model for $\Delta P$ Prediction	<ul style="list-style-type: none"> <li>▪ Dukler's method used for mixture viscosity calculation.</li> <li>▪ Showed satisfactory prediction of pressure drop</li> </ul>	Kawahara et al. <sup>66</sup>	No
<b><i>Phase Holdup</i></b>			
Holdup determination by using homogenous quality (Linear or Armand type correlations)	<ul style="list-style-type: none"> <li>▪ Gas phase holdup (<math>\epsilon_G</math>) can be determined by volumetric gas quality (<math>\beta=Q_G/(Q_G+Q_L)</math>) with a linear correlation</li> <li>▪ Decrease in channel hydraulic diameter increases deviation from the linear trend</li> </ul>	Choi et al. <sup>67</sup> Xiong and Chung <sup>68</sup>	No
Holdup determination by using homogenous quality (Nonlinear correlations)	Linear Armand-type correlations (such as $\epsilon = 0.88 \beta$ ) are not sufficiently accurate for two-phase flow in microchannels.	Kawahara et al. <sup>66</sup> Chung and Kawaji <sup>69</sup>	No
<b><i>RTD and axial dispersion</i></b>			
RTD dependence on microchannel aspect ratio	For a fixed cross sectional area and throughput, RTDs become narrower as the aspect ratio decreases	Aubin et al. <sup>70</sup>	No
RTD in meandering microchannels	For larger capillary numbers, the effect of axial dispersion increases due to an increase in the liquid film thickness	Trachsel et al. <sup>71</sup>	No
<b><i>Flow field velocity determination</i></b>			
Micro-particle image velocimetry ( $\mu$ -PIV)	<ul style="list-style-type: none"> <li>▪ For liquid-liquid flow in microchannel, the refractive indices (<math>n_1</math> and <math>n_2</math>) should be matched to get field velocity vectors representing the same depth in both phases</li> <li>▪ For gas-liquid flow in straight symmetrical microchannels, the small non-symmetries observed in velocity vectors could be due to micron sized wall roughness or compressibility of the gas phase</li> </ul>	Kim et al. <sup>72</sup> Miessner et al. <sup>73</sup> Günther et al. <sup>74</sup>	No

**Table 0-6.** Path 2, how to build research foundations on micro-packed beds by their comparison with macro-packed beds (similarity of operation)

<b>Path 2: Packed beds vs Micro-packed beds</b>			
<b>Subjects of study on packed beds</b>	<b>Key point(s)</b>	<b>Selected references</b>	<b>Similar study on micro-packed beds?</b>
<b><i>Flow regimes and transitions</i></b>			
Trickle-to-pulse flow transition & flow regime maps	<ul style="list-style-type: none"> <li>▪ Higher pressures (at a given superficial gas velocity) shift the trickle-to-pulse flow transition toward higher liquid throughputs.</li> <li>▪ A packed bed using extrudates instead of spheres displays a trickle-to-pulse transition boundary at higher gas flow rates.</li> <li>▪ Explicit correlations have been developed based on databases of flow regime transitions</li> </ul>	Wammes et al. <sup>75</sup> Trivizadakis et al. <sup>76</sup> Larachi et al. <sup>77</sup> Charpentier and Favier <sup>78</sup>	Yes but very briefly <sup>28</sup>
<b><i>Pressure drop</i></b>			
Pressure drop correlations	<ul style="list-style-type: none"> <li>▪ The developed correlation is valid for trickle and pulse flow regimes operated at atmospheric conditions</li> <li>▪ Require knowledge on single-phase <math>\Delta P</math> (function of bed properties)</li> </ul>	Kan and Greenfield <sup>79</sup>	No
	<ul style="list-style-type: none"> <li>▪ The developed correlations are valid for a wider range of operating conditions compared to Kan and Greenfield <sup>79</sup></li> </ul>	Saez and Carbonell <sup>80</sup> Sai and Varma <sup>81</sup>	
	<ul style="list-style-type: none"> <li>▪ Correlations using modified Lockhart-Martinelli number instead of single-phase pressure drop.</li> <li>▪ Covering operating pressure in the range of 0.1-10 MPa</li> </ul>	Ellman et al. <sup>82</sup> Larachi et al. <sup>83</sup>	
	<ul style="list-style-type: none"> <li>▪ Correlations extended from Ergun equation for the two-phase flow through packed beds</li> </ul>	Wammes et al. <sup>75</sup> Benkrid et al. <sup>84</sup>	
<b><i>Phase Holdup</i></b>			
Liquid holdup correlations	<ul style="list-style-type: none"> <li>▪ Correlations demonstrate the dependency of dynamic liquid holdup to the particle diameter and interfacial area in low and high interaction regimes.</li> <li>▪ Correlations are valid for a bed operated at atmospheric conditions.</li> </ul>	Burghardt et al. <sup>85</sup> Specchia and Baldi <sup>86</sup>	No
	<ul style="list-style-type: none"> <li>▪ Correlation using Lockhart-Martinelli number (same as <math>\Delta P</math> correlations)</li> <li>▪ Derived from experimental data of air and various liquids (cyclohexene, kerosene, and polyethyleneglycol) for <math>D/d_p=20.83</math></li> </ul>	Morsi et al. <sup>87</sup>	No

<b>Path 2: Packed beds vs Micro-packed beds</b>			
<b>Subjects of study on packed beds</b>	<b>Key point(s)</b>	<b>Selected references</b>	<b>Similar study on micro-packed beds?</b>
Liquid holdup correlations	<ul style="list-style-type: none"> <li>Extension of Morsi et al.<sup>87</sup> approach to include the effect of various shapes of the particles for the low &amp; high interaction regimes</li> </ul>	Rao et al. <sup>88</sup>	No
	<ul style="list-style-type: none"> <li>Correlation based on Reynolds and Galileo number</li> </ul>	Wammes and Westerterp <sup>89</sup>	No
<b><i>Hysteresis and wetting efficiency</i></b>			
Solid phase wetting efficiency and hysteresis in hydrodynamic parameters	<ul style="list-style-type: none"> <li>Wetting efficiency in packed bed is dependent on particle diameter (use of tracer method)</li> <li>For each packing element, the area wetting fraction correlated with the number of contact points of one packing element with others in the bed (use of MRI method followed by image processing)</li> <li>No hysteresis in liquid holdup, <math>\Delta P</math> and the flow-regime transitions at elevated pressures.</li> <li>Extent of hysteresis in pressure drop and liquid holdup reduces with increase in particle diameter</li> <li>Huge difference in pressure drops and mass transfer coefficients depending on different bed pre-wetting methods</li> </ul>	Mills and Dudukovic <sup>90</sup> Sederman and Gladden <sup>91</sup> Wammes et al. <sup>75</sup> Gunjal et al. <sup>92</sup> Loudon et al. <sup>93</sup> van Howelingen et al. <sup>94</sup>	Quite briefly <sup>95</sup>
<b><i>Mass transfer coefficients</i></b>			
Gas-liquid mass transfer coefficient	<ul style="list-style-type: none"> <li>Correlations for G-L mass transfer including pressure drop and liquid holdup terms</li> <li>G-L mass transfer coefficient correlations based on physical properties as well as bed and particle diameters</li> </ul>	Iliuta and Thyriou <sup>96</sup> Wild et al. <sup>97</sup>	No
Liquid-solid mass transfer coefficient	<ul style="list-style-type: none"> <li>L-S mass transfer coefficient and wetting efficiency were not presented separately due to their dependency</li> <li>L-S mass transfer coefficient and wetting efficiency were separately evaluated from two-phase and full-liquid operations</li> <li>Threefold increase in L-S mass transfer coefficient by shifting from low interaction to high interaction flow regime</li> </ul>	Latifi et al. <sup>98</sup> Lakota and Levec <sup>99</sup> Rao and Drinkenburg <sup>100</sup>	Only single-phase liquid flow <sup>29</sup> (No study for two-phase flow)



### 1.6.3 Literature on the hydrodynamic study of micro-packed beds

As mentioned earlier, and as can be inferred from Tables 1.4 and 1.5, micro-packed beds unlike micro-channels have received much less attention. Therefore, a systematic review of the literature (like what has been done for micro-channels<sup>101</sup>) is not possible for micro-packed beds and thus in what follows, four contributions that have been published on the hydrodynamic of micro-packed beds are discussed. To the best of the author's knowledge, these four works are believed to be the only studies conducted up to now in this field (Other than those prepared within the scope of this thesis).

#### a) *Scaling down trickle bed reactors*

van Herk et al.<sup>102</sup> fabricated two sets of packed microreactors. One in which the Hydrodesulphurization (HDS) process takes place and one cold-setup as a replicate to investigate the hydrodynamics of a so-called scaled-down trickle bed reactor. For both systems, the microreactor diameter is 2mm packed with particles of 100 $\mu$ m in diameter. The cold-setup uses ethanol and nitrogen as liquid and gas feeds respectively. For the subtraction of inlet effects, experiments were done for two cases: without column and with column. This way, the authors claimed that only the column effects have been taken into account for residence time and tracer spread evaluation as:

$$\sigma_L^2 = \sigma_{L,tot}^2 - \sigma_{L,blank}^2 \quad (1-1)$$

$$\tau_L = \tau_{L,tot} - \tau_{L,blank} \quad (1-2)$$

RTD experiments are done with tracer injection method for both single-phase liquid flow mode and gas-liquid two-phase flow mode and the F-curves have been plotted (representing a step change in tracer concentration). Tracers in these experiments are dyes which are detected by spectroscopy. Results are all depicted in terms of dimensionless residence time, dimensionless axial dispersion (column Péclet number) and particle Péclet number according to the following equations:

$$\tau_{\theta} = \frac{\tau_L}{L/(u_G + u_L)} \quad (1-3)$$

$$Pe_L = \frac{2 \cdot \tau^2 L}{\sigma_L^2} = \frac{L \cdot u_L}{D_{ax}} \quad (1-4)$$

$$Pe_p = \frac{d_p \cdot u_L}{D_{ax}} = Pe_L \frac{d_p}{L} \quad (1-5)$$

The main conclusions drawn from their work can be summarized below:

- Minimal deviations from plug flow were observed
- Effect of gas flow rate on liquid residence time was more pronounced in micro-packed beds as compared to macro-scale trickle bed reactors.
- With increasing the gas fraction in flow, the bypass of gas increases due to a segregated gas-flow pattern and this will in turn, increase the liquid residence time.

It should be noted that the notion of trickle bed in micro-packed beds may not be appropriate as the gravitational forces causing the liquid to trickle down in macro-scale packed beds have minimal effects in micro-scale while capillary forces are regarded as the governing one.

#### ***b) Dispersion and Holdup in Multiphase Packed Bed Microreactors***

Márquez et al.<sup>103</sup> studied dispersion and holdup in randomly packed microreactors with respect to variations in flow conditions and fluid properties. The work is based on the hypothesis that due to small scale of the microreactor, capillary forces are dominant in a way that liquid holdup is quite high and therefore, dispersion in multiphase flow resembles that of the single-phase liquid flow with minor deviations resulting from gas-liquid interactions in the former. The experiments are carried out in intermediate flow rates between the low velocity diffusion-only limit and the high velocity limit where full mixing conditions prevail.

The experimental setup for the work (Figure 1-7) is similar to the previous work regarding the column diameter and particle size. Yet, instead of using

spectroscopy, the tracer detection system is a differential refractive cell index. Also, to cancel out the effects of tracer dispersion in sections outside the packed bed, two micro-packed beds of different lengths (97 cm and 7 cm) were tested and results from these two setups are subtracted from each other. This was tantamount to performing experiments with a 90cm bed in the absence of inlet effects (as the convection-dispersion equation is linear in concentration and the convective fluxes dominate disperse fluxes at the boundary of subtraction i.e., 7 cm into the packed bed). Various organic chemicals were used as tracer and dilute solutions of each of them in Tetradecane were prepared as samples.

Two-phase flow leaving the bed shall be subjected to phase separation before the liquid flows into the refractive index flow cell for RTD measurements (gas bubble in liquid negatively affects the refractive cell). To do so, the two-phase flow is siphoned off through a metal membrane (pore size = 10  $\mu\text{m}$ ) for separation. Achieving a complete gas-liquid separation requires that the pressure downstream of the membrane is less than the capillary pressure of gas moving through the pores.

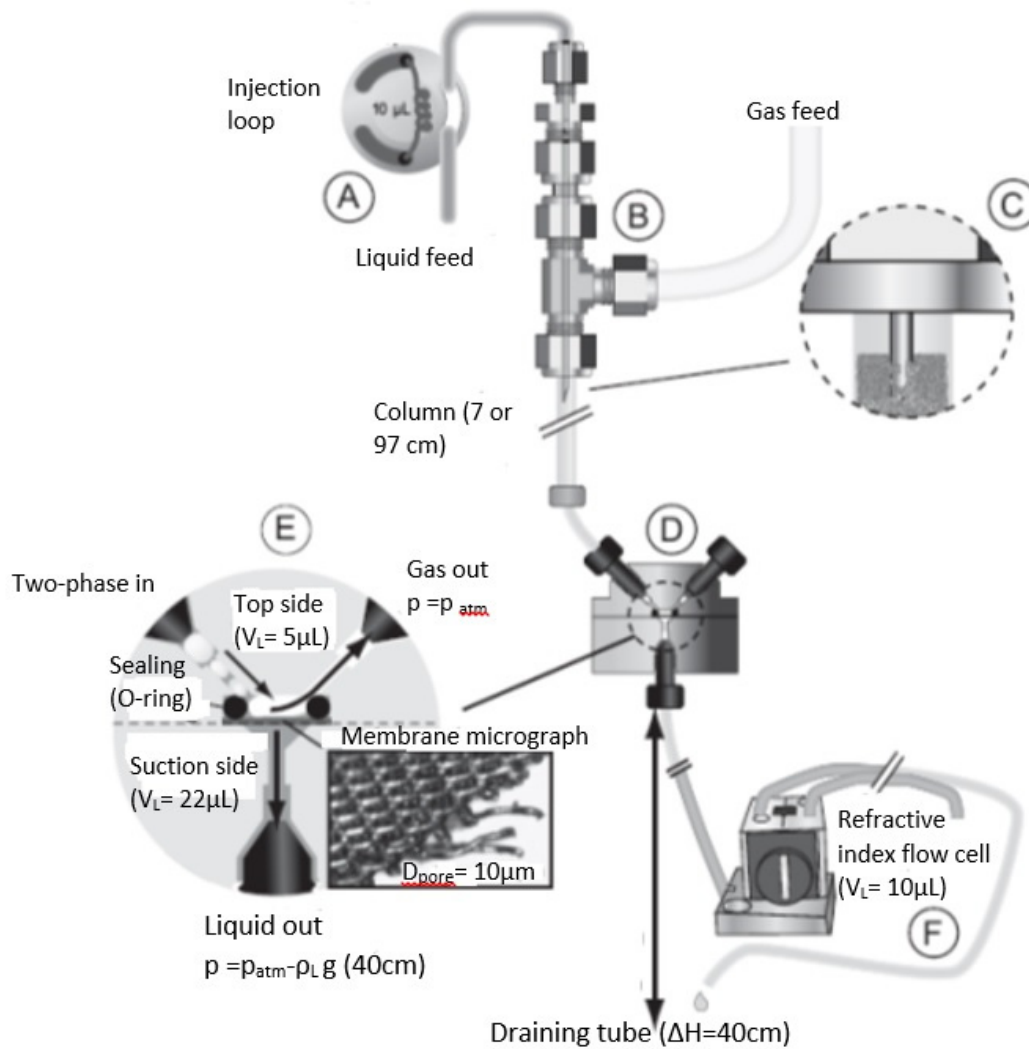


**Figure 0-7.** Experimental setup for contribution b) by Márquez et al.<sup>103</sup>

The conclusions from this work are as follows:

- High holdup values (it should be noted that in this work, the two terms *holdup* and  *saturations* have been used interchangeably) and almost full wetting with 100 $\mu\text{m}$  particles
- For low Re numbers, gas-liquid interaction is limited and neither holdup nor dispersion are strongly affected by the gas flow rate
- Molecular diffusivity and volatility of the tracer had nearly no effect on dispersion whereas the latter only affects the residence time.

- Dispersion in multiphase micro-packed beds is very similar to single-phase liquid systems with only a factor of two or three differences between the two cases.

**c) *Transient Behavior and Stability in Miniaturized Multiphase Packed Bed Reactors***

Márquez et al.<sup>95</sup> studied the hydrodynamic behavior of multiphase randomly packed microreactors with different startup procedures. Macro-scale packed bed reactors, pre-wetting the bed has a large impact on its hydrodynamic behavior as compared to the case operations starting with a dry bed. The item of key interest for this work was to evaluate the time required to achieve steady state as this is an important factor for high-throughput catalyst testing in order to shift from one catalyst option to another.

The experimental setup to this work is identical to the previous work. Pressure drop and liquid holdup are determined for two modes: dry startup and wet startup. For dry startup, the bed is initially flushed with nitrogen. Then the gas flow is kept constant while liquid flow rate is first increased up to a certain flow rate and subsequently decreased to its initial value. For dry startup it was revealed that liquid saturation is a function of flow rate alone, regardless of the flow history. For wet startup, the bed is first subjected to a constant gas and liquid flow and after 24 hours, the liquid flow rate is first increased and then decreased.

The conclusions to this study can be summarized as:

- Minimal hysteresis was observed by working in different startup modes
- High values of liquid saturation inside the micro-packed bed (as a result of strong capillary forces) leads to more stable hydrodynamic conditions as compared to macro-scale trickle bed reactors.
- Startup and switching times (the time for achieving steady state upon a step change) are in the order of 3-4 residence times
- The long characteristic time of response to a step change in these beds is claimed to be dependent on the compressibility in the gas-feed section and flow resistance in the packed bed itself such that a large volume in the feed section gives a large capacity that delays the new steady state.

- Since the hydrodynamic of micro-packed beds give insights on the kinetic data that can be further obtained from these systems, it is recommended that kinetic studies should be taken at times when transient behaviours are over and a complete steady state has achieved.

***d) Two-phase flow in packed-bed microreactors: Experiments, model and simulations***

Iliuta et al.<sup>104</sup> tailored a 2D hydrodynamic model based on the volume-averaged mass and momentum balance equations to describe concurrent two phase flow in packed microreactors. First of all, experiments were done with Water and Air as the working fluids flowing over a fixed of solids with particles of 55 $\mu$ m in diameter.

Then, based on these conditions, a 2D model was developed by writing the steady-state momentum and continuity balance equations for the gas and liquid along with the appropriate boundary conditions. These equations had to be coupled with three other sets of equations namely: 1) closure equations for the interfacial drag forces 2) momentum balance for the gas-liquid interface and 3) radial porosity distribution models.

- *Closure equations*: the interaction forces (written in the momentum balance equation) exerted on the liquid and gas phases can be evaluated using the two most common models developed for macro-scale trickle bed reactors by Holub et al.<sup>105</sup> and Attou et al.<sup>106</sup>
- *Momentum balance for gas-liquid interface*: it is also required to account for the discontinuity in pressure between the gas and liquid phases (capillary pressure). For this work, authors used the correlation developed by Attou and Ferschneider.<sup>107</sup>
- *Radial porosity distribution*: four different correlations developed for macro-scale packed beds are used in this contribution: 1) Vortmeyer and Schuster<sup>108</sup>, 2) Cohen and Metzner<sup>109</sup>, 3) Müller<sup>110</sup> and 4) de Klerk.<sup>111</sup>

Results of model validation reveal that the best predictions for pressure drop are for the case of combining Holub et al.<sup>105</sup> closure equations and Cohen and

Metzner<sup>109</sup> radial porosity distribution correlation. However, for liquid holdup, this combination shows a slight under-prediction.

For the final part of the work, a simulation has been carried out to investigate the effect of bed-to-particle diameter ( $D/d_p$ ) and capillary pressure on the gas and liquid velocity and holdup in the bed. The simulation utilizes the combinations of Holub et al.<sup>105</sup> closure equations and Cohen and Metzner<sup>109</sup> radial porosity distribution correlation.

Simulation results indicate that the model is quite sensitive to capillary pressure. Since the simulations were performed for the two cases: 1) absence of capillary pressure 2) presence of capillary pressure, the comparison of these two cases showed that capillary pressure has a tendency to stabilize the liquid flow structure (in contrast with inertial forces which act against stability). Capillary pressure causes the liquid phase to displace from the high-porosity region to the low-porosity region of the bed and consequently lead to a decrease in liquid channelling and an increase of liquid flow in the center. Obviously the opposite trend exists for the gas phase.

The concluding remark to this work, as authors claim, is that with increasing the availability of hydrodynamic data in micro-packed beds there will be a chance to refine the closure equations that were derived for macro-scale packed beds and customize them according to the physics of flow in miniaturized packed beds.

#### **1.6.4 Visualizations in micro-packed beds**

Micro-scale flow visualization is a key to understand, analyze, develop and evaluate novel micro-scale systems. Visualization are mostly performed for flow regime observations in order to see the effect of changes in operating variables (such as gas and liquid flow rates) on flow regimes and their transitions.<sup>53, 59, 60</sup> As a result of the drastic reduction in length scales upon miniaturization, the number of feasible probing methods diminishes as opposed to a large number of options for macro-scale multiphase flow visualization including intrusive and non-intrusive techniques.<sup>112, 113</sup> As for the gas-liquid flow in microchannels, microscopic visualizations through the transparent walls of microreactors provide valuable information regarding the flow regimes and their transitions (non-intrusive method). The

common experimental setup for such kind of visualizations is a high speed camera or a microscope coupled with a camera (with a high frequency for image acquisition). Figure 1-8 shows a series of visualizations for gas-liquid flow in a microchannel where changing the L/G ratio gives rise to the evolution of different flow regime. Flow regimes for gas-liquid flow in microchannels are not within the scope of this thesis, however, there are comprehensive reviews in this field.<sup>101</sup>

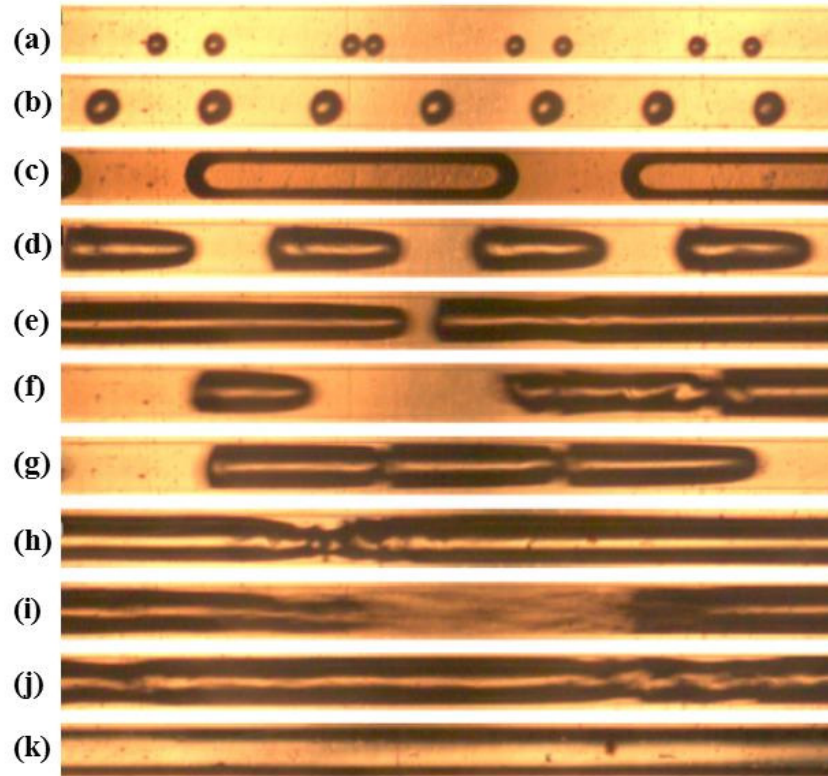


**Figure 0-8.** Typical images encountered during CO<sub>2</sub>-water flow in the micro-channel with  $d_h = 400 \mu\text{m}$  (flow from left to right with observation point at a distance of 3 cm from entrance): (a) bubbly flow ( $j_G = 0.16 \text{ m/s}$ ,  $j_L = 1.0 \text{ m/s}$ ); (b) bubbly flow ( $j_G = 0.29 \text{ m/s}$ ,  $j_L = 1.0 \text{ m/s}$ ); (c) Taylor flow ( $j_G = 0.16 \text{ m/s}$ ,  $j_L = 0.04 \text{ m/s}$ ,  $Ca = 0.0028$ ,  $Re_L = 80$ ); (d) Taylor flow ( $j_G = 1.28 \text{ m/s}$ ,  $j_L = 1.0 \text{ m/s}$ ,  $Ca = 0.031$ ,  $Re_L = 913$ ); (e) unstable slug flow ( $j_G = 1.74 \text{ m/s}$ ,  $j_L = 0.51 \text{ m/s}$ ); (f) unstable slug flow ( $j_G = 2.14 \text{ m/s}$ ,  $j_L = 0.51 \text{ m/s}$ ); (g) bubble-train slug flow ( $j_G = 2.07 \text{ m/s}$ ,  $j_L = 1.0 \text{ m/s}$ ); (h) slug-annular flow ( $j_G = 7.51 \text{ m/s}$ ,  $j_L = 0.20 \text{ m/s}$ ); (i) churn flow ( $j_G = 12.7 \text{ m/s}$ ,  $j_L = 1.0 \text{ m/s}$ ); (j) churn flow ( $j_G = 31 \text{ m/s}$ ,  $j_L = 0.51 \text{ m/s}$ ); (k) annular flow ( $j_G = 21.5 \text{ m/s}$ ,  $j_L = 0.02 \text{ m/s}$ ), Adapted from Yue et al. (2008)<sup>53</sup>

Utilizing a high speed camera for image capturing, it is also possible to determine residence time distribution for gas-liquid flow in microchannels by injecting a dye tracer and monitoring the change of color in the fluid within a specific field of view (as shown in Figure 1-9).<sup>71, 74</sup>



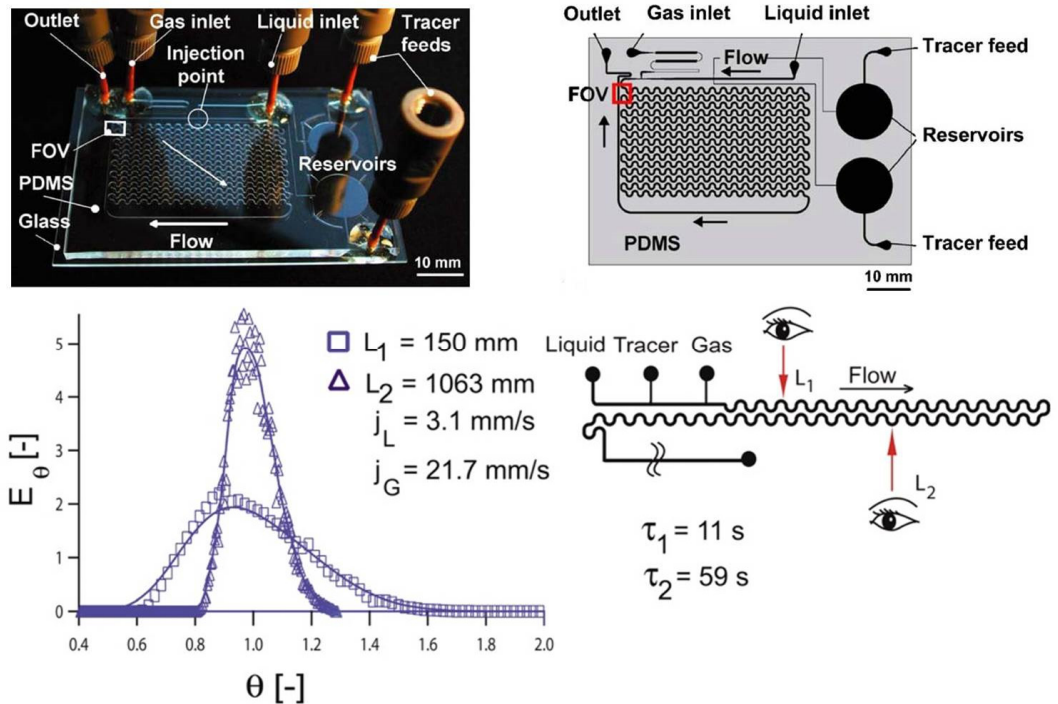


**Figure 0-9.** Experimental setup for the meandering microchannel (top-left), Schematic of the microchannel; network and the field of view (top-right) and RTD curves for segmented gas–liquid flow ( $j_L = 3.1 \text{ mm/s}$ ,  $j_G = 21.7 \text{ mm/s}$ ) at different lengths along device (bottom). Adapted from Trachsel et al. (2005)<sup>71</sup> and Günther et al. (2004)<sup>74</sup>

For a micro-packed bed, even if the optical transparency of the wall is maintained, visualizations become tricky as the presence of solid phase gives rise to the diffraction of light and therefore, it is not possible to have visualizations from the core of the bed and the images and related interpretations are only limited to the wall region. Here the visualization is also performed by the integration of microscope and CCD camera. The acquired images may require subsequent processing as will be shown in the next chapters.

## 1.7 Mass transfer study of micro-packed beds

Mass transfer in micro-packed beds (like other types of microreactors) is greatly improved compared to conventional or laboratory-scale units. In the study of mass transfer in micro-packed beds fast catalytic reactions such as hydrogenation of a liquid hydrocarbon (G-L-S system) are chosen as candidates since the chemical kinetics is often limited by mass transfer of hydrogen through the liquid and to the surface of solid catalyst. For the case of

hydrogenation in a typical macro-scale packed bed the low solubility of hydrogen in the solvent makes mass transfer complicated<sup>114</sup> and therefore, the operation is carried out at extremely high pressures. This will in turn increase the risk of explosion at a large scale unit.

However, in a safe micro-scale operation, Losey et al.<sup>28</sup> performed hydrogenation of cyclohexene on Pt/Al<sub>2</sub>O<sub>3</sub> catalyst particles (53-74 μm) in a micro-packed bed at much lower pressures (setup shown in Figure 1-1). The overall mass transfer resistance (1/K<sub>LA</sub>) was assumed to be the lump of mass transfer resistance for hydrogen absorption into the liquid (1/k<sub>la</sub>) and for its diffusion through the liquid and to the surface of the solid catalyst (1/k<sub>cas</sub>). The overall mass transfer coefficient (K<sub>LA</sub>) in their micro-packed bed was in the range of 5-15 s<sup>-1</sup> which is two orders of magnitude larger than that in their macro-scale counterparts (0.01-0.08 s<sup>-1</sup>).

In a similar attempt, Inoue et al.<sup>42</sup> performed the direct synthesis of hydrogen peroxide by feeding hydrogen, deuterium, oxygen and nitrogen along with the liquid reactant solution (H<sub>2</sub>SO<sub>4</sub>, H<sub>3</sub>PO<sub>4</sub> and NaBr) into a microreactor packed with Pt/C catalyst particles. The overall mass transfer coefficient (K<sub>LA</sub>) was 3.8 s<sup>-1</sup> and consistent with what Losey et al. had previously achieved.

Mass transfer studies in micro-packed beds are not limited to the determination of overall mass transfer coefficient. For example, Tidona et al.<sup>29</sup> focused on the evaluation of liquid-solid mass transfer coefficient at different ratios of channel-to-particle diameters (N) as well as different channel geometries using the copper dissolution method. Dissolution of sparingly soluble solids into liquids has been repeatedly used in macro-scale packed beds<sup>115</sup> and the adoption of this method for a micro-packed bed comes from the similarity between packed beds and micro-packed beds mentioned in section 1.6.2. Tidona et al.<sup>29</sup> used 80μm spherical copper particles packed in micro-tubes followed by tube shaking and vacuum application to densify the bed while the solution of potassium dichromate and sulphuric acid is flown through the micro-packed bed (see Figure 1-10). They assumed that the existing macro-scale correlations developed for liquid-solid mass transfer coefficient (in terms of Sherwood number) are not valid and attempted to propose their own correlation for micro-scale and for different channel-to-particle diameter ratios. They found out that at constant N, the shape of the channel has no influence on the liquid-solid mass transfer.

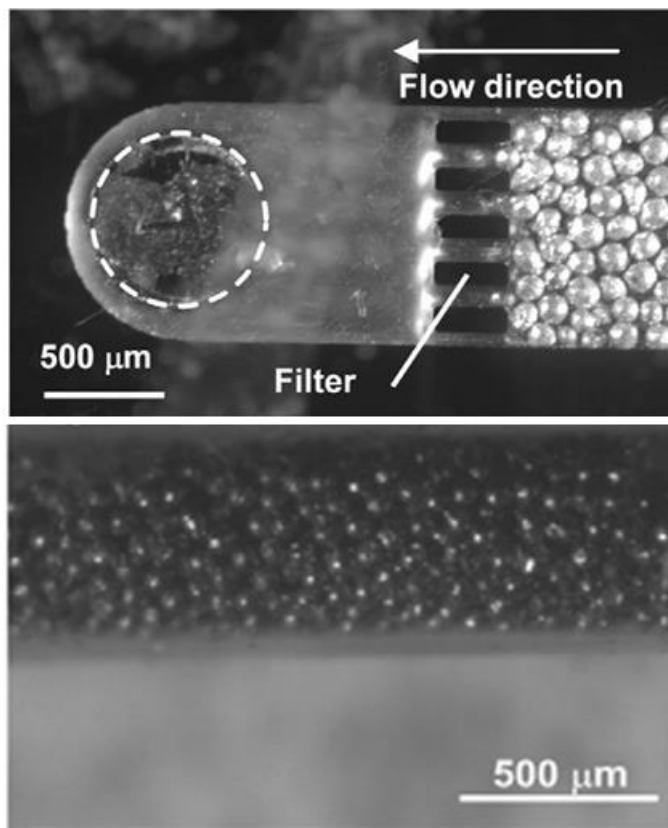


**Figure 0-10.** Top view of the micro-packed bed outlet filter for solids immobilization (a) and 320µm fused-silica square microchannel packed with 80µm copper particles (b). Adapted from Tidona et al. (2012)<sup>29</sup>

## 1.8 Scope of thesis

The scope of the current research project is mainly on hydrodynamic study of micro-packed beds as a sub-category of microreactors which are seemingly under-recognized as the open literature suggests. Our strategy is to build research foundations on micro-packed beds by comparing it with other units with which it has the most similarities (either from scale or operation point of view). The same approach will be more or less followed in the mass transfer study of micro-packed beds. The hypothesis for hydrodynamic studies in this thesis is that the difference between the relative importance of forces (as demonstrated in Table 1-4) might cause different hydrodynamic behaviour in micro-packed beds as compared to the macro-scale packed beds. This hypothesis is supposed to be put into test in the subsequent hydrodynamic studies.

Flow regimes and their transitions have always been of paramount importance in hydrodynamic studies of both macro-scale packed beds and microchannels as they are depictions of how different phases (mainly gas and liquid) interact with each other as their flow ratio through these units is altered. In chapter 2 the flow regimes in micro-packed beds will be studied and characterized by means of microscopic wall visualizations along with image processing. Images taken from the wall region of the micro-packed bed will also be processed for the study of hydrodynamic multiplicity (hysteresis). The idea is to verify whether this phenomenon (which is rather well-known in macro-scale packed beds) is also observed in micro-packed beds. One of the biggest obstacles in hydrodynamic study of micro-packed beds, according to author's discussions in a number of scientific conferences was attributed to the numerous challenges encountered in these studies such as high pressure drops and the possibility of tube failures and non-reproducibility of the results. In chap 3 the aims is to address these problems and suggest recommendation to surpass the challenges methodically and through a cause-and-effect logic in performing the experiments. Chapter 4 is in continuation of chapter 2 where the effects of solid particle size and channel geometry on flow regime, wetting pattern hysteresis and transient behaviour are discussed. Chapter 5 deals with liquid-solid mass transfer in micro-packed beds where a commonly employed method for determining the liquid-solid mass transfer coefficient in macro-scale packed beds (limiting-current technique) is tested on a micro-packed bed.

## 1.9 Nomenclature

Bo	Bond number (-)
c	Concentration (%w/w)
Ca	Capillary number (-)
$d_p$	Particle diameter (L)
$D_{ax}$	Axial dispersion coefficient ( $L^2T^{-1}$ )
Fr	Froude number (-)
g	Gravitational acceleration ( $LT^{-2}$ )
L	Length (L)
n	Refractive Index (-)
$Pe_L$	Axial Péclet number (-)
$Pe_p$	Particle Péclet number (-)
Q	Flow rate ( $L^3T^{-1}$ )
Re	Reynolds number (-)
T	Temperature ( $\theta$ )
u	Velocity ( $LT^{-1}$ )
$u_g$	Gas velocity ( $LT^{-1}$ )
$u_L$	Liquid velocity ( $LT^{-1}$ )
W	Width (L)

We Weber number (-)

### **Greek letters**

$\beta$  Homogenous void Fraction in two phase flow (-)

$\Delta t$  Time lag between two laser pulses (T)

$\mu$  Viscosity ( $ML^{-1}T^{-1}$ )

$\rho$  Density ( $ML^{-3}$ )

$\tau$  Mean residence time (T)

$\tau_0$  Dimensionless residence time (-)

$\sigma$  Surface tension of liquid phase ( $MT^{-2}$ )

$\sigma^2$  Tracer spread in the RTD curve (-)

### **Subscripts**

G,g Gas

L,l Liquid

total Microreactor setup with column

blank Microreactor setup without column

## 1.10 References

1. Stankiewicz, A. I.; Moulijn, J. A., Process intensification: Transforming chemical engineering. *Chemical Engineering Progress* **2000**, 96, (1), 22-34.
2. Keil, F. J. E., *Modeling of Process Intensification*. Wiley-VCH: **2007**.
3. Hessel, V.; Löwe, H.; Müller, A.; Kolb, G., *Chemical Micro Process Engineering, Processing and Plants*. Wiley-VCH: **2005**.
4. Reed, B. W. e. a., Membrane Separations Technology: Principles and Applications. In Noble, R. D.; Stern, S. A., Eds. Elsevier Science B.V.: **1995**; p 478.
5. Oroskar, A. R. In *IMRET-5: 5th International Conference on Microreaction Technology*, Strasbourg, **2001**; Springer: Strasbourg, **2001**.
6. Salic, A.; Tusek, A.; Zelic, B., Application of microreactors in medicine and biomedicine. *Journal of Applied Biomedicine* **2012**, 10, (3), 137-153.
7. Wang, Y. E.; Holladay, J. D. E., *Microreactor Technology and Process Intensification*. ACS symposium series ed.; **2005**.
8. Ehrfeld, W.; Hessel, V.; Löwe, H., *Microreactors*. Wiley-VCH: **2000**.
9. Hessel, V.; Hardt, S.; Löwe, H., *Chemical Micro Process Engineering, Fundamentals, Modelling and Reactions*. Wiley-VCH: **2004**.
10. Jensen, K. F., Microreaction engineering - is small better? *Chem. Eng. Sci.* **2001**, 56, (2), 293-303.
11. McGovern, S.; Harish, G.; Pai, C. S.; Mansfield, W.; Taylor, J. A.; Pau, S.; Besser, R. S., Multiphase flow regimes for hydrogenation in a catalyst-trap microreactor. *Chem. Eng. J.* **2008**, 135, S229-S236.
12. Chakraborty, S. E., *Microfluidics and Microfabrication*. Springer: **2010**.
13. Ajmera, S. K.; Losey, M. W.; Jensen, K. F.; Schmidt, M. A., Microfabricated packed-bed reactor for phosgene synthesis. *Aiche J.* **2001**, 47, (7), 1639-1647.
14. Elvira, K. S.; Solvas, X. C. i.; Wootton, R. C. R.; deMello, A. J., The past, present and potential for microfluidic reactor technology in chemical synthesis. *Nature Chemistry* **2013**, 5, (11), 905-915.
15. Gavriilidis, A.; Angeli, P.; Cao, E.; Yeong, K. K.; Wan, Y. S. S., Technology and applications of microengineered reactors. *Chemical Engineering Research & Design* **2002**, 80, (A1), 3-30.

16. Roberge, D. M.; Ducry, L.; Bieler, N.; Cretton, P.; Zimmermann, B., Microreactor technology: A revolution for the fine chemical and pharmaceutical industries? *Chem. Eng. Technol.* **2005**, 28, (3), 318-323.
17. See <http://www.icis.com/resources/news/2009/05/04/9211877/microreactors-gain-popularity-among-producers/>
18. See <http://pubs.acs.org/cen/news/8226/8226earlysci2.html>
19. Losey, M. W.; Jackman, R. J.; Firebaugh, S. L.; Schmidt, M. A.; Jensen, K. F., Design and fabrication of microfluidic devices for multiphase mixing and reaction. *J. Microelectromech. Syst.* **2002**, 11, (6), 709-717.
20. Yeong, K. K.; Gavriilidis, A.; Zapf, R.; Hessel, V., Catalyst preparation and deactivation issues for nitrobenzene hydrogenation in a microstructured falling film reactor. *Catal. Today* **2003**, 81, (4), 641-651.
21. Klemm, E.; Mathivanan, G.; Schwarz, T.; Schirmer, S., Evaporation of hydrogen peroxide with a microstructured falling film. *Chem. Eng. Process.* **2011**, 50, (10), 1010-1016.
22. Abdallah, R.; Meille, V.; Shaw, J.; Wenn, D.; de Bellefon, C., Gas-liquid and gas-liquid-solid catalysis in a mesh microreactor. *Chemical Communications* **2004**, (4), 372-373.
23. Wenn, D. A.; Shaw, J. E. A.; Mackenzie, B., A mesh microcontactor for 2-phase reactions. *Lab Chip* **2003**, 3, (3), 180-186.
24. Renken, A.; Kiwi-Minsker, L., Microstructured Catalytic Reactors. In *Advances in Catalysis, Vol 53*, Gates, B. C.; Knozinger, H.; Jentoft, F. C., Eds. Elsevier Academic Press Inc: San Diego, 2010; Vol. 53, pp 47-122.
25. Tsoligkas, A. N.; Simmons, M. J. H.; Wood, J., Two phase gas-liquid reaction studies in a circular capillary. *Chem. Eng. Sci.* **2007**, 62, (18-20), 5397-5401.
26. Tsoligkas, A. N.; Simmons, M. J. H.; Wood, J.; Frost, C. G., Kinetic and selectivity studies of gas-liquid reaction under Taylor flow in a circular capillary. *Catal. Today* **2007**, 128, (1-2), 36-46.
27. Pattekar, A. V.; Kothare, M. V., A radial microfluidic fuel processor. *J. Power Sources* **2005**, 147, (1-2), 116-127.
28. Losey, M. W.; Schmidt, M. A.; Jensen, K. F., Microfabricated multiphase packed-bed reactors: Characterization of mass transfer and reactions. *Ind. Eng. Chem. Res.* **2001**, 40, (12), 2555-2562.



29. Tidona, B.; Desportes, S.; Altheimer, M.; Ninck, K.; von Rohr, P. R., Liquid-to-particle mass transfer in a micro packed bed reactor. *Int. J. Heat Mass Transf.* **2012**, *55*, (4), 522-530.
30. Pattekar, A. V.; Kothare, M. V., A microreactor for hydrogen production in micro fuel cell applications. *J. Microelectromech. Syst.* **2004**, *13*, (1), 7-18.
31. Guettel, R.; Turek, T., Assessment of micro-structured fixed-bed reactors for highly exothermic gas-phase reactions. *Chem. Eng. Sci.* **2010**, *65*, (5), 1644-1654.
32. Knobloch, C.; Guettel, R.; Turek, T., Holdup and Pressure Drop in Micro Packed-Bed Reactors for Fischer-Tropsch Synthesis. *Chemie Ingenieur Technik* **2013**, *85*, (4), 455-460.
33. Wilhite, B. A.; Jensen, K. F.; Hill, T. F.; Velasquez-Garcia, L. F.; Epstein, A. H.; Livermore, C., Design of a silicon-based microscale trickle-bed system for singlet-oxygen production. *Aiche J.* **2008**, *54*, (9), 2441-2455.
34. Wada, Y.; Schmidt, M. A.; Jensen, K. F., Flow distribution and ozonolysis in gas-liquid multichannel microreactors. *Ind. Eng. Chem. Res.* **2006**, *45*, (24), 8036-8042.
35. Tourvieille, J. N.; Philippe, R.; de Bellefon, C., Milli-channel with metal foams under an applied gas-liquid periodic flow: Flow patterns, residence time distribution and pulsing properties. *Chem. Eng. Sci.* **2015**, *126*, 408-426.
36. AlDahhan, M. H.; Larachi, F.; Dudukovic, M. P.; Laurent, A., High-pressure trickle-bed reactors: A review. *Ind. Eng. Chem. Res.* **1997**, *36*, (8), 3292-3314.
37. Al-Naimi, S. A.; Al-Sudani, F. T. J.; Halabia, E. K., Hydrodynamics and flow regime transition study of trickle bed reactor at elevated temperature and pressure. *Chem. Eng. Res. Des.* **2011**, *89*, (7A), 930-939.
38. Faridkhou, A.; Hamidipour, M.; Larachi, F., Hydrodynamics of gas-liquid micro-fixed beds - Measurement approaches and technical challenges. *Chem. Eng. J.* **2013**, *223*, 425-435.
39. Tadepalli, S.; Qian, D. Y.; Lawal, A., Comparison of performance of microreactor and semi-batch reactor for catalytic hydrogenation of o-nitroanisole. *Catal. Today* **2007**, *125*, (1-2), 64-73.
40. Bellos, G. D.; Papayannakos, N. G., The use of a three phase microreactor to investigate HDS kinetics. *Catal. Today* **2003**, *79*, (1-4), 349-355.

41. Knochen, J.; Guettel, R.; Knobloch, C.; Turek, T., Fischer-Tropsch synthesis in milli-structured fixed-bed reactors: Experimental study and scale-up considerations. *Chem. Eng. Process.* **2010**, 49, (9), 958-964.
42. Inoue, T.; Schmidt, M. A.; Jensen, K. F., Microfabricated multiphase reactors for the direct synthesis of hydrogen peroxide from hydrogen and oxygen. *Ind. Eng. Chem. Res.* **2007**, 46, (4), 1153-1160.
43. Ajmera, S. K.; Delattre, C.; Schmidt, M. A.; Jensen, K. F., Microfabricated cross-flow chemical reactor for catalyst testing. *Sens. Actuator B-Chem.* **2002**, 82, (2-3), 297-306.
44. Suh, J. S.; Lee, M. T.; Greif, R.; Grigoropoulos, C. R., A study of steam methanol reforming in a microreactor (vol 173, pg 458, 2007). *J. Power Sources* **2008**, 183, (2), 817-817.
45. Park, H. G.; Malen, J. A.; Piggott, W. T.; Morse, J. D.; Greif, R.; Grigoropoulos, C. P.; Havstad, M. A.; Upadhye, R., Methanol steam reformer on a silicon wafer. *J. Microelectromech. Syst.* **2006**, 15, (4), 976-985.
46. Bakhtiary-Davijany, H.; Hayer, F.; Phan, X. K.; Myrstad, R.; Venvik, H. J.; Pfeifer, P.; Holmen, A., Characteristics of an Integrated Micro Packed Bed Reactor-Heat Exchanger for methanol synthesis from syngas. *Chem. Eng. J.* **2011**, 167, (2-3), 496-503.
47. Trachsel, F.; Hutter, C.; von Rohr, P. R., Transparent silicon/glass microreactor for high-pressure and high-temperature reactions. *Chem. Eng. J.* **2008**, 135, S309-S316.
48. Tidona, B.; Urakawa, A.; von Rohr, P. R., High pressure plant for heterogeneous catalytic CO<sub>2</sub> hydrogenation reactions in a continuous flow microreactor. *Chem. Eng. Process.* **2013**, 65, 53-57.
49. Haruta, M.; Yamada, N.; Kobayashi, T.; Iijima, S., Gold catalysts prepared by coprecipitation for low-temperature oxidation of hydrogen and of carbon-monoxide. *Journal of Catalysis* **1989**, 115, (2), 301-309.
50. Enache, D. I.; Edwards, J. K.; Landon, P.; Solsona-Espriu, B.; Carley, A. F.; Herzing, A. A.; Watanabe, M.; Kiely, C. J.; Knight, D. W.; Hutchings, G. J., Solvent-free oxidation of primary alcohols to aldehydes using Au-Pd/TiO<sub>2</sub> catalysts. *Science* **2006**, 311, (5759), 362-365.
51. Cao, E. H.; Sankar, M.; Firth, S.; Lam, K. F.; Bethell, D.; Knight, D. K.; Hutchings, G. J.; McMillan, P. F.; Gavriilidis, A., Reaction and Raman spectroscopic studies of alcohol

oxidation on gold-palladium catalysts in microstructured reactors. *Chem. Eng. J.* **2011**, 167, (2-3), 734-743.

52. Lindken, R.; Rossi, M.; Grosse, S.; Westerweel, J., Micro-Particle Image Velocimetry (mu PIV): Recent developments, applications, and guidelines. *Lab Chip* **2009**, 9, (17), 2551-2567.

53. Yue, J.; Luo, L. G.; Gonthier, Y.; Chen, G. W.; Yuan, Q., An experimental investigation of gas-liquid two-phase flow in single microchannel contactors. *Chem. Eng. Sci.* **2008**, 63, (16), 4189-4202.

54. Coleman, J. W.; Garimella, S., Characterization of two-phase flow patterns in small diameter round and rectangular tubes. *Int. J. Heat Mass Transf.* **1999**, 42, (15), 2869-2881.

55. Zhao, T. S.; Bi, Q. C., Co-current air-water two-phase flow patterns in vertical triangular microchannels. *Int. J. Multiph. Flow* **2001**, 27, (5), 765-782.

56. Waelchli, S.; von Rohr, P. R., Two-phase flow characteristics in gas-liquid microreactors. *Int. J. Multiph. Flow* **2006**, 32, (7), 791-806.

57. Zhang, T.; Cao, B.; Fan, Y. L.; Gonthier, Y.; Luo, L. G.; Wang, S. D., Gas-liquid flow in circular microchannel. Part I: Influence of liquid physical properties and channel diameter on flow patterns. *Chem. Eng. Sci.* **2011**, 66, (23), 5791-5803.

58. Barajas, A. M.; Panton, R. L., The effects of contact-angle on 2-phase flow in capillary tubes. *Int. J. Multiph. Flow* **1993**, 19, (2), 337-346.

59. Cubaud, T.; Ulmanella, U.; Ho, C. M., Two-phase flow in microchannels with surface modifications. *Fluid Dyn. Res.* **2006**, 38, (11), 772-786.

60. Serizawa, A.; Feng, Z. P.; Kawara, Z., Two-phase flow in microchannels. *Exp. Therm. Fluid Sci.* **2002**, 26, (6-7), 703-714.

61. Triplett, K. A.; Ghiaasiaan, S. M.; Abdel-Khalik, S. I.; Sadowski, D. L., Gas-liquid two-phase flow in microchannels - Part I: two-phase flow patterns. *Int. J. Multiph. Flow* **1999**, 25, (3), 377-394.

62. Qian, D. Y.; Lawal, A., Numerical study on gas and liquid slugs for Taylor flow in a T-junction microchannel. *Chem. Eng. Sci.* **2006**, 61, (23), 7609-7625.

63. Haverkamp, V.; Hessel, V.; Lowe, H.; Menges, G.; Warnier, M. J. F.; Rebrov, E. V.; de Croon, M.; Schouten, J. C.; Liauw, M. A., Hydrodynamics and mixer-induced bubble

formation in micro bubble columns with single and multiple-channels. *Chem. Eng. Technol.* **2006**, 29, (9), 1015-1026.

64. Yue, J.; Chen, G. W.; Yuan, Q., Pressure drops of single and two-phase flows through T-type microchannel mixers. *Chem. Eng. J.* **2004**, 102, (1), 11-24.

65. Kreutzer, M. T.; Kapteijn, F.; Moulijn, J. A.; Kleijn, C. R.; Heiszwolf, J. J., Inertial and interfacial effects on pressure drop of Taylor flow in capillaries. *Aiche J.* **2005**, 51, (9), 2428-2440.

66. Kawahara, A.; Chung, P. M. Y.; Kawaji, M., Investigation of two-phase flow pattern, void fraction and pressure drop in a microchannel. *Int. J. Multiph. Flow* **2002**, 28, (9), 1411-1435.

67. Choi, C. W.; Yu, D. I.; Kim, M. H., Adiabatic two-phase flow in rectangular microchannels with different aspect ratios: Part I - Flow pattern, pressure drop and void fraction. *Int. J. Heat Mass Transf.* **2011**, 54, (1-3), 616-624.

68. Xiong, R. Q.; Chung, J. N., An experimental study of the size effect on adiabatic gas-liquid two-phase flow patterns and void fraction in microchannels. *Phys. Fluids* **2007**, 19, (3), 8.

69. Chung, P. M. Y.; Kawaji, M., The effect of channel diameter on adiabatic two-phase flow characteristics in microchannels. *Int. J. Multiph. Flow* **2004**, 30, (7-8), 735-761.

70. Aubin, J.; Prat, L.; Xuereb, C.; Gourdon, C., Effect of microchannel aspect ratio on residence time distributions and the axial dispersion coefficient. *Chem. Eng. Process.* **2009**, 48, (1), 554-559.

71. Trachsel, F.; Gunther, A.; Khan, S.; Jensen, K. F., Measurement of residence time distribution in microfluidic systems. *Chem. Eng. Sci.* **2005**, 60, (21), 5729-5737.

72. Kim, B. J.; Liu, Y. Z.; Sung, H. J., Micro PIV measurement of two-fluid flow with different refractive indices. *Meas. Sci. Technol.* **2004**, 15, (6), 1097-1103.

73. Miessner, U.; Lindken, R.; Westerweel, J.; Asme, Velocity measurements in microscopic two-phase flows by means of micro PIV. *Proceedings of the 6th International Conference on Nanochannels, Microchannels, and Minichannels, Pts a and B* **2008**, 1111-1118.

74. Gunther, A.; Khan, S. A.; Thalmann, M.; Trachsel, F.; Jensen, K. F., Transport and reaction in microscale segmented gas-liquid flow. *Lab Chip* **2004**, 4, (4), 278-286.

75. Wammes, W. J. A.; Middelkamp, J.; Huisman, W. J.; Debaas, C. M.; Westerterp, K. R., Hydrodynamics in a cocurrent gas-liquid trickle bed at elevated pressures. *Aiche J.* **1991**, 37, (12), 1849-1862.
76. Trivizadakis, M. E.; Giakoumakis, D.; Karabelas, A. J., A study of particle shape and size effects on hydrodynamic parameters of trickle beds. *Chem. Eng. Sci.* **2006**, 61, (17), 5534-5543.
77. Larachi, F.; Iliuta, I.; Chen, M.; Grandjean, B. P. A., Onset of pulsing in trickle beds: Evaluation of current tools and state-of-the-art correlation. *Can. J. Chem. Eng.* **1999**, 77, (4), 751-758.
78. Charpentier, J. C.; Favier, M., Some liquid holdup experimental-data in trickle-bed reactors for foaming and non-foaming hydrocarbons. *Aiche J.* **1975**, 21, (6), 1213-1218.
79. Kan, K. M.; Greenfield, P. F., Pressure-drop and holdup in 2-phase cocurrent trickle flows through beds of small packings. *Industrial & Engineering Chemistry Process Design and Development* **1979**, 18, (4), 740-746.
80. Saez, A. E.; Carbonell, R. G., Hydrodynamic parameters for gas-liquid cocurrent flow in packed-beds. *Aiche J.* **1985**, 31, (1), 52-62.
81. Sai, P. S. T.; Varma, Y. B. G., Pressure-drop in gas-liquid downflow through packed-beds. *Aiche J.* **1987**, 33, (12), 2027-2036.
82. Ellman, M. J.; Midoux, N.; Laurent, A.; Charpentier, J. C., A new, improved pressure-drop correlation for trickle-bed reactors. *Chem. Eng. Sci.* **1988**, 43, (8), 2201-2206.
83. Larachi, F.; Laurent, A.; Midoux, N.; Wild, G., Experimental-study of a trickle-bed reactor operating at high-pressure- 2-phase pressure-drop and liquid saturation. *Chem. Eng. Sci.* **1991**, 46, (5-6), 1233-1246.
84. Benkrid, K.; Rode, S.; Midoux, N., Prediction of pressure drop and liquid saturation in trickle-bed reactors operated in high interaction regimes. *Chem. Eng. Sci.* **1997**, 52, (21-22), 4021-4032.
85. Burghardt, A.; Bartelmus, G.; Jaroszynski, M.; Kolodziej, A., Hydrodynamics and mass-transfer in a 3-phase fixed-bed reactor with cocurrent gas-liquid downflow. *Chem. Eng. J. Biochem. Eng. J.* **1995**, 58, (2), 83-99.
86. Specchia, V.; Baldi, G., Pressure-drop and liquid holdup for 2-phase concurrent flow in packed-beds. *Chem. Eng. Sci.* **1977**, 32, (5), 515-523.

87. Morsi, B. I.; Midoux, N.; Charpentier, J. C., Flow patterns and some holdup experimental-data in trickle-bed reactors for foaming, nonfoaming, and viscous organic liquids. *Aiche J.* **1978**, 24, (2), 357-360.
88. Rao, V. G.; Ananth, M. S.; Varma, Y. B. G., Hydrodynamics of 2-phase co-current downflow through packed-beds. 2. Experiments and correlations. *Aiche J.* **1983**, 29, (3), 473-483.
89. Wammes, W. J. A, Westerterp, K. R., The influence of reactor pressure on the hydrodynamics in a cocurrent gas-liquid trickle-bed reactor. *Chem. Eng. Sci.* **1990**, 45, (3), 2247-2254.
90. Mills, P. L.; Dudukovic, M. P., Evaluation of liquid-solid contacting in trickle-bed reactors by tracer methods. *Aiche J.* **1981**, 27, (6), 893-904.
91. Sederman, A. J.; Gladden, L. F., Magnetic resonance imaging as a quantitative probe of gas-liquid distribution and wetting efficiency in trickle-bed reactors. *Chem. Eng. Sci.* **2001**, 56, (8), 2615-2628.
92. Gunjal, P. R.; Kashid, M. N.; Ranade, V. V.; Chaudhari, R. V., Hydrodynamics of trickle-bed reactors: Experiments and CFD modeling. *Ind. Eng. Chem. Res.* **2005**, 44, (16), 6278-6294.
93. Loudon, D.; van der Merwe, W.; Nicol, W., Multiple hydrodynamic states in trickle flow: Quantifying the extent of pressure drop, liquid holdup and gas-liquid mass transfer variation. *Chem. Eng. Sci.* **2006**, 61, (22), 7551-7562.
94. van Howelingen, A. J.; Van der Merwe, W.; Wales, N.; Heydenrych, M.; Nicol, W., The effect of hydrodynamic multiplicity on liquid phase trickle flow axial dispersion. *Chem. Eng. Res. Des.* **2009**, 87, (5A), 677-683.
95. Marquez, N.; Castano, P.; Moulijn, J. A.; Makkee, M.; Kreutzer, M. T., Transient Behavior and Stability in Miniaturized Multiphase Packed Bed Reactors. *Industrial & Engineering Chemistry Research* **2010**, 49, (3), 1033-1040.
96. Iliuta, I.; Thyrion, F. C., Gas-liquid mass transfer in fixed beds with two-phase cocurrent downflow: Gas/Newtonian and non-Newtonian liquid systems. *Chem. Eng. Technol.* **1997**, 20, (8), 538-549.

97. Wild, G.; Larachi, F.; Charpentier, J.-C., Heat and mass transfer in gas-liquid-solid fixed bed reactors. In *Heat and mass transfer in porous media*, Quintard, M.; Todorovic, M., Eds. Elsevier: **1992**.
98. Latifi, M. A.; Laurent, A.; Storck, A., Liquid solid mass-transfer in a packed-bed with downward cocurrent gas-liquid flow- An organic liquid-phase with high Schmidt number. *Chem. Eng. J. Biochem. Eng. J.* **1988**, 38, (1), 47-56.
99. Lakota, A.; Levec, J., Solid-liquid mass-transfer in packed-beds with cocurrent downward 2-phase flow. *Aiche J.* **1990**, 36, (9), 1444-1448.
100. Rao, V. G.; Drinkenburg, A. A. H., Solid-liquid mass-transfer in packed-beds with cocurrent gas-liquid downflow. *Aiche J.* **1985**, 31, (7), 1059-1068.
101. Shao, N.; Gavriilidis, A.; Angeli, P., Flow regimes for adiabatic gas-liquid flow in microchannels. *Chem. Eng. Sci.* **2009**, 64, (11), 2749-2761.
102. van Herk, D.; Kreutzer, M. T.; Makkee, M.; Moulijn, J. A., Scaling down trickle bed reactors. *Catalysis Today* **2005**, 106, (1-4), 227-232.
103. Marquez, N.; Castano, P.; Makkee, M.; Moulijn, J. A.; Kreutzer, M. T., Dispersion and holdup in multiphase packed bed microreactors. *Chemical Engineering & Technology* **2008**, 31, (8), 1130-1139.
104. Iliuta, I.; Hamidipour, M.; Schweich, D.; Larachi, F., Two-phase flow in packed-bed microreactors: Experiments, model and simulations. *Chemical Engineering Science* **2012**, 73, 299-313.
105. Holub, R. A.; Dudukovic, M. P.; Ramachandran, P. A., A phenomenological model for pressure-drop, liquid holdup, and flow regime transition in gas-liquid trickle flow. *Chemical Engineering Science* **1992**, 47, (9-11), 2343-2348.
106. Attou, A.; Boyer, C.; Ferschneider, G., Modelling of the hydrodynamics of the cocurrent gas-liquid trickle flow through a trickle-bed reactor. *Chemical Engineering Science* **1999**, 54, (6), 785-802.
107. Attou, A.; Ferschneider, G., A two-fluid hydrodynamic model for the transition between trickle and pulse flow in a cocurrent gas-liquid packed-bed reactor. *Chemical Engineering Science* **2000**, 55, (3), 491-511.

108. Vortmeyer, D.; Schuster, J., Evaluation of steady flow profiles in rectangular and circular packed-beds by a variational method. *Chemical Engineering Science* **1983**, 38, (10), 1691-1699.
109. Cohen, Y.; Metzner, A. B., Wall effects in laminar-flow of fluids through packed-beds. *Aiche Journal* **1981**, 27, (5), 705-715.
110. Mueller, G. E., Prediction of radial porosity distributions in randomly packed fixed-beds of uniformly sized spheres in cylindrical containers. *Chemical Engineering Science* **1991**, 46, (2), 706-708.
111. de Klerk, A., Voidage variation in packed beds at small column to particle diameter ratio. *Aiche Journal* **2003**, 49, (8), 2022-2029.
112. Boyer, C.; Duquenne, A. M.; Wild, G., Measuring techniques in gas-liquid and gas-liquid-solid reactors. *Chemical Engineering Science* **2002**, 57, (16), 3185-3215.
113. Chaouki, J.; Larachi, F.; Dudukovic, M. P., Noninvasive tomographic and velocimetric monitoring of multiphase flows. *Industrial & Engineering Chemistry Research* **1997**, 36, (11), 4476-4503.
114. Mills, P. L.; Chaudhari, R. V., Multiphase catalytic reactor engineering and design for pharmaceuticals and fine chemicals. *Catal. Today* **1997**, 37, (4), 367-404.
115. Saroha, A. K., Solid-liquid mass transfer studies in trickle bed reactors. *Chem. Eng. Res. Des.* **2010**, 88, (5-6A), 744-747.



## 2 Hydrodynamics of gas-liquid cocurrent flows in micro-packed beds - Wall visualization study

**Résumé** Une technique de microscopie inversée a été mise en place pour examiner l'hydrodynamique aux parois lors d'un écoulement co-courant gaz-liquide dans les micros lits-fixes. L'analyse d'image a permis la caractérisation de deux régimes d'écoulement contigus et leur transition ainsi que du phénomène d'hystérèse. Des régimes à faible et haute interactions comprenant, respectivement, les déplacements lents et rapides de l'interface gaz-liquide ont été identifiés. L'apparition de la transition de régime a été délimitée en distinguant le comportement fluctuant dans le temps des longueurs caractéristiques extraites des zones occupées par le gaz et le liquide dans le champ de vision. La carte des régimes d'écoulement de Charpentier et Favier délimitant les régimes de basse et de haute interaction dans les macros lits-fixes a été réexaminée à la lumière des résultats de transition dans les micros lits-fixes pour trois systèmes gaz-liquide différents (air-eau, argon-eau et argon-saccharose). La carte des régimes d'écoulement suggère que la transition se produit dans les lits-fixes aux mêmes valeurs  $L/G$ . La manifestation de l'hystérèse dans les micros lits garnis a été appréhendée par des mesures de perte de charge et la détermination de la fraction mouillée à la fois par modes d'imbibition et drainage. En accord avec les observations sur les macro-lits fixes, la méthode de drainage a révélé une plus grande perte de charge et une plus grande fraction mouillée comparativement à la méthode d'imbibition pour le même type de garnissage et débits de fluide.

**Abstract** An inverted microscopy technique was implemented to scrutinize the wall-region hydrodynamics of gas-liquid cocurrent flows in micro-packed beds. Digital image analysis enabled characterization of two contiguous flow regimes, hysteresis and transition thereof. A low- and high-interaction regimes featuring, respectively, slow and rapid displacements of gas-liquid boundary were identified. The onset of regime changeover was delineated by distinguishing the fluctuating behavior in time of characteristic lengths extracted from the areas occupied by gas and liquid in the field of view. A Charpentier and Favier flow regime map demarcating low and high interaction regimes in conventional macro-scale trickle beds was elaborated for the sake of comparison of micro-packed bed transitions for three different gas-liquid systems (air-water, argon-water and argon-sucrose solution). The flow regime map suggests that micro-packed bed transition occurs at rather the same L/G values. Manifestation of hysteresis in micro-packed beds was apprehended via pressure drop measurements and wetting fraction determination both in imbibition and drainage modes. In agreement with macro-scale packed bed observations, the drainage branch revealed larger pressure drop and wetting fraction compared with the imbibition branch for the same set of bed and fluid flow rates.

## 2.1 Introduction

Process Intensification (PI) is often mentioned as one of the most promising development paths for the chemical process industry having major progress areas for chemical engineering research as well.<sup>1</sup> Microreactors are one of the tools which fulfill the aims of process intensification and are increasingly explored in different sectors of chemical industry. They offer a number of advantages compared to their macroscopic counterparts, i.e., higher surface to volume ratios leading to higher heat and mass transfer coefficients. This allows reactions to be performed under more aggressive conditions with higher yields that are not achievable in macro-scale reactors.<sup>2,3</sup> Furthermore, rapid screening of numerous catalysts<sup>4</sup> as well as safe synthesis of hazardous materials<sup>5,6</sup> can be considered as other advantages that triggered increased research on microreactors.

Although an important body of literature revolves around kinetic and mass transfer studies in multiphase microreactors<sup>7-10</sup> to improve their performance, it should be noted that equal awareness about the hydrodynamics of such systems is of paramount importance. Any success in correctly addressing the flow phenomena and optimizing the contacting schemes at this scale culminates to an even more increase in efficiency. Over the last two decades, several hydrodynamic studies have been conducted on two-phase flow in different types of miniaturized flow systems such as microchannels,<sup>11-18</sup> internally-structured microreactors<sup>19-23</sup> and mesh microreactors.<sup>24,25</sup> However, despite the rather wide application of micro-packed beds in kinetic and mass transfer studies, their hydrodynamic characteristics are still under-recognized and poorly addressed in the open literature. Few experimental attempts necessitate in-depth investigations to unveil their hydrodynamic behavior. This work is aimed at filling the currently existing gap by studying some of the hydrodynamic aspects of two-phase cocurrent gas-liquid flow in micro-packed beds.

Regardless of the differences stemming from working at different scales, micro-packed beds have the most similarity with macro-scale trickle bed reactors wherein both gas and liquid phases flow over a fixed bed of solid particles from one side and exit from the other side of bed. Therefore, one general approach to build research foundations in this field is to identify the key parameters in the operation of macro-scale trickle-bed reactors and then develop experimental methods to study the same parameters, if feasible, in micro-scale

packed beds. For trickle bed reactors, some of the key parameters are *flow regimes*, *pressure drop*, *RTD*, *liquid holdup*, *wetting efficiency* and *interfacial area*. These parameters can be studied by a number of intrusive and non-intrusive visualization/measurement methods in macro-scale.<sup>26</sup> For micro-packed beds, however, these methods mostly fail to be adopted. This is due to a drastic change in characteristic lengths on one side and the paucity of appropriate and well-established probing technologies on the other. Another approach to fuel hydrodynamic research in micro-packed beds comes from its comparison with micro-channels as the scales are rather the same for both units. Since a plethora of hydrodynamic studies have been conducted on micro-channels covering a wide variety of subjects,<sup>27</sup> it is also possible to identify those ideas that seem relevant to be investigated for micro-packed beds as well. Although this approach has not gained enough popularity as the first one, it seems to be a promising approach for improving our knowledge on the hydrodynamics of micro-packed beds.

As for the first approach, RTD measurements for gas-liquid flow in micro-packed beds has been done by van Herk et al.<sup>28</sup> who reported minimal deviation from plug flow behavior and more pronounced effect of gas flow rate on liquid residence time as compared to macro-scale trickle beds. Márquez et al. also performed RTD tests to determine liquid holdup in micro-packed beds using non-volatile<sup>29</sup> and volatile<sup>30</sup> tracers. Nevertheless, they reported their holdups as a single global value not reflecting its axial variation due to high pressure gradients existing in micro-packed beds. Transient behavior of micro-packed beds upon employing several startup procedures was also investigated by Márquez et al.<sup>31</sup> and they observed minor deviations in the achieved steady state. Although obtaining visualizations from macro-scale packed beds provided valuable insight into the flow nature,<sup>32</sup> none of the abovementioned works took research initiatives in this direction for micro-packed beds. The studies were also focused on a flow regime where gas-liquid interactions were quite limited (low interaction regime) and transition to high interaction regimes skipped investigation.

Therefore, in the current study, microscopic imaging is utilized to obtain visualizations within the transparent walls of micro-packed bed at the layer adjacent to the wall. The focus of the work is on flow regimes, onset of flow regime transition and the

contributory roles of fluid physical properties and finally hysteresis. For the latter, pressure drop measurements are also reported along with wetting percentages in both imbibition (ascending liquid flow rate) and drainage (descending liquid flow rate) paths.

## **2.2 Experimental**

### **2.2.1 Setup**

The schematic of the setup for performing the experiments is shown in Figure 2-1. It consists of a transparent borosilicate tube with square cross-section having a hydraulic diameter of 1 mm and length of 11.5 cm packed with spherical glass beads with diameters in the range of 106-125  $\mu\text{m}$  serving as the micro-packed bed. The bed has optically accessible windows for microscopic visualization. Liquid delivery to the bed is enabled by a syringe pump (Teledyne ISCO, 500D) while gas is fed via mass flow controller (EL-Flow Bronkhorst). Introduction of gas and liquid into the micro-packed bed is such that their mixing takes place right at the start of the packed bed. Otherwise, the existence of any void space upstream of the micro-packed bed bringing gas and liquid phases in contact prior to entering the packed section, will lead into instabilities and thus should be avoided.<sup>7</sup> It should be noted that the pressure drop is measured at the gas-liquid entrance to the bed. The micro-packed bed is mounted horizontally on an inverted microscope (Olympus GX-51) and visualized through a 10X objective lens (MPlanFLN-BD series) at a constant light intensity. It is noteworthy to mention that at such small scales as the micro-packed bed, strong capillary forces simply outweigh gravitational effects.<sup>29</sup> This means that horizontal and vertical arrangement of the micro-packed bed will lead to identical results. The microscope is coupled with a camera (TSI, PowerView<sup>TM</sup> Plus) which is itself connected to a computer with a frame-grabber port and image acquisition is performed using Insight3G software.

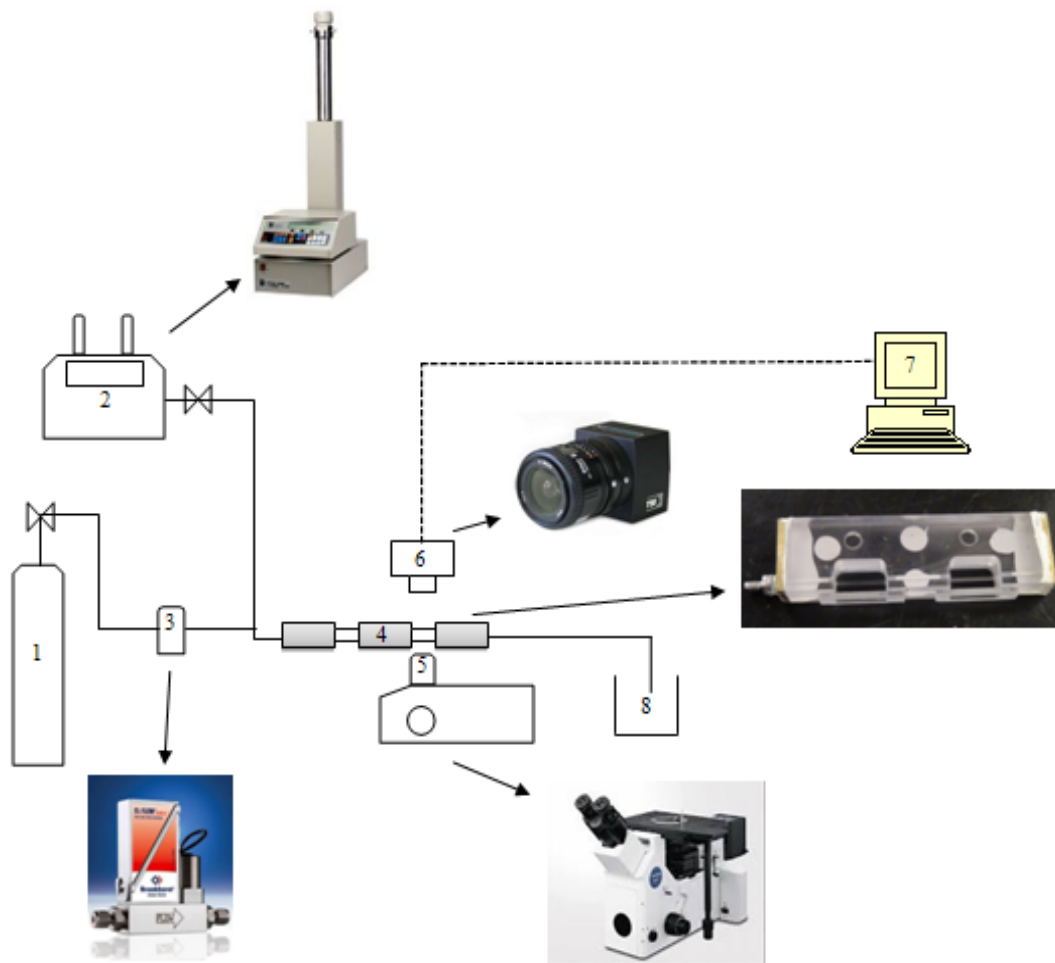


**Figure 2-1.** Experimental Setup: 1) Gas cylinder; 2) Syringe pump; 3) Gas mass flow controller; 4) Microreactor; 5) Inverted microscope and objective lens; 6) Camera with frame grabber port; 7) Computer for image acquisition; 8) Drain

### 2.2.2 Methodology

To begin each set of experiments, the capillary was densely packed with the glass beads by frequent tapping. For flow regime transition experiments, air and argon were used as the gas phase while water and aqueous sucrose solutions were fed as liquid phase. Table 2-1 summarizes the fluids' physical properties. Three gas-liquid combination sets: air-water, argon-water and air-aqueous sucrose solution have been tested flowing at different superficial velocities through the micro-packed bed at room temperature. Upon reaching a constant pressure drop at each set of gas and liquid superficial velocities (indicating steady state conditions), a set of 150 images were taken at 15 Hz rate from the bed. The transition

from low interaction to high interaction regime can be observed by microscopic visualization and subsequently verified by statistical analysis as will be described in the image processing section.

**Table 2-1.** Properties of Working Fluids

<b>Fluid</b>	<b>Density (kg/m<sup>3</sup>)</b>	<b>Viscosity (mPa.s)</b>	<b>Surface Tension (N/m)</b>
<b>Water</b>	997	1.00	0.0728
<b>Sucrose solution (0.24 w/w%)</b>	1096	1.92	0.0601
<b>Air</b>	1.21	0.018	-
<b>Argon</b>	1.66	0.021	-

In another set of experiments, air and water were used for hysteresis observations in the micro-packed bed. After packing the bed, the superficial gas velocity was held constant at 25.5 cm/s while the superficial liquid velocity was steadily increased from 1.1 mm/s to 19.2 mm/s (forward or imbibition mode) with equal increments and then decreased to the initial point (backward or drainage mode). It is noteworthy to mention that the superficial velocities are related to the bed entrance. At each liquid velocity, for both imbibition and drainage paths, 150 images were taken from the bed after pressure drop stabilization in order to compare visualizations from the bed texture at same superficial liquid velocities in both increasing and decreasing paths. Pressure drops corresponding to each liquid velocity and path were also recorded at the same time as the images were being acquired. It should be emphasized that in image acquisition process since only the bed wall region can be observed with inverted microscopy, results and interpretations originating from image processing are limited to this range. All the experiments were repeated to ensure reproducibility.

### **2.2.3 Image Processing**

The acquired images at each stage are processed using MATLAB image processing toolbox. Since processing of the acquired images is based on the gray level intensity analysis of the pixels within each image, the intensity of light from the microscope to the microreactor shall be kept constant throughout the entire experiments. Due to curvatures at the corners of the square tube (wall boundary) showing themselves as blurs on the top and bottom edges,

each raw image has been cropped from the edges prior to image processing. Pre-processing operations were also performed to obtain images with a smooth gas-liquid boundary. Then, for each image, the regions occupied with gas (brighter regions) and liquid (darker regions) phases were separated by grayscale thresholding followed by image binarization to label all the pixels within the image as either gas (white) or liquid (black). Afterwards, the weighted mean area of the separate liquid (or gas) regions ( $A_L$  or  $A_G$ ) were determined and based on that area, a characteristic length ( $\Lambda$ ) has been defined for liquid (or gas) as:

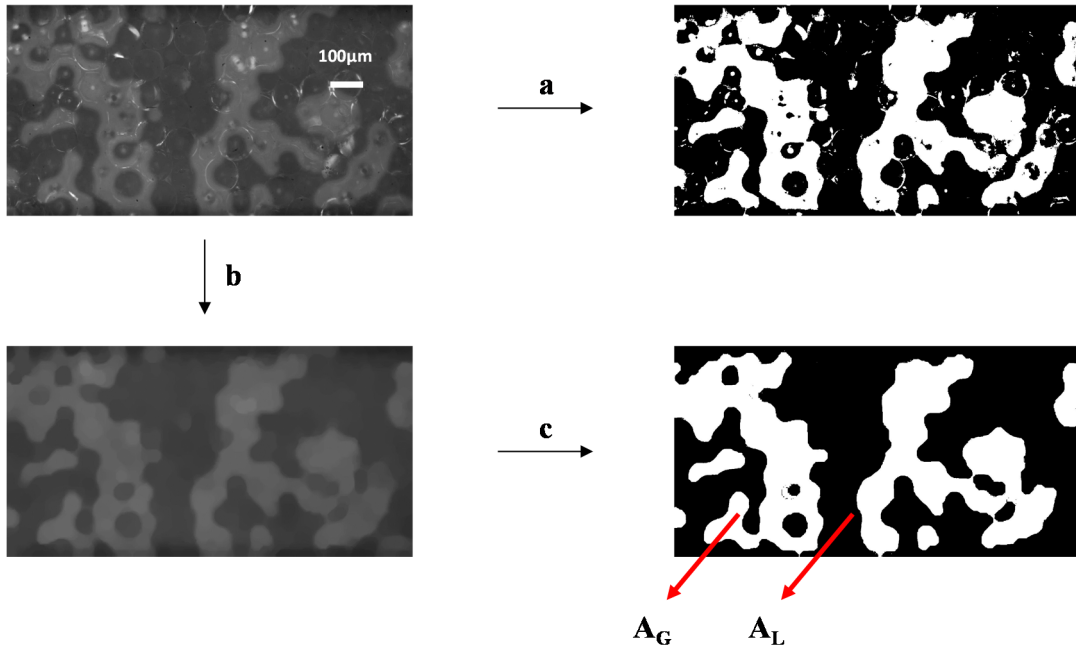


**Figure 2-2.** Image processing procedure starting from raw image (top-left): a) image binarization without preprocessing b) image pre-processing c) binarization of pre-processed image and obtaining liquid and gas occupied mean areas.

$$\Lambda_L = \sqrt{\frac{4A_L}{\pi}} \quad (2-1)$$

$$\Lambda_G = \sqrt{\frac{4A_G}{\pi}} \quad (2-2)$$

The procedure is shown in Figure 2-2. For flow regime studies, where characteristic lengths are concerned, images will be processed on a frame-by-frame basis and characteristic lengths for gas and liquid phases are calculated for each of the 150 images taken at different



liquid superficial velocities. Each frame consists of  $976 \times 1881$  pixels filling a field of view  $0.7 \times 1.3 \text{ mm}^2$  in area and a depth of focus equal 15 microns taken 4 cm downstream from bed entrance. In order to determine the onset of flow regime transition from low interaction to high interaction, a moment method has been used which relies on calculating the coefficient of variation from variance and arithmetic mean as the 2<sup>nd</sup> order and 1<sup>st</sup>-order moments, respectively. This method has already been used for macro-scale trickle bed reactors to predict trickle-to-pulse flow regime transition using electrical conductivity as the fluctuating signal.<sup>33</sup> In this study, however, the coefficient of variation (COV) is based on liquid phase characteristic length ( $\Lambda_L$ ):

$$\text{COV}(\Lambda_L) = \frac{\sqrt{\sigma^2(\Lambda_L)}}{\underline{\mu}(\Lambda_L)} \quad (2-3)$$

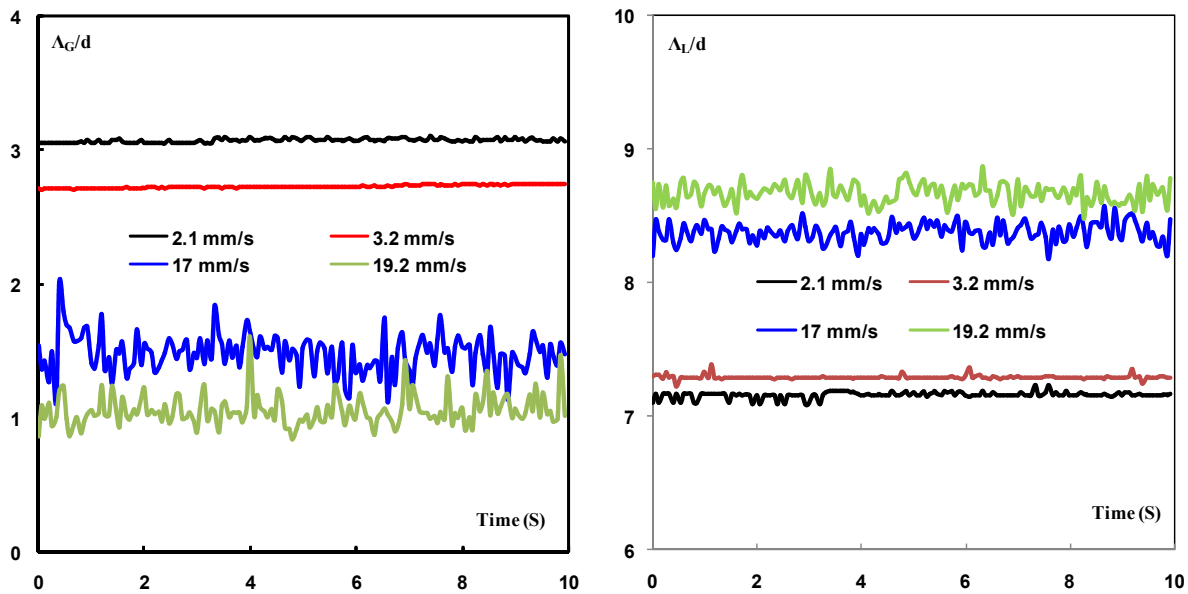
In which  $\sigma^2$  and  $\underline{\mu}$  are variance and mean value, respectively, of liquid characteristic length. The maxima observed in each of the  $\text{COV}(\Lambda_L)$  versus  $U_{LS}$  plots will then correspond to the point of flow regime transition. To perform hysteresis studies, each set of 150 images will be time-averaged and the resulting single image will be processed, i.e., thresholded and binarized, for the study of wetting patterns. In addition, by subtracting time-averaged binarized images of imbibitions from drainages at the same superficial velocities, one can distinguish three distinct regions in the bed texture: a) regions dry in imbibition and wet in drainage b) regions wet in imbibition and dry in drainage c) regions undergoing the same situation (either both wet or both dry) in imbibition and drainage.

## 2.3 Results and discussion

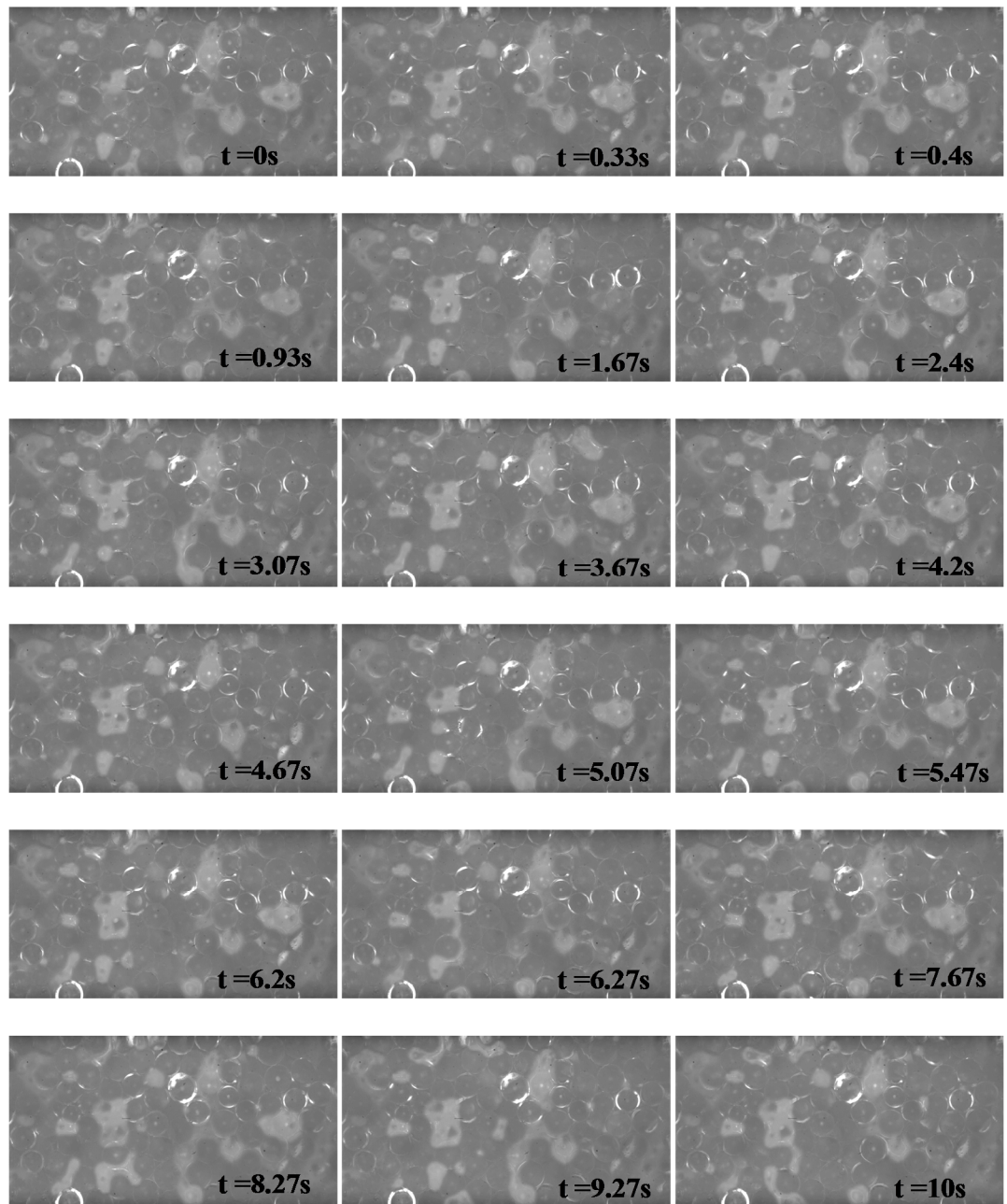
### 2.3.1 Flow Regimes

Figure 2-3 shows dynamic variations of both liquid (left) and gas (right) characteristic lengths in dimensionless form at four different liquid superficial velocities and constant gas superficial velocity (25.5 cm/s) where  $d$  is the solid particle diameter. As can be observed from both Figures, at low liquid superficial velocities, the characteristic lengths of both gas and liquid phases which are representatives of gas-liquid boundary movement have a monotonic trend indicating that low interaction flow regime prevails. At this flow regime,

gas and liquid phases have a rather constant share of the bed voidage without significantly perturbing each other. However, at increased liquid superficial velocities a competition arises between the two phases for the void spaces in the bed and high interaction flow regime is reached manifesting itself as fluctuations in both gas and liquid characteristic lengths. Note that at constant gas velocity, an increase in liquid superficial velocity leads to an increase (decrease) in the areas occupied by liquid (gas) which is translated as an increase (decrease) in liquid (gas) characteristic length. Some visualization from the high interaction flow regime are also shown in Figure 2-4 and as was explained, the movements in gas-liquid boundary are visible in this regime as gas-occupied and liquid-occupied regions repeatedly displace each other due to strong phase exchanges with innermost layers, i.e., towards bed center.



**Figure 2-3.** Dynamic variations of characteristic lengths for liquid (right) and gas (left) at four liquid superficial velocities.



**Figure 2-4.** Sequence of images taken for air and water system in the high interaction regime at  $U_{GS}=25.5$  cm/s and  $U_{GL}=19$  mm/s.

### 2.3.2 Onset of Flow Regime Transitions

In Figure 2-5, coefficients of variation of the liquid are plotted against liquid superficial velocities for three gas-liquid systems: air-water, argon-water and air-sucrose solution all at one superficial gas velocity, as an example. As depicted in the Figure, the maxima on each of the plots are points where transition from low interaction to high interaction flow regime takes place for that particular gas-liquid system. By comparing the curves for air-water and argon-water systems, one can sense the effect of gas density on the onset of flow regime transition. The exit pressure was 0.1 MPa while the entrance pressure was 0.85 MPa, 0.98 MPa and 0.96 MPa, respectively, for the air-water, argon-water and air-sucrose systems.

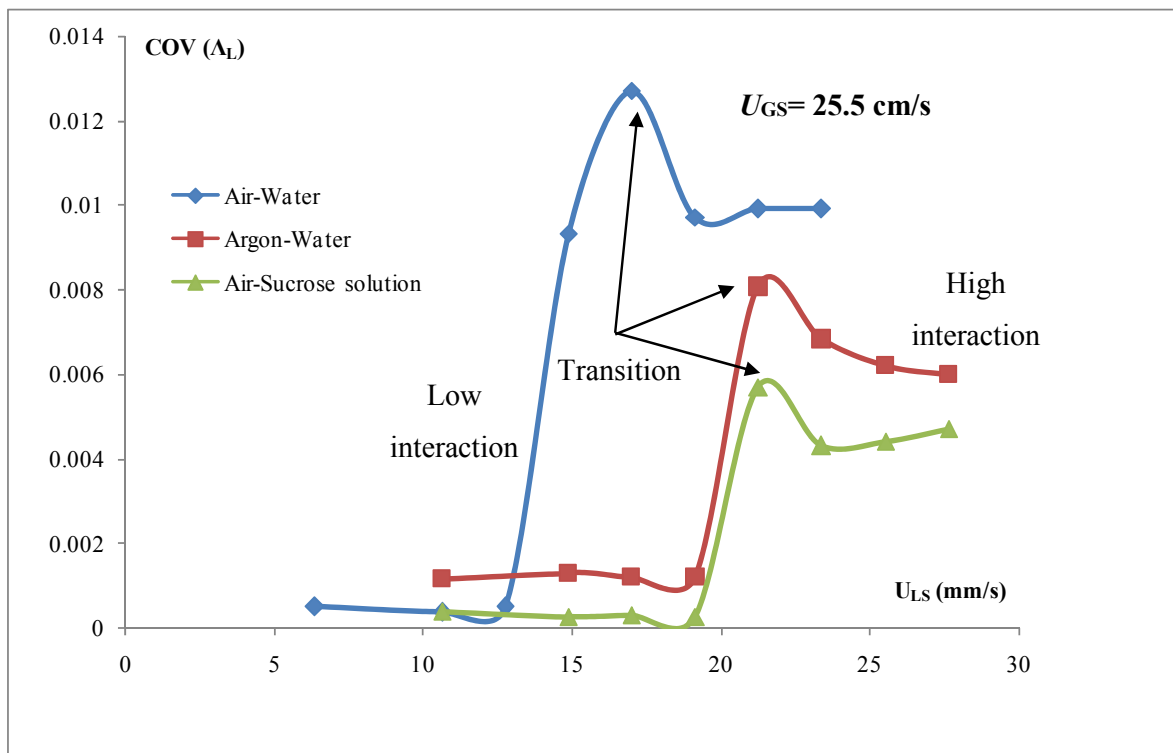


**Figure 2-5.** Coefficient of variation of liquid as a function of liquid superficial velocity and constant gas superficial velocity: Maxima on curves correspond to transitions from low to high interaction flow regime.

In macro-scale trickle beds, the low-to-high interaction flow regime transition at a given liquid (respectively gas) superficial velocity shifts toward higher gas (respectively

liquid) superficial velocities the higher the pressures (or the gas densities).<sup>34</sup> This makes trickle flow operating region in macro-scale trickle beds wider at elevated pressure. As stated by Attou and Ferschneider<sup>35</sup> increase in gas density leads to a decrease in inertial forces and therefore transition occurs at higher gas and liquid velocities. Hence, it appears that either the fact that the fluid dynamics, as captured nearby the wall, or the miniature scale of the micro-packed bed under study are at the origin of a similar trend. This behavior seems coherent with the precocious transition of air-water system with respect to that of argon-water system.

The effect of liquid surface tension on flow regime transition in macro-scale packed beds is due to variations of the capillary force exerted at the gas-liquid interface. That to what extent this statement is valid for micro-packed beds and if there are other phenomena contributing to flow regime transition at micro-scale requires more detailed studies on phase interactions at this scale. For example, as shown in Figure 2-5 at constant gas superficial velocity, relative decrease of surface tension by 17% appeared to have shifted the transition point to higher liquid superficial velocities (or equivalently higher superficial mass flow rates by considering the liquid densities in table 2-1) which is somewhat interesting and in contrast with the findings for macro-scale packed beds. As a matter of fact, the transition of low surface tension liquids was found to exhibit a very peculiar trend as higher liquid transitional velocities can also occur at higher, rather than at lower superficial gas velocities.<sup>36</sup> Such peculiarities are real and were observed on some data of Chou et al.<sup>37</sup> and of Clements and Halfacre.<sup>38</sup> Furthermore, since liquid viscosity for the sucrose solution is 92% larger than that of water (table 2-1), ascribing all the variability to solely liquid surface tension might be an overstatement. It is known that a significant drop of liquid transitional velocity in trickle beds accompanies an increasing liquid viscosity.<sup>36</sup> This is unlike what Figure 2-5 shows which is in favor of dominant effects driven by capillary forces than by viscous forces.

Based on the observations on flow regime transition as well as the statistical analysis stated above at various gas and liquid superficial velocities, it is possible to build up a flow regime map separating the low interaction and high interaction flow regimes for different gas-liquid combinations. Each of the maxima observed on Figure 2-5, representing the flow regime transition point, corresponds to one point on the flow regime map. Figure 2-6 shows

a flow regime map of such kind with Baker's flow parameter coordinates adopted from the work of Charpentier and Favier<sup>39</sup> as:

$$\lambda = \sqrt{\frac{\rho_G \rho_L}{\rho_{\text{air}} \rho_{\text{wat}}}} \quad (2-4)$$

$$\psi = \frac{\sigma_{\text{wat}}}{\sigma_L} \left( \frac{\mu_L}{\mu_{\text{wat}}} \right)^{1/3} \left( \frac{\rho_{\text{wat}}}{\rho_L} \right)^{2/3} \quad (2-5)$$

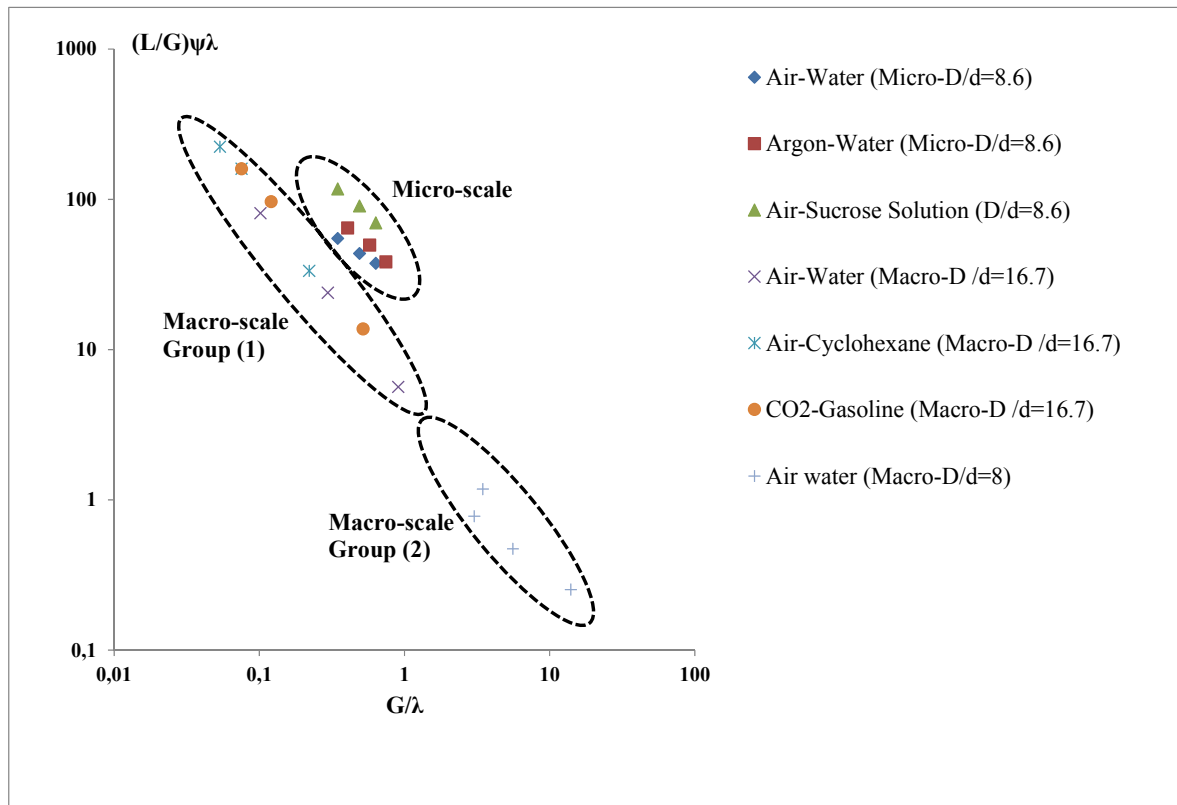


**Figure 2-6.** Comparative flow regime map based on Charpentier and Favier coordinates. Regions to the left of each group represent low interaction flow regime while regions to the right indicate high interaction flow regime. Results for macro-scale groups I and II are extracted from Charpentier and Favier (1975).<sup>39</sup>

As illustrated in Figure 2-6, and by comparing our experimental points with those obtained from the macro-scale counterparts, it can be observed that in micro-packed beds the

transition from low interaction to high interaction flow regime takes place at almost the same liquid-to-gas throughput ratios. Two groups have been depicted for macro-scale units: group (1) having larger column-to-particle diameter ratios than the current work (non-similar geometric ratios and group (2) corresponding to macro-scale setups with very close column-to-particle diameter ratios as this study. The comparison shows no considerable impact of scale on flow regime transition which might represent a benefit associated with using micro-packed beds from the perspective of process intensification (achieving the same conditions in a smaller system). This will enable researches (such as catalyst testing) to be performed at micro-scale packed beds (with much lower catalyst intake) at lower flow rates compared to macro-scale (though keeping the same flow ratio) and at nearly the same flow regime envelope as macro-scale units. The closeness of micro-scale transition points to those of macro-scale group (1) might suggest that the flow regime transitions are rather insensitive to column-to-particle diameter ratio.

Losey et al.<sup>7</sup> had also presented a flow regime map to show transitions from what they called “trickle to pulse flow regime”. Two issues are worth commenting from their contribution: first, the notion of “trickle” flow in micro-packed beds where gravitational forces have virtually no role in driving liquid flow across the micro-packed bed does not seem to be appropriate. Second, the pulse flow in their micro-packed bed is caused by flow instabilities due to the gas and liquid phases merging together upstream of the packed section meaning that its *ex situ* origin is somewhere upstream and outside the packed bed section which is obviously different from what is typically known as *in situ* pulse flow in packed beds.

### 2.3.3 Hysteresis

Hysteresis reflecting hydrodynamic multiplicity is a phenomenon normally observed in packed bed reactors showing itself as a difference in pressure drop, liquid holdup or wetting efficiency between flow increasing and decreasing modes of operation. There are many factors contributing to hysteresis in macro-scale packed beds including start-up procedures (dry/wet), packing sizes, presence of surfactants, porous/nonporous packing, operating flow ranges, gas flow rate, column diameters, and inlet liquid distributions.<sup>40</sup> Figure 2-7 depicts pressure drop measurements for air-water system in both imbibition

(increasing liquid superficial velocity, lower curve) and drainage (decreasing liquid superficial velocity, upper curve) modes at constant gas superficial velocity ( $U_{GS} = 25.5$  cm/s). Higher pressure drops observed for the drainage curve results from the higher liquid holdup in this path (since the bed is pre-wetted) which is in agreement with classic macro-scale packed beds (trickle beds). In contrast to Márquez et al.<sup>31</sup> who reported negligible hydrodynamic multiplicity in their micro-packed bed (column-to-particle diameter  $\approx 20$ ), a rather considerable pressure drop hysteresis is observed in the current work (column-to-particle diameter  $\approx 10$ ) with a maximum difference of nearly 2 bars between imbibition and drainage curves in the low interaction regime. In fact, despite the contributory role of liquid superficial velocity on the hysteresis occurrence, Márquez et al.<sup>31</sup> based their interpretations on a limited number of experimental points in a narrow range of liquid superficial velocities with its maximum being even less than where our hysteresis loop started.

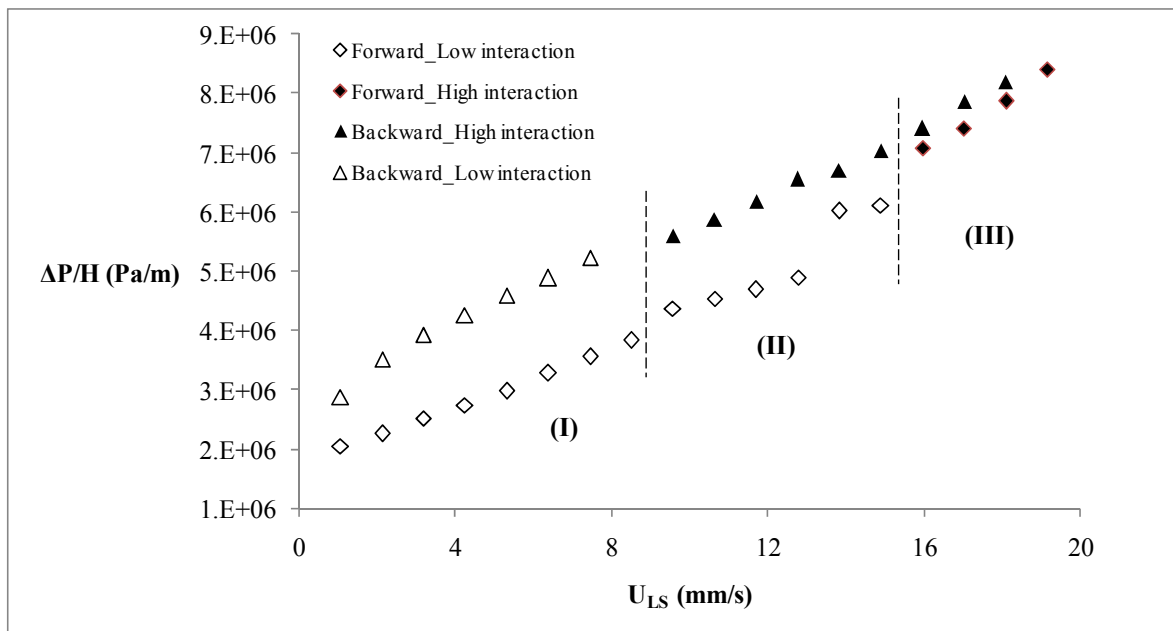


**Figure 2-7.** Two-phase flow pressure drop versus liquid superficial velocity at constant gas superficial velocity ( $U_{GS} = 25.5$  cm/s). Lower curve: ascending liquid velocity (imbibition or forward mode), upper curve: descending liquid velocity (drainage or backward mode).

As can be noticed from Figure 2-7, upon increasing liquid flow rate, pressure drop gradually increases until the transition from low interaction to high interaction flow regime occurs at  $U_{LS} = 16$  mm/s and continues up to end of the imbibition path. As the liquid velocity



starts to decrease from its maximum ( $U_{LS} = 19.2$  mm/s) on the drainage curve, it is interestingly observed that the flow regime transition point from high interaction to low interaction is shifted to lower liquid velocities extending the high interaction regime on the descending liquid velocity path. This can be due to liquid holdup increase in the drainage curve which makes the gas-liquid competition go on to lower liquid superficial velocities. Therefore, the pressure drop hysteresis loop can be divided into three zones from the flow regime transition point of view in both forward and backward curves: zone (I) with low interaction at both imbibition and drainage, zone (II) with low interaction on the imbibition and high interaction on the drainage curve and zone (III) where high interaction regime prevails for both operation paths.

Hysteresis is also evidenced in terms of the area fraction occupied (wetted) by the liquid phase as well as the wetting patterns in the bed texture within the low interaction regime. Figure 8 compares the wetted area percentages for time-averaged images of the bed for respective imbibition and drainage modes at different liquid superficial velocities (with constant gas superficial velocity of 25.5 cm/s). As expected from pressure drop hysteresis loop in Figure 2-7, it is observed from Figure 2-8 that the wetted area percentages are different in imbibition and drainage paths with higher wetted percentages in drainage as compared to imbibition path. Although this plot only compares wetted percentages in the wall region, it can be inferred from pressure drop hysteresis curve (Figure 2-7) that the same statement holds true for overall wetted volumes as well.

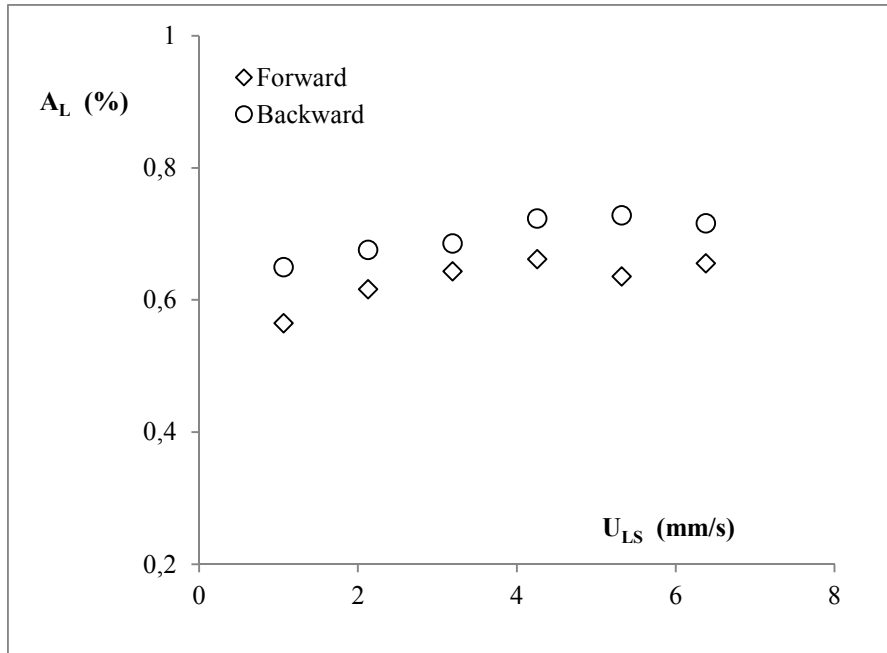


**Figure 2-8.** Fraction of liquid occupying bed texture nearby wall, as inferred from image analysis and processing, both in forward and backward conditions within zone (I) of pressure drop hysteresis curve.

It would be interesting to check if dry/wetted areas retain their status or there might be some changes in the wetting patterns distinguishing between drainage and imbibition modes. Figure 2-9 shows a comparison between the wetting patterns in imbibition (Figures 2-9.a and 2-9.c) and drainage (Figures 2-9.b and 2-9.d) modes at  $U_{LS} = 1.1$  mm/s and  $U_{GS} = 25.5$  cm/s. In Figures 2-9.a and 2-9.b, representing imbibition and drainage conditions, respectively, it can be seen that the distribution of wetted and dry regions are not quite identical for the two cases which is an indication of wetting pattern hysteresis. For the ease of analysis, wetted and dry regions are separated by image binarization (Figures 2-9.c and 2-9.d) where pixels labeled as 0 (black) represent wetted regions and those labeled as 1 (white) stand for dry regions. In order to identify areas that had undergone a change in wetting (either dry-to-wet or wet-to-dry), the images for imbibition can be subtracted from those of drainage so that the differences in wetting pattern could be visibly detected in the obtained difference image. The result is shown in Figure 2-9.e. One can verify simply by comparing the two binarized images that red color pixels indicate dry areas in the imbibition phase that became wet during drainage while blue colors represent the opposite behavior. Green regions also

signify areas that remained indifferent to the operation path and maintained their condition (either wet in both paths or dry in both paths).

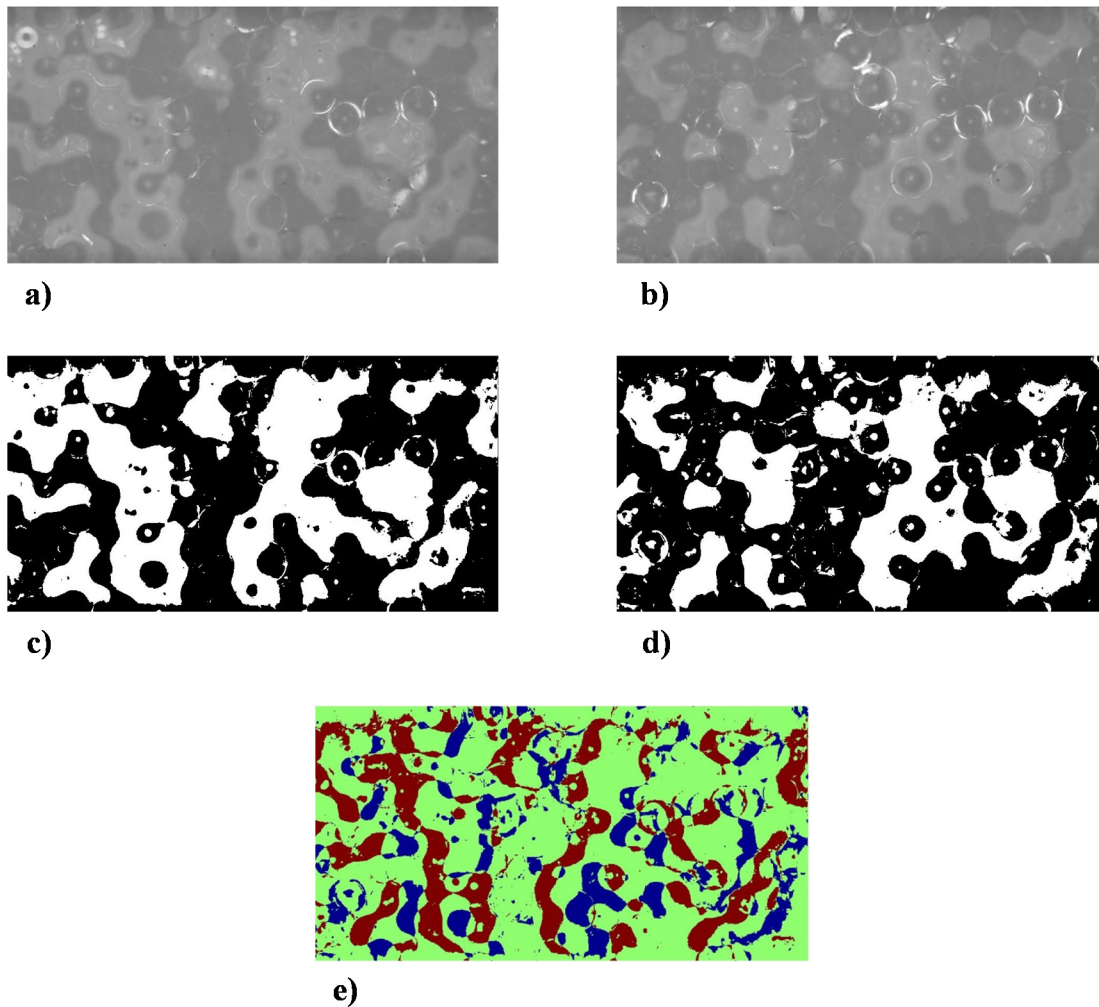


**Figure 2-9.** Comparison of the wetting patterns at the same gas and liquid superficial inlet velocities ( $U_{GS}= 25.5$  cm/s,  $U_{LS}= 1.1$  mm/s). a) original imbibition image, b) original drainage image, c) binarized imbibition image, d) binarized drainage image and e) comparative difference image of c) and d).

Difference images can be made for all liquid superficial velocities within the zone (I) (as shown in Figure 2-7) and the distribution of different wetted sections be plotted in a comparative scheme. The result is presented in Figure 2-10. It demonstrates that a major fraction of the bed texture remains unbiased with respect to imbibition and drainage modes of operation (green color). On the other hand, the fraction of the regions that were dry in imbibition and then became wet in drainage is slightly higher than the fraction of the regions

which followed the opposite trend. This behavior is in accordance with the nature of hysteresis in macro-scale packed beds in which wetting percentage is higher in drainage than in imbibition. Unbiased regions can be further divided into two zones with respect to remaining either constantly dry or constantly wet during the entire imbibition and drainage paths. Figure 2-11 shows the differentiation between these two zones. As can be observed, the tendency to remain wet is quite higher as compared to staying dry which is due to the capillary forces retaining the liquid phase within the pores of the micro-packed bed. At increased liquid superficial velocities, the ratio of the constantly wet region to constantly dry region increases gradually.

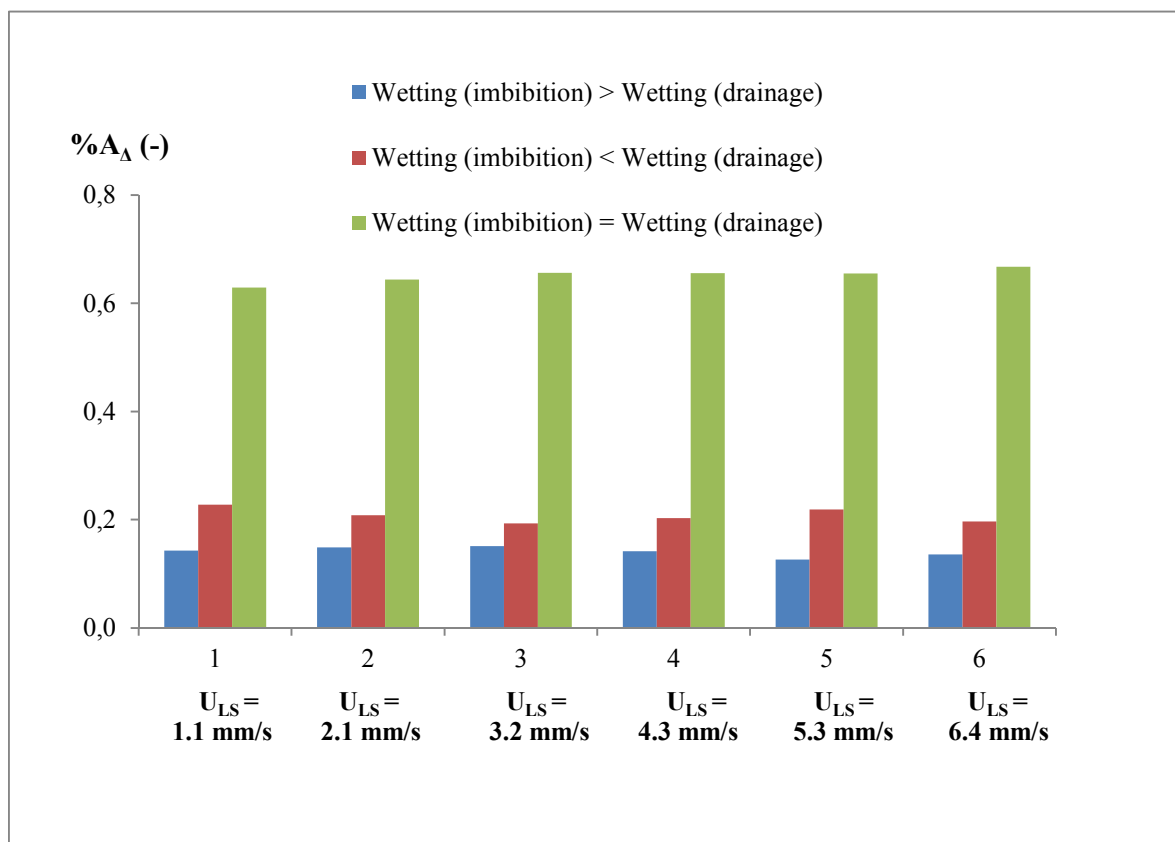


**Figure 2-10.** Fraction of liquid occupying bed texture in both forward and backward conditions within zone (I) of the pressure drop hysteresis curve.

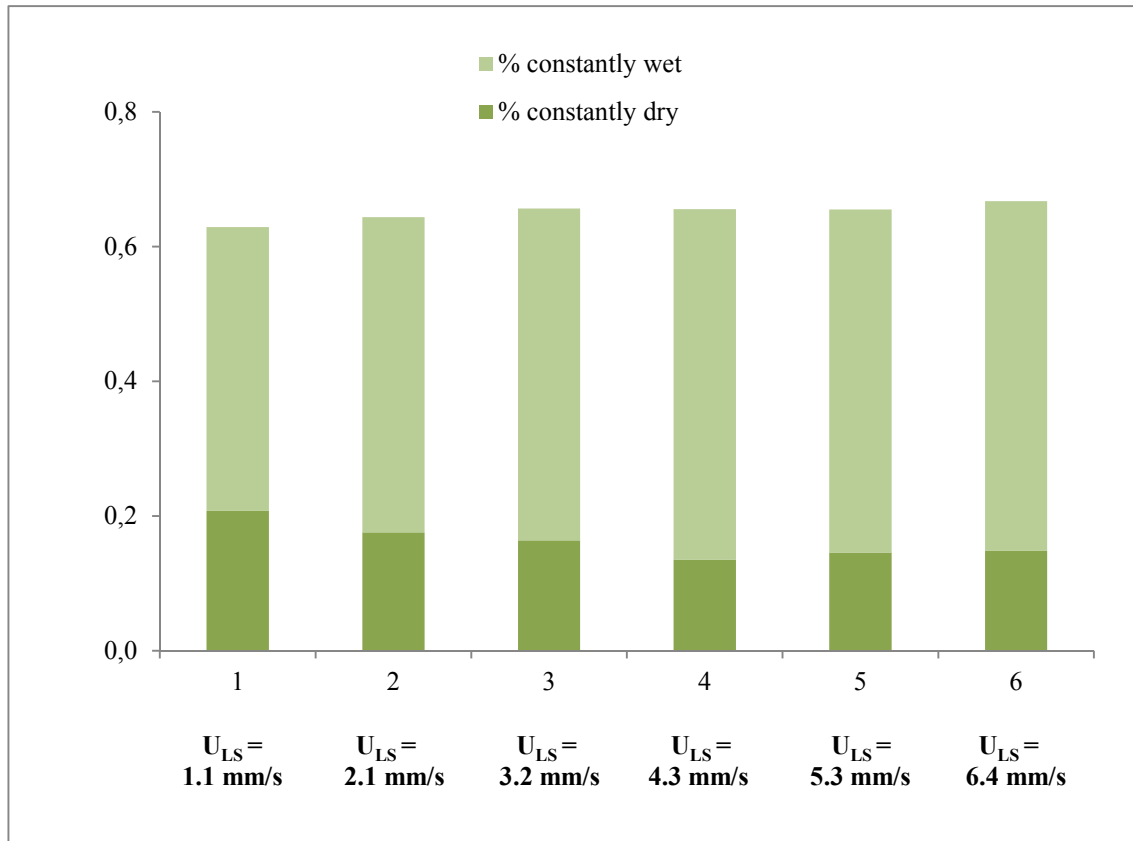


**Figure 2-11.** Comparative percentage of the indifferent regions (green parts of Figure 9) within zone (I) of the pressure drop hysteresis curve.

## 2.4 Conclusions

In the current work the hydrodynamics of micro-packed beds are investigated in terms of flow regimes, flow regime transition and hysteresis. The emphasis was mostly on microscopic visualization followed by processing the acquired images. Two major flow regimes were identified: low interaction flow regime with minor movements in gas-liquid boundary and high interaction flow regime characterized by rapid displacements of the gas and liquid phases causing fluctuations in the defined characteristic lengths. Statistically, the onset of flow regime transition could be identified by introducing the coefficient of variation of the liquid characteristic length. The results were employed to build a flow regime map demarcating regions for low and high interaction regimes. It was shown that flow regime

transitions occur at much lower liquid-to-gas throughput ratios in micro-packed beds than in their macro-scale counterparts. As for the hysteresis analysis, pressure drops measurements revealed important hydrodynamic non-unicity (or multiplicity) behavior especially in zone (I) where low interaction flow regimes prevail in both imbibition and drainage curves. Also, based on wetting pattern hysteresis three distinct regions were identified within the bed texture: 1) regions that were wet in the imbibition path and then became dry during drainage, 2) regions that were dry during imbibition path and which became wet upon drainage and 3) regions that retained their status (either wet or dry) regardless of the operation mode.

The current work carries the potential to be extended in two different directions in the future works. From one hand, by using appropriate methods such as matching the refractive indices of solid and liquid phases visualizations are enabled to be performed at layers beyond the wall region and into the core of the bed. On the other hand, the effect of using particles of various sizes on the onset of flow regime transitions as well as the hysteresis in the low interaction regime could be studied.

## 2.5 Nomenclature

$A$	Area occupied by either gas or liquid phase ( $L^2$ )
COV	Coefficient of variation
$G$	Superficial gas mass flow rate (Figure 6) ( $ML^{-2}T^{-1}$ )
$L$	Superficial liquid mass flow rate (Figure 6) ( $ML^{-2}T^{-1}$ )
$U_{GS}$	Superficial gas velocity ( $LT^{-1}$ )
$U_{LS}$	Superficial liquid velocity ( $LT^{-1}$ )

### Greek letters

$\Lambda$	Baker flow parameter, $\lambda = \sqrt{\frac{\rho_G}{\rho_{air}} \frac{\rho_L}{\rho_{wat}}}$
$\mu$	Dynamic viscosity ( $ML^{-1}T^{-1}$ )
$\bar{\mu}$	Arithmetic average
$\rho$	Density ( $ML^{-3}$ )
$\sigma$	Surface tension ( $MT^{-2}$ )
$\sigma^2$	Variance
$\psi$	Baker flow parameter, $\psi = \frac{\sigma_{wat}}{\sigma_L} \left( \frac{\mu_L}{\mu_{wat}} \right)^{1/3} \left( \frac{\rho_{wat}}{\rho_L} \right)^{2/3}$
$\Delta$	Difference
$\Lambda$	Characteristic length (L)

### Subscripts

G	Gas
L	Liquid

## 2.6 References

1. Van Gerven, T.; Stankiewicz, A., Structure, Energy, Synergy, Time-The Fundamentals of Process Intensification. *Industrial & Engineering Chemistry Research* **2009**, 48, (5), 2465-2474.
2. Jensen, K. F., Microreaction engineering - is small better? *Chemical Engineering Science* **2001**, 56, (2), 293-303.
3. de Mas, N.; Gunther, A.; Schmidt, M. A.; Jensen, K. F., Microfabricated multiphase reactors for the selective direct fluorination of aromatics. *Industrial & Engineering Chemistry Research* **2003**, 42, (4), 698-710.
4. Ajmera, S. K.; Delattre, C.; Schmidt, M. A.; Jensen, K. F., Microfabricated cross-flow chemical reactor for catalyst testing. *Sensors and Actuators B-Chemical* **2002**, 82, (2-3), 297-306.
5. Ajmera, S. K.; Losey, M. W.; Jensen, K. F.; Schmidt, M. A., Microfabricated packed-bed reactor for phosgene synthesis. *Aiche Journal* **2001**, 47, (7), 1639-1647.
6. Inoue, T.; Schmidt, M. A.; Jensen, K. F., Microfabricated multiphase reactors for the direct synthesis of hydrogen peroxide from hydrogen and oxygen. *Industrial & Engineering Chemistry Research* **2007**, 46, (4), 1153-1160.
7. Losey, M. W.; Schmidt, M. A.; Jensen, K. F., Microfabricated multiphase packed-bed reactors: Characterization of mass transfer and reactions. *Industrial & Engineering Chemistry Research* **2001**, 40, (12), 2555-2562.
8. Chen, J. F.; Chen, G. Z.; Wang, J. X.; Shao, L.; Li, P. F., High-Throughput Microporous Tube-in-Tube Microreactor as Novel Gas-Liquid Contactor: Mass Transfer Study. *Aiche Journal* **2011**, 57, (1), 239-249.
9. Su, H. J.; Wang, S. D.; Niu, H. N.; Pan, L. W.; Wang, A. J.; Hu, Y. K., Mass transfer characteristics of H<sub>2</sub>S absorption from gaseous mixture into methyldiethanolamine solution in a T-junction microchannel. *Separation and Purification Technology* **2010**, 72, (3), 326-334.



10. Wilhite, B. A.; Jensen, K. F.; Hill, T. F.; Velasquez-Garcia, L. F.; Epstein, A. H.; Livermore, C., Design of a silicon-based microscale trickle-bed system for singlet-oxygen production. *Aiche Journal* **2008**, 54, (9), 2441-2455.
11. Barajas, A. M.; Panton, R. L., The effects of contact-angle on 2-phase flow in capillary tubes. *International Journal of Multiphase Flow* **1993**, 19, (2), 337-346.
12. Triplett, K. A.; Ghiaasiaan, S. M.; Abdel-Khalik, S. I.; Sadowski, D. L., Gas-liquid two-phase flow in microchannels - Part I: two-phase flow patterns. *International Journal of Multiphase Flow* **1999**, 25, (3), 377-394.
13. Zhao, T. S.; Bi, Q. C., Co-current air-water two-phase flow patterns in vertical triangular microchannels. *International Journal of Multiphase Flow* **2001**, 27, (5), 765-782.
14. Akbar, M. K.; Plummer, D. A.; Ghiaasiaan, S. M., On gas-liquid two-phase flow regimes in microchannels. *International Journal of Multiphase Flow* **2003**, 29, (5), 855-865.
15. Cubaud, T.; Ho, C. M., Transport of bubbles in square microchannels. *Physics of Fluids* **2004**, 16, (12), 4575-4585.
16. Vandu, C. O.; Liu, H.; Krishna, R., Mass transfer from Taylor bubbles rising in single capillaries. *Chemical Engineering Science* **2005**, 60, (22), 6430-6437.
17. Yue, J.; Luo, L. G.; Gonthier, Y.; Chen, G. W.; Yuan, Q., An experimental investigation of gas-liquid two-phase flow in single microchannel contactors. *Chemical Engineering Science* **2008**, 63, (16), 4189-4202.
18. Jovanovic, J.; Rebrov, E. V.; Nijhuis, T. A.; Kreutzer, M. T.; Hessel, V.; Schouten, J. C., Liquid-Liquid Flow in a Capillary Microreactor: Hydrodynamic Flow Patterns and Extraction Performance. *Industrial & Engineering Chemistry Research* **2012**, 51, (2), 1020-1031.
19. Losey, M. W.; Jackman, R. J.; Firebaugh, S. L.; Schmidt, M. A.; Jensen, K. F., Design and fabrication of microfluidic devices for multiphase mixing and reaction. *Journal of Microelectromechanical Systems* **2002**, 11, (6), 709-717.

20. Wada, Y.; Schmidt, M. A.; Jensen, K. F., Flow distribution and ozonolysis in gas-liquid multichannel microreactors. *Industrial & Engineering Chemistry Research* **2006**, *45*, (24), 8036-8042.
21. Krishnamurthy, S.; Peles, Y., Gas-liquid two-phase flow across a bank of micropillars. *Physics of Fluids* **2007**, *19*, (4), 14.
22. Krishnamurthy, S.; Peles, Y., Two-phase flow pattern transition across micropillars: Size scale effect at the microscale. *Physics of Fluids* **2008**, *20*, (2), 6.
23. Krishnamurthy, S.; Peles, Y., Surface tension effects on adiabatic gas-liquid flow across micro pillars. *International Journal of Multiphase Flow* **2009**, *35*, (1), 55-65.
24. Kulkarni, A. A.; Gorasia, A. K.; Ranade, V. V., Hydrodynamics and liquid phase residence time distribution in mesh microreactor. *Chemical Engineering Science* **2007**, *62*, (24), 7484-7493.
25. Amador, C.; Wenn, D.; Shaw, J.; Gavriilidis, A.; Angeli, P., Design of a mesh microreactor for even flow distribution and narrow residence time distribution. *Chemical Engineering Journal* **2008**, *135*, S259-S269.
26. Boyer, C.; Duquenne, A. M.; Wild, G., Measuring techniques in gas-liquid and gas-liquid-solid reactors. *Chemical Engineering Science* **2002**, *57*, (16), 3185-3215.
27. Shao, N.; Gavriilidis, A.; Angeli, P., Flow regimes for adiabatic gas-liquid flow in microchannels. *Chemical Engineering Science* **2009**, *64*, (11), 2749-2761.
28. van Herk, D.; Kreutzer, M. T.; Makkee, M.; Moulijn, J. A., Scaling down trickle bed reactors. *Catalysis Today* **2005**, *106*, (1-4), 227-232.
29. Marquez, N.; Castano, P.; Makkee, M.; Moulijn, J. A.; Kreutzer, M. T., Dispersion and holdup in multiphase packed bed microreactors. *Chemical Engineering & Technology* **2008**, *31*, (8), 1130-1139.
30. Marquez, N.; Musterd, M.; Castano, P.; Berger, R.; Moulijn, J. A.; Makkee, M.; Kreutzer, M. T., Volatile tracer dispersion in multi-phase packed beds. *Chemical Engineering Science* **2010**, *65*, (13), 3972-3985.

31. Marquez, N.; Castano, P.; Moulijn, J. A.; Makkee, M.; Kreutzer, M. T., Transient Behavior and Stability in Miniaturized Multiphase Packed Bed Reactors. *Industrial & Engineering Chemistry Research* **2010**, 49, (3), 1033-1040.
32. Chaouki, J.; Larachi, F.; Dudukovic, M. P., Noninvasive tomographic and velocimetric monitoring of multiphase flows. *Industrial & Engineering Chemistry Research* **1997**, 36, (11), 4476-4503.
33. Aydin, B.; Larachi, F., Trickle bed hydrodynamics and flow regime transition at elevated temperature for a Newtonian and a non-Newtonian liquid. *Chemical Engineering Science* **2005**, 60, (23), 6687-6701.
34. Al-Dahhan, M.H.; Larachi, F.; Dudukovic, M. P.; Laurent, A., High-pressure trickle-bed reactors: A review. *Industrial & Engineering Chemistry Research* **1997**, 36, (8), 3292-3314.
35. Attou, A.; Ferschneider, G., A two-fluid hydrodynamic model for the transition between trickle and pulse flow in a cocurrent gas-liquid packed-bed reactor. *Chemical Engineering Science* **2000**, 55, (3), 491-511.
36. Larachi, F.; Iliuta, I.; Chen, H.; Grandjean, B.P.A., Onset of pulsing in trickle beds: Evaluation of current tools and state-of-the-art correlation. *Canadian Journal of Chemical Engineering* **1999**, 77, (4), 751-758.
37. Chou, T.S.; Worley, F.L.; Luss, D., Transition to pulsed flow in mixed-phase cocurrent downflow through a fixed bed. *Ind. Eng. Chem. Process Design & Development* **1979**, 16, (3), 424-427.
38. Clements, L.D.; Halfacre, G., Liquid composition and flow regime effects in gas and liquid downflow in packed beds. 72<sup>nd</sup> AIChE meeting, session 76, San Francisco, **1979**, pp. 25-29.
39. Charpentier, J. C.; Favier, M., Some liquid holdup experimental-data in trickle-bed reactors for foaming and nonfoaming hydrocarbons. *Aiche Journal* **1975**, 21, (6), 1213-1218.
40. Maiti, R.; Khanna, R.; Nigam, K. D. P., Hysteresis in trickle-bed reactors: A review. *Industrial & Engineering Chemistry Research* **2006**, 45, (15), 5185-5198.



### **3 Hydrodynamics of gas-liquid micro-fixed beds – Measurement approaches and technical challenges**

**Résumé** Malgré le grand nombre de domaines qui sont ouverts à l'étude hydrodynamique dans les microréacteurs à lit-fixe, effectuer des recherches dans ce domaine est principalement entravé par de nombreux défis expérimentaux. Ce travail fournit un résumé des défis techniques, problèmes et interprétations erronées qui pourraient être rencontrés dans la réalisation d'expériences hydrodynamiques sur les microréacteurs à lit-fixe. Certaines de ces questions seront soulignées lors de la comparaison des mesures de la distribution des temps de séjour (DTS) obtenus à l'aide de sondes de conductivité électrique à l'échelle du micro lit-fixe avec une méthode DTS obtenue près des parois par visualisation de l'élution d'un traceur coloré et le suivi dans le temps de la variation de l'intensité de niveau de gris des images. La moyenne latérale de l'intensité du niveau de gris aux deux extrémités, amont et aval, des zones d'intérêt près des parois, a servi comme section d'entrée et de sortie pour la méthode d'Aris des deux mesures. Le principal résultat de ce travail a été la confirmation expérimentale de la vitesse maximale du liquide dans la zone de forte porosité, proche de la paroi, prédite théoriquement. Enfin, les résultats expérimentaux de perte de charge et de saturation liquide obtenus en suivant rigoureusement les protocoles expérimentaux sont présentés.

**Abstract** Despite many areas that are open to investigation in the hydrodynamic study of micro-fixed bed reactors, conducting research in this field is mostly hampered by a number of experimental challenges that have made many attempts ineffectual. This work provides a summary of the technical challenges, problems and misconstrues one might encounter in performing hydrodynamic experiments on micro-fixed bed reactors. Some of these issues will be pointed out upon comparing classical residence time distribution (RTD) measurements through electrical conductivity probes at micro-fixed bed scale with near-wall RTD obtained via visualizations of dye-tracer elution and monitoring the changes in gray level intensity of the images. Laterally-averaged gray level intensity at both upstream and downstream extremities of the wall regions of interest acted as inlet and outlet curves for the Aris method. The major outcome of this work was experimental confirmation of theoretically predicted maximum liquid velocity in the high porosity zone close to the wall. Finally, the experimental results on pressure drop and liquid holdup obtained upon following the right experimental protocols are presented.

### 3.1 Introduction

The emergence of microreactors was the outcome of a worldwide demand for smaller, cleaner, safer and more energy efficient process units. High surface-to-volume ratios promote heat and mass transfer in these miniaturized units making them suitable for highly exothermic<sup>1</sup> and mass transfer limited reactions.<sup>2</sup> Due to small testing volumes and short residence times, they can also be employed safely for fast catalyst screening purposes to transfer laboratory results into production more rapidly.<sup>3</sup> The *numbering up* possibility for micro-structured devices is another feature which, although still in its infancy, has the potential to be applied in industry.<sup>4</sup> Today, on the other hand, chemical industries highly rely on multiphase catalytic reactions in which gas and liquid phases flow concurrently through a fixed bed of solids. This flow pattern provides efficient contact between the phases and thus has a wide variety of applications.<sup>5</sup> Having combined the pool of benefits for both microreactors and fixed bed reactors, micro-fixed beds (also known as micro-packed beds) are promising candidates to take the industry to the next level. This, in effect, led to a number of researches mainly focused on reaction engineering<sup>6,7</sup> and mass transfer<sup>2,8</sup> in microreactors each confirming their enhanced performance as compared to macro-scale units.

Even in micro-scale reactors, despite the advantages cited, there exist offsets from what is ideally expected in terms of conversion, mass transfer and so forth. These are attributed to deviations from the ideal fluid flow patterns and contacting schemes the extent of which could be addressed by hydrodynamic studies. Results of such analyses might bring modifications to the existing designs for boosted performance and efficiency. Micro-fixed bed reactors are no exception in this regard and thus, hydrodynamic experiments such as those performed on their macro-scale counterpart (trickle bed reactors) are required to measure (or determine) the hydrodynamic parameters including: pressure drop, liquid holdup, residence time distribution (RTD), etc. Also, microscopic visualizations can be utilized for flow regime studies and provide valuable information on the different contacting patterns between the phases. As for the hydrodynamic studies in this field, the attempt to perform RTD measurements for gas-liquid flow in micro-packed beds has been done by van Herk et al.<sup>9</sup> and later by Márquez et al. who performed RTD tests to determine liquid holdup in micro-packed beds using non-volatile<sup>10</sup> and volatile<sup>11</sup> tracers. Transient behavior of micro-

packed beds in several startup procedures was also investigated by Márquez et al.<sup>12</sup> and minor deviations in the achieved steady state were observed. In spite of the valuable insights that could be obtained by microscopic visualizations, studies of this kind such as flow regime investigations are quite scarce.<sup>13</sup>

It can be perceived from above that there is a huge research potential in this field and yet a dearth of experimental works and publications. This mainly stems from several challenges and problems that arise upon hydrodynamic study of micro-fixed bed reactors during experimentation phase precluding accurate and reliable experiments as compared to hydrodynamic tests on other types of microreactors such as micro-channels. There are a number of significant details in hydrodynamic studies of micro-fixed beds that have been either overlooked and caused successive failures or kept as the know-hows to the previous experimenters. Therefore, the authors' objective in this work is to reveal the bag of tricks gained through experience and following a cause and effect learning logic in this subject so that the prospective experiments on micro-fixed bed reactors could be performed as immaculately as possible. In what follows, the experimental setups and methodologies for both precise RTD studies and visualizations are described first along with useful and detailed guidelines for implementation. Afterwards, the results demonstrate the major challenges during experimentation by illustrations drawn from problematic and/or modified experiments, wherever necessary. Finally, a number of experimental results on pressure drop and liquid holdup obtained by committing to the correct experimental procedures are presented.

## **3.2 Experimental section**

### **3.2.1 Microreactor packing procedure**

Micro-reactor packing is one of the crucial steps which, if done correctly, ensures reproducibility and reliability of the experimental results. Particles could be easily loaded inside the micro-tube through a handmade tiny metal funnel within multiple steps in each of which a certain portion of the total bed volume is loaded with particles. Frequent tappings are required between the steps to completely densify the bed. Loose packings will adversely affect reproducibility of the experiments (especially in case of pressure drop measurements)



and once the gas and liquid are both fed, gaps may start to develop at different locations within the length of packed bed or flow instabilities upstream of the bed might occur and halting the experiment would be inevitable.

### **3.2.2 RTD setup fabrication and methodology**

High-pressure gradients within the length of micro-fixed bed reactors (in the order of  $10^3$  kPa/m) necessitate materials for fabrication that could withstand elevated pressures without mechanical failure and subsequent leakages. If microscopic visualizations are not intended (such as in RTD measurements), walls of micro-fixed beds could be made of thick glass or even metals whereas in case of visualizations (e.g., for flow regime studies<sup>13</sup>) the walls should only be made of transparent pristine materials that might be mechanically strengthened by methods such as etching.<sup>14</sup> Installation of electric conductivity probes in the walls of those micro-fixed beds that are utilized for RTD studies was first inspired by the conductivity ring electrodes commonly used for macro-scale packed beds.<sup>15</sup> Figure 3-1 (left) shows a schematic of such micro-ring electrodes constructed through inserting perforated metal plates within lateral cuts across the reactor wall and fixed by applying a layer of epoxy glue around it. However, this appeared to be one of the major challenges for the authors as high pressure gradients increase the risk of fluids leakage which led to a series of failures in RTD experiments. As a consequence, the design was modified by inserting two point electrodes (instead of rings) via two holes drilled in micro-reactor wall without causing perturbations in the main flow and applying epoxy glue for fixing them as illustrated in Figure 3-1 (right) (and Figure 3-2). Subsequent experiments proved the efficiency of this modification and no leakage was observed.

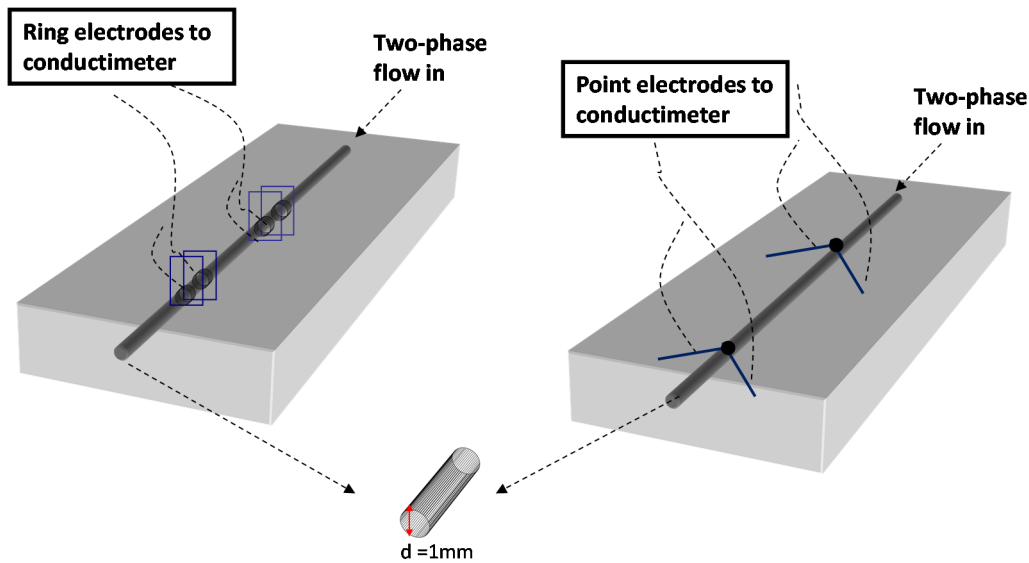


**Figure 3-1.** Two types of electrode configuration proposed for for RTD measurements. Old design of ring electrodes (left) and new design of point electrodes (right) installed on microreactor.

The experimental setup for RTD studies is shown in Figure 3-2. Three gases (Argon, Air and Hydrogen) were tested versus water (with a tinge of NaCl dissolved) as the liquid. Gas and liquid phases flow co-currently through a 1mm (ID) circular glass tube packed with nearly monodisperse glass beads of two different size ranges (53-63)  $\mu\text{m}$  and (106-125)  $\mu\text{m}$ . Liquid delivery to the bed is enabled by a syringe pump (Teledyne ISCO, 500D) while gas is fed via a mass flow controller (EL-Flow Bronkhorst). Gas and liquid phases are brought into contact by a T-junction located upstream of the packed bed consisting of a coaxial arrangement. Liquid passes through the inner tube while the gas flows within the annular area between liquid line and the outer tube. To avoid flow instabilities within the bed caused by fluid initial maldistribution, the first contact between the two phases should take place at the start of the packed bed. This will be discussed in detail in section 3.6.2. By placing a stainless steel grid at the reactor exit, it is ensured that solid phase stays put upon two-phase flow experiments. Pressure drop measurement is performed between the gas-feed line (inlet section) and bed outlet via a piezoelectric differential pressure transducer.

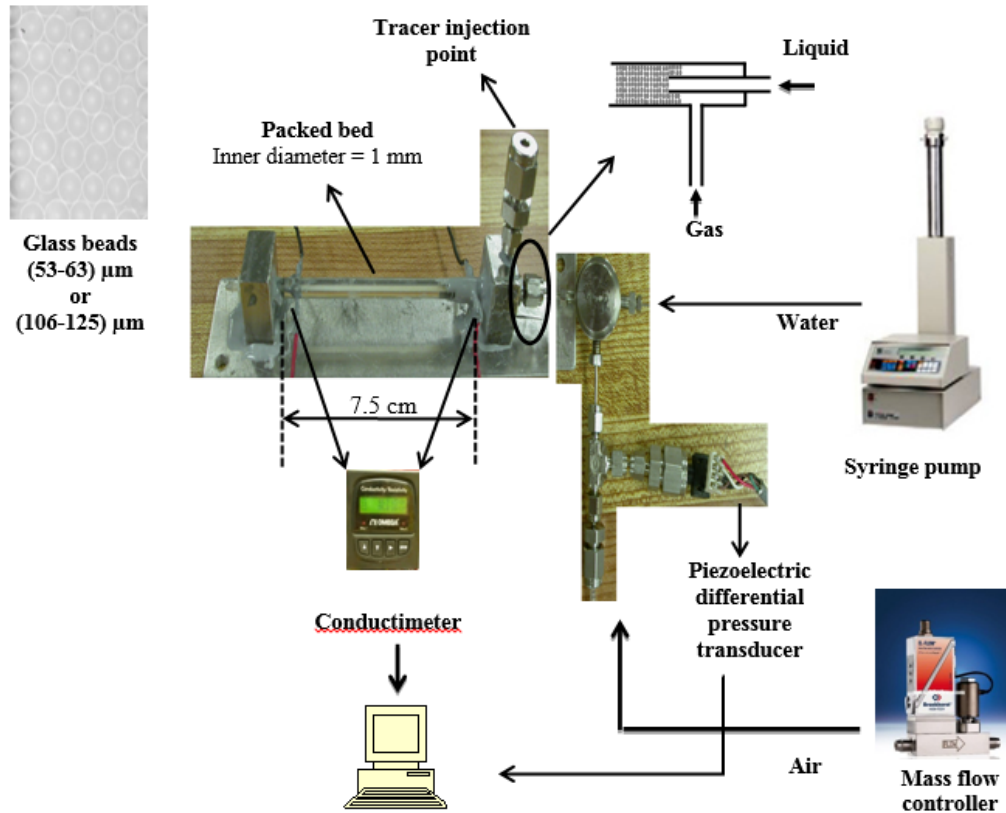


**Figure 3-2.** Experimental setup of the micro-fixed bed reactor for RTD and holdup determination

For RTD and liquid holdup determination, Aris's impulse method has been employed in the current experimental setup according to similar works relying on linear correlation of conductivity and ion concentration for NaCl solutions (Kohlrausch law).<sup>16</sup> Small and equal amounts (0.2  $\mu\text{L}$ ) of 3M NaCl solution were injected at the start of the packed bed without causing perturbations or viscosity alteration in the main liquid flow.<sup>17</sup> A manual syringe (Agilent Technologies, Inc) was used for the injection. To avoid potential leakages during injection, syringe needle passes through a septum incorporated at the injection point. Two sets of electric conductivity probes each placed at one end of the packed bed and yet downstream of the tracer injection point, transfer the response signals to a conductimeter (Omega model CDCN-91) as the measuring device. The data are also registered on-line by means of a data acquisition system. Injections at each set of gas and liquid flowrates were repeated at least three times to ensure reproducibility. Analysis of the responses entails estimations of liquid space time,  $\tau$ , (which could be translated into liquid holdup) and liquid

Péclet number (indication of axial dispersion). For this purpose, the plug flow model with axial dispersion (PD) and open-open boundary conditions was used and the above two parameters were estimated by a non-linear least-squares fitting between the outlet measured signal and the RTD-convoluted simulated outlet signal.<sup>16</sup> It is noteworthy to mention that using pure water as the liquid phase in the very initial RTD experiments led to peculiar behaviors in both inlet and outlet signals as shown in Figures 3-3.a and 3-3.b. The conductivity meter is unresponsive below a certain threshold; therefore, quite small amounts of NaCl (0.6 gr per liter) was added to the feed to move the baseline above the sensitivity limit of the conductivity meter.

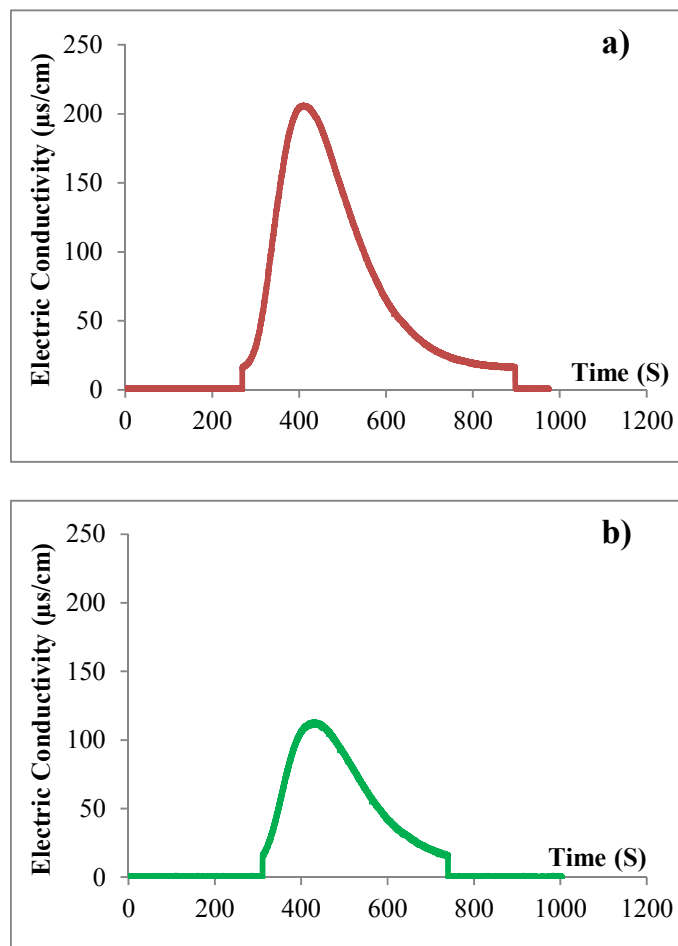


**Figure 3-3.** Conductivity signals for the inlet (a) and outlet (b) upon using pure water as the liquid phase  $U_{GS}=21.3$  cm/s,  $U_{LS}=1$  mm/s

In another methodology different to ours, Márquez et al.<sup>10</sup> used dye tracer injection in the liquid feeding line upstream of the packed bed and single detection of the signal via refractometer downstream of the packed bed. Since the assumption of imposing an ideal pulse tracer to the micro-fixed bed reactor does not appear realistic, RTD results drawn from single detection of the signal are not likely to reflect the actual hydrodynamic behavior of micro-fixed bed. However, downstream *double* detection of the signal has the advantage of obtaining more precise RTDs from the two sets of conductivity probes by signals deconvolution whether or not the initial pulse injection is ideal.

Furthermore, employing refractometers for signal measurement as described by Márquez et al.<sup>10</sup> has the drawback of phase separation as a prerequisite for RTD measurement in that the gas-liquid flow leaving the micro-fixed bed is passed through a phase separator (membrane-type) and the separated liquid phase flows through the refractive index flow cell. This phase separator has a substantial contribution in the spread of the E-curve for which the assumption of linearity has yet to be experimentally verified. However, this problem of uncertainty is virtually surpassed upon in-situ RTD measurement using two sets of conductivity probes and conductimeter.

### **3.2.3 Visualization setup and methodology**

To perform visualization studies with the setup shown in Figure 3-4, air and water are fed (in the same way as above) to a micro-reactor consisting of transparent borosilicate tube with square cross-section ( $D_H=1$ ,  $H=11.5$  cm, wall thickness = 0.4 mm) packed with spherical glass beads of 106-125  $\mu\text{m}$  in diameter. The bed has optically accessible windows for microscopic visualization while the rest of tube was inserted in carved plexiglass block such that the bare parts of the tube are protected against any inadvertent stroke. The micro-packed bed is mounted on an inverted microscope (Olympus GX-51) and visualized through a 10X objective lens (MPlanFLN-BD series) with a working distance of 6.5 mm. Before any visualization attempt, the wall thickness of micro-fixed beds should be chosen in accordance with the working distance of the available objective lens (e.g., increased thickness entails the use of objectives with higher working distance). The microscope is coupled with a camera (TSI, PowerView<sup>TM</sup> Plus) which is itself connected to a computer with a frame-grabber port and image acquisition is performed using Insight3G software. Upon reaching a constant

pressure drop at each set of experiments, a set of 150 images were taken at 15 Hz rate from the bed to see how the phases interact at the wall vicinity. It should be noted that in image acquisition process only the bed wall region can be observed with inverted microscopy and all the results and interpretations drawn from image processing are related to this range.

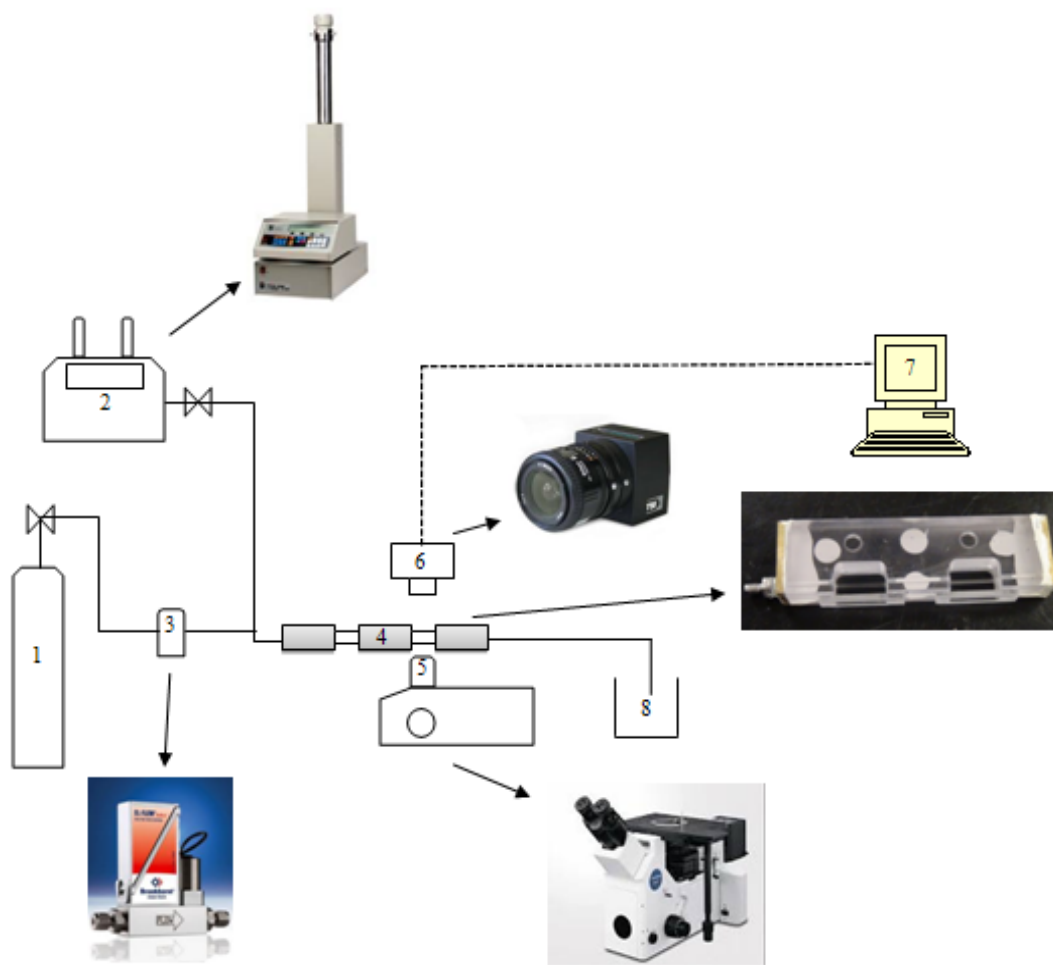


**Figure 3-4.** Experimental Setup for visualization experiments: 1) Gas cylinder 2) Syringe pump 3) Gas mass flow controller 4) Micro-reactor 5) Inverted Microscope and Objective lens 6) Camera with frame grabber port 7) Computer for image acquisition 8) Drainage

The acquired images at each stage are processed using MATLAB image processing toolbox. Since processing of the acquired images is based on the gray level intensity analysis of the pixels within each image, the intensity of light from the microscope to the microreactor shall be kept constant throughout the entire experiments. Processing of images includes

cropping the edges to remove the blurs observed at the wall boundary due to curvature, pre-processing operations to obtain images with a smooth gas-liquid boundary and finally performing the gray scale thresholding and binarization to separate the regions occupied with gas (brighter regions) and liquid (darker regions) phases as done in our previous work.<sup>13</sup> The weighted mean area of the liquid phase ( $\Lambda_L$ ) can be used to define its characteristic length.

In another task, as delineated in Figures 3-5 and 3-6, an innovative approach was implemented for the first time and wall visualizations along with image processing were used to determine RTD in micro-fixed beds by injecting a dye tracer at the start of the bed packed with (106-125)  $\mu\text{m}$  particles and monitoring the changes in the gray level intensity of the images taken (150 images) within a frame downstream of the injection point. Two different methods are employed: 1) Assuming an ideal pulse injection of dye and monitoring the changes in overall averaged grayscale value of the pixels within the entire image (Figure 3-5) and 2) dye injection and monitoring the changes in laterally-averaged gray level intensity at both left and right extremities of the pictures (Figure 3-6). The distance between the left and right extremes in the acquired images is 1881 pixels (1.34 mm upon calibration) which could be virtually imagined as two probes located 1.34 mm apart from each other.

The RTD curves obtained in both methods will exhibit minima rather than maxima that are commonly observed in RTD tests. This is due to the nature of image processing in MATLAB which ascribes lower grayscale values on the pixels that become darker (as a result of dye injection). To convert the signals into those showing maxima, the complementary value of each pixel has been calculated (by subtracting each pixel value from 256 as the maximum pixel grayscale value) and the results are redrawn. Illustrative examples of the curves showing minima and maxima in method 2 (mentioned above) are presented in Figures 3-7.a and 3-7.b, respectively.

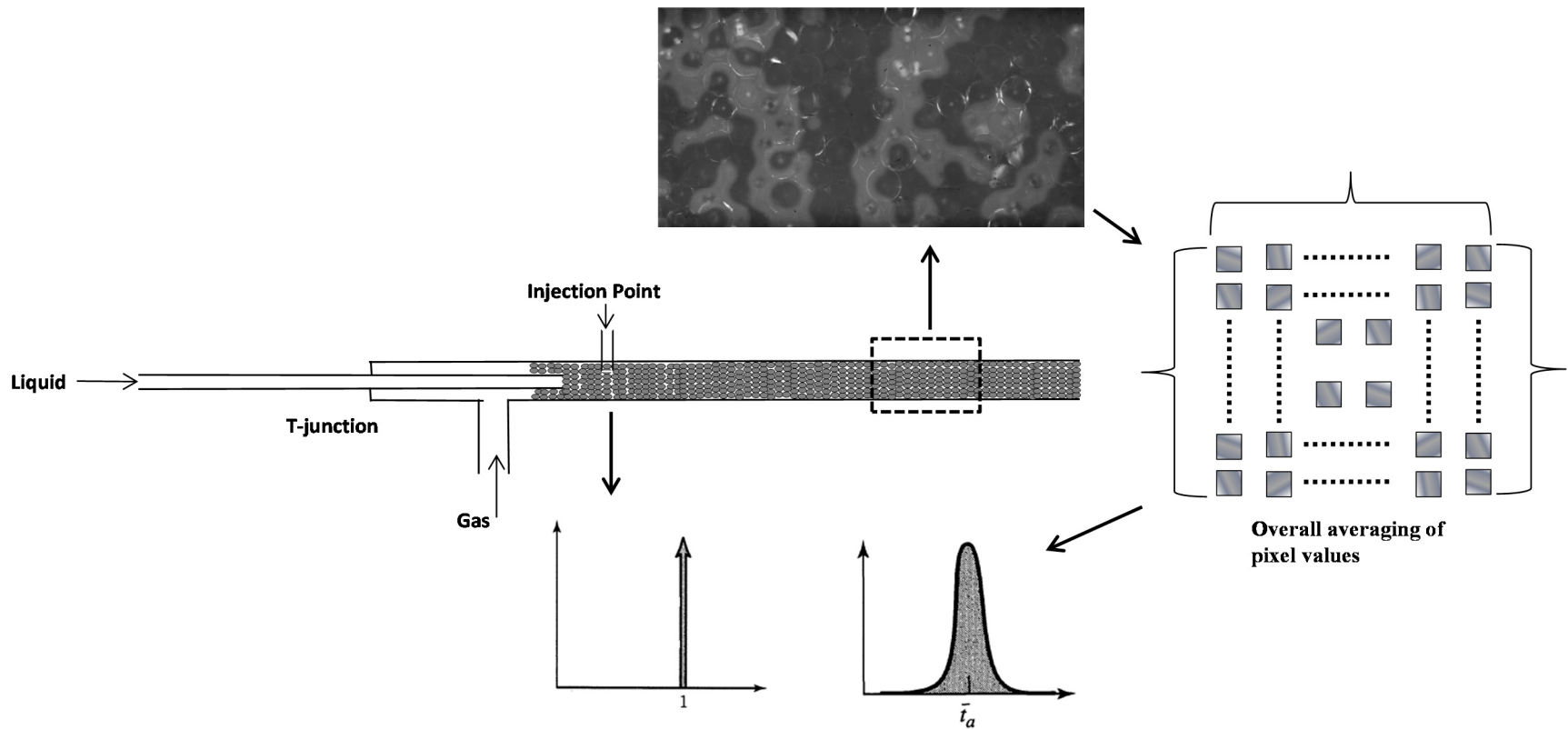


**Figure 3-5.** Schematics of method 1 for RTD determination by microscopic imaging and dye injection (assuming ideal pulse injection) and monitoring the overall-averaged pixel values within the image ( $U_{GS} = 10.6$  cm/s and  $U_{LS} = 1.6$  mm/s)



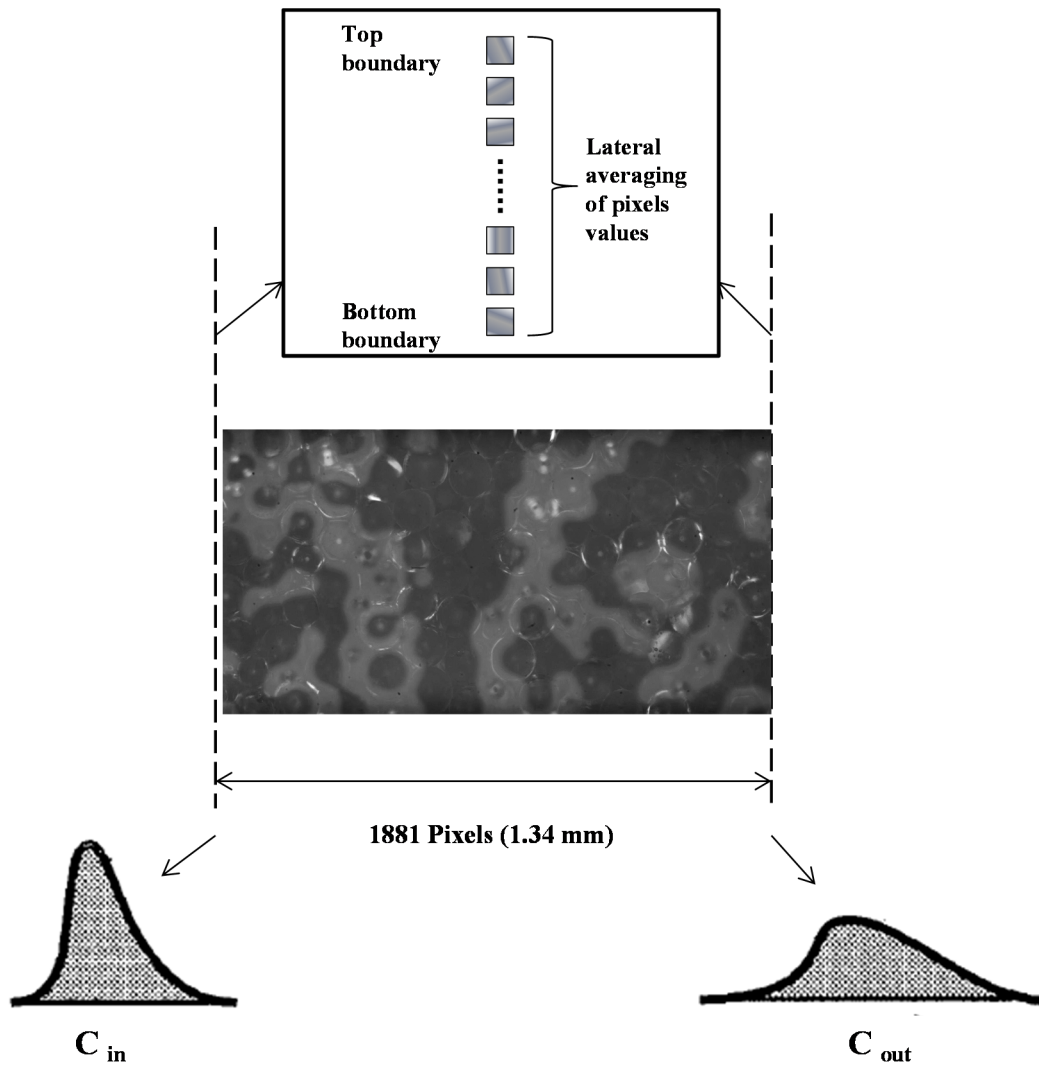


**Figure 3-6.** Schematics of method 2 for RTD determination by microscopic imaging and dye injection by double detection and monitoring of the laterally averaged pixel values at the two left and right extremes of the image ( $U_{GS}= 10.6$  cm/s and  $U_{LS}= 1.6$  mm/s)

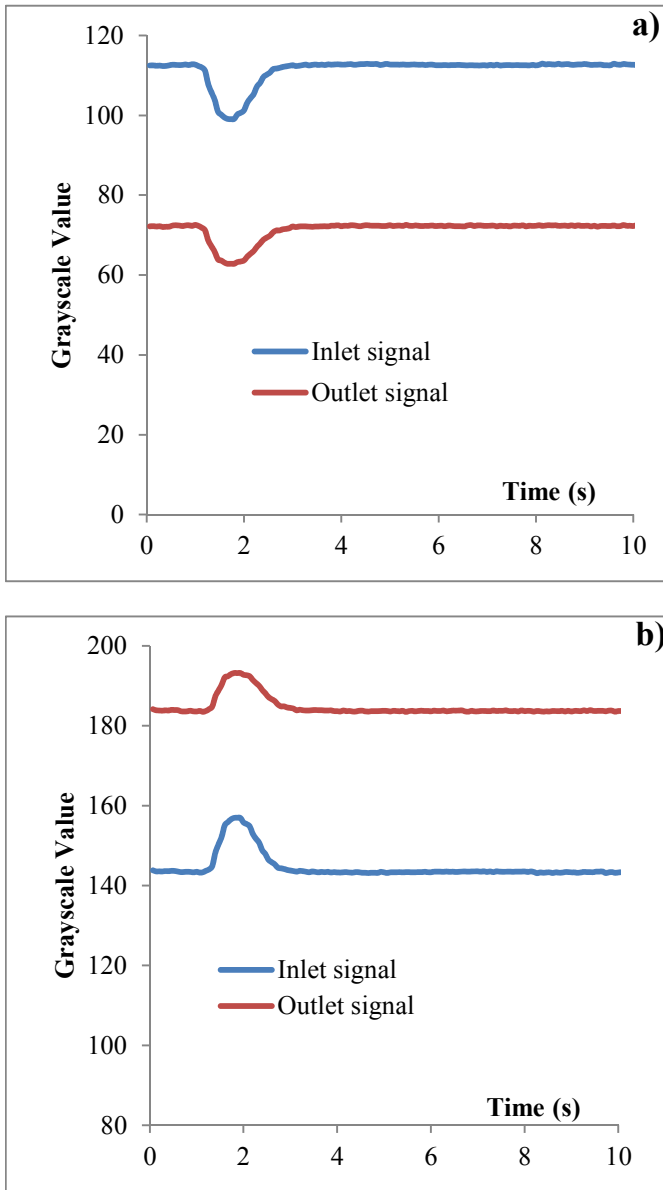


**Figure 3-7.** Illustrative example of inverting the initially obtained RTD curves from microscopic imaging and dye injection into those commonly used. a) Initially obtained curves showing minima b) Inverted curves showing maxima.

### 3.3 Results and discussion

#### 3.3.1 Effect of tracer input location

Choosing the right point for tracer injection was found to be a challenge in RTD studies for which the final configuration, as shown in Figure 3-2, had to be decided through

experimentation. Figure 3-8 pictures two locations that were initially thought out for tracer injection: 1) in liquid phase line and upstream of the micro-fixed bed before gas-liquid contact (Figure 3-8.a) and 2) in micro-fixed bed reactor after gas-liquid contact within the bed (Figure 3-8.b). Theoretically, the entire arrangement in the former case could be considered virtually as one single phase micro-channel (liquid feed line) put in series with one multiphase micro-fixed bed and hence, when tracer is injected in the liquid feeding line, axial dispersion in the single-phase liquid tube (upstream of the micro-fixed bed) broadens the pulse-like injection signal before it enters the micro-fixed bed. Therefore, the results drawn from RTD curves in this case would not represent solely the micro-fixed bed reactor. To avoid this complexity, Figure 3-8.b was proposed as an alternative to the location of tracer input where injections are made downstream of the gas-liquid merging point within the packed section.

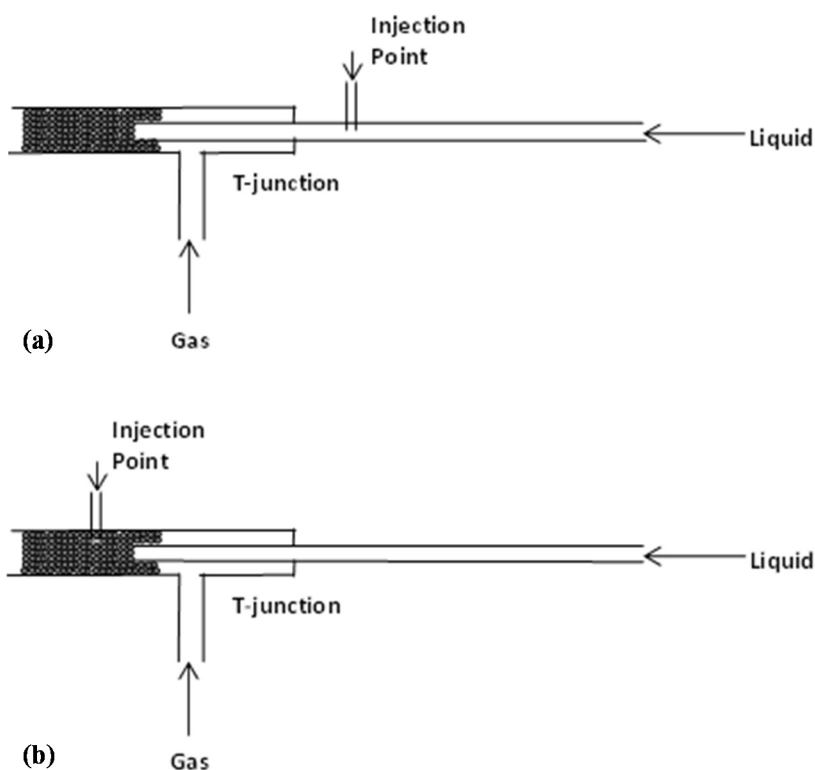


**Figure 3-8.** Two alternatives for tracer injection during hydrodynamic test on micro-fixed bed reactors. a) in liquid phase before gas-liquid contact b) in packed bed after gas-liquid contact

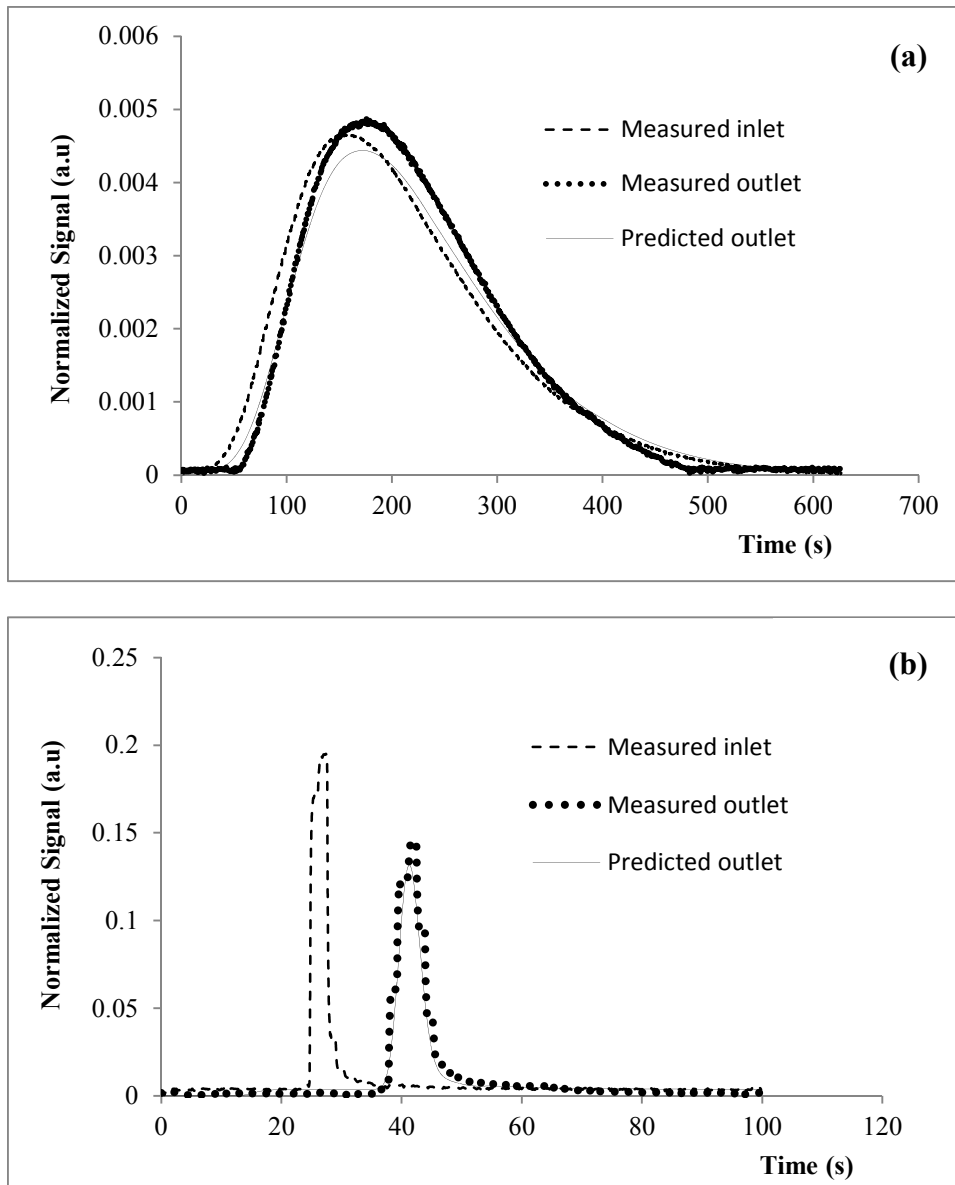


**Figure 3-9.** Experimental inlet and outlet electrical conductance response curves with the fit of outlet response using a two-parameter PD RTD model for two cases: a) tracer injection in the liquid feeding line b) tracer injection in the packed bed downstream of the gas-liquid merging point. ( $U_{GS} = 21.3$  cm/s and  $U_{LS} = 1$  mm/s for both cases)

Both configurations were experimentally tested while other parameters such as fluids flow rate, packing size, micro-fixed bed length, etc. have been kept unaltered and the results are compared in Figure 3-9. As can be observed in Figure 3-9.a, where tracer is injected in the liquid feed line (6cm upstream of micro-fixed bed reactor), there is a rather complete interference between the inlet and outlet signals. Upon performing the least-squares fitting for RTD calculations, as explained earlier, a value of  $P_{\text{EL}} = 2.5$  was calculated indicating a

high degree of dispersion which sounded unlikely at such scale. This gave rise to the hypothesis that the interference of signals could contribute to the false estimation of liquid Péclet number by curve fitting algorithm. On the other hand, Figure 3-9.b demonstrates the results of the experiments conducted by using the configuration in Figure 3-8.b in order to verify the hypothesis. The new arrangement led to an accurate curve fitting for the outlet signal and a massive change in liquid Péclet number ( $PéL > 100$ ) indicating plug flow behaviour within micro-fixed bed. The RTD tests carried out by Márquez et al.<sup>10</sup> also adopts the method in Figure 3-8.a for tracer injection which is arguably not an appropriate one as explained above. Moreover, a careful examination of both measured outlet signal curve in Figure 3-9.a and the one for 7-cm column obtained by Márquez et al.<sup>10</sup> reveals that they would be similar to each other in terms of spread if plotted on the same time scale.

### 3.3.2 Misconstrue in flow regime designation

Upon feeding the micro-fixed bed reactor with gas and liquid phases during microscopic observations, wall visualizations reveal that two main types of flow regimes (*low interaction* and *high interaction*) prevail depending on the ratio of gas-to-liquid flow rates for which there are methods enabling characterisation and demarcation as shown in our previous work.<sup>13</sup> There are sporadic cases in visualization, however, in which a seemingly high interaction flow regime is observed at gas-to-liquid ratios that in fact correspond to the low interaction flow regime according to several repeated experiments. Figure 3-10 shows a sequence of four images taken from the wall region of the bed at such condition ( $U_{LS} = 16 \text{ mm/s}$ ,  $U_{GS} = 21.3 \text{ cm/s}$ ) in which brighter and darker regions represent gas and liquid phase, respectively. As can be viewed, at  $t = 0 \text{ s}$  (and  $t = 1.8 \text{ s}$ ) gas and liquid phases have a specific share of the bed while at  $t = 0.6 \text{ s}$  (and  $t = 2.4 \text{ s}$ ) a pulse of liquid phase sweeps away parts of the gas phase. Binarized images are also depicted.

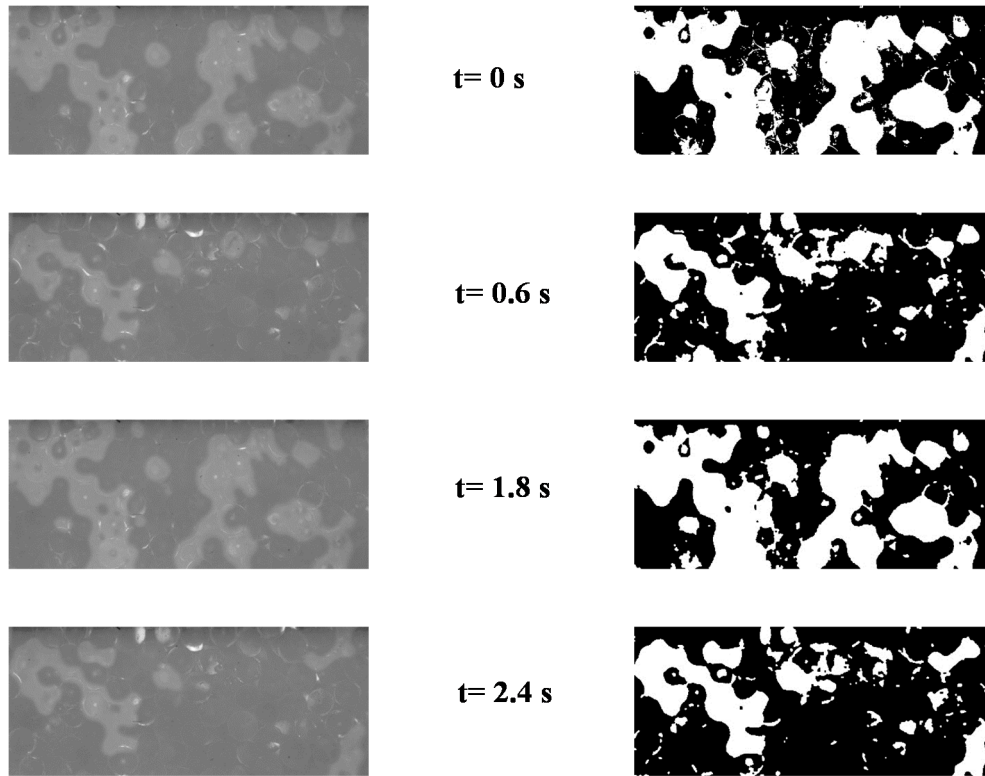


**Figure 3-10.** Sequence of four images taken for air and water system in during flow instability at  $U_{GS}= 21.3$  cm/s and  $U_{LS}= 1.6$  mm/s (left) and the binarized images (right).

This can be attributed to flow instabilities (as reported by Losey et al.<sup>2</sup>) caused by the void space existing upstream of the packed bed allowing an early competition between gas and liquid phase in this region before they reach the packed bed itself. The flow instabilities can also be illustrated in terms of fluctuations observed in the dimensionless liquid phase characteristic length as in Figure 3-11.a where  $d_p$  is the solid particle diameter. Peaks in the Figure represent instances where pulses of liquid pass through and sweep away major parts of the gas phase leading to a sudden increase in the liquid phase characteristic length. On the opposite, dense packing by the procedure mentioned in section 3.2.1 results in a rather monotonic behavior in liquid phase characteristic length (Figure 3-11.b). Observations of this type of instability could also be cross-validated by using the circular micro-fixed bed equipped with conductivity probes.

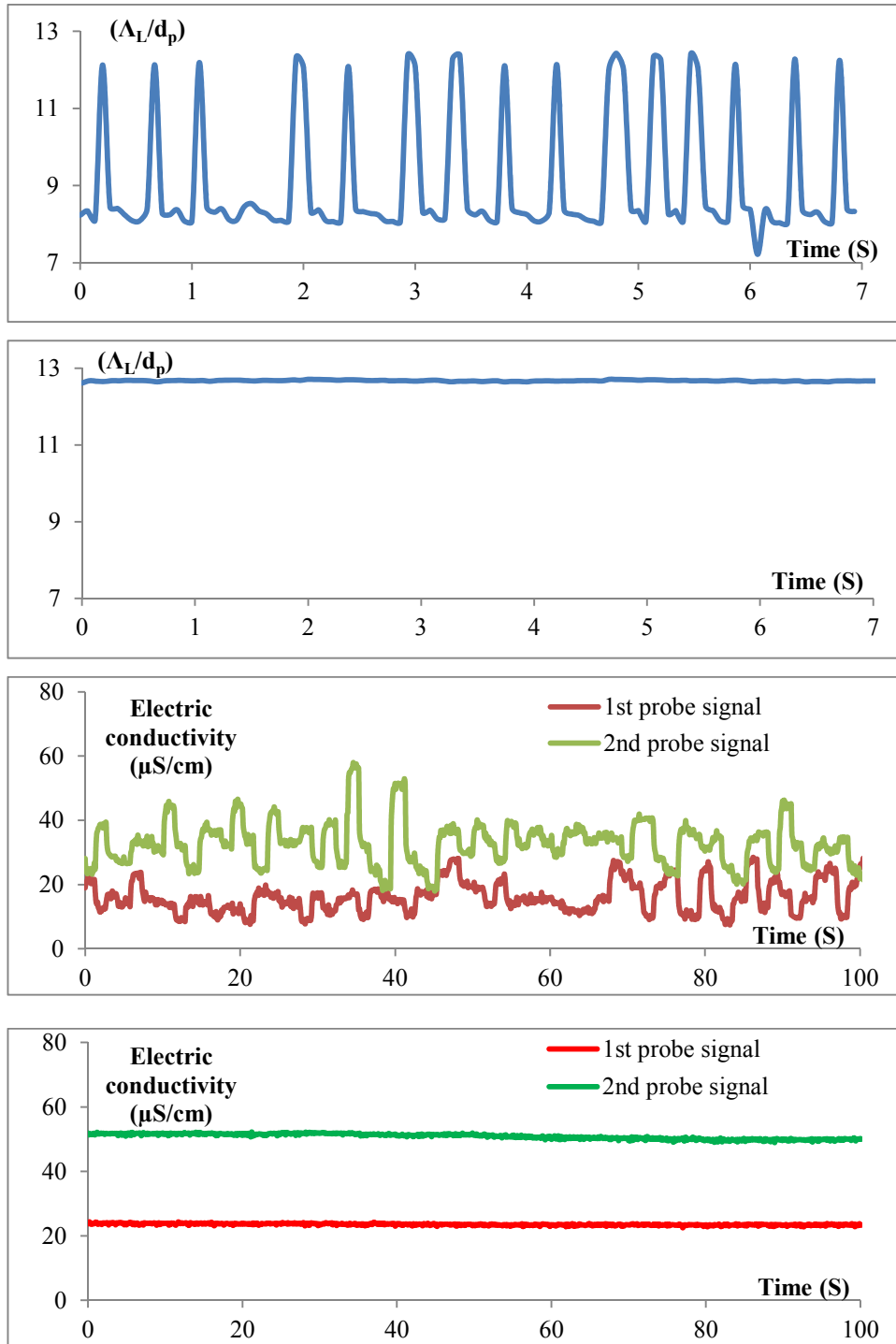


**Figure 3-11.** Variations in dimensionless liquid phase characteristic length (a,b) and electric conductivity (c,d) at  $U_{GS}= 21.3$  cm/s and  $U_{LS}= 1.6$  mm/s. a) dimensionless liquid phase characteristic length during flow instabilities due to loose packing b) dimensionless liquid phase characteristic length in dense-packing c) electric conductivity signals during flow instabilities due to loose packing d) electric conductivity signals in dense-packing

Figure 3-11.c shows the same fluctuations on both electric conductivity signals recorded by the first and second sets of probes can be seen when the micro-reactor is not densely packed (which makes RTD measurements impossible due to lack of a stable baseline) while Figure 3-11.d illustrates same signals upon dense packing. Conductivity signals appear to be more fluctuating with respect to microscopy measurements as they reveal localized behavior of the bed cross section. Therefore, to avoid misconstrues in flow regime designation, care must be taken that the bed is fully and densely packed with particles such that the fluids first confrontation takes place in the packed bed.

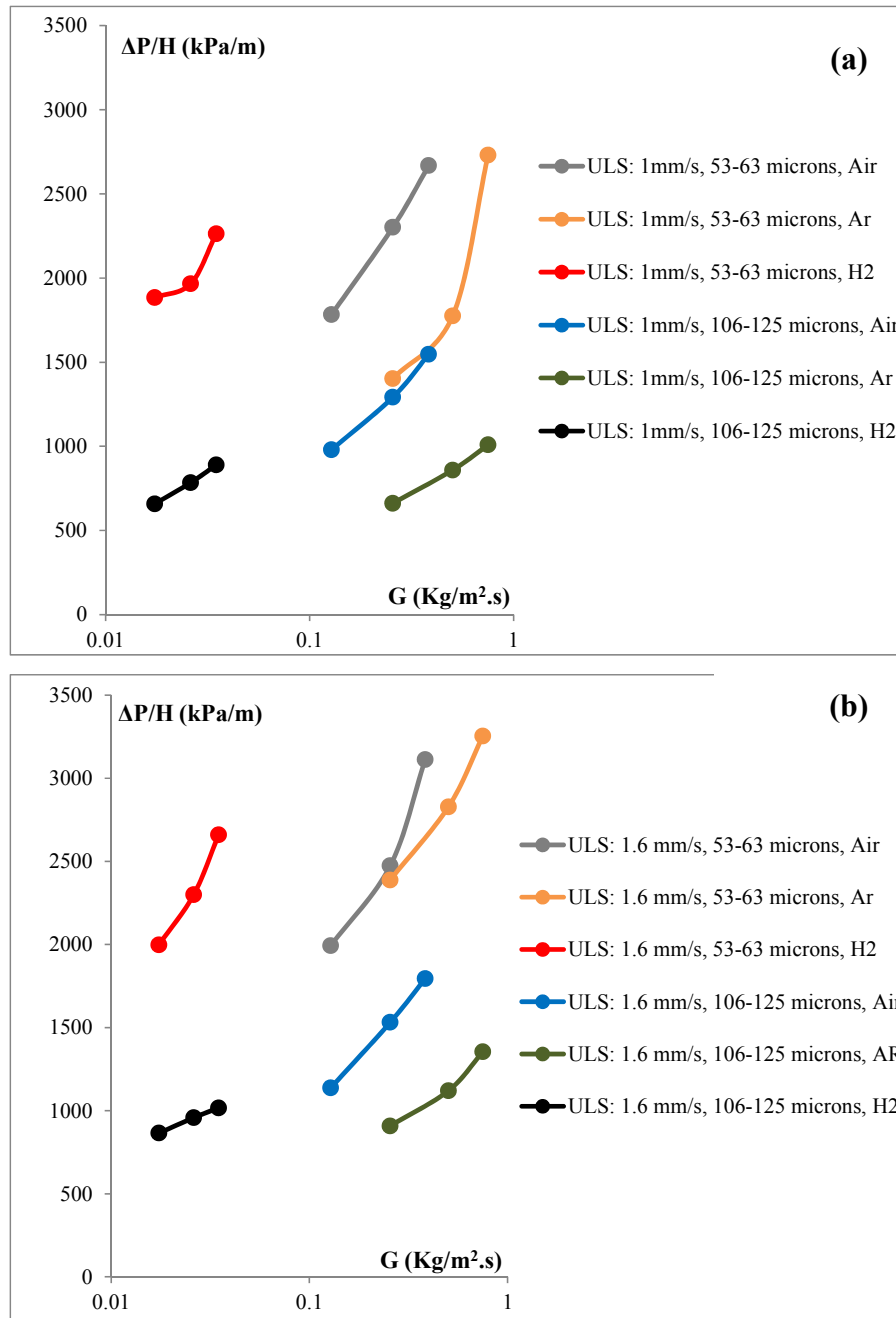
### 3.3.3 Pressure drop, bed porosity and liquid holdup

Figure 3-12 depicts variations in pressure drop with respect to gas mass flux ( $G$ ) for three systems: Air-Water, Argon-Water and Hydrogen-Water at two different liquid superficial inlet velocities ( $U_{LS} = 1$  mm/s in Figure 3-12.a and  $U_{LS} = 1.6$  mm/s in Figure 3-12.b) and two different solid particle sizes. As can be observed from both Figures 3-12.a and 3-12.b, pressure drops for a specific gas-liquid combination increase as the solid particles diameter decreases since the resistance to flow rises upon using smaller particles and fluids have to flow within more tortuous paths. It can also be seen that pressure drop decreases with an increase in gas density at constant gas mass fluxes. Moreover, increases in both gas and liquid superficial velocities ( $U_{LS}$  and  $U_{GS}$ ) end up in an increase in pressure drop.

Although there exist a number of methods in the literature for porosity determination in macro-scale packed bed reactors<sup>18-20</sup>, this becomes a major challenge in the case of micro-fixed bed reactors due to the reduced scale and paucity of appropriate probing methods. Therefore, liquid holdup determination for single-phase liquid flow (enabled by blocking the gas entry on the T-junction) could be regarded as a solution to determine the bed porosity. As for the liquid holdup, single-phase flow experiments yield to a bed porosity of 0.408 and 0.424 for particles of (55-63)  $\mu\text{m}$  and (106-125)  $\mu\text{m}$  in diameter, respectively. For two-phase flow tests, it can be seen from Figure 3-13 that increases in gas density result in an increase in liquid holdup at constant gas mass fluxes. Comparisons between Figures 3-13.a and 3-13.b reveal that liquid holdups increase upon increasing the liquid superficial inlet velocity for a specific gas-liquid combination while other parameters are held constant because of the gas phase displacement by the liquid. In contrast, increased gas superficial inlet velocities



(increased gas mass flux) decreases liquid holdup since more liquid is swept away from the bed by the gas phase. Finally, smaller solid particle sizes increase the liquid holdup as more liquid is retained in the bed due to stronger capillary forces at reduced particle sizes.



**Figure 3-12.** Pressure drop data for air-water, argon-water and hydrogen-water systems at (a)  $U_{LS}=1 \text{ mm/s}$  and (b)  $U_{LS}=1.6 \text{ mm/s}$

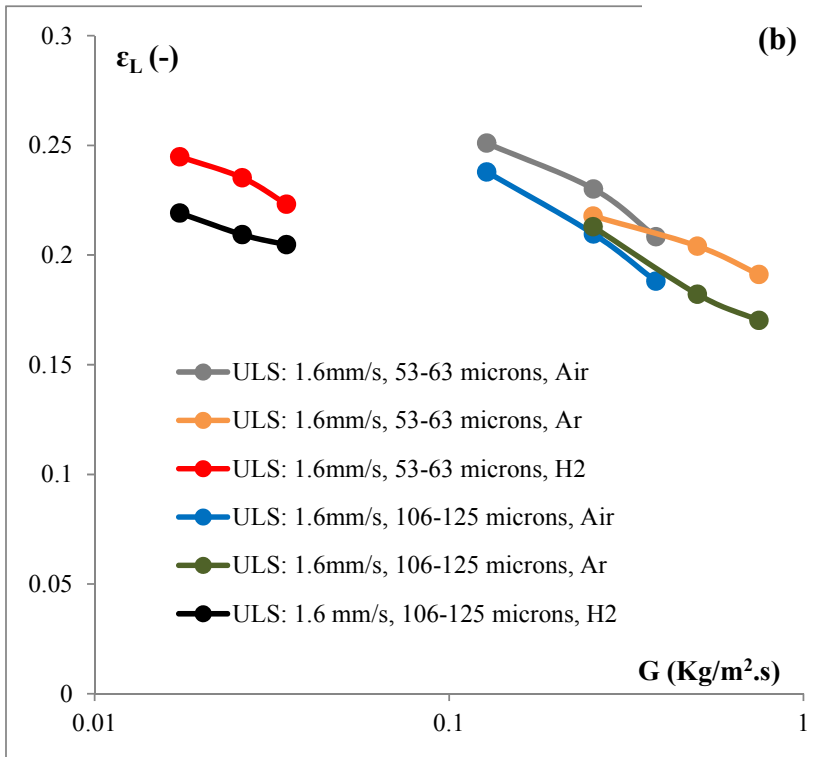
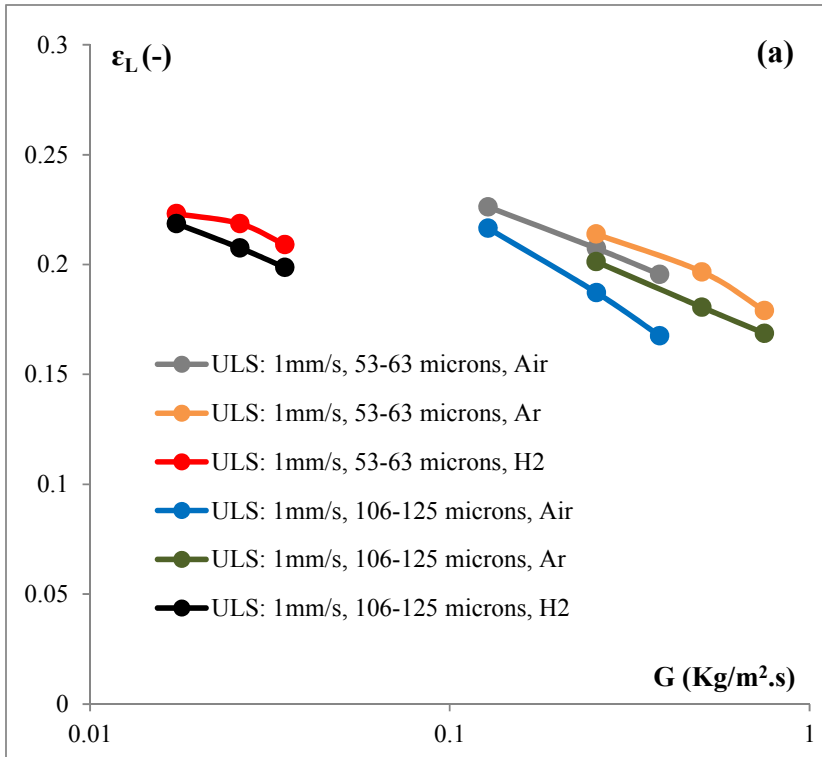


**Figure 3-13.** Liquid holdup data for air-water, argon-water and hydrogen-water systems at (a)  $U_{LS}=1$  mm/s and (b)  $U_{LS}=1.6$  mm/s

### 3.3.4 Near wall RTD determination

Dotted trend lines in both Figures 3-14.a and 3-14.b show the results of near wall RTD tests performed (according to the methodology depicted in Figure 3-5) at  $U_{Gs}= 10.6$  cm/s and  $U_{Ls}= 1.6$  mm/s. To examine if the assumption of ideal pulse injection holds true for this method, the normalized RTD signals acquired from overall averaged pixel values were fitted against two types of curves, one representing small deviations from plug flow (or  $D/UL < 0.01$  as in Figure 3-14.a) and one representing large deviations from plug flow (or  $D/UL > 0.01$  as in Figure 3-14.b) where  $D/UL$  is the dispersion number. The equations for these two cases have been abundantly mentioned in the literature.<sup>21</sup> As observed in Figure 3-14.a, the best fit to actual RTD curve is obtained at  $D/UL= 0.04$  (solid line) under the assumption of small deviations from plug flow. However, this value of  $D/UL$  is beyond the limiting value of 0.0128 for which the assumption can be made.<sup>21</sup> As for the Figure 3-14.b, the best fit to the actual RTD curve is for  $D/UL= 0.042$  if large deviations from plug flow are assumed to prevail. Yet, as mentioned in section 3.3.1, the experiments carried out by RTD setup in Figure 3-2 indicate low levels of dispersion for the two phase flow in micro-fixed bed reactors and therefore, it can be concluded that near wall RTD determination by following the procedure shown in Figure 3-5 (assuming ideal pulse injection of dye and monitoring the changes in overall averaged pixel value) does not seem as an appropriate method.

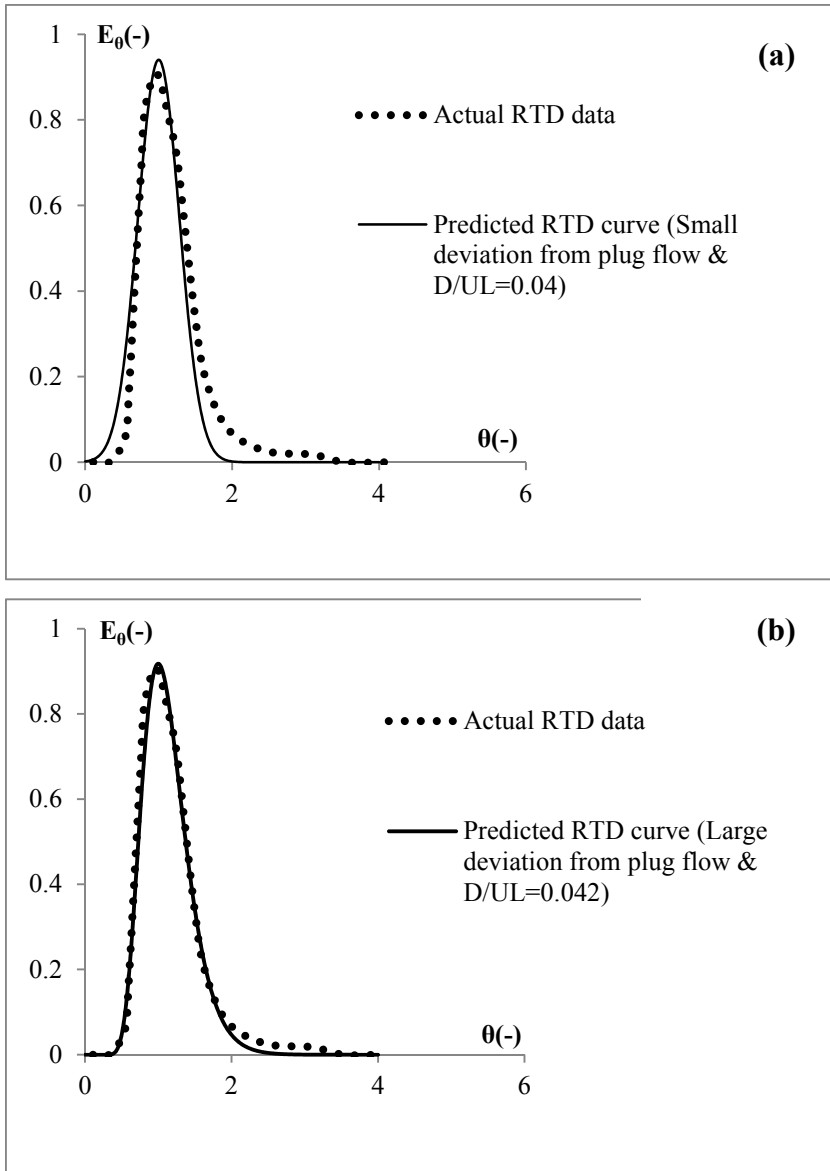


**Figure 3-14.** Actual RTD data obtained by monitoring the changes in the overall averaged pixel values and fitted against the curves representing a) small deviations from plug flow and b) large deviations from plug flow

Alternatively, using method 2 for RTD determination as illustrated in Figure 3-6 (at  $U_{GS} = 10.6$  cm/s and  $U_{LS} = 1.6$  mm/s) and inverting the signals (according to Figure 3-7) results in Figure 3-15. The Figure presents the results of the response analysis by the same procedure mentioned in section 3.2.2 by depicting the match between the measured and predicted outlet curves. A value of 0.06 s for liquid space time was also calculated. Since the  $(L/U_{LS})$  ratio in the current visualization experiments is close to unity, liquid space time and

liquid holdup take values close to each other. Figure 3-13.b illustrates that, under similar operating conditions, an average value of about 0.2 s can be expected for liquid space time. However, close to wall RTD measurements reveal much lower value indicating that liquid velocity is significantly higher in this region. In previous work of our group, Iliuta et al.<sup>16</sup> simulated the two-phase flow in packed bed microreactors by solving a two-dimensional hydrodynamic model based on the volume-averaged mass and momentum conservation equations. Radial non-uniform porosity distribution relations were incorporated in the model. The liquid and gas velocity fields were characterized by a significant non-uniformity due to the non-uniform presence of the solid phase. The major variation of liquid and gas velocities was observed in a region extending up to  $2d_p$  from the wall with a maximum located in the high porosity zone just close to the wall.

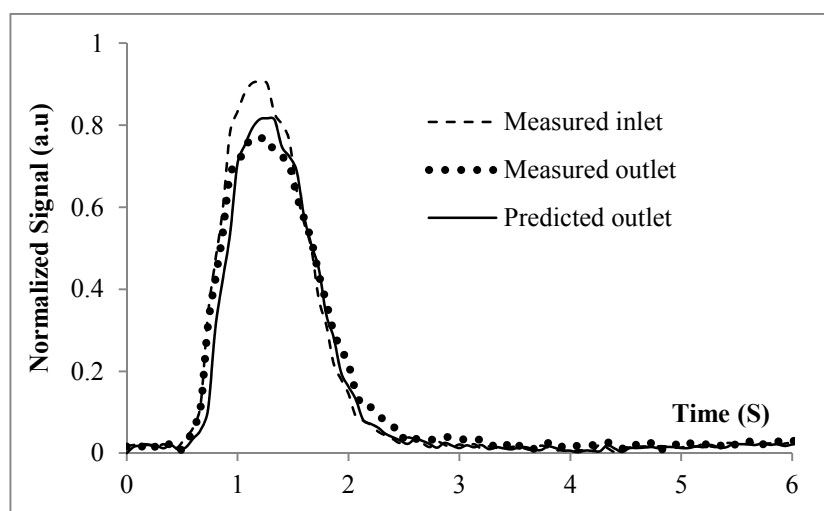


**Figure 3-15.** Experimental inlet and outlet gray level variation response curves (obtained by image acquisition from wall visualization) with the fit of outlet response using a two-parameter PD RTD model. ( $U_{GS}= 10.6$  cm/s and  $U_{LS}= 1.6$  mm/s)

In fact, the experimental results confirm the previous theoretical predictions. However, some caution should be exercised regarding the absolute values as the imaging frequency of the existing camera is relatively low (15 frames/s). As for the future experiments, three recommendations could be made. First, the imaging system (including camera, microscope and data acquisition) could be duplicated enabling image recording at selected distances (as far as the physical interference of the two systems allows) to produce separated RTD curves. Alternatively, less costly modifications could be implemented on the

current setup. One can either utilize objective lenses with broader field of view (lower magnification) in order to increase the actual distance between the edges of the pictures taken and separate the obtained signals or use cameras with higher imaging frequency ( $\gg 15$  Hz) to acquire more intermediate images between each two images that were taken in the current work.

### **3.4 Conclusion**

The challenges commonly faced in the hydrodynamic study of micro-fixed bed reactors were discussed in different sections of the text. Some of the significant details were explained in experimental setup and methodology while the more substantial issues that became clear to the authors through following a cause and effect learning logic were subjected to more scrutiny. As for the challenges, it can be concluded that the location of tracer input is a major factor in reliability of RTD experiments. The comparisons made between the two proposed arrangements suggested that it should be located downstream of the point where gas and liquid phases merge and upstream of the first pair of point electrodes. Micro-reactor packing is the second most important issue that, if performed correctly, not only guarantees reproducibility of experiments but also enables the precise flow regime distinction beyond any shadow of scepticism. It should also be noted that the idea of using point electrodes instead of ring-type ones along with its installation was a key achievement in surpassing the challenge of fluid leakage. Pressure drop and liquid holdup values indicate that increases in solid particle size (while other parameters are unaltered) give rise to a decrease in both pressure drop and liquid holdup. Furthermore, increases in superficial liquid velocity, increases liquid holdup whereas increase in superficial gas velocity leads to its decrease (while other parameters are kept constant). Near-wall RTD was measured via injecting a dye tracer at the start of the bed and monitoring the changes in the gray level intensity of the images taken within a frame downstream of the injection point. Laterally-averaged gray level intensity at both left and right extremities of the pictures acted as inlet and outlet curves for the Aris method. The major outcome of this work was experimental confirmation of theoretically predicted maximum velocity in the high porosity zone close to the wall.

### 3.5 Nomenclature

$d_p$	Solid particle diameter (L)
$D_H$	Hydraulic diameter (L)
$G$	Gas mass velocity ( $\text{ML}^{-2}\text{T}^{-1}$ )
$H$	Microreactor length (L)
$L$	Field of view length (L)
$Pé_L$	Liquid phase Péclet number (-)
$\Delta P$	Two-phase flow pressure drop ( $\text{ML}^{-1}\text{T}^{-2}$ )
$t$	Time (T)
$U_{GS}$	Gas phase superficial velocity ( $\text{L T}^{-1}$ )
$U_{LS}$	Liquid phase superficial velocity ( $\text{L T}^{-1}$ )

#### **Greek letters**

$\varepsilon_L$	Liquid holdup (-)
$\lambda_L$	Liquid characteristic length (L)
$\tau_l$	Liquid space time (T)

#### **Subscripts**

G, g	Gas
L, l	Liquid

### 3.6 References

1. de Mas, N.; Gunther, A.; Schmidt, M. A.; Jensen, K. F., Microfabricated multiphase reactors for the selective direct fluorination of aromatics. *Industrial & Engineering Chemistry Research* **2003**, 42, (4), 698-710.
2. Losey, M. W.; Schmidt, M. A.; Jensen, K. F., Microfabricated multiphase packed-bed reactors: Characterization of mass transfer and reactions. *Industrial & Engineering Chemistry Research* **2001**, 40, (12), 2555-2562.
3. Ehrfeld, W.; Hessel, V.; Löwe, H., *Microreactors*. Wiley-VCH: **2000**.
4. Hessel, V.; Löwe, H.; Müller, A.; Kolb, G., *Chemical Micro Process Engineering, Processing and Plants*. Wiley-VCH: **2005**.
5. AlDahhan, M. H.; Larachi, F.; Dudukovic, M. P.; Laurent, A., High-pressure trickle-bed reactors: A review. *Industrial & Engineering Chemistry Research* **1997**, 36, (8), 3292-3314.
6. Guettel, R.; Turek, T., Assessment of micro-structured fixed-bed reactors for highly exothermic gas-phase reactions. *Chemical Engineering Science* **2010**, 65, (5), 1644-1654.
7. Ajmera, S. K.; Delattre, C.; Schmidt, M. A.; Jensen, K. F., Microfabricated cross-flow chemical reactor for catalyst testing. *Sensors and Actuators B-Chemical* **2002**, 82, (2-3), 297-306.
8. Tidona, B.; Desportes, S.; Altheimer, M.; Ninck, K.; von Rohr, P. R., Liquid-to-particle mass transfer in a micro packed bed reactor. *International Journal of Heat and Mass Transfer* **2012**, 55, (4), 522-530.
9. van Herk, D.; Kreutzer, M. T.; Makkee, M.; Moulijn, J. A., Scaling down trickle bed reactors. *Catalysis Today* **2005**, 106, (1-4), 227-232.
10. Marquez, N.; Castano, P.; Makkee, M.; Moulijn, J. A.; Kreutzer, M. T., Dispersion and holdup in multiphase packed bed microreactors. *Chemical Engineering & Technology* **2008**, 31, (8), 1130-1139.



11. Marquez, N.; Musterd, M.; Castano, P.; Berger, R.; Moulijn, J. A.; Makkee, M.; Kreutzer, M. T., Volatile tracer dispersion in multi-phase packed beds. *Chemical Engineering Science* **2010**, 65, (13), 3972-3985.
12. Marquez, N.; Castano, P.; Moulijn, J. A.; Makkee, M.; Kreutzer, M. T., Transient Behavior and Stability in Miniaturized Multiphase Packed Bed Reactors. *Industrial & Engineering Chemistry Research* **2010**, 49, (3), 1033-1040.
13. Faridkhou, A.; Larachi, F., Hydrodynamics of Gas-Liquid Cocurrent Flows in Micropacked Beds—Wall Visualization Study. *Industrial & Engineering Chemistry Research* **2012**, 51, (50), 16495-16504.
14. Trachsel, F.; Hutter, C.; von Rohr, P. R., Transparent silicon/glass microreactor for high-pressure and high-temperature reactions. *Chemical Engineering Journal* **2008**, 135, S309-S316.
15. Aydin, B.; Larachi, F., Trickle bed hydrodynamics and flow regime transition at elevated temperature for a Newtonian and a non-Newtonian liquid. *Chemical Engineering Science* **2005**, 60, (23), 6687-6701.
16. Iliuta, I.; Hamidipour, M.; Schweich, D.; Larachi, F., Two-phase flow in packed-bed microreactors: Experiments, model and simulations. *Chemical Engineering Science* **2012**, 73, 299-313.
17. Kestin, J.; Khalifa, H. E.; Correia, R. J., Tables of the dynamic and kinematic viscosity of aqueous NaCl solutions in the temperature range 20-150 °C and the pressure range 0.1-35 MPa. *Journal of Physical and Chemical Reference Data* **1981**, 10, (1), 71-87.
18. Tsochatzidis, N. A.; Karabelas, A. J.; Giakoumakis, D.; Huff, G. A., An investigation of liquid maldistribution in trickle beds. *Chemical Engineering Science* **2002**, 57, (17), 3543-3555.
19. Gotz, J.; Zick, K.; Heinen, C.; Konig, T., Visualisation of flow processes in packed beds with NMR imaging: determination of the local porosity, velocity vector and local dispersion coefficients. *Chemical Engineering and Processing* **2002**, 41, (7), 611-629.

20. Nguyen, N. L.; van Buren, V.; Reimert, R.; von Garnier, A., Determination of porosity and flow distribution in packed beds by magnetic resonance imaging. *Magnetic Resonance Imaging* **2005**, 23, (2), 395-396.
21. Levenspiel, O., *Chemical Reaction Engineering*. John Wiley & Sons, Inc.: 1999.

## **4 Two-phase flow hydrodynamic study in micro-packed beds – The effect of bed geometry and particle size**

**Résumé** Les visualisations microscopiques à proximité de la région de la paroi d'un micro lit-fixe et des mesures hydrodynamiques en écoulement biphasique gaz-liquide ont été réalisées dans le but d'étudier l'effet de la taille des particules et de la forme du tube sur la perte de charge du lit, la transition du régime d'écoulement, l'hystérèse et la réponse transitoire du lit aux perturbations du débit. La visualisation par microscopie inversée a révélé qu'une diminution de la taille des particules conduit au déclenchement précoce d'un régime d'écoulement de haute interaction alors que le changement de la forme de la section passante du capillaire de circulaire à carrée n'a eu aucun effet sur la transition du régime d'écoulement. L'effet de la taille des particules sur le phénomène d'hystérèse du mouillage dans le fixe de section carrée a également été étudié par les voies de drainage et d'imbibition. Enfin, le comportement transitoire des micros lits-fixes de géométries circulaire et carrée remplis de particules de deux tailles différentes a été étudié en mesurant les variations de pertes de charge du lit lors suite à des perturbations contrôlées des débits de liquide à débit de gaz constant. Les particules de grandes tailles et la géométrie carrée ont montré des temps de transitions courts en comparaison de ceux associés aux petites particules et à une géométrie circulaire du canal.

**Abstract** Microscopic visualizations nearby the wall region of micro-fixed beds and hydrodynamic measurements during gas-liquid two-phase flows were carried out with an aim to investigate the effect of particle size and capillary tube shape on the bed pressure drop, flow regime transition, hysteresis and bed transient response to flow-rate step perturbations. Visualizations through inverted microscopy revealed that a decrease in particle size leads to early inception of a high interaction flow regime whereas changing capillary shape from circular to square had no effect on flow regime changeover. The effect of particle size on the wetting pattern hysteresis in square micro-packed beds was also investigated in both imbibition and drainage paths. It was found that wetting pattern hysteresis decreases with a decrease in particle size. Finally, the transient behavior of micro-fixed beds of circular and square geometries packed with particles of two different sizes were studied by monitoring the bed pressure drop variations upon step changes in liquid flow rate at iso-G (constant gas mass flux) conditions. Larger particle sizes and square geometry showed shorter transient times as compared to smaller particle sizes and circular geometry.

## 4.1 Introduction

Miniaturized reactors currently serve as the basic tool for kinetic studies, synthesis and catalyst testing due to their high surface-to-volume ratios, enhanced heat transfer, safety, etc. This is especially the case for heterogeneously catalyzed highly exothermic reactions carried out in micro-fixed bed reactors.<sup>1-3</sup> Although the literature is rife with studies on micro-fixed beds<sup>1, 2, 4-6</sup> with the aim of enhancing their efficiencies in terms of conversion, mass transfer, etc., only a few of them went beyond and to the root cause, that is, the nature of contacting patterns between the phases.<sup>7-9</sup> This is what hydrodynamic studies attempt to address so that by adjusting the contacting scheme of the phases involved, multiphase reactions in micro-reactors could proceed toward more favorable conditions and performances.<sup>7</sup> Occasional examples of combining hydrodynamic analysis with mass transfer and reaction studies in microreactors can be found in the literature.<sup>10-12</sup>

Possible research initiatives in this field come from two different aspects: 1) similarity between micro-fixed beds and macro-scale fixed beds (packed beds) from the operation point of view and 2) resemblance between micro-fixed beds and micro-channels from the scale perspective. The two approaches have major benefits; first, there are a number of key parameters concerning the hydrodynamics of both packed beds and micro-channels that could be suggestive to prospective investigations on micro-fixed beds (e.g., pressure drop, liquid holdup, residence time distribution (RTD), system geometry, etc.). Second, the appropriate method that could be adopted for measuring/determining the above parameters on micro-fixed beds can be decided by customizing the available methods used for packed beds<sup>13, 14</sup> or micro-channels.<sup>15, 16</sup> However, there is still a narrow band of knowledge on micro-fixed beds hydrodynamics as compared to existing information about other miniaturized flow devices due to the numerous challenges and difficulties that arise in the experiments. Description of the common technical challenges and measurement approaches in micro-fixed bed experiments has been addressed recently.<sup>17</sup>

As for studies on micro-fixed beds in particular, Márquez et al. did RTD tests to determine a global liquid holdup in micro-fixed beds using non-volatile<sup>8</sup> and volatile<sup>18</sup> tracers. They also observed minor hysteresis in pressure drop and liquid holdup in micro-fixed beds.<sup>9</sup> Faridkhou and Larachi<sup>7</sup>, on the other hand, reported a major hysteresis in

pressure drop and wetting patterns by combining pressure drop measurements with microscopic wall visualizations at higher gas and liquid flow-rates as compared to Márquez et al.<sup>9</sup> Flow regimes study was also carried out<sup>7</sup> by processing images taken from the wall region at different gas-to-liquid flow ratios and introducing a phase characteristic length as a measure to differentiate the two observed flow regimes. Near-wall RTD measurements were also performed by injecting a dye tracer at the entrance of the micro-fixed bed and monitoring variations in the gray level intensity of the images taken within a frame downstream of the injection point.<sup>17</sup> The results were in accordance with the theoretically predicted maximum velocity in the high porosity zone close to the wall.<sup>19</sup>

To further extend knowledge about the hydrodynamics of micro-fixed beds, the current work studies the effect of channel shape and particle size (or tube-to-particle size ratio) on the bed pressure drop, flow regime transition point, hysteresis and transient behavior. Since the utilization of square tubes rather than round ones offers more compact systems, as shown in the case of heat exchangers<sup>20</sup>, the comparison between the two geometries at micro-scale hydraulic diameters becomes appealing. Also, numerous works have been done on microchannel geometry and its effect on hydrodynamics<sup>20-22</sup> and heat transfer<sup>23</sup> while similar studies on micro-fixed beds is still lacking in the literature. Despite a number of researches carried out on the effect of particle size (or column-to-particle size ratio) on the hydrodynamics of packed beds<sup>24-27</sup>, studies of such kind have yet to be performed in their micro-scale lookalikes and hence, will be subjected to investigation in this contribution. Finally, since micro-fixed beds are ultimately aimed for commercial applications, the study of their transient behavior (which is an industrially important parameter especially during equipment startups) and factors affecting it seems crucial.

## 4.2 Experimental

### 4.2.1 Setup

The schematic of the setup for performing the experiments is shown in Figure 4-1. It consists of two separate transparent borosilicate tubes one with square ( $W \times H = 1 \text{ mm} \times 1 \text{ mm}$ ,  $L = 11.5 \text{ cm}$ ) and another with circular cross-section ( $D = 1 \text{ mm}$ ,  $L = 10.8 \text{ cm}$ ) used as micro-beds. The capillaries are inserted in carved plexiglass blocks so that they could be protected

against any inadvertent stroke. The tubes are packed with spherical glass beads with diameters in the ranges of either 106-125  $\mu\text{m}$  or 55-63  $\mu\text{m}$  (depending on the experiment) serving as the micro-packed bed. Both beds have optically accessible windows for microscopic visualization. Liquid (water with  $\sigma = 0.0728 \text{ N/m}$ ) and gas (air) delivery to the micro-fixed bed are enabled by a syringe pump (Teledyne ISCO, 500D) and mass flow controller (EL-Flow Bronkhorst), respectively. Introduction of gas and liquid into the bed is such that their mixing takes place right at the start of the packed bed. Otherwise, the existence of any void space upstream of the micro-fixed bed bringing gas and liquid phases in contact prior to entering the packed section, will lead to instabilities and therefore, should be avoided.<sup>4,17</sup> The micro-fixed bed is mounted on an inverted microscope (Olympus GX-51) and visualized through a 10X objective lens (MPlanFLN-BD series, resolution: 1.12  $\mu\text{m}$ ) at a constant light intensity. The microscope is coupled with a camera (TSI, PowerView<sup>TM</sup> Plus) which is itself connected to a computer with a frame-grabber port and image acquisition is performed at a frequency of 15 Hz using Insight3G software. Pressure drop measurement in all the experiments is performed between the gas-feed line (inlet section) and bed outlet via a piezoelectric differential pressure transducer.

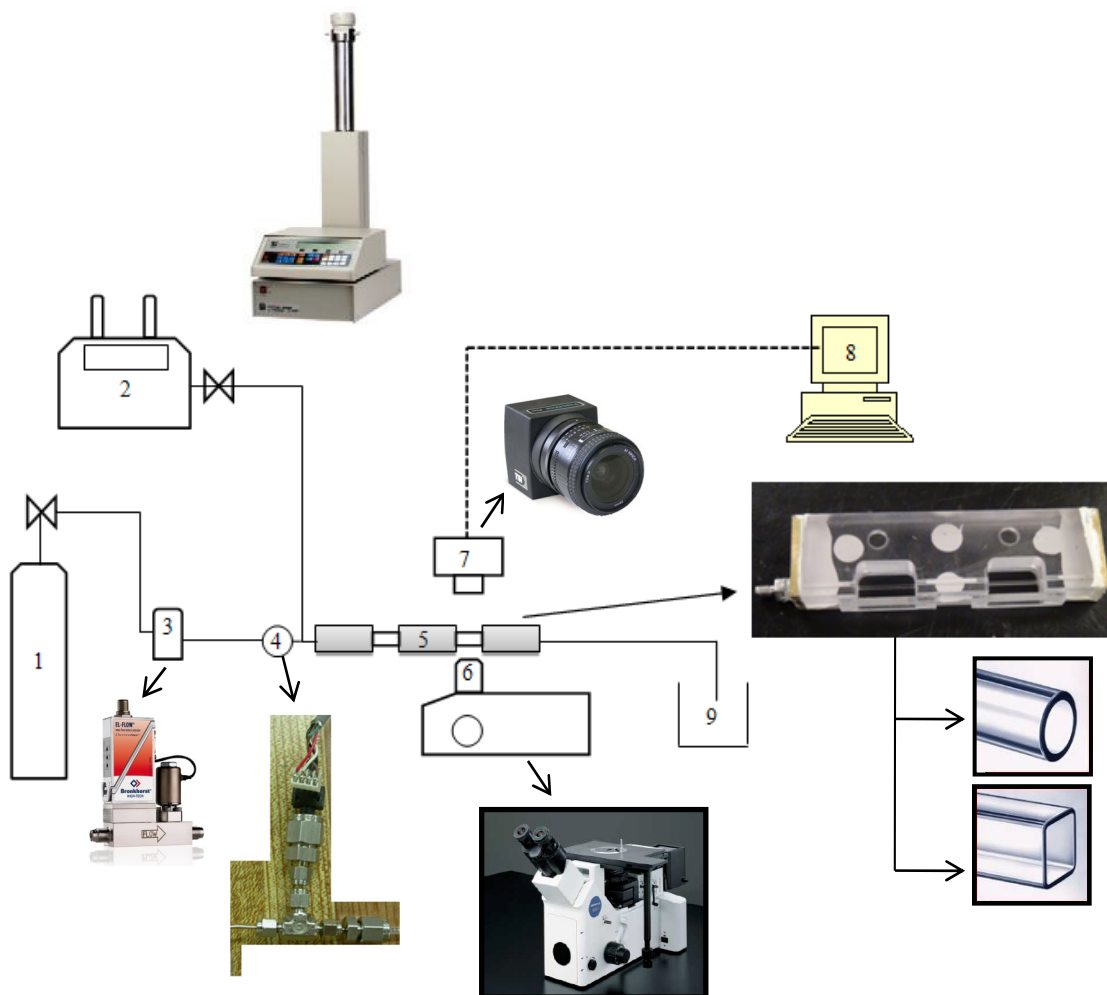


**Figure 4-1.** Experimental Setup: 1) Gas cylinder; 2) Syringe pump; 3) Gas mass flow controller; 4) Differential pressure transducer; 5) Micro-reactor made with round/square capillary tube; 6) Inverted microscope and objective lens; 7) Camera with frame grabber port; 8) Computer for image acquisition; 9) Drain.

#### 4.2.2 Methodology

To begin each set of experiments, the micro-beds were densely packed with glass beads. Particles could be easily loaded inside the micro-tube through a handmade tiny metal funnel within multiple steps in each of which a certain portion of the total bed volume is loaded with particles. Frequent tappings are required between the steps to completely densify the bed.<sup>17</sup> For the first part of flow regime transition experiments, only the square micro-fixed bed is used as it not only enables microscopic visualizations but also provides images with appropriate quality for subsequent processings due to its flat wall (the latter is not the case for circular geometry). Air superficial velocity is kept constant (21.3 cm/s) while water



flows at different superficial velocities (12.8, 14.9, 17.0 and 19.2 mm/s) through the micro-fixed bed at room temperature. Upon reaching a constant pressure drop at each set of gas and liquid superficial velocities (indicating steady state conditions), a set of 50 images were taken at 15 Hz rate from each of the four regions within the bed as shown in Figure 4-2. Two of the regions are located at the first half of the bed and the other two at the second half of it and imaging is performed successively from regions of one extreme to the other by turning the x-axis stage knob of the microscope for axial displacement through the micro-fixed bed. The aim of this part is to show how the flow regime transition starts sequentially within the bed length. The transition from low interaction to high interaction regime can be observed by microscopic visualization and graphically depicted via changes in the dimensionless liquid phase characteristic length ( $\Lambda_L/d_p$ ).<sup>7</sup> The characteristic length for the liquid phase is based on the weighted mean area it occupies on each image determined by image thresholding and binarization in MATLAB software.<sup>7,17</sup> A smooth evolution of the characteristic length with time indicates low interaction flow regime whereas abrupt jerks are signs for high interaction flow regime.

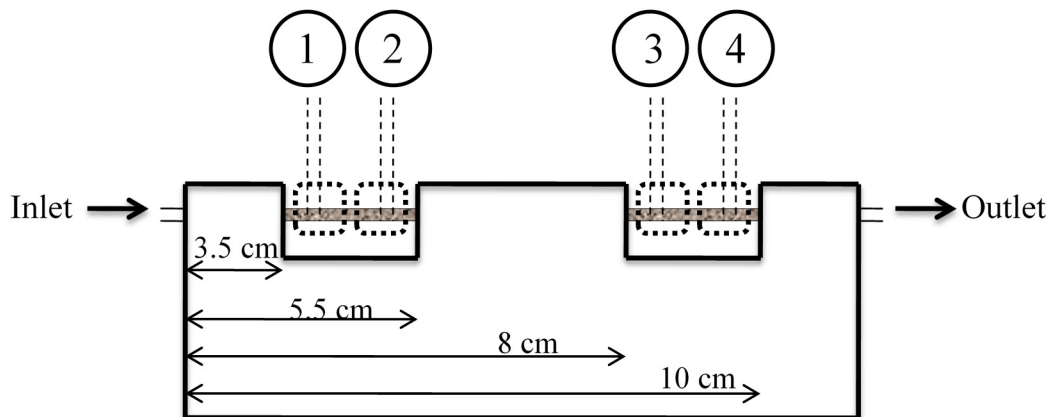


**Figure 4-2.** Regions within the square micro-fixed bed axial length used for visualization on flow regime transition.

To study the effect of tube cross-sectional shape and particle size (or tube-to-particle diameter ratio) on pressure drop, flow regime transition point and bed dynamics, micro-fixed beds of both geometries were packed with glass beads of both size distributions and tested at different operating conditions according to Table 4-1. Upon increasing liquid flow from  $L_i$  to  $L_j$  (at iso-G conditions), steady state pressure drop was registered (at a frequency of 10

Hz) by first maintaining the liquid flow rate at  $L_i$  for 30 s and then switching to  $L_j$  until establishment of a new steady state. Meanwhile, microscopic visualizations from the near-inlet windows of both micro-fixed beds monitored the prevailing flow regimes within the bed. If the initial steady state pressure drop (for the initial liquid flow,  $L_i$ ) and the final steady state pressure drop (for the final liquid flow,  $L_j$ ) are named as  $\Delta P_i$  and  $\Delta P_j$ , respectively, then the transient time for the bed (as a measure of the bed dynamic behavior) is taken as the time when pressure drop values starts to exceed  $\Delta P_i + \sigma_i$  and reach  $\Delta P_j - \sigma_j$  where  $\sigma_i$  and  $\sigma_j$  are the standard deviations for pressure drop data at the initial and final steady states (designated as  $\Delta P_i$  and  $\Delta P_j$ ), respectively. This has been shown schematically in Figure 4-3 where the transient time is the time span between the blue and red bands representing the ascending part of the pressure drop variations versus time in Figure 4-3 (bottom).

**Table 4-1.** Operating conditions for studying the effect of capillary shape and particle size on pressure drop, flow regimes and micro-packed bed transient behavior ( $U_{GS} = 21.3$  cm/s).

<b>Micro-fixed bed cross-sectional geometry</b>	<b>Particle size (<math>\mu\text{m}</math>)/ (<math>D/d_p</math>)</b>	<b>Minimum liquid superficial velocity (mm/s)</b>	<b>Maximum liquid superficial velocity (mm/s)</b>
Square	106-125 $\mu\text{m}$ / $\approx 10$	$U_{LS} = 1.1$	$U_{LS} = 23.4$
Square	53-63 $\mu\text{m}$ / $\approx 20$	$U_{LS} = 1.1$	$U_{LS} = 14.9$
Circular	106-125 $\mu\text{m}$ / $\approx 10$	$U_{LS} = 1.1$	$U_{LS} = 23.4$
Circular	53-63 $\mu\text{m}$ / $\approx 20$	$U_{LS} = 1.1$	$U_{LS} = 14.9$

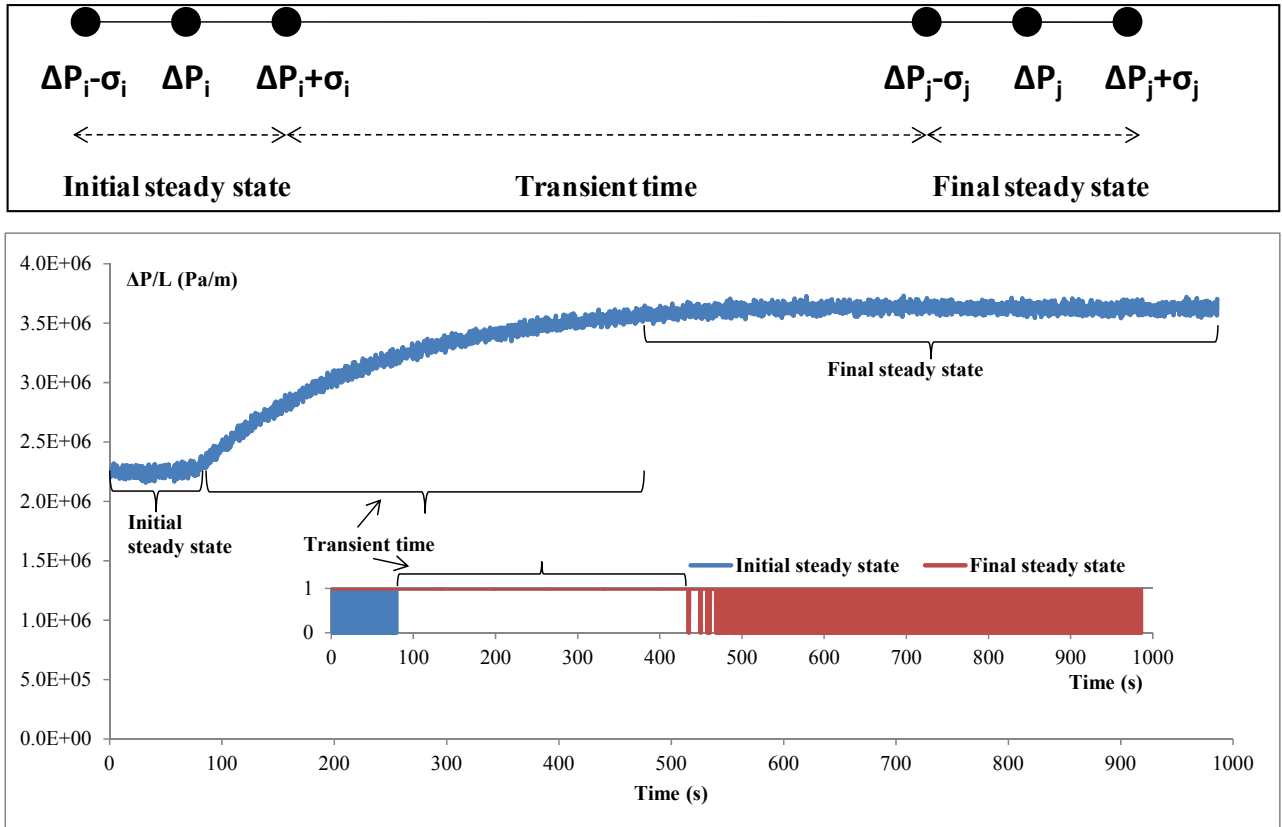


**Figure 4-3.** Definition of transient time taken as the time span between two steady states (top) and the method for its determination (bottom).

As for the study of wetting pattern hysteresis in micro-fixed beds, Faridkhou and Larachi<sup>7</sup> performed the experiments for  $D/d_p \approx 10$  with particles in the range of 106-125  $\mu\text{m}$  by taking wall-region images from the bed texture during both imbibition (increasing liquid flow rate) and drainage (decreasing liquid flow rate) paths within the low interaction flow regime. To investigate the effect of using smaller particle size (or increased tube-to-particle ratios) on the wetting patterns, particles in the range of 55-63  $\mu\text{m}$  are used in the current work ( $D/d_p \approx 20$ ). The gas superficial velocity is fixed at 25.5 cm/s while liquid superficial velocity is gradually increased from 1.1 mm/s to 13.8 mm/s and then decreased to its initial value. At each liquid velocity, for both imbibition and drainage paths, 150 images were taken from the bed after pressure drop stabilization in order to compare visualizations from the bed texture at same superficial liquid velocities in both increasing and decreasing paths. The acquired images at each liquid flow rate (in both imbibition and drainage) are time-averaged and the resulting single images will be subjected to thresholding,

binarization and subtraction to get the respective difference images and analyze the wetting pattern hysteresis. The results will be compared against the previous results of Faridkhou and Larachi.<sup>7</sup>

## 4.3 Results and discussion

### 4.3.1 Flow regime transition within the bed

Figure 4-4 depicts dynamic variations in dimensionless liquid-phase characteristic length ( $\Lambda_L/d_p$ : refer to chapter 2) at four regions within the axial length of the square micro-fixed bed according to Figure 4-2 and at iso-G condition. As can be seen in Figures 4-4-1-a and 4-4-1-b (for  $U_{LS} = 12.8$  mm/s) where a low interaction flow regime prevails in all four regions down the reactor length, variations in dimensionless liquid-phase characteristic lengths are quite monotonous indicating minor movements at the gas and liquid boundaries. As the liquid superficial velocity increases to  $U_{LS} = 14.9$  mm/s, regions (3) and (4) located within the second half of the micro-fixed bed come to the verge of a flow regime transition as evidenced by fluctuations in dimensionless liquid-phase characteristic lengths in Figure 4-4-2-b. However, regions (1) and (2) are still unaffected by the change in liquid superficial velocity maintaining the low interaction flow regime, as Figure 4-4-2-a suggests.

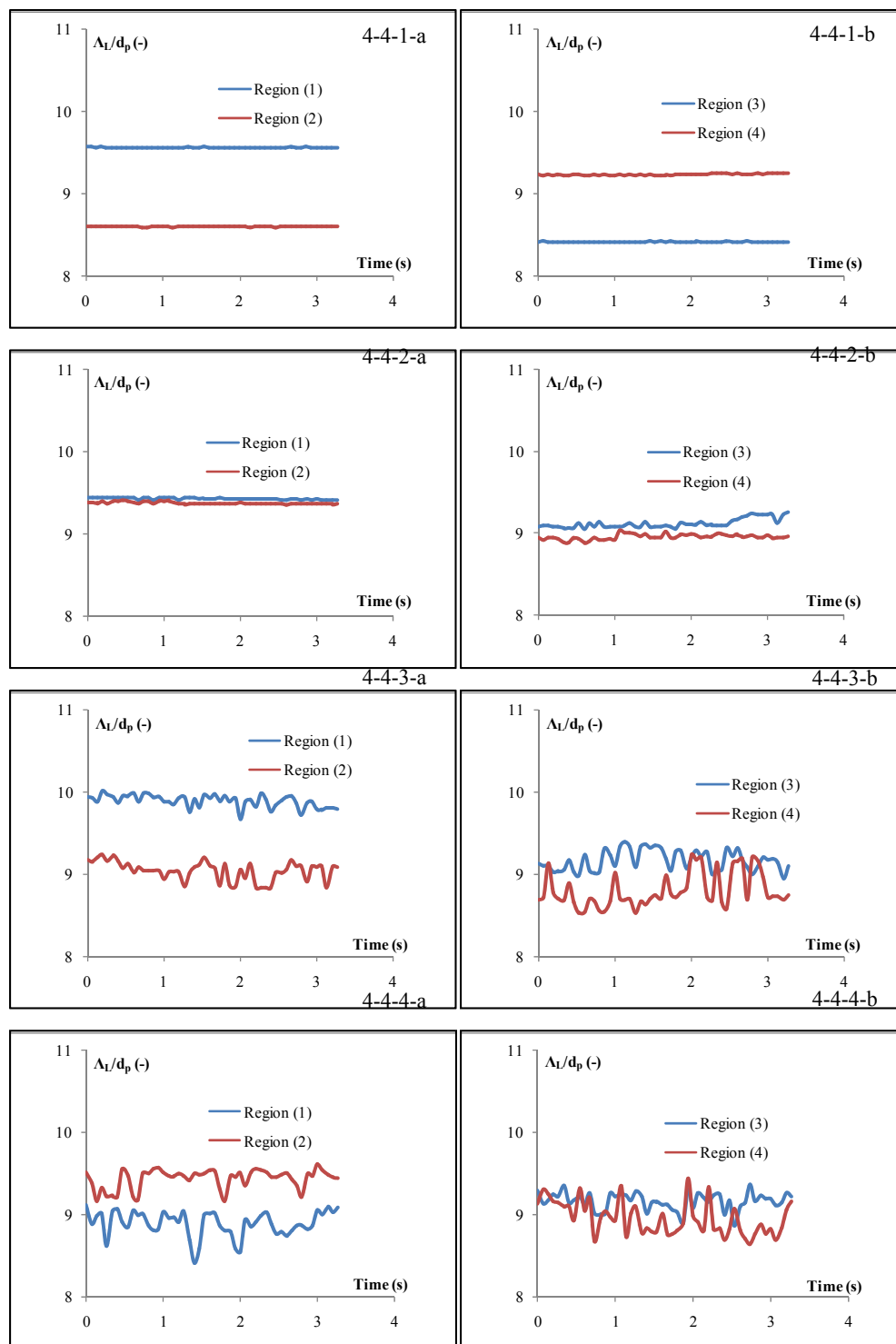


**Figure 4-4.** Dynamic variations in dimensionless liquid-phase characteristic length at  $U_{GS} = 21.3$  cm/s and for four regions within the axial length of the square micro-fixed bed with particles of 106-125  $\mu\text{m}$  (columns (a) and (b) represent first and second half of micro-fixed bed, respectively, according to Figure 2).  $U_{LS} = 12.8$  mm/s (4-4-1-a and 4-4-1-b),  $U_{LS} = 14.9$  mm/s (4-4-2-a and 4-4-2-b),  $U_{LS} = 17.0$  mm/s (4-4-3-a and 4-4-3-b) and  $U_{LS} = 19.2$  mm/s (4-4-4-a and 4-4-4-b).

Further increase in liquid superficial velocity ( $U_{Ls} = 17.0$  mm/s) will not only cause fluctuations of higher amplitudes in regions (3) and (4), but also shifts the flow regime transition into regions (1) and (2) which are closer to the micro-fixed bed inlet as illustrated in Figures 4-4-3-a and 4-4-3-b. As the liquid superficial velocity is raised to 19.2 mm/s, high interaction flow regime prevails within the entire bed according to Figures 4-4-4-a and 4-4-4-b. The reason why the high interaction flow regime initiated at the near-end of the bed and then gradually propagated toward the micro-fixed bed inlet could be due to the fact that lower pressures at near-outlet extreme of the micro-bed cause the expansion of the gas phase which will in turn lead to higher interactions with the liquid phase while higher liquid flow rates are required to cause a flow regime transition at regions closer to the bed inlet. Similar observations have been frequently reported for macro-scale packed beds.<sup>28-30</sup> It should be stated that the same behavior was observed in the micro-fixed bed of circular geometry as well. However, due to the tube curvature and the resulting blurry regions within the field of view, translation of gas-liquid boundary movements into a liquid-phase characteristic length was not possible and solely the microscopic visualization could confirm flow regime transitions in each region.

Figures 4-5a,b illustrate pressure drop variations with liquid superficial velocity at conditions and show the effect of solid particle size (or tube-to-particle diameter ratio) on pressure drop and the onset of flow regime change in micro fixed beds of circular and square geometry, respectively. As for the pressure drop, the data at low interaction regime (at very low liquid superficial velocities) are rather comparable to those obtained by Knobloch et al (for particles in the range of 55-63  $\mu\text{m}$ ) who did pressure drop measurements during a Fischer-Tropsch synthesis in a micro-fixed reactor.<sup>10</sup> Based on earlier discussions regarding inception of the high interaction flow regime at near-outlet regions of the micro-fixed bed (and its subsequent propagation to the upstream regions), all the flow regime visualizations were made within a region quite close to the micro-fixed bed inlet to ensure that flow regime transition has taken place throughout the entire bed length.

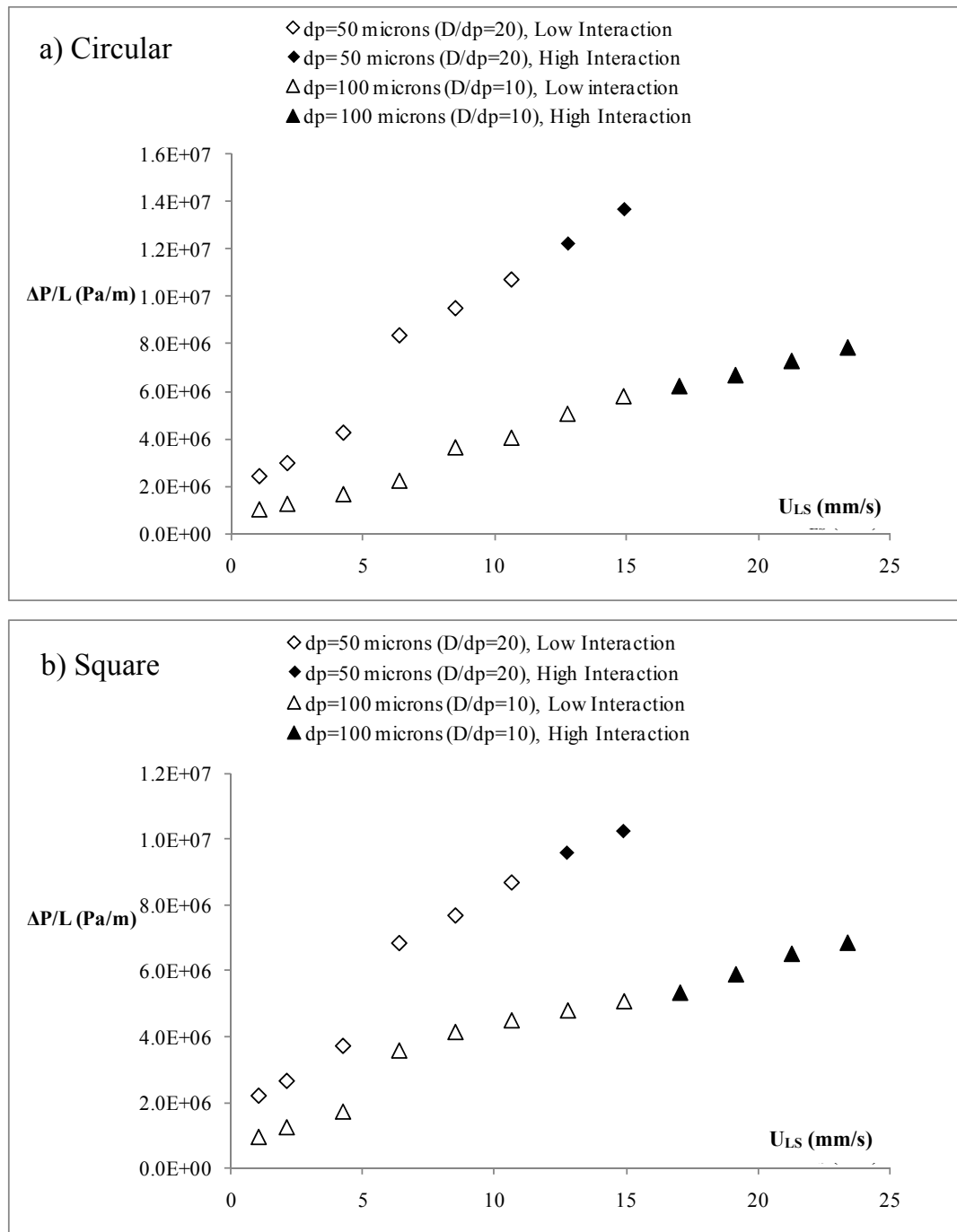


**Figure 4-5.** Pressure drop variations against liquid superficial velocity (at iso-G conditions) for a) circular geometry and b) square geometry.

As can be observed from both Figures 4-5a,b, pressure drop increases with a decrease in particle size as the fluids have to flow through more tortuous paths in the micro-fixed bed. Both geometries display sharp increases in pressure drop for  $D/d_p \approx 20$  and to a lesser extent for  $D/d_p \approx$

10 once the liquid superficial velocity exceeds 4.3 mm/s. This could be either the result of a change in the gas-liquid contacting pattern in the core of the bed (which may not be discernible through wall visualization), or due to the inception of transitions in flow regime at the very near-outlet region (between region 4, according to Figure 4-2, and the bed outlet where microscopic observation is impeded). However, none of these possibilities have affected the entire bed cross section and length unless the liquid flow rate is further increased. Moreover, for  $D/d_p \approx 10$  flow regime transition occurs at  $U_{LS} = 17.0$  mm/s whereas at  $D/d_p \approx 20$ , a change in the flow regime takes place at a lower liquid superficial velocity ( $U_{LS} = 12.8$  mm/s) at the expense of a higher pressure drop. Earlier inception of high interaction flow regime at reduced particle sizes could be the consequence of smaller pore sizes having more tendency to be filled with the liquid phase at lower liquid flow rates (due to stronger capillary forces at micro-scale) which will block the passages for the gas phase, thus causing a more intense competition between the phases at lower liquid superficial velocities. Same results had already been obtained by Ng<sup>28</sup> for macro-scale packed beds. Therefore, if high interactions between the gas and liquid phases are desirable at lower liquid flow rates, it would be at the expense of much higher energy costs due to the increased pressure drop.

Figures 4-6a and b illustrate the effect of micro-fixed bed geometry on pressure drop and flow regime transition point at two different ranges of particle size (e.g.,  $D/d_p \approx 20$  and  $D/d_p \approx 10$ , respectively). It can be perceived that the onset of flow regime transition is seemingly dependent on gas-to-liquid flow rates and particle size rather than capillary tube shape. It can be observed that at  $D/d_p \approx 20$  (Figure 4-6-a), pressure drop data for both circular and square geometries are quite close at lower liquid superficial velocities (up to 4.3 mm/s) when flow is gas phase-dominant. However, upon further increase in liquid flow rate, the pressure drop data for circular geometry start to gradually outweigh those of the square geometry especially after a rather sharp jump in pressure drop when the liquid superficial velocity increases from  $U_{LS} = 4.3$  mm/s to  $U_{LS} = 6.4$  mm/s. This could be due to nearly 27% larger cross-sectional area of the flow for the square geometry (although the hydraulic diameters for both geometries are the same) making the difference in pressure drops more apparent. Bypassed liquid flow from the corners of the square micro-fixed bed without passing through the porous bed is another contributory factor in this regard.



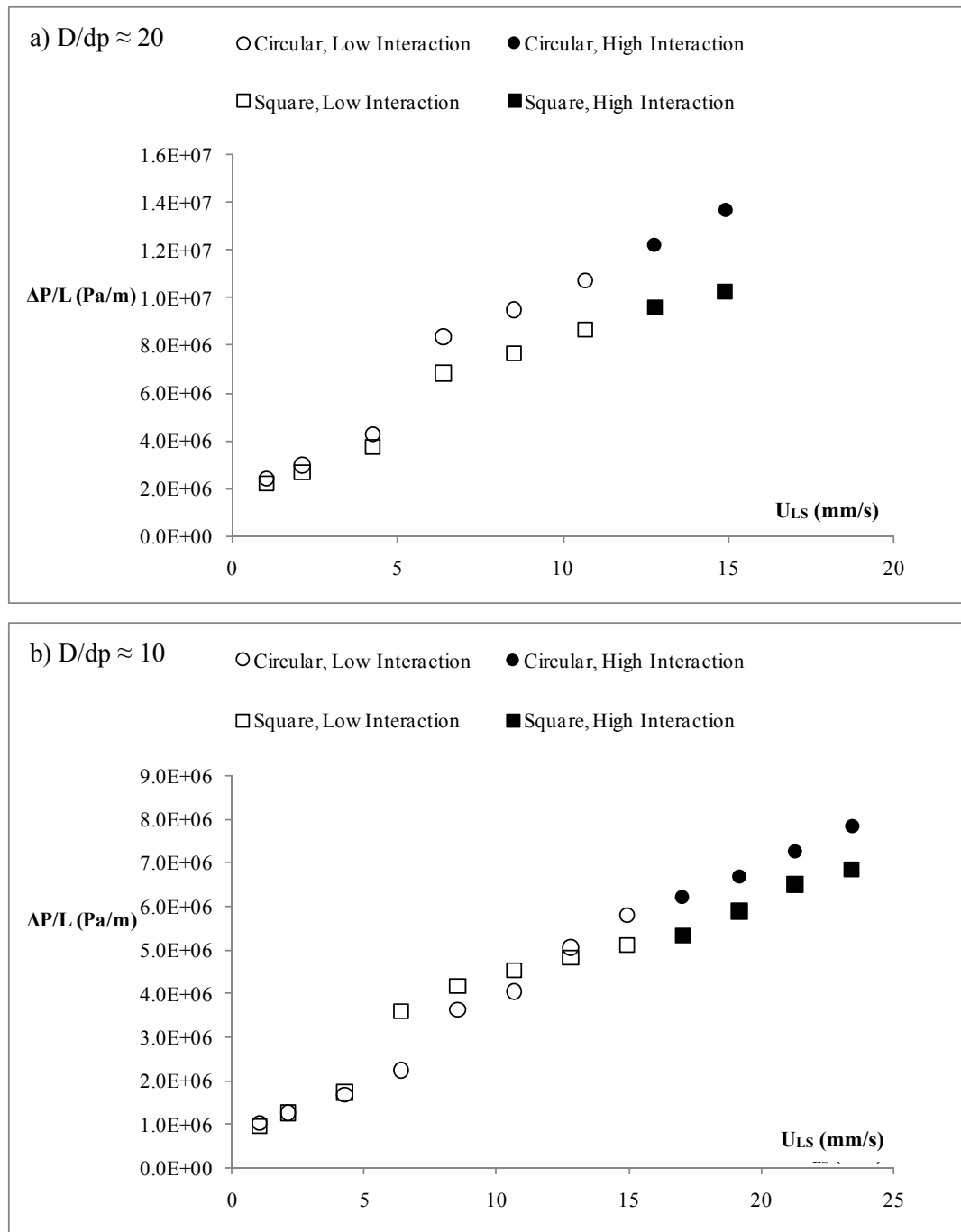


**Figure 4-6.** Pressure drop variations against liquid superficial velocity (at iso-G conditions) at two different range of particle sizes: a)  $D/d_p \approx 20$  and b)  $D/d_p \approx 10$ .

As for the case of  $D/d_p \approx 10$  (Figure 4-6-b), almost the same trend as Figure 4-6-a is observed except for a region between  $U_{LS} = 6.4$  mm/s and  $U_{LS} = 10.6$  mm/s where pressure drops for the square tube become significantly larger than those for the circular one first and then steadily drops down such that beyond  $U_{LS} = 10.6$  mm/s pressure drop data for square

geometry lie below those of the circular. This interesting, and yet peculiar, observation for the abovementioned region (between  $U_{LS} = 6.4$  mm/s and  $U_{LS} = 10.6$  mm/s) could be explained as follows. According to Coleman and Garimella<sup>20</sup>, who did two-phase flow experiments in square and circular micro-channels, surface tension has a more pronounced effect in square tubes as compared to circular ones in that the liquid phase is more readily pulled into the corners of the square tube. By increasing  $U_{LS}$  at iso-G conditions (and at  $D/d_p \approx 10$  suggesting wall effects), liquid phase starts to become the dominant phase and replaces the gas phase mostly at the corners of the square channel due to capillary forces. This interaction between the two phases at the corners of the square channel will ultimately cause pressure drop values to exceed those of the circular one. Further increase in liquid flow rate leads to the same trend observed previously for  $D/d_p \approx 20$ .

#### **4.3.2 Hysteresis and the effect of particle size**

Hysteresis in micro-fixed beds can be spotted by wall visualizations and depicted in terms of wetting patterns in the bed texture within the low interaction regime.<sup>7</sup> Faridkhou and Larachi<sup>7</sup> used image binarization to differentiate between the areas occupied by gas phase (dry) and liquid phase (wet) in both imbibition and drainage paths as illustrated in Figure 4-7-a for a micro-fixed bed at  $D/d_p \approx 10$ . Subtraction of the two binary images led to the difference image in Figure 4-7-a with three distinct regions: regions in red color indicate dry areas in the imbibition phase (path of ascending liquid flow rate) that became wet during drainage (path of descending liquid flow rate) while blue colors represent the opposite behavior. Green regions also signify areas that remained indifferent to the operation path and maintained their condition (either wet or dry in both paths).

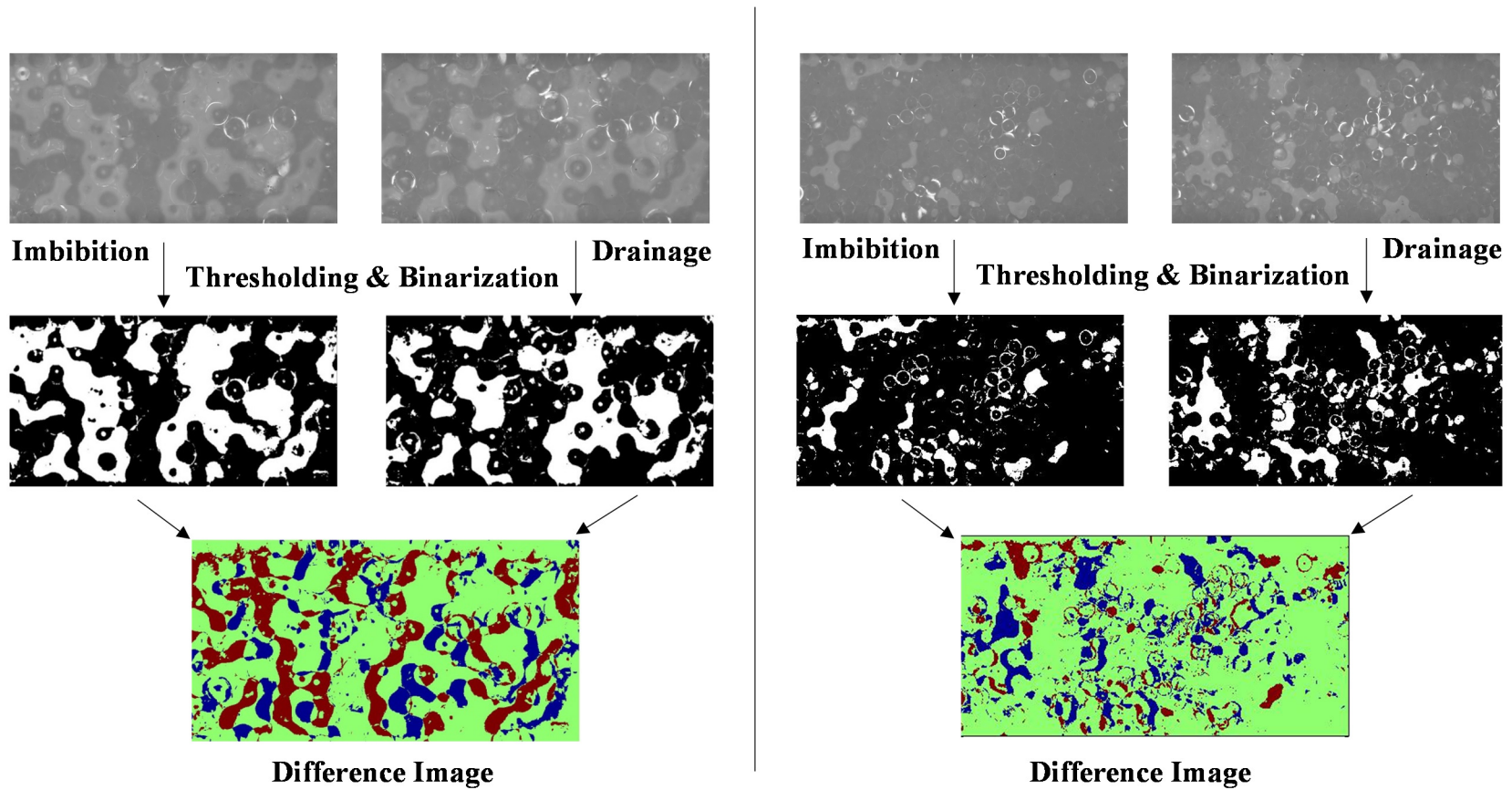


**Figure 4-7.** Effect of decreasing particle size (increasing  $D/d_p$  ratio) on wetting pattern hysteresis at the same gas and liquid superficial velocities ( $U_{GS} = 25.5$  cm/s,  $U_{LS} = 1.1$  mm/s) for a)  $D/d_p \approx 10$  (adapted from Faridkhou and Larachi [7]) and b)  $D/d_p \approx 20$  (current work).

It would be of interest to examine how and to what extent the hysteresis manifests itself in the wall region of micro-fixed beds by decreasing the particle size (increasing the tube-to-particle diameter ratio). The results for image binarization and subtraction are shown in the difference image of Figure 4-7-b. It can be viewed that in comparison with Figure 4-7-a, wetting pattern hysteresis in the wall vicinity has diminished upon a decrease in particle size as can be inferred from the larger fraction of green regions in Figure 4-7-b. The relative distribution of the green, red and blue regions shown in Figure 4-7 as well as the differentiation between the indifferent regions for both particle sizes are depicted in Figures 4-8a-d. Figures 4-8a,c represent particles in the range of 106-125  $\mu\text{m}$  or  $D/d_p \approx 10$  (adapted from Faridkhou and Larachi <sup>7</sup>) and Figures 4-8b,d stand for particles in the range of 53-63  $\mu\text{m}$  (or  $D/d_p \approx 20$ ). Comparison of Figures 4-8a,c versus 4-8b,d reveals that at smaller particle sizes, not only the fraction of the bed maintaining its wetting condition in both imbibition and drainage conditions increases drastically but also the bed texture is more prone to stay constantly wet rather than constantly dry as Figure 4-8d suggests in comparison with Figure 4-8b. This stems from stronger capillary forces in smaller particles which gives rise to a higher tendency of the bed texture to become wet by the liquid phase. Even within the drainage path, the smaller pores of the smaller particle are more inclined to retain the liquid phase as compared to the larger particle sizes.

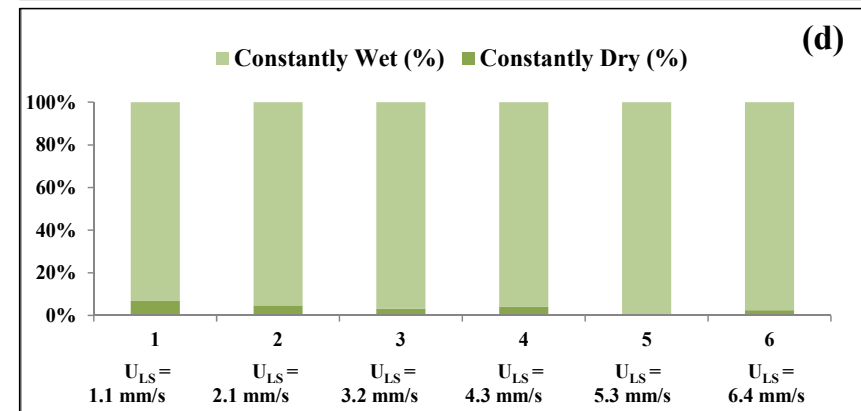
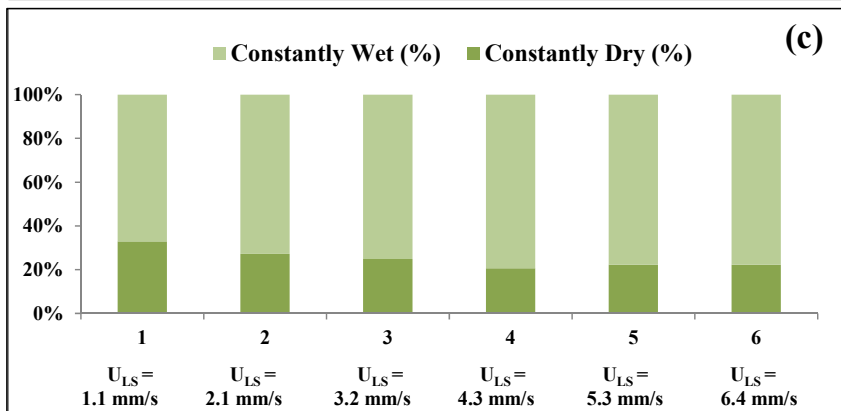
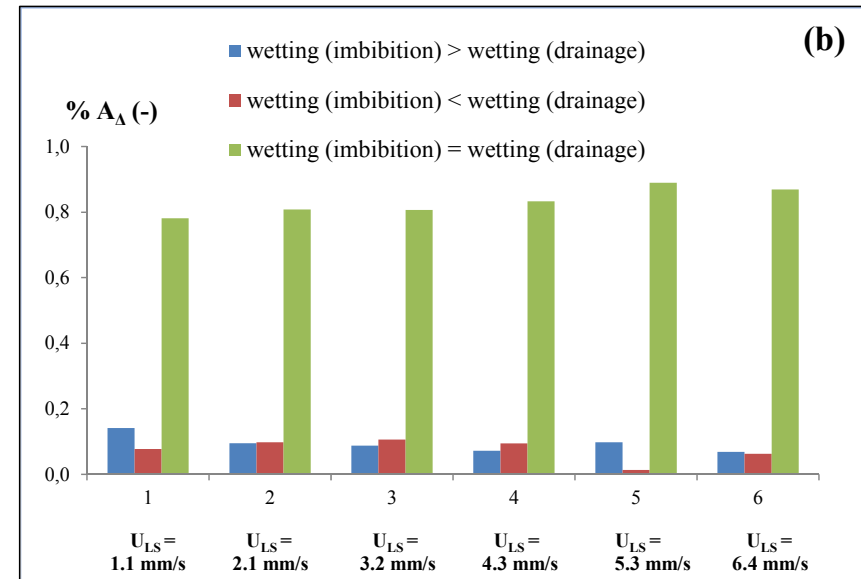
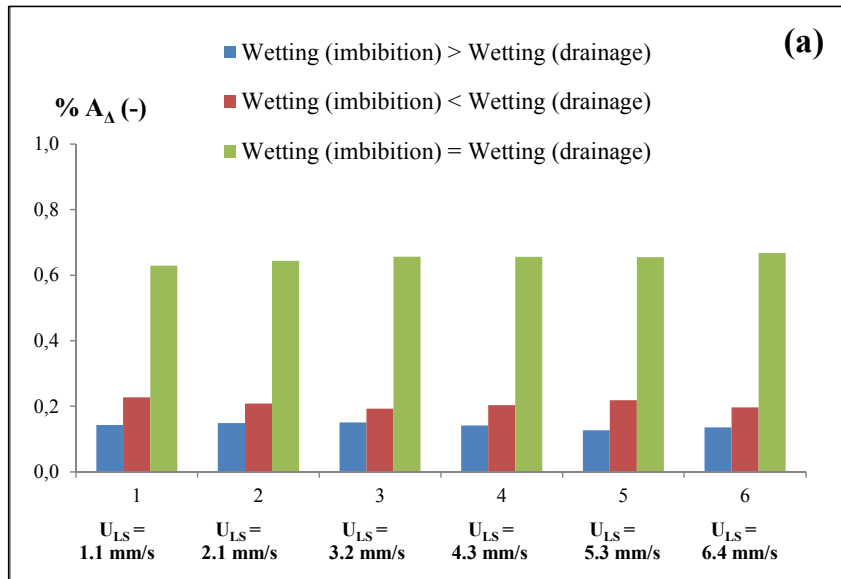


**Figure 4-8.** (a, c): Fraction of liquid occupying bed texture in both imbibition and drainage, and comparative percentage of indifferent regions (green parts of Figure 8a) adapted from Faridkhou and Larachi [7], for  $D/d_p \approx 10$ . (b, d): Fraction of liquid-occupying bed texture in both imbibition and drainage, and the comparative percentage of the indifferent regions (green parts of Figure 8b) as current work for  $D/d_p \approx 20$ .

### 4.3.3 Transient behavior

As for the dynamics of the micro-fixed beds at iso-G conditions, Figures 4-9a,b depict the effect of bed geometry on the transient behavior for two different particle sizes. The parameter  $\theta$  is the dimensionless form of the transient time ( $t_t$ ) defined as:

$$\theta = \frac{t_t}{\frac{l_{MFB}}{U_{LS}}} \quad (4-1)$$

Where  $l_{MFB}$  is the micro-fixed bed length and  $U_{LS}$  is the superficial liquid velocity according to the geometry. For both particle size ranges of 53-63  $\mu\text{m}$  and 106-125  $\mu\text{m}$  corresponding to  $D/d_p \approx 20$  and  $D/d_p \approx 10$ , respectively, it can be observed from Figures 4-9a,b that micro-fixed beds of square geometry exhibit a shorter transient time in comparison with the circular geometry. The difference in transient times is more pronounced as the liquid superficial velocity increases according to the embedded plots in Figures 4-9a,b where the ratio of the dimensionless transient times are plotted against  $U_{LS}$ . The reason for this could be due to the stabilizing effect of the liquid film pulled to the corners of the square micro-fixed bed due to surface tension forces which shortens the transient time by damping the interactions between gas and liquid phase. The effect of solid particle size (or column-to-particle diameter ratio) on transient time for square and circular geometries are illustrated in Figures 4-10a,b, respectively. As can be seen the transient time in both geometries decreases for larger particle sizes (smaller  $D/d_p$  ratios). This could be due to a higher porosity and lesser tortuous paths in beds of larger particle sizes making faster and more efficient contact between gas and liquid phases which will in turn reduce the transient time. Nevertheless, as the embedded plots in Figures 4-10a,b suggest, the ratio of the transient times do not exhibit a regular increasing or decreasing trend with respect to liquid superficial velocity. The results are also in agreement with the model results of Andersson and Holmedal<sup>31</sup> obtained in macro-scale for fluid flow through porous media.

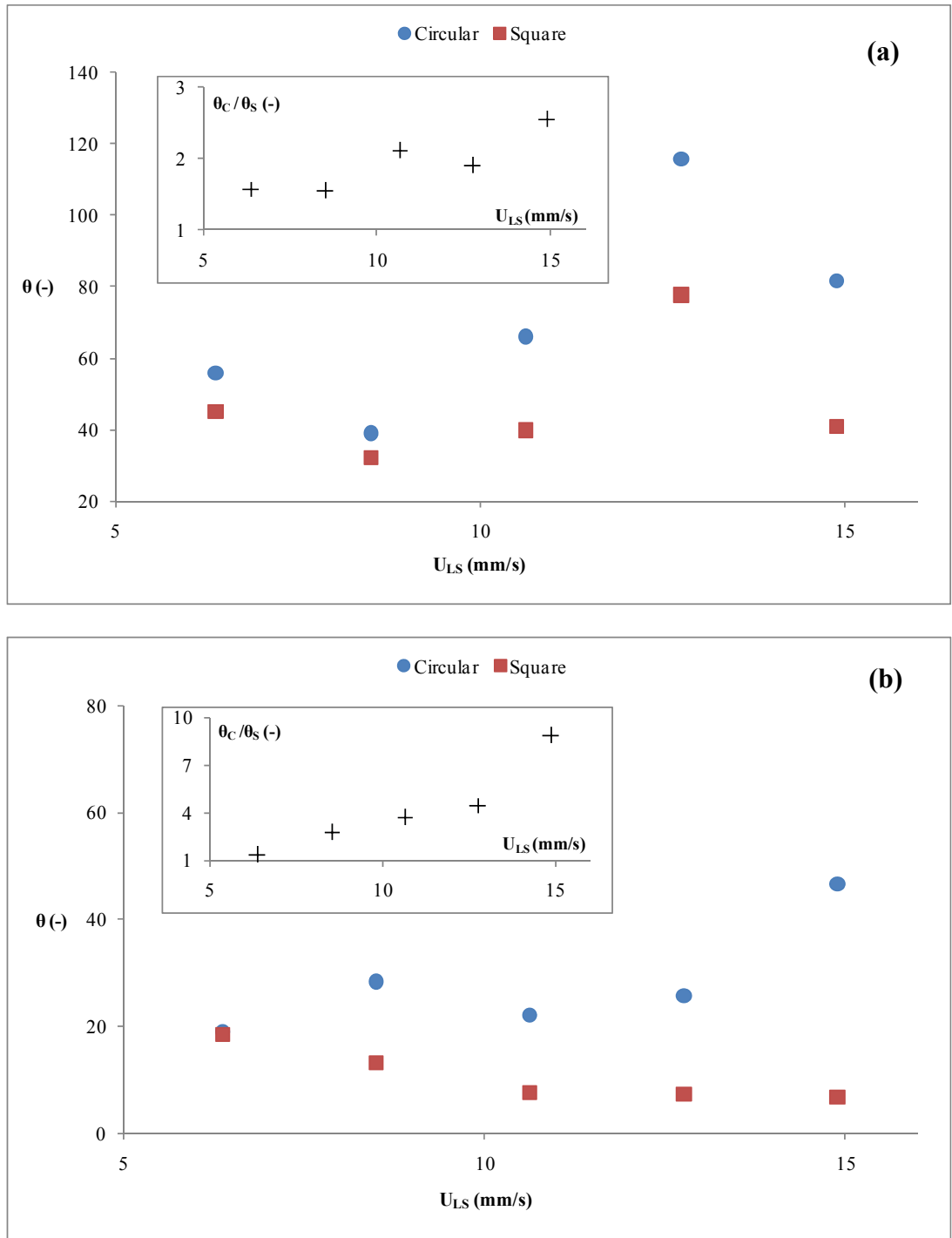


**Figure 4-9.** Effect of geometry on the dimensionless transient time of micro-fixed beds at a)  $D/d_p \approx 20$  and b)  $D/d_p \approx 10$ .

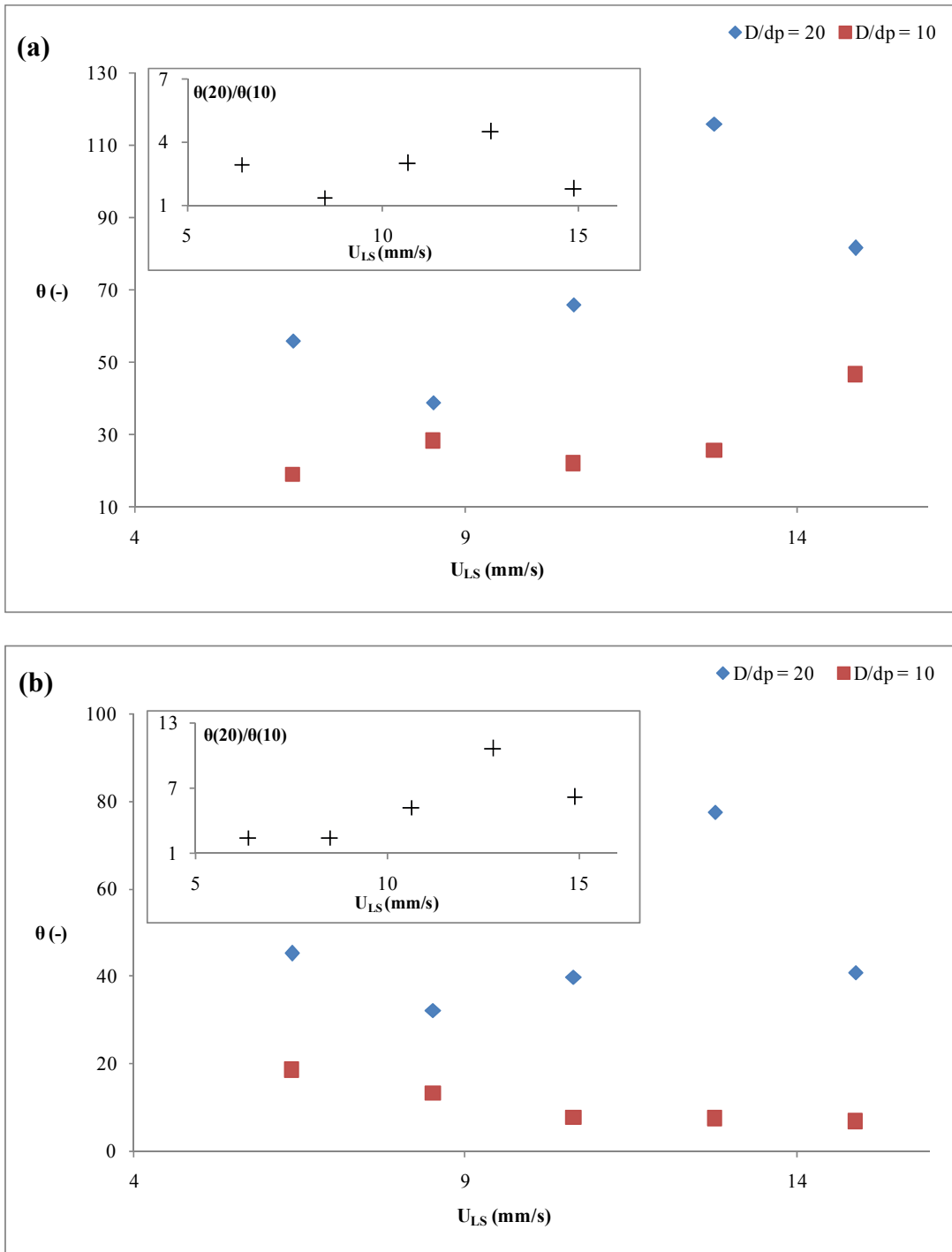


**Figure 4-10.** Effect of particle size (column-to-particle diameter ratio) on the dimensionless transient time in micro-fixed bed of a) circular geometry and b) square geometry.



## 4.4 Conclusion

In the current work, the effects of solid particle size and bed cross-sectional geometry on a number of hydrodynamic parameters of micro-fixed beds were subjected to investigation. The parameters included: bed pressure drop, flow regime transition point, hysteresis and the bed transient behavior. Based on microscopic observations, it was observed that high interactions between gas and liquid phases start at the near-outlet zone of the bed and are gradually propagated toward the near-inlet zone. For this reason, visual observations at near-inlet zones can confirm whether or not the high interaction flow regime prevails within the entire bed. Using smaller particle sizes at similar gas-liquid flow ratios caused an earlier inception of the high interaction regime whereas cross-sectional geometry of the bed did not affect the point of flow regime transition. Wetting pattern hysteresis in micro-fixed bed was shown to be strongly influenced by changes in solid particle size (or tube-to-particle diameter ratio). The time required for the bed pressure drop to achieve a new steady state upon a step change in liquid flow rate (as a measure of the micro-fixed bed transient behavior) was determined and it was revealed that larger particle sizes and square geometry possess shorter transient times as compared to smaller particle sizes and circular geometry. Although wall visualizations can address parts of the hydrodynamic aspects of micro-fixed beds, there exist other methods which can be applied successfully for more in-depth studies and interpretations such as micro-computed tomography for visualizing gas-liquid interactions and their distribution at any depth within the bed or micro-particle image velocimetry ( $\mu$ -PIV) for flow field velocity determination which are within the scope of the future works.

## 4.5 Nomenclature

$\%A$	Area percentage (Figure 8) (-)
$d_p$	Solid particle diameter (L)
$D$	Tube (Column) diameter (L)
$G$	Gas mass flow ( $MT^{-1}$ )
$l$	Microreactor length (L)
$L$	Liquid mass flow ( $MT^{-1}$ )
$P$	Pressure ( $ML^{-1}T^{-2}$ )
$t_t$	Transient time (T)
$U_{GS}$	Gas phase superficial velocity ( $L T^{-1}$ )
$U_{LS}$	Liquid phase superficial velocity ( $L T^{-1}$ )

### Greek letters

$\Delta$	Difference (-)
$\theta$	Dimensionless transient time (-)
$\lambda_L$	Liquid characteristic length (L)
$\sigma$	Standard deviation

### Subscripts

$i$	Initial steady state
$j$	Final steady state
$L$	Liquid phase
$MFB$	Micro-fixed bed

## 4.6 References

1. Inoue, T.; Schmidt, M. A.; Jensen, K. F., Microfabricated multiphase reactors for the direct synthesis of hydrogen peroxide from hydrogen and oxygen. *Industrial & Engineering Chemistry Research* **2007**, 46, (4), 1153-1160.
2. Guettel, R.; Turek, T., Assessment of micro-structured fixed-bed reactors for highly exothermic gas-phase reactions. *Chemical Engineering Science* **2010**, 65, (5), 1644-1654.
3. Renken, A.; Kiwi-Minsker, L., Microstructured Catalytic Reactors. In *Advances in Catalysis, Vol 53*, Gates, B. C.; Knozinger, H.; Jentoft, F. C., Eds. Elsevier Academic Press Inc: San Diego, 2010; Vol. 53, pp 47-122.
4. Losey, M. W.; Schmidt, M. A.; Jensen, K. F., Microfabricated multiphase packed-bed reactors: Characterization of mass transfer and reactions. *Industrial & Engineering Chemistry Research* **2001**, 40, (12), 2555-2562.
5. Ajmera, S. K.; Delattre, C.; Schmidt, M. A.; Jensen, K. F., Microfabricated cross-flow chemical reactor for catalyst testing. *Sensors and Actuators B-Chemical* **2002**, 82, (2-3), 297-306.
6. Tadepalli, S.; Qian, D. Y.; Lawal, A., Comparison of performance of microreactor and semi-batch reactor for catalytic hydrogenation of o-nitroanisole. *Catalysis Today* **2007**, 125, (1-2), 64-73.
7. Faridkhou, A.; Larachi, F., Hydrodynamics of Gas-Liquid Cocurrent Flows in Micropacked Beds-Wall Visualization Study. *Industrial & Engineering Chemistry Research* **2012**, 51, (50).
8. Marquez, N.; Castano, P.; Makkee, M.; Moulijn, J. A.; Kreutzer, M. T., Dispersion and holdup in multiphase packed bed microreactors. *Chemical Engineering & Technology* **2008**, 31, (8), 1130-1139.
9. Marquez, N.; Castano, P.; Moulijn, J. A.; Makkee, M.; Kreutzer, M. T., Transient Behavior and Stability in Miniaturized Multiphase Packed Bed Reactors. *Industrial & Engineering Chemistry Research* **2010**, 49, (3), 1033-1040.
10. Knobloch, C.; Guettel, R.; Turek, T., Holdup and Pressure Drop in Micro Packed-Bed Reactors for Fischer-Tropsch Synthesis. *Chemie Ingenieur Technik* **2013**, 85, (4), 455-460.

11. Haase, S.; Weiss, M.; Langsch, R.; Bauer, T.; Lange, R., Hydrodynamics and mass transfer in three-phase composite minichannel fixed-bed reactors. *Chemical Engineering Science* **2013**, 94, 224-236.
12. Aubin, J.; Prat, L.; Xuereb, C.; Gourdon, C., Effect of microchannel aspect ratio on residence time distributions and the axial dispersion coefficient. *Chemical Engineering and Processing* **2009**, 48, (1), 554-559.
13. Chaouki, J.; Larachi, F.; Dudukovic, M. P., Noninvasive tomographic and velocimetric monitoring of multiphase flows. *Industrial & Engineering Chemistry Research* **1997**, 36, (11), 4476-4503.
14. Boyer, C.; Duquenne, A. M.; Wild, G., Measuring techniques in gas-liquid and gas-liquid-solid reactors. *Chemical Engineering Science* **2002**, 57, (16), 3185-3215.
15. Yue, J.; Luo, L. G.; Gonthier, Y.; Chen, G. W.; Yuan, Q., An experimental investigation of gas-liquid two-phase flow in single microchannel contactors. *Chemical Engineering Science* **2008**, 63, (16), 4189-4202.
16. Waelchli, S.; von Rohr, P. R., Two-phase flow characteristics in gas-liquid microreactors. *International Journal of Multiphase Flow* **2006**, 32, (7), 791-806.
17. Faridkhou, A.; Hamidipour, M.; Larachi, F., Hydrodynamics of gas-liquid micro-fixed beds - Measurement approaches and technical challenges. *Chemical Engineering Journal* **2013**, 223, 425-435.
18. Marquez, N.; Musterd, M.; Castano, P.; Berger, R.; Moulijn, J. A.; Makkee, M.; Kreutzer, M. T., Volatile tracer dispersion in multi-phase packed beds. *Chemical Engineering Science* **2010**, 65, (13), 3972-3985.
19. Iliuta, I.; Hamidipour, M.; Schweich, D.; Larachi, F., Two-phase flow in packed-bed microreactors: Experiments, model and simulations. *Chemical Engineering Science* **2012**, 73, 299-313.
20. Coleman, J. W.; Garimella, S., Characterization of two-phase flow patterns in small diameter round and rectangular tubes. *International Journal of Heat and Mass Transfer* **1999**, 42, (15), 2869-2881.
21. Triplett, K. A.; Ghiaasiaan, S. M.; Abdel-Khalik, S. I.; Sadowski, D. L., Gas-liquid two-phase flow in microchannels - Part I: two-phase flow patterns. *International Journal of Multiphase Flow* **1999**, 25, (3), 377-394.

22. Cubaud, T.; Ho, C. M., Transport of bubbles in square microchannels. *Physics of Fluids* **2004**, 16, (12), 4575-4585.
23. Liu, N.; Li, J. M.; Sun, J.; Wang, H. S., Heat transfer and pressure drop during condensation of R152a in circular and square microchannels. *Experimental Thermal and Fluid Science* **2013**, 47, 60-67.
24. Attou, A.; Ferschneider, G., A two-fluid hydrodynamic model for the transition between trickle and pulse flow in a cocurrent gas-liquid packed-bed reactor. *Chemical Engineering Science* **2000**, 55, (3), 491-511.
25. Sai, P. S. T.; Varma, Y. B. G., Pressure-drop in gas-liquid downflow through packed-beds. *Aiche Journal* **1987**, 33, (12), 2027-2036.
26. Larachi, F.; Laurent, A.; Midoux, N.; Wild, G., Experimental study of a trickle bed reactor operating at high pressure- 2-Phase pressure-drop and liquid saturation. *Chemical Engineering Science* **1991**, 46, (5-6), 1233-1246.
27. Larachi, F.; Laurent, A.; Wild, G.; Midoux, N., Some experimental liquid saturation results in fixed-bed reactors operated under elevated pressure in cocurrent upflow and downflow of the gas and the liquid. *Industrial & Engineering Chemistry Research* **1991**, 30, (11), 2404-2410.
28. Ng, K. M., A model for flow regime transitions in cocurrent down-flow trickle bed reactors. *Aiche Journal* **1986**, 32, (1), 115-122.
29. Holub, R. A.; Dudukovic, M. P.; Ramachandran, P. A., Pressure-drop, liquid-holdup, and flow regime transition in trickle flow. *Aiche Journal* **1993**, 39, (2), 302-321.
30. Krieg, D. A.; Helwick, J. A.; Dillon, P. O.; McCready, M. J., Origin of disturbances in cocurrent gas-liquid packed-bed flows. *Aiche Journal* **1995**, 41, (7), 1653-1666.
31. Andersson, H. I.; Holmedal, L. E., Start-up flow in a porous-medium channel. *Acta Mechanica* **1995**, 113, (1-4), 155-168.



## **5 Determination of liquid-solid mass transfer coefficient in micro-packed beds using the limiting current technique**

**Résumé:** La détermination expérimentale du coefficient de transfert de masse liquide-solide ( $k_{LS}$ ) par la technique électrochimique (polarisation linéaire) a été effectuée dans un micro-lit fixe rempli de couches de particules de graphite non-sphériques servant de cathode et d'anode. La réaction électrochimique choisie pour le travail a été la réaction d'oxydo-réduction des ions ferri- et ferrocyanures. Les expériences ont été réalisées pour un écoulement monophasique (solution d'électrolyte contenant du ferri- et le ferrocyanure de potassium, avec de la soude comme électrolyte de référence) et en régime de diffusion limitée. Afin de déterminer les déviations liées à la géométrie sphérique, à la surface spécifique et totale des particules de graphite, des traitements d'image 2D des particules de graphite ont été utilisés. Deux approches (moyenne arithmétique et logarithmique de la concentration) ont permis de tenir compte de l'incidence de la variation axiale de concentration le long du lit pour déterminer le coefficient de transfert de masse liquide-solide. Finalement, la correspondance de valeurs de  $k_{LS}$  avec les corrélations construites sur la base d'études sur les lits fixes à l'échelle macroscopique (en termes de nombre de Sherwood, pour l'écoulement monophasique) a été étudiée.

**Abstract:** Experimental determination of liquid-solid mass transfer coefficient ( $k_{LS}$ ) via a linear polarization method was carried out in a micro-packed bed filled with layers of non-spherical graphite particles serving as cathode and anode for the Redox ferri/ferrocyanide electrochemical reaction. Experiments concerned single-phase liquid flow (electrolyte solution containing potassium ferri- and ferrocyanide along with NaOH as the background electrolyte) within the diffusion-limited regime. Particle size analysis and image processing were used to evaluate deviations from spherical geometry of the graphite particles while two concentration averaging approaches (logarithmic and arithmetic) were used to account for the species concentration variations with bed length to determine liquid-solid mass transfer coefficient. Finally, the correspondence of  $k_{LS}$  values with macro-scale packed bed correlations (in terms of Sherwood number and for single-phase liquid flow) was discussed.



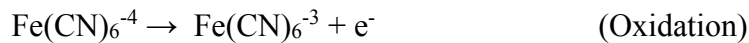
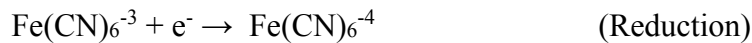
## 5.1 Introduction

Chemical processing at micro-scales has undisputed advantages such as high surface to volume ratios, enhanced heat and mass transfer rates, increased productivity and improved safety. The emergence of micro-reactors has thus triggered a wide range of scientific investigations and researches in a variety of domains.<sup>1</sup> As a subcategory of microreactors, micro-packed beds are micro-scale versions of the packed beds ubiquitously employed in industry. These units possess the advantages of micro-scale operation on one hand and those of macro-scale packed beds (e.g. efficient contact between phases) on the other hand.<sup>2</sup> Thus far, micro-packed beds have been used promisingly for processes such as Fischer-Tropsch synthesis,<sup>3</sup> hydrogenation,<sup>4</sup> oxidation,<sup>5</sup> reforming,<sup>6</sup> and so forth.

Despite a number of kinetic studies performed on micro-packed beds, studies on mass transfer especially on the liquid-solid contribution are quite scarce.<sup>7</sup> Therefore, in order to build a research strategy for mass transfer studies in micro-packed beds, one could review the open literature in search for similar studies on their macro-scale lookalikes. The experimental procedures and methodologies adopted in such kind of works could be then customized to their micro-scale versions.<sup>8</sup> As for macro-scale packed beds, a number of experimental methods have been devised to determine liquid-solid mass transfer coefficients,<sup>9</sup> among which two have gained more popularity: 1) dissolution of soluble solids in liquids<sup>9-11</sup> and 2) electrochemical techniques.<sup>12-17</sup> Despite the widespread use of dissolution method in liquid-solid mass transfer studies, there are drawbacks associated with this method. As pointed out by Al-Dahhan et al.,<sup>9</sup> the method suffers from underestimating the solid-liquid mass transfer rate in low interaction regime which is attributed to partial particle wetting by the liquid. These authors also argued that the dissolution method works well for packed beds operating at atmospheric pressures, however, once operating pressure is increased, losses of dissolved material was observed at the outlet stream requiring modifications of the experimental procedure.<sup>11</sup>

To the best of the authors' knowledge, Tidona et al.<sup>7</sup> were the first who have attempted a determination of liquid-solid mass transfer coefficients in microscale objects using the dissolution method. This latter consists of feeding a solution of potassium dichromate and sulfuric acid through a packed bed of copper particles and where the mass

transfer coefficients were estimated based on the assumption of constant copper particle size (neglecting shrinkage of particles in contact with potassium dichromate and sulfuric acid). As an alternative to the dissolution method in both macro- and micro-scale setups, the electrochemical method (also known as limiting-current technique) is a well-established method for determining liquid-solid mass transfer coefficients<sup>9,16</sup> and has been increasingly employed in mass transfer studies to determine the liquid-solid mass transfer coefficient at macro-scale. The working principle of the limiting-current technique is to monitor and measure the current at the working electrode by applying a range of potentials (also known as potential scan or linear sweep voltammetry) to the electrochemical cell. The electrochemical cell consists of electrodes as well as the electrolyte solution containing reducing and oxidizing reactants (for a list of model reactions and redox couples used in limiting-current mass transfer studies, one can refer to Selaman and Tobias<sup>18</sup>). One of the most popular reaction models is the redox reaction of ferricyanide ( $\text{Fe}(\text{CN})_6^{-3}$ ) and ferrocyanide ( $\text{Fe}(\text{CN})_6^{-4}$ ) ions<sup>14,17,19</sup> which proceeds as follows:



The resulting current-potential (or I-V) curve obtained from the sweep voltammetry is schematically shown in Figure 5-1. At the start of the potential scan the kinetic regime prevails characterized by the rather sharp increase of current with changes in potential. In this region, the intrinsic reaction rate of the redox reaction controls the current.<sup>17</sup> After further increase in potential, the current reaches a saturation level ( $I_{lim}$ ) as illustrated in Figure 5-1. This region coincides with the diffusion-limited plateau where the rate of transfer of the charged species from the electrolyte solution onto the electrode surface is the limiting factor. The effective liquid-solid mass transfer coefficient is calculated based on the limiting current as follows:

$$\phi k_{LS} = \frac{I_{lim}}{n_e F A_e C} \quad (5-1)$$

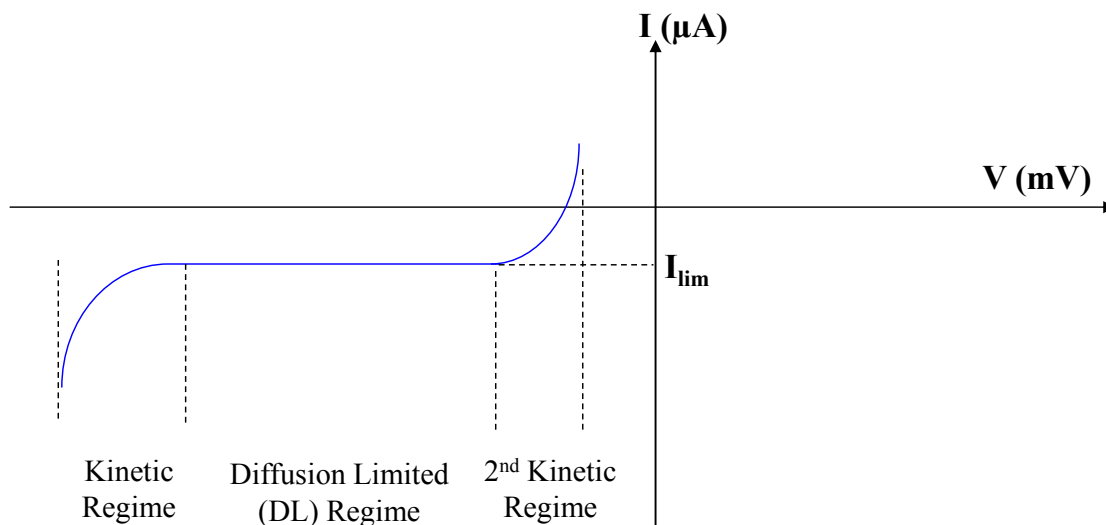


**Figure 5-1.** Schematic of the I-V curve obtained from limiting-current technique

where  $\phi_{k_{LS}}$  is the product of wetting efficiency ( $\phi$ ) and liquid-solid mass transfer coefficient ( $k_{LS}$ ) termed as effective liquid-solid mass transfer coefficient,  $I_{lim}$  is the limiting current,  $n_e$  is the number of redox-exchanged electrons,  $F$  is the faraday number,  $A_e$  is electrode surface area and  $C$  is the bulk concentration of the reducing reactant (ferricyanide). In single-phase liquid flow,  $\phi = 1$ . The objective of the current work is provide preliminary measurements of liquid-solid mass transfer coefficients in micro-packed beds and discuss the challenges surrounding the use of the limiting-current technique with the redox reaction of ferri- and ferrocyanide as model reaction in obtaining this crucial information.

## 5.2 Experimental

### 5.2.1 Setup

The experimental setup for the mass transfer study is shown in Figure 5-2. For single-phase liquid flow tests, an aqueous solution of 1M NaOH (provided from VWR), 0.02M  $K_4Fe(CN)_6$  and 0.003M  $K_3Fe(CN)_6$  (supplied from Laboratoire Mat-Québec) was used as an electrolyte. The physical properties of the solution are reported elsewhere.<sup>15,17,19,20</sup> The use of high concentrations of NaOH as background and inert supporting electrolyte is to suppress the ion flux contributed by migration and increase the solution electrical conductivity.<sup>18</sup> The

electrolyte solution is delivered by a syringe pump (Orion Sage model M365) and passes through a circular capillary tube (ID = 1mm) packed with layers of spherical micron size glass beads (supplied from Mo-Sci Co.) and graphite particles (purchased from Alfa Aesar). The packing remained stationary in the packed tube owing to a stainless steel grid located at the bed exit.

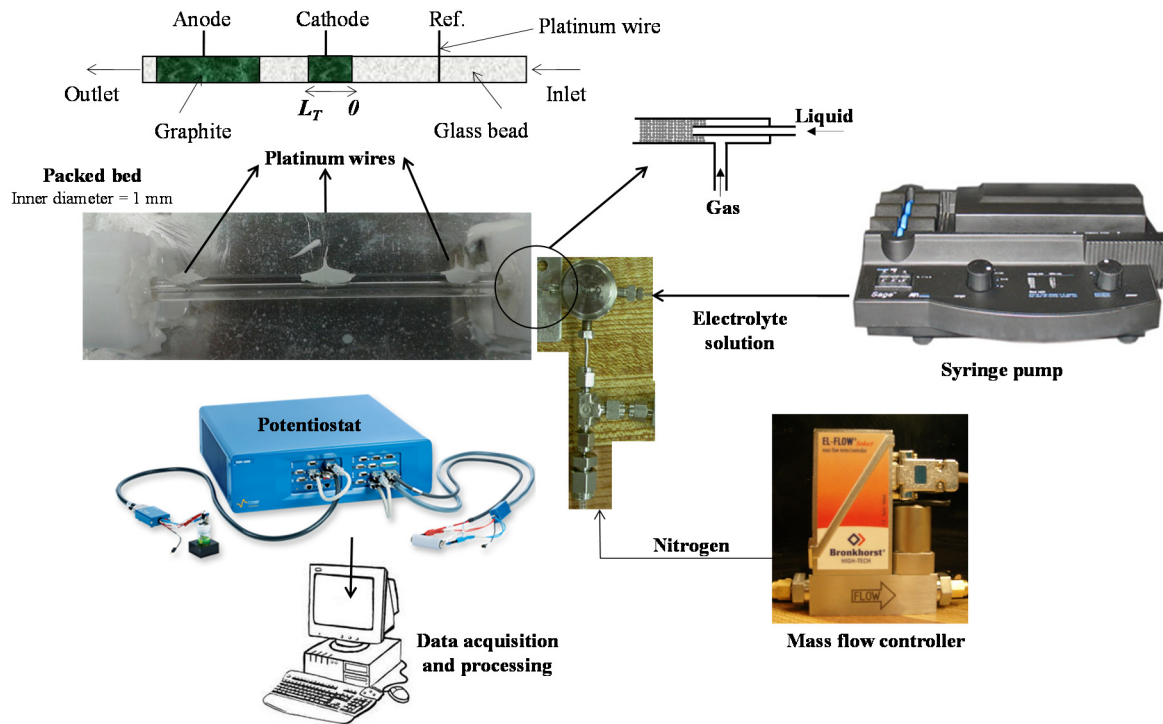


**Figure 5-2.** Experimental setup of the micro-fixed bed reactor for liquid-solid mass transfer studies

It should be noted that nickel particles were initially used instead of graphite particles. Peculiar behaviour of the current in the would-be plateau region led to the observation of very low currents in the mass transfer limited region which was attributed to gradual deactivation of nickel particles due to nickel oxide layer formation. This led to abandon the nickel electrochemical system. The graphite flakes were crushed and sieved to the same size distribution as the glass beads serving to serve as cathode and anode (see Figure 5-2). Two groups of particles were used: group A, graphite particles retained in between 53 $\mu$ m and 63 $\mu$ m sieves and group B, particles retained in-between 125 $\mu$ m and 150 $\mu$ m sieves. Three platinum wires were inserted perpendicular to flow direction in the capillary tube, two of which were in contact with the anode and cathode graphite layers while the third one was

inserted within the glass bead section serving as a reference electrode. The other ends of the three platinum wires were clip-connected to a potentiostat (model VSP-27 from Bio-Logic SA) to monitor applied voltage and current generated according to a linear polarization (LP) technique.

In the two-phase flow experiments, liquid is fed by the same syringe pump while the gas phase (N<sub>2</sub>) is fed via a mass flow controller (EL-Flow Bronkhorst). Gas and liquid phases are brought into contact by a T-junction located upstream of the packed bed consisting of a coaxial arrangement. Liquid passes through the inner tube while the gas flows within the annular area between liquid line and the outer tube and both are then concurrently fed to the tube. A graduated cylinder is placed at the outlet to collect the liquid and it is used as a double check for liquid flow rate specified for the syringe pump. Upon achieving the steady state at each flow rate, the potentiostat is triggered to perform a sweep voltammetry at 15 mV/s scan rate. Each scan for each given flow rates was repeated at least thrice to ensure reproducibility.

### **5.2.2 Methodology**

Determination of liquid-solid mass transfer in a micro-packed bed partly filled with graphite particles encountered a number of challenges each will be explained in detail as follows:

*Preparation:* A number of experimental details should be thoroughly taken care of during preparation for performing the experiments in order to obtain a plateau with acceptable reproducibility:

1) The presence of miscellaneous ions in the water leads to changes in the shape of the I-V curve as unexpected bump(s) will appear at the start of the diffusional plateau zone (which is the sign for an undesirable electrochemical reaction). To ensure that the ionic species present in tap water will not negatively affect the results, the electrolyte solution should be prepared with deionized water. In the current work, deionized water with resistivity of 18.2 MΩ-cm was used and no bump in the diffusion limited regime was observed.

2) The electrolyte solution must be used as fresh before each set of experiment and its direct exposure to air and sunlight must be avoided. Therefore, the fresh solution (from which the syringe pump is refilled) is constantly kept in an opaque container while nitrogen

is being bubbled into it. Meanwhile, the liquid line from the syringe pump to the micro-packed bed is covered by aluminium foil to prevent light exposure.

3) The capillary tube along with platinum wires were washed with diluted sulphuric acid after each set of experiment and rinsed with deionized water to ensure that there will not be any source of contamination for the subsequent set of experiment.

*Concentration gradient within bed length:* According to Figure 5-2, the electrolyte solution containing ferricyanide and ferrocyanide first passes through the cathode where ferricyanide reduction to ferrocyanide takes place. Upon voltage application to the electrochemical cell, electrons discharge through the platinum wire into the cathodic graphite layer. This could be considered as identical to mass transfer in catalytic packed beds of length  $L$  in which a rapid surface reaction takes place. The equation for calculating the axial concentration profile could be found elsewhere: <sup>21</sup>

$$C_L = C_0 e^{-\frac{k_{LS}aL}{U}} \quad (5-2)$$

Where  $C_0$  is the initial concentration of ferricyanide,  $a$  is the specific surface area and  $U$  is the superficial velocity. Due to the high specific surface area of the graphite particles ( $a$ ) which is inherent to micro-scale packed beds, the cathode length ( $L_T$ ) should be as small as possible (a few millimetres) to ensure that its entire length has been actively used for ferricyanide reduction otherwise, there will be a depletion of ferricyanide ion at a length shorter than  $L_T$ . Since variations in axial concentration (through the cathode) are not negligible, the concentration term in equation (1) should be replaced by an averaged value:

which can be either: 1)  $\frac{1}{L_T} \int_0^{L_T} C_0 e^{-\frac{k_{LS}ax}{u}} dx$  or 2) the arithmetic average of concentrations at the two extremes of the cathode length  $C_M = (C_{L_T} + C_0)/2$  where  $C_{L_T}$  is determined from equation (5-2). Combining the integrally averaged concentration term with equation (5-1) assuming single-phase liquid flow ( $\phi=1$ ) gives:

$$k_{LS} = -\alpha \ln(1 - \beta) \quad (5-3)$$

where

$$\alpha = \frac{u}{aL_T} \quad (5-4)$$

$$\beta = \frac{IL_T}{n_eFA_eC_0u} \quad (5-5)$$

While substitution of the arithmetically averaged concentration in equation (5-1) gives:

$$k_{LS} = \frac{I_{lim}}{n_eFA_eC_M} \quad (5-6)$$

**Geometry of graphite particles** The issue with graphite particles is their non-spherical shape making the calculations for specific surface area and total surface less straightforward. One approach to deal with this problem is to use the sphericity factor ( $\Psi$ ) and equivalent diameter ( $d_{eq}$ ) to account for deviations from spherical geometry.<sup>22,23</sup> This is achieved by taking multiple 2D images from graphite particles (around 20 images from each size distribution) to represent the average particle geometries. Figures 5-3.a and 5-3.b shows images taken from the two size distributions. The acquired images are processed using ImageJ software. The image processing task includes fitting (approximating) the graphite particles with ellipses characterized by parameters such as major axis, minor axis, aspect ratio and circularity. The final step of image processing entails: 1) assigning surface areas (A) to the particles (based on which an equivalent diameter can be defined as:  $d_{eq} = \sqrt{4A/\pi}$  and 2) classifying the particles based on their surface area in the form of a frequency histogram (from which the distributions for particle size, volume and mass could be deduced). The particle size distributions (based on equivalent diameter) are shown in Figures 5-4.a and 5-4.b for groups A and B. As for the non-spherical graphite particles, it is reasonable to assume that the 3D term of sphericity can also be represented by circularity ( $C$ ) which is a 2D term<sup>24</sup> and can be drawn from image processing. Having evaluated the circularity for graphite particles, the specific surface area and total area should be corrected so that deviation from spherical geometry is accounted for according to equations 7 and 8:

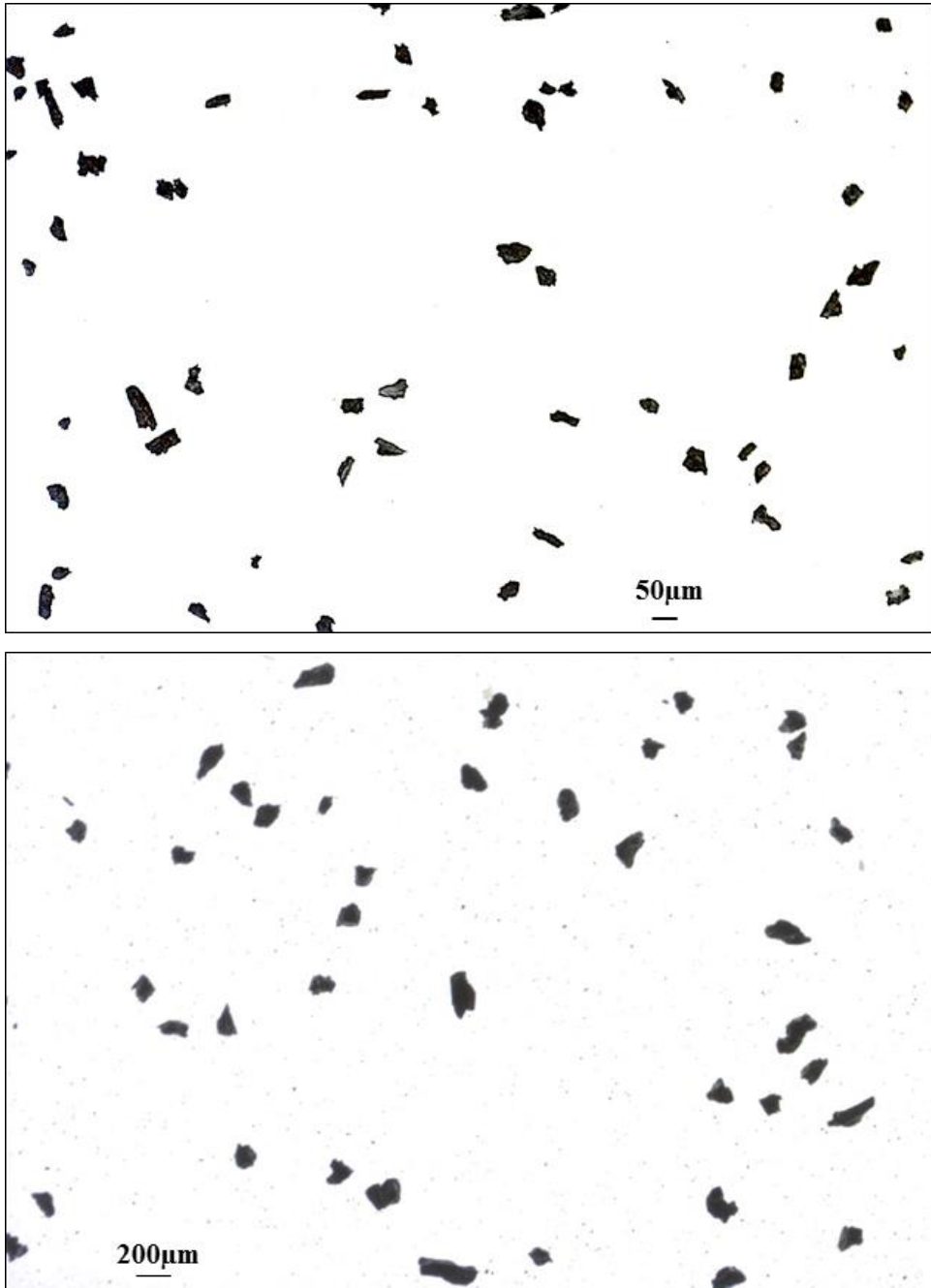


**Figure 5-3.** Images of graphite particles of two different sizes: Group A (top) Group B (bottom)

$$a_{corrected} = \frac{a}{\zeta} \quad (5-7)$$



$$A_{corrected} = \frac{A}{\zeta} \quad (5-8)$$

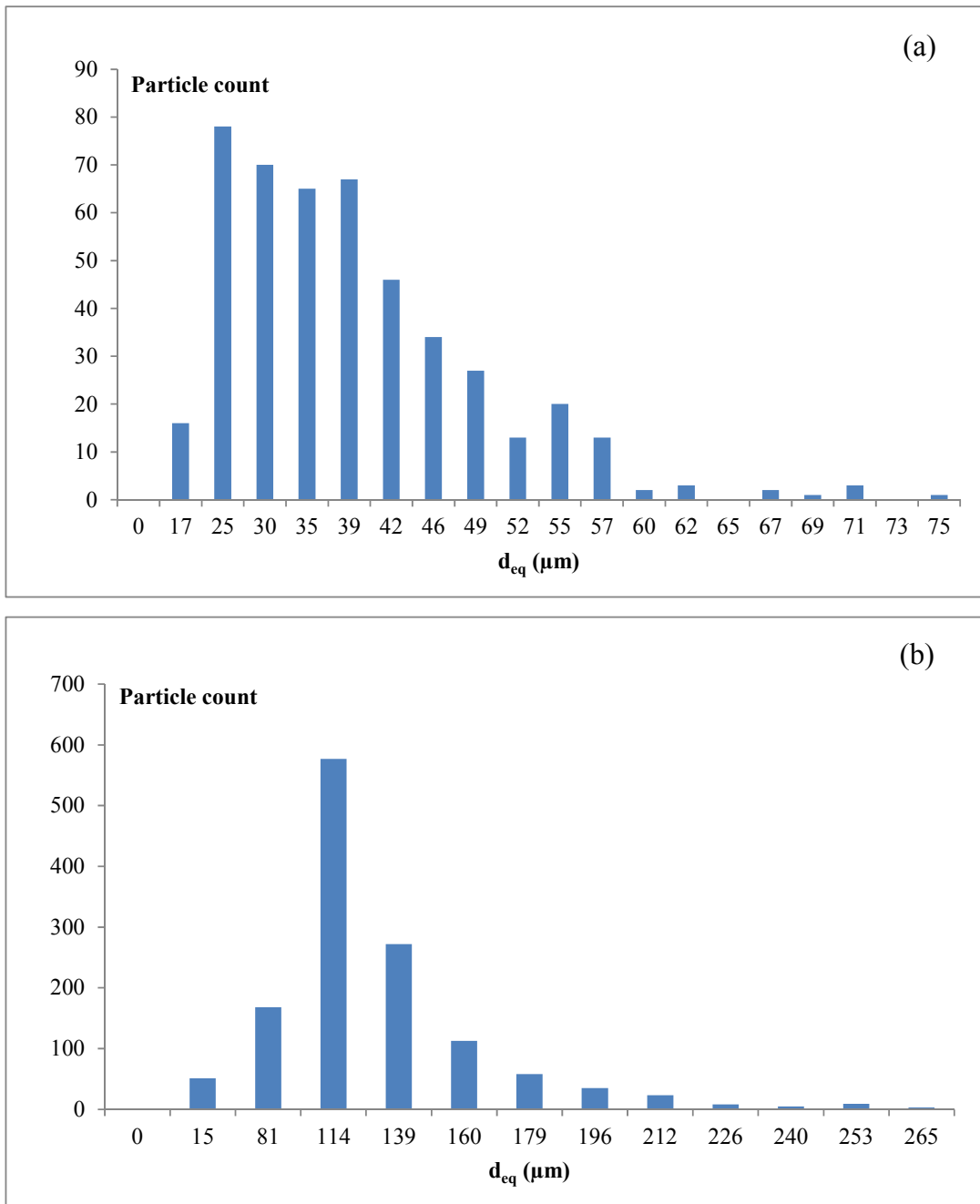


**Figure 5-4.** Size distribution based on equivalent diameter for graphite particles of a) Group A and b) Group B.

The average values for circularity are 0.6 and 0.64 for particles of group A and B, respectively.

## 5.3 Results and discussions

### 5.3.1 Single-phase liquid flow

Figures 5-5.a and 5-5.b depict I-V curves for particles of group A and group B, respectively, where the negative currents correspond to the cathodic ferricyanide reduction. As can be seen, the mass-transfer-controlled current plateau is expectably shifting toward more negative currents upon increasing liquid velocity merely mirroring the monotonic dependence of the mass transfer coefficient,  $k_{LS}$ , with respect to liquid superficial velocity through the bed.

Current plateaus for each liquid velocity are converted through equations (5-3) and (5-6) to liquid-solid mass transfer coefficients. Unfortunately for group A graphite particles (smaller size), it is not possible to evaluate the liquid-solid mass transfer coefficient from eq. (5-3) as with the existing experimental parameters (specific surface area, total surface area, cathode length and superficial velocity)  $C_{LT}$  approaches zero (100% conversion of ferricyanide at  $L_T$ ). As an explanation for logarithmic approach, this means that the length of the cathodic section ( $L_T$ ) is longer than actual length where the ferricyanide ion in the solution is totally depleted (due to higher mass transfer coefficient compared to group B particles). In case of the arithmetic averaging for concentration, the 100% conversion of ferricyanide at  $L_T$  means that the total depletion has occurred at a length  $L$  ( $L < L_T$ ) for which the total surface area, and thus the liquid-solid mass transfer coefficient from equation (5-6), cannot be readily determined. In order to obtain real values of liquid-solid mass transfer coefficient for group A graphite particles we should have tried to achieve a very short length of cathode (shorter than 2 mm) which was not feasible with our current packing protocol.

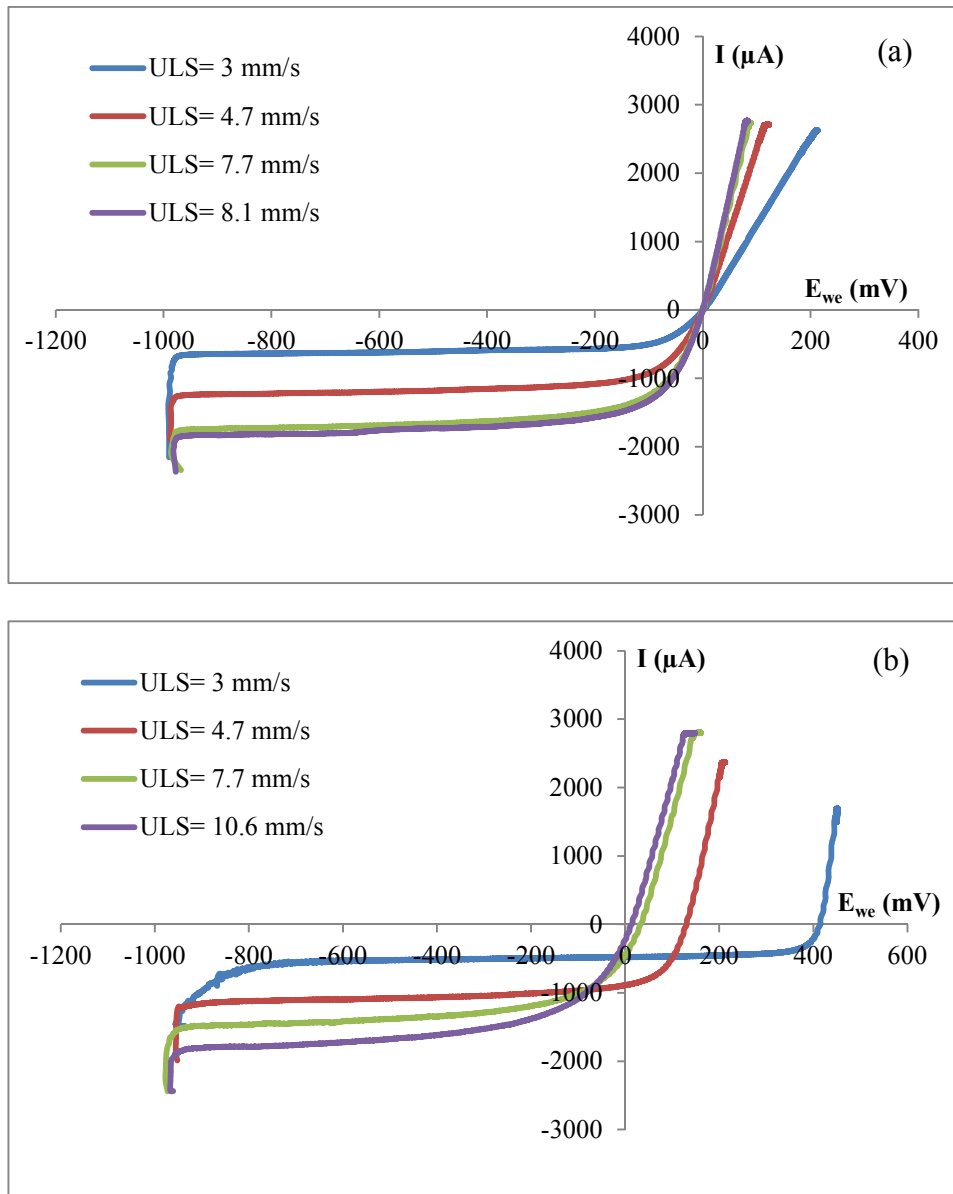


**Figure 5-5.** I-V curve in single-phase liquid flow experiments for graphite particles of a) Group A and b) Group B

The results for group B graphite particles determined from both logarithmic and arithmetic approaches are shown directly in Figure 5-6.a and in the dimensionless form (Sherwood vs. Reynolds number) in Figure 5-6.b. The increase in mass transfer coefficient with respect to velocity is consistent with what prevails in the diffusion-limited regime. As the logarithmic average for ferricyanide concentration is always smaller than its arithmetic average,  $k_{LS}$  values obtained for the logarithmic method are slightly higher than those evaluated with the arithmetic method. Furthermore, according to several correlations

proposed in macro-scale for Sherwood number as a function of Reynolds number<sup>25-27</sup>, it can be observed that  $k_{LS}$  (or  $Sh$ ) changes with  $U^b$  (or  $Re^b$ ) where  $b$  is often in the range of 0.33-0.58. This explains the asymptotic trend of  $k_{LS}$  and Sherwood number with respect to velocity and Reynolds number, respectively.

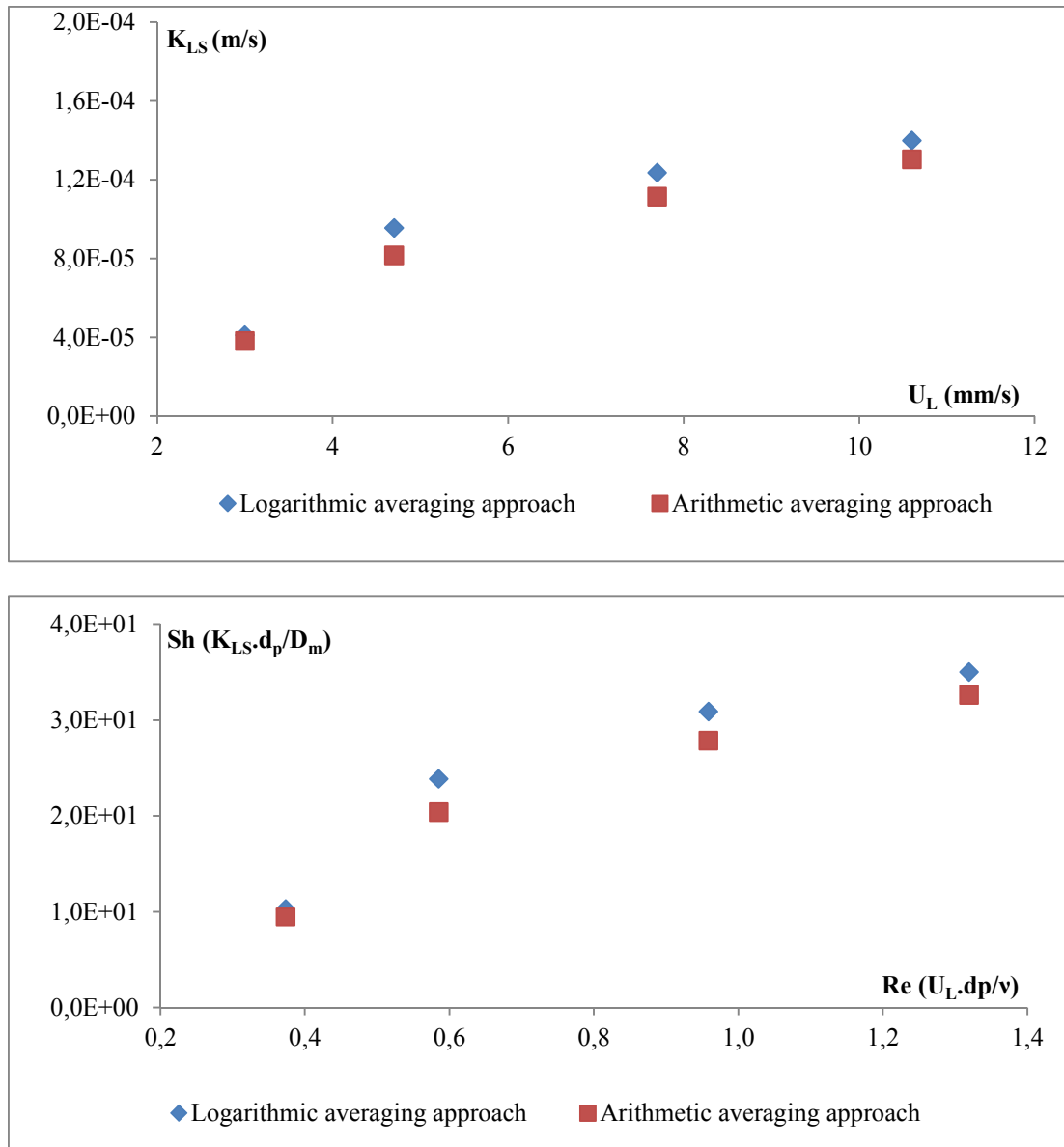


**Figure 5-6.** Liquid-solid mass transfer coefficients for group B graphite particles in both a) direct and b) dimensionless form comparing the logarithmic and arithmetic averaging approach for evaluating ferricyanide concentration

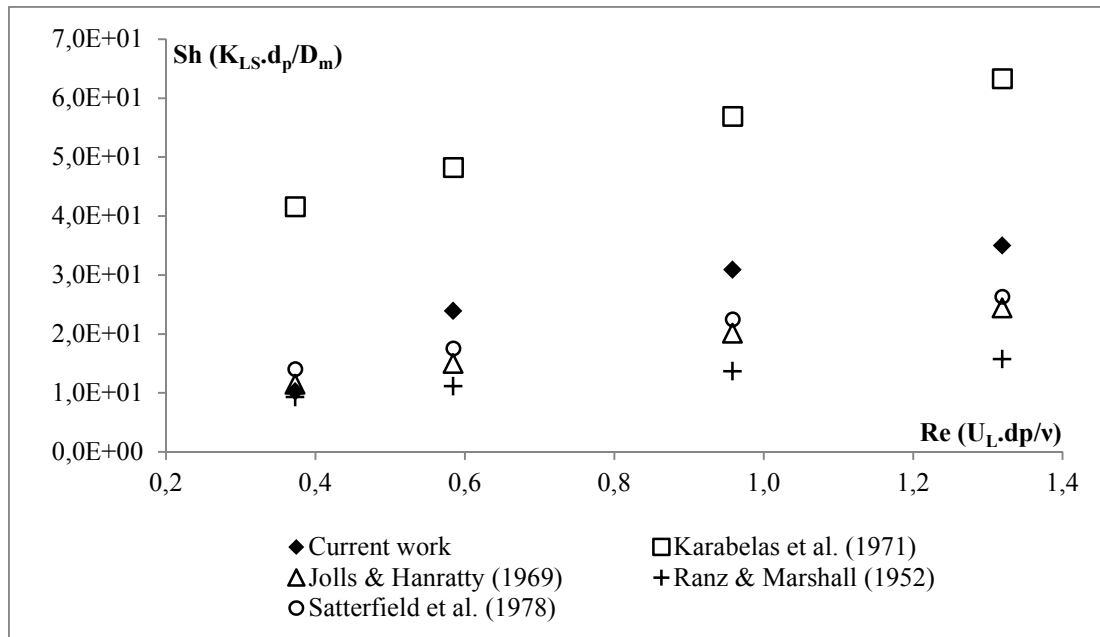
It is interesting to investigate whether or not current measurements for liquid-solid mass transfer coefficient at micro-scale are adequately captured by means of existing macro-scale correlations available in the literature for single-phase flow. The correlations are often in the form  $Sh = C_1 + C_2 Re^{C_3} Sc^{C_4}$  where  $C_i$  often takes one of the 0 or 2 values. Four samples of such correlations are presented in Table 5-1. In Figure 5-7, the experimental results obtained for liquid-solid mass transfer coefficient (for group B graphite particles) are compared against values predicted by the four macro-scale correlations developed for single-phase liquid flow in packed beds: i) Ranz and Marshall<sup>28</sup> ii) Jolls and Hanratty<sup>25</sup> iii) Karabelas et al.<sup>26</sup> and iv) Satterfield et al.<sup>10</sup>.

**Table 5-1.** Selected macro-scale correlations (in terms of Sherwood number) proposed for determination of liquid-solid mass transfer coefficient

Author(s)	Correlation	Remark
Ranz and Marshall <sup>28</sup>	$Sh = 2 + 0.6Re_L^{0.50}Sc^{1/3}$	Developed for evaporating drops
Jolls and Hanratty <sup>25</sup>	$Sh = 1.64(\varepsilon Re_L)^{0.60}Sc^{1/3}$	Random packing of monodisperse spheres ( $\varepsilon = 0.41$ )
Karabelas et al. <sup>26</sup>	$Sh = 4.58(\varepsilon Re_L)^{1/3}Sc^{1/3}$	Regular packed beds of uniform spheres ( $\varepsilon = 0.26$ )
Satterfield et al. <sup>10</sup>	$Sh = 1.15Re_L^{1/2}Sc^{1/3}$	Packed beds of cylindrical 3 × 3 mm and 6 × 6 mm tablets

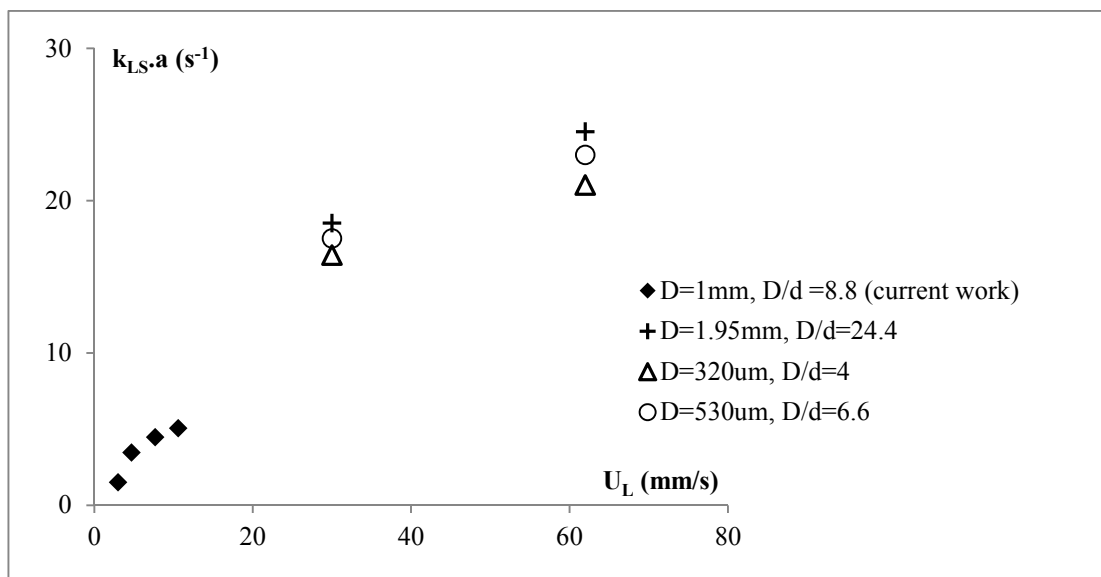
As can be observed from Figure 5-7, the correlations proposed by Karabelas et al. and Ranz and Marshall results, respectively, in significant over-prediction and under-prediction. However, the correlations by Satterfield et al. and Jolls and Hanratty are found to perform almost equally well in being the closest to experimental data though underestimating these latter systematically as Re number increases. Interestingly, both of these correlations were developed for mm-size non-spherical packings. In general, some degree of caution has to be applied in predicting micro-scale results of liquid-solid mass transfer coefficient with the macro-scale correlations as the nature of the flow in the two scales are markedly different, e.g., tube-to-particle diameter ratio and marginal role played by gravitational forces in micro-scale. It should be noted that Tidona et al.<sup>7</sup> derived several correlations for liquid-solid mass

transfer coefficient at micro-scale, however, each correlation was based on a limited number of experimental results within a narrow range of Reynolds number and specific to a certain geometry and tube aspect ratio. For this reason, none of the correlations proposed by Tidona et al.<sup>7</sup> was able to match to our experimental data as they were obtained at lower Reynolds numbers and different tube dimensions and particle sizes.



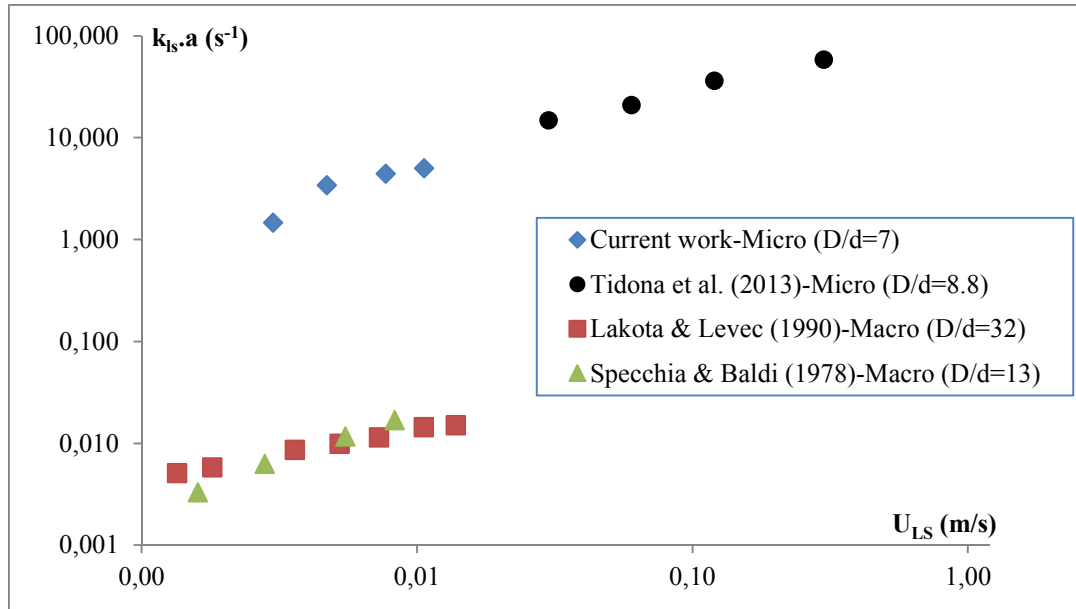
**Figure 5-7.** Experimental liquid-solid mass transfer coefficients for group B graphite particles versus predicted results with macro-scale correlations.

Figure 5-8 shows variations in volumetric liquid-solid mass transfer coefficients ( $k_{LS,a}$ ) of the current work along with those obtained in other micro-packed beds using dissolution method for  $k_{LS}$  evaluation with spherical particle sizes of  $80\mu\text{m}$ .<sup>7</sup> As can be seen, the range of liquid velocities in the two works is different because of technical constraints in our study and the possibility of glass tube fracture limited the range of liquid velocity. However, had it been possible to perform experiments at increased liquid velocities, it could have been expected for our data to merge onto those data of Tidona et al.<sup>7</sup> with probably some offset originating from difference between particle sizes in the two cases.



**Figure 5-8.** Volumetric liquid-solid mass transfer coefficients for group B graphite particles (◆) compared with those determined by Tidona et al. (2013) with 80 $\mu$ m particles and different D/d ratios. All data are for single-phase liquid flow experiments.

As a comparison between volumetric liquid-solid mass transfer coefficients in both micro- and macro-scale, Figure 5-9 depicts the results of current work along with the results of Specchia and Baldi<sup>29</sup> and Lakota and Levec<sup>27</sup> (macro-scale results) and Tidona et al. (micro-scale test).<sup>7</sup> All the results presented are for single-phase liquid flow experiments. The D/d ratios for Lakota & Levec and Specchia & Baldi results were 32 and 13, respectively, whereas the ratio was around 7 in the current work and 8.8 for Tidona et al. As can be seen from Figure 5-9, the macro-scale  $k_{LS,a}$  values are several orders of magnitude lower than those obtained for micro-scale setups showing the effect of aggressive phase interactions at constricted volumes as well as high surface-to-volume ratios associated with microreactors. Although the data from Tidona et al.<sup>7</sup> shows higher volumetric mass transfer coefficients, they are acquired at the expense of higher liquid phase velocities (at least by one order of magnitude) justifying these high values compared to the current work.



**Figure 5-9.** Comparison of volumetric liquid-solid mass transfer coefficients for single-phase liquid flow experiments at micro- and macro-scale.

Among the existing correlations recommended for estimation of liquid-solid mass transfer coefficients, the correlations developed by Larachi et al.<sup>30</sup> for macro-scale packed beds (using artificial neural network and dimensional analysis in the presence of a comprehensive database of mass- and heat-transfer data) are shown to exhibit unparalleled accuracy with nearly ten times less scatter and have also been phenomenologically examined for consistency. These type of correlations use normalized inputs based on a number of dimensionless numbers including Reynolds, Stokes, Galileo and Schmidt number. To investigate whether these types of correlations are able to predict micro-scale mass-transfer result, Figures 5-10.a and 5-10.b show the experimental data versus the predicted ones. As can be observed, there is a significant difference between the experimental data and the predictions from the correlation of Larachi et al.<sup>30</sup> One reason to these markedly different results could be due to the fact that normalized inputs used to build the structure of these correlations are partly based on dimensionless numbers which describe the macro-scale phenomena. For instance, the Stokes and Galileo number are used for describing the systems in which gravitational forces are not negligible. However, this is not the case in micro-scale systems such as the current work. Another probable reason for such a difference in liquid-solid mass transfer coefficient results could be from the domain of applicability aspect where



the Reynold numbers for in the current work where outside the range proposed by the correlation.

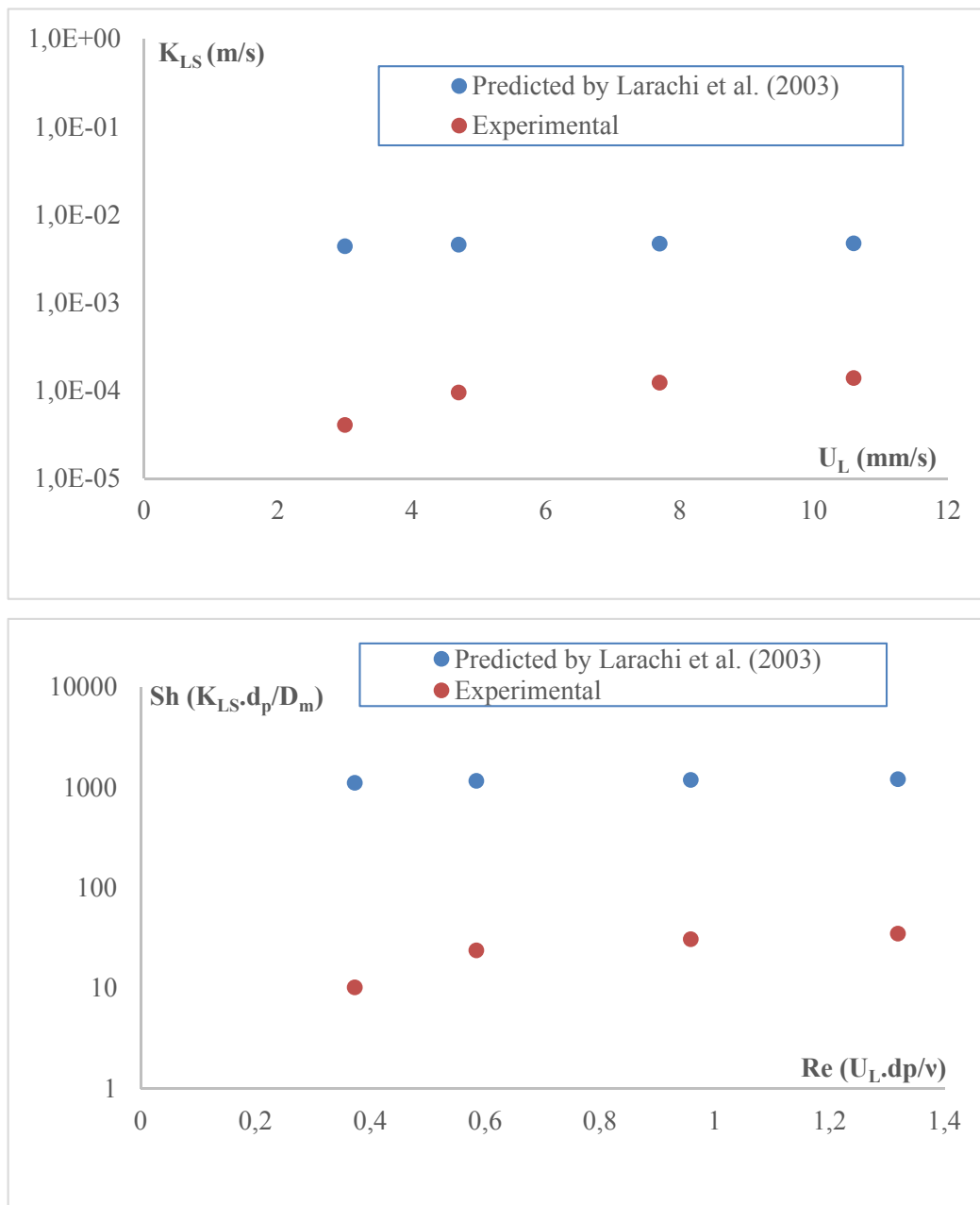


**Figure 5-10.** Comparison of experimental liquid-solid mass transfer coefficients with predictions of Larachi et al. (2003) correlation a)  $k_{LS}$  vs  $U_{LS}$ , b) Sherwood number vs. Reynolds number

### 5.3.2 Gas-liquid flow

As for the two-phase flow experiments electrolyte solution and nitrogen were both fed to the micro-packed bed. Unlike the macro-scale packed beds in the literature where flat I-V curves in the diffusional regime had been obtained for two-phase flow, the I-V curve for our micro-packed bed showed different shapes of fluctuations in this regime. Examples of such rise and falls in current are shown in Figure 5-11. In Figure 5-11.a fluctuations start at the second half of the diffusion-limited regime which might be due to approaching the 2<sup>nd</sup> kinetic regime and evolution of bubbles. On the other hand, Figure 5-11.b shows fluctuations that are, in contrast with Figure 10.a, following a more or less regular pattern. This type of signal in the diffusion-limited regime could be originating from intense interactions between gas and liquid (a pulse-like flow of gas and liquid) within the bed. Samples of such kind of fluctuations have been previously demonstrated by Faridkhou et al.<sup>2</sup> indicating the intermittent flow of gas and liquid inside the bed. However, the signals were not reproducible and did not enable us to deduce reliable liquid-solid mass transfer coefficient values from the linear polarization curves. One possible way to eliminate the fluctuation in the diffusional plateau is to decrease the high  $U_{G0}/U_{L0}$  ratio by using gas flow meters that deliver the gas phase at much lower flowrates (lower gas superficial velocities) than the one being currently used.

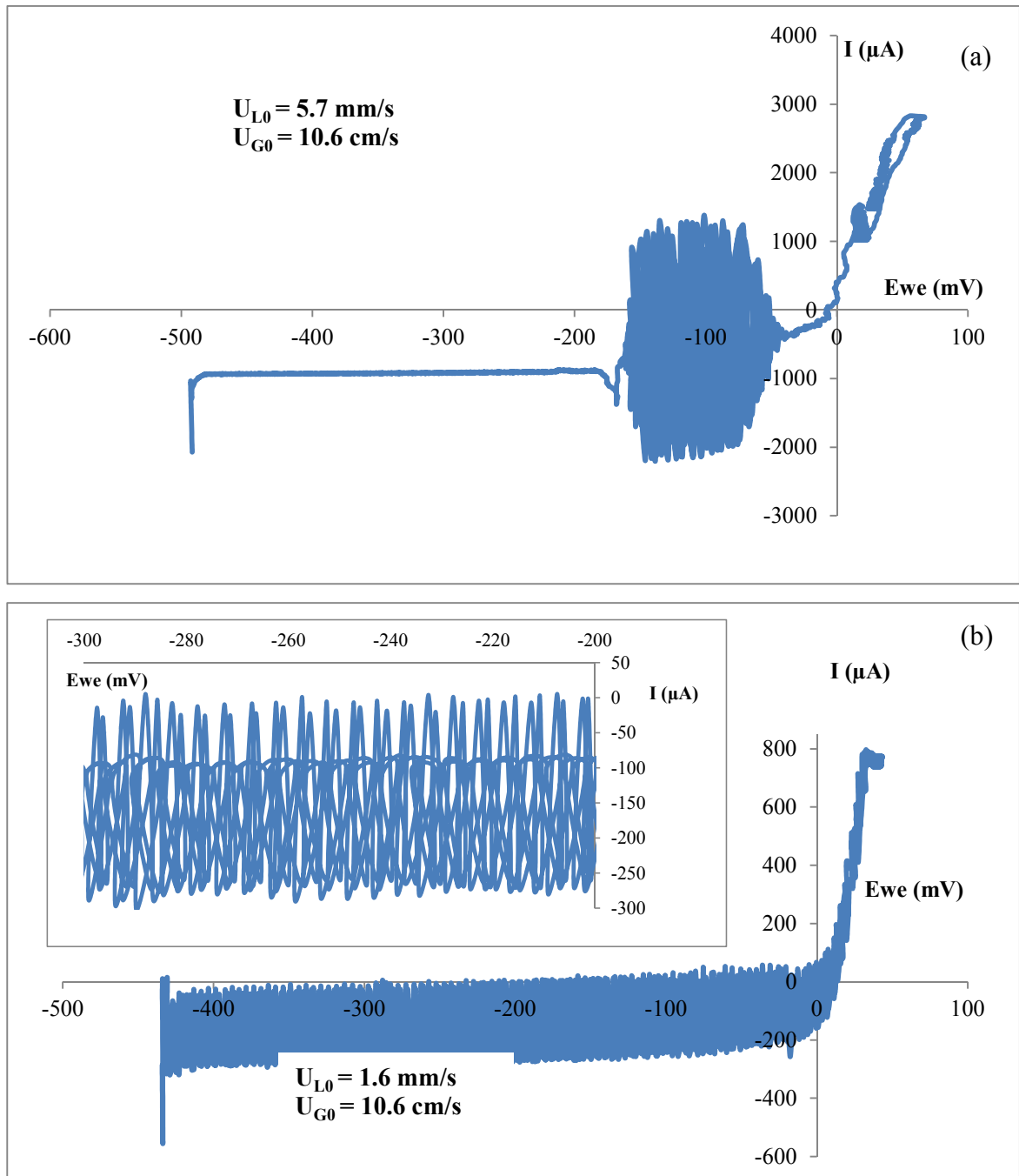


**Figure 5-11.** Examples of peculiar results obtained for two-phase flow experiments presumably due to the high flow rate of the gas phase compared to the liquid phase.

## 5.4 Conclusions

Limiting current technique was used in the current work to determine liquid-solid mass transfer coefficient. The electrolyte solution passes through a micro-tube which is partly packed with layers of non-spherical graphite particles representing cathode and anode. Processing the 2D images acquired from non-spherical graphite samples allows determination of particles average circularity, their specific surface area and total surface area required in evaluating the liquid-solid mass transfer coefficient. Two methods have been proposed to account for variations in ferricyanide concentration and the results for both cases were compared. Having studied on how the micro-scale results for liquid-solid mass transfer coefficient correspond to previously suggested macro-scale correlations, it was found out that the correlation proposed by Satterfield et al. (for packings with cylindrical shape) shows closer predictions but still shows some degrees of under-prediction. A macro- versus micro-scale comparison in terms of volumetric liquid-solid mass transfer coefficient shows significantly higher  $k_{LS,a}$  values for micro-packed beds stemming from higher solid-liquid interaction in confined spaces and high surface-to-volume ratio provided by micro-packed bed. As for the future works in this field, one can use gas flow meters with flowrates in the same order as the liquid phase to determine  $k_{LS}$  at two-phase flow conditions. Once the liquid-solid mass transfer coefficient data from two-phase flow and single-phase liquid flow are available, it is possible to determine the wetting efficiency (as was already done by Lakota and Levec<sup>27</sup> in macro-scale packed beds) and its variation along the length of micro-packed bed (due to the expansion of the gas phase at near-outlet regions of the micro-packed bed). Ultimately, inspired from the work of Larachi et al.<sup>30</sup>, it is possible to develop correlations for predicting liquid-solid mass transfer coefficient using inputs (dimensionless numbers) that portray the phenomena specific to micro-scale system. This will inevitably require a large number of experimental data for mass transfer coefficient at micro-scale to test its consistency.

## 5.5 Nomenclatures

$a$	Specific surface area ( $L^{-1}$ )
$A$	Surface area ( $L^2$ )
$C_0$	Initial concentration of ferricyanide ( $mol.L^{-3}$ )
$C_{L_T}$	Concentration of ferricyanide at $L_T$ ( $mol.L^{-3}$ )
$C_M$	Averaged ferricyanide concentration ( $mol.L^{-3}$ )
$d_{eq}$	Equivalent diameter (L)
$F$	Faraday constant ( $9.65 \times 10^4$ C/mol)
$I$	Current (A)
$k_{LS}$	Liquid-solid mass transfer coefficient ( $LT^{-1}$ )
$L_T$	Total length of cathode section (L)
$n_e$	Number of electrons (-)
$Re$	Reynolds number (-)
$Sc$	Schmidt number (-)
$Sh$	Sherwood number (-)
$U_L$	Superficial velocity ( $LT^{-1}$ )
Greek letters	
$\alpha$	Equation (5-4)
$\beta$	Equation (5-5)

$\Psi$	Sphericity (-)
$\zeta$	Circularity (-)

## 5.6 References

- Hessel, V.; Angeli, P.; Gavriilidis, A.; Lowe, H., Gas-liquid and gas-liquid-solid microstructured reactors: Contacting principles and applications. *Ind. Eng. Chem. Res.* **2005**, 44, (25), 9750-9769.
- Faridkhou, A.; Hamidipour, M.; Larachi, F., Hydrodynamics of gas-liquid micro-fixed beds - Measurement approaches and technical challenges. *Chem. Eng. J.* **2013**, 223, 425-435.
- Guettel, R.; Turek, T., Assessment of micro-structured fixed-bed reactors for highly exothermic gas-phase reactions. *Chem. Eng. Sci.* **2010**, 65, (5), 1644-1654.
- Tadepalli, S.; Qian, D. Y.; Lawal, A., Comparison of performance of microreactor and semi-batch reactor for catalytic hydrogenation of o-nitroanisole. *Catal. Today* **2007**, 125, (1-2), 64-73.
- Cao, E. H.; Sankar, M.; Firth, S.; Lam, K. F.; Bethell, D.; Knight, D. K.; Hutchings, G. J.; McMillan, P. F.; Gavriilidis, A., Reaction and Raman spectroscopic studies of alcohol oxidation on gold-palladium catalysts in microstructured reactors. *Chem. Eng. J.* **2011**, 167, (2-3), 734-743.
- Suh, J. S.; Lee, M. T.; Greif, R.; Grigoropoulos, C. R., A study of steam methanol reforming in a microreactor (vol 173, pg 458, 2007). *J. Power Sources* **2008**, 183, (2), 817-817.
- Tidona, B.; Desportes, S.; Altheimer, M.; Ninck, K.; von Rohr, P. R., Liquid-to-particle mass transfer in a micro packed bed reactor. *Int. J. Heat Mass Transf.* **2012**, 55, (4), 522-530.
- Faridkhou, A.; Larachi, F., Two-phase flow hydrodynamic study in micro-packed beds - Effect of bed geometry and particle size. *Chem. Eng. Process.* **2014**, 78, 27-36.
- Saroha, A. K., Solid-liquid mass transfer studies in trickle bed reactors. *Chem. Eng. Res. Des.* **2010**, 88, (5-6A), 744-747.
- Satterfield, C. N.; Vaneek, M. W.; Bliss, G. S., Liquid-solid mass-transfer in packed-beds with downward concurrent gas-liquid flow. *Aiche J.* **1978**, 24, (4), 709-717.
- Al-Dahhan, M.; Highfill, W.; Ong, B. T., Drawbacks of the dissolution method for measurement of the liquid-solid mass-transfer coefficients in two-phase flow packed-bed reactors operated at low and high pressures. *Ind. Eng. Chem. Res.* **2000**, 39, (8), 3102-3107.
- Chau, P. C., Local liquid solid mass-transfer measurement in a trickle film flow model using an electrochemical technique. *Int. J. Heat Mass Transf.* **1987**, 30, (11), 2305-2317.

13. Highfill, W.; Al-Dahhan, M., Liquid-solid mass transfer coefficient in high pressure trickle bed reactors. *Chem. Eng. Res. Des.* **2001**, 79, (A6), 631-640.
14. Gostick, J.; Doan, H. D.; Lohi, A.; Pritzker, M. D., Investigation of local mass transfer in a packed bed of pall rings using a limiting current technique. *Ind. Eng. Chem. Res.* **2003**, 42, (15), 3626-3634.
15. Hassan, I.; Zahran, R. R.; Mansour, I. S.; Sedahmed, G. H., Liquid-solid mass transfer at a fixed bed of lessing rings, in relation to electrochemical reactor design. *Ind. Eng. Chem. Res.* **2005**, 44, (15), 5761-5767.
16. Trivizadakis, M. E.; Karabelas, A. J., A study of local liquid/solid mass transfer in packed beds under trickling and induced pulsing flow. *Chem. Eng. Sci.* **2006**, 61, (23), 7684-7696.
17. Joubert, R.; Nicol, W., Trickle flow liquid-solid mass transfer and wetting efficiency in small diameter columns. *Can. J. Chem. Eng.* **2013**, 91, (3), 441-447.
18. Selman, J. R.; Tobias, C. W., Mass-transfer measurements by the limiting-current technique. *Adv. Chem. Eng.* **1978**, 10:211.
19. Mohammed, I.; Bauer, T.; Schubert, M.; Lange, R., Liquid-solid mass transfer in a tubular reactor with solid foam packings. *Chem. Eng. Sci.* **2014**, 108, 223-232.
20. Bourne, J. R.; Dellava, P.; Dossenbach, O.; Post, T., Densities, viscosities, and diffusivities in aqueous sodium-hydroxide potassium ferricyanide and ferrocyanide solutions. *Journal of Chemical and Engineering Data* **1985**, 30, (2), 160-163.
21. Fogler, H. S., *Elements of Chemical Reaction Engineering*. Prentice Hall International Series ed.; **2005**.
22. Li, L.; Ma, W., Experimental Study on the Effective Particle Diameter of a Packed Bed with Non-Spherical Particles. *Transport in Porous Media* **2011**, 89, (1), 35-48.
23. Chikhi, N.; Coindreau, O.; Li, L. X.; Ma, W. M.; Taivassalo, V.; Takasuo, E.; Leininger, S.; Kulenovic, R.; Laurien, E., Evaluation of an effective diameter to study quenching and dry-out of complex debris bed. *Annals of Nuclear Energy* **2014**, 74, 24-41.
24. Cavarretta, I.; O'Sullivan, C.; Coop, M. R. In *Applying 2D shape analysis techniques to granular materials with 3D particle geometries*, 6th International Conference on the Micromechanics of Granular Media, Golden, CO, 2009, Jul 13-17, 2009; Golden, CO, 2009; pp 833-836.
25. Jolls, K. R.; Hanratty, T. J., Use of electrochemical techniques to study mass transfer rates and local skin friction to a sphere in a dumped bed. *Aiche J.* **1969**, 15, (2), 199-&.
26. Karabelas, A. J.; Wegner, T. H.; Hanratty, T. J., Use of asymptotic relations to correlate mass transfer data in packed beds. *Chem. Eng. Sci.* **1971**, 26, (10), 1581-&.

27. Lakota, A.; Levec, J., Solid-liquid mass-transfer in packed-beds with cocurrent downward 2-phase flow. *Aiche J.* **1990**, 36, (9), 1444-1448.
28. Ranz, W. E.; Marshall, W. R., Evaporation from drops .1. *Chem. Eng. Prog.* **1952**, 48, (3), 141-146.
29. Specchia, V.; Baldi, G.; Gianetto, A., Solid-liquid mass-transfer in concurrent 2-phase flow through packed-beds. *Industrial & Engineering Chemistry Process Design and Development* **1978**, 17, (3), 362-367.
30. Larachi, F.; Belfares, L.; Iliuta, I.; Grandjean, B, Heat and mass transfer in cocurrent gas-liquid packed beds. Analysis, recommendation, and new correlations. *Ind. Eng. Chem. Res.* **2003**, 42, (1), 222-242.



## 6 Thesis conclusion

### 6.1 Key contributions

In chapter 2, the hydrodynamics of micro-packed beds were studied. The focus of this chapter was on flow regimes, flow regime transition and hysteresis and mostly relied on microscopic visualization followed by processing the acquired images. Visualization of micro-packed bed identified two major flow regimes: low-interaction flow regime, characterized by minor movements in gas-liquid boundary and high interaction flow regimes showing rapid displacements of the gas and liquid phases. Subsequent image processing enables differentiation between the two regimes by defining characteristic lengths. Statistical analysis (based on the coefficient of variation of the characteristic length versus liquid superficial velocity) led to the identification of flow regime transition point and building a flow regime map demarcating regions for low and high interaction regimes. Hysteresis study of the micro-packed bed was carried out by both pressure drop measurements and bed wetting pattern analysis (in imbibition ( $L\uparrow$ ) and drainage ( $L\downarrow$ ) modes) where major hysteresis was observed in both cases. Based on the wetting pattern hysteresis, three distinct regions were identified within the bed texture: (1) regions that were wet in the imbibition path and then became dry during drainage, (2) regions that were dry during imbibition path and which became wet upon drainage, and (3) regions that retained their status (either wet or dry) regardless of the operation mode.

Chapter 3 was an overview of the challenges that had been encountered in the hydrodynamic study of micro-packed beds and led to the dearth of publications in this field. Some of the small but important details were mentioned in the experimental setup and methodology while some of the major challenges surpassed by performing experiments with a cause and effect logic were subjected to more scrutiny. Starting from RTD experiments it was concluded that the location of tracer input does matter in reliability of RTD experiments. Among the two possible options for tracer injection it was found out that it should be injected somewhere in between the gas-liquid merging point (start of the packed bed) and the first pair of point electrodes. The importance of solid packing (to obtain reproducible RTD results) and modification of conductivity probes were the next important issues discussed in chapter

3. Pressure drop measurements along with liquid holdup determination reveal that increases in solid particle size decreased both pressure drop and liquid holdup. Also, increases in superficial liquid velocity led to an increase in liquid holdup. The opposite trend was observed by increasing the superficial gas velocity. Wall RTD tests were done by injecting a dye tracer and monitoring the gray level intensity changes of the images taken within a frame downstream of the injection. Experimental results confirmed the theoretically predicted maximum velocity in the wall region (having high porosity).

As for chapter 4, the effects of solid particle size and bed cross-sectional geometry (circular vs. square) on a number of hydrodynamic parameters of micro-fixed beds (bed pressure drop, flow regime transition point, hysteresis and the bed transient behavior) were investigated. From the two-phase flow visualizations it was observed that flow regime transition from low to high interaction initiates at the near-outlet zone of the bed and gradually propagates toward the near-inlet zone. Using smaller particle sizes at same L/G flow ratios caused an earlier inception of the high interaction regime while cross-sectional geometry of the bed did not affect the point of flow regime transition. Study of wetting pattern hysteresis showed that hysteresis in micro-packed beds is strongly affected solid particle size. Monitoring the bed transient behavior revealed that larger particle sizes and square geometry possess shorter transient times in comparison with smaller particle sizes and circular geometry.

In chapter 5, the limiting current technique was adopted to determine liquid-solid mass transfer coefficient in a micro-tube packed with glass beads and graphite particles (serving as electrodes) in single-phase liquid flow conditions. The electrochemical reaction under investigation was the redox reaction of ferri- and ferrocyanide. 2D imaging and subsequent processings along with statistical analysis enabled determination of circularity for graphite particles to account for deviations from spherical geometry. The single-phase liquid flow experiments revealed much higher volumetric liquid-solid mass transfer coefficients ( $k_{LS,a}$ ) as compared to macro-scale packed beds. This was due to higher solid-liquid interaction in confined spaces and high surface-to-volume ratio provided by micro-packed bed.

## 6.2 Suggested future work

It was shown in the introduction section that hydrodynamic studies of micro-packed beds, unlike microchannels, have received little coverage in the open literature. In case of microchannels many different aspects such as flow regimes, factors affecting flow regimes, pressure drop, phase holdup, residence time distribution have been extensively and thoroughly studied. The number of publications in the open literature focusing only on flow in micro-channels nearly exceeds 1000. In contrast, investigations on micro-packed beds are still in their infancy with only a small number of publications in the literature as mentioned throughout this thesis. Very few works that have been published indicate that there are still many gaps to be filled in this realm. Although there are many challenges that arise in studying the hydrodynamics of micro-packed beds in terms of both fabrication and operation, once they are successfully surpassed there will be a huge research gradient in this field. For example, a comprehensive set of investigations can be conducted on the subject of flow regimes and factors contributing to its transitions by getting inspirations from the pool of research available on microchannels<sup>1-3</sup> and use them as platform for the current studies. For example, there are some catalytic processes in which water-repellent (hydrophobic or super-hydrophobic) catalysts are employed. As a micro-scale cold setup for such processes it is stimulating to see how the wettability of both wall and solid particles in micro-packed beds will affect the point of flow regime change, pressure drop and liquid holdup. Using hydrophobic/hydrophilic materials or coatings for both wall and solid particles will make four combinations that can be compared to each other for the effect of wettability.

In chapter 2, studies on flow regimes and flow regime transition were presented all relying on visualization from layers adjacent to the wall and therefore all discussions and interpretations are limited to the wall region. Although wall visualizations can address parts of the hydrodynamic aspects of micro-fixed beds, there exist other methods which can be applied successfully for more in-depth studies such as micro-computed tomography for visualizing gas-liquid interactions and their distribution at any depth within the bed or micro-particle image velocimetry ( $\mu$ -PIV) with refractive index matching for flow field velocity determination.

It was shown in chapter 3 that the results obtained from wall RTD measurements (using the microscopic imaging and subsequent image processing) are in agreement with naïve expectation of higher liquid velocity in the wall region due to higher porosity. However, the low imaging frequency (15 frames/sec) and the narrow field of view of the objective lens necessitate some degree of caution in the interpretation of the obtained values. To allow further interpretations and in order to obtain more accurate results, there are three recommendations that could be implemented and will improve the wall RTD experiments in future studies. The first option could be the side-by-side installation of two separate visualization systems (including microscope and camera) and fixing a specific distance to produce separated RTD curves. The next two options, which will be less costly as compared to the first option, are to keep the structure of experimental setup mentioned in chapter 3 but either replace the objective lens with those having a broader field of view (lower magnification) to cover a wider length of the micro-packed bed or use a camera with much higher frequency of imaging ( $\gg 15$  Hz) to acquire more intermediate images between each two images that are being taken with the current setup mentioned in chapter 3.

It was shown in chapter 4 that by increasing the liquid flow rate at constant gas mass flow rate, flow regime transition in micro-packed beds starts from the near-outlet zone and then progressively shifts with respect to bed length (opposite to flow direction) to the near-inlet regions. This means that the pressure gradient within the bed length and gradual expansion of the gas phase as it flows toward the outlet contribute to gas-liquid contacting patterns that are more or less different with respect to bed length. Also, by carefully examining the results presented in the very few contributions on micro-packed beds<sup>4-6</sup> it can be observed that liquid holdups that have been determined in micro-packed beds by using tracer injection method are reported as one single global value. This view on liquid holdup of micro-packed beds does not seem to be appropriate as the very large pressure gradients within the micro-packed beds length suggest that liquid holdups vary with respect to length which is not the case for macro-scale packed beds. Therefore, a potential idea to shed light upon this issue is to design and fabricate micro-packed bed setups with multiple tracer concentration probes between the two ends and determine liquid holdup at each interval from

upstream to downstream (at least at three intervals:  $[0, L/3]$ ,  $[L/3, 2L/3]$ ,  $[2L/3, L]$ ) to compare the obtained values.

Since the liquid-solid mass transfer coefficient in micro-packed beds, discussed in chapter 5, is also dependent on liquid holdup, it would also be interesting to design and fabricate a micro-packed bed with multiple platinum wires inserted in the tube and change the position of cathode and anode within the length of the bed to determine liquid-solid mass transfer coefficient at different intervals (at least at three intervals:  $[0, L/3]$ ,  $[L/3, 2L/3]$ ,  $[2L/3, L]$ ). The experiments could be conducted at both low interaction and high interaction flow regimes depending on the design pressure of the tube. If liquid-solid mass transfer coefficients for two-phase gas-liquid flow are desired, one can use gas flow meters with flowrates in the same order as the liquid phase to determine  $k_{LS}$  at two-phase flow conditions. Upon comparing these values with those of single-phase flow experiments, it is also possible to determine the wetting efficiency as was done by Lakota and Levec<sup>7</sup> for macro-scale packed beds.

### 6.3 References

1. Shao, N.; Gavriilidis, A.; Angeli, P., Flow regimes for adiabatic gas-liquid flow in microchannels. *Chem. Eng. Sci.* **2009**, 64, (11), 2749-2761.
2. Akbar, M. K.; Plummer, D. A.; Ghiaasiaan, S. M., On gas-liquid two-phase flow regimes in microchannels. *Int. J. Multiph. Flow* **2003**, 29, (5), 855-865.
3. Triplett, K. A.; Ghiaasiaan, S. M.; Abdel-Khalik, S. I.; Sadowski, D. L., Gas-liquid two-phase flow in microchannels - Part I: two-phase flow patterns. *Int. J. Multiph. Flow* **1999**, 25, (3), 377-394.
4. Marquez, N.; Castano, P.; Makkee, M.; Moulijn, J. A.; Kreutzer, M. T., Dispersion and holdup in multiphase packed bed microreactors. *Chem. Eng. Technol.* **2008**, 31, (8), 1130-1139.
5. Marquez, N.; Castano, P.; Moulijn, J. A.; Makkee, M.; Kreutzer, M. T., Transient Behavior and Stability in Miniaturized Multiphase Packed Bed Reactors. *Ind. Eng. Chem. Res.* **2010**, 49, (3), 1033-1040.
6. Faridkhou, A.; Hamidipour, M.; Larachi, F., Hydrodynamics of gas-liquid micro-fixed beds - Measurement approaches and technical challenges. *Chem. Eng. J.* **2013**, 223, 425-435.
7. Lakota, A.; Levec, J., Solid-liquid mass-transfer in packed-beds with cocurrent downward 2-phase flow. *Aiche J.* **1990**, 36, (9), 1444-1448.

